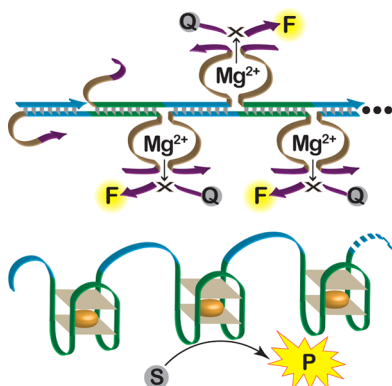


From Cascaded Catalytic Nucleic Acids to Enzyme–DNA Nanostructures: Controlling Reactivity, Sensing, Logic Operations, and Assembly of Complex Structures

Fuan Wang,[‡] Chun-Hua Lu,[‡] and Itamar Willner*

Institute of Chemistry, The Center for Nanoscience and Nanotechnology, The Hebrew University of Jerusalem, Jerusalem 91904, Israel



CONTENTS

1. Introduction	2881
2. Enzyme-Free Nucleic Acid-Activated Chain Reactions	2883
2.1. Hybridization Chain Reactions (HCR) for Sensing and Tailoring Nanostructures	2884
2.2. Catalytic Hairpin Assembly (CHA) Reactions for Amplified Sensing and Programmed Nanostructuring	2888
2.3. Cascaded Strand-Displacement Processes for Logic Gates and DNA Machines	2893
3. DNAzyme-Activated Chain Reactions	2896
3.1. Isothermal DNAzyme-Activated Catalytic Cascades	2896
3.2. Isothermal Autonomous DNAzyme-Activated Catalytic Cascades	2899
3.3. DNAzyme-Activated Autonomous Cascaded Logic Gates and DNA Machines	2903
4. Enzyme/DNAzyme Coupled Catalytic Cascades	2906
4.1. Biocatalytic Cascades Driven by Coupled DNAzymes and Rolling Circle Amplification (RCA) Processes	2906
4.2. Biocatalytic Cascades Driven by Coupled DNAzymes and Endonucleases/Nicking Enzymes	2910
4.3. Biocatalytic Transformations Driven by Coupled Polymerase/Nicking Enzyme DNAzyme Cascades	2913
4.4. Coupled Ligation-Triggered DNAzyme Cascades	2915
4.5. DNAzyme-Amplified Detection of Telomerase Activity	2917

4.6. Logic Gates with Cascaded Enzyme/DNAzyme Systems	2919
5. Enzyme–Nucleic Acid Systems for Controlled Chemical Processes	2919
5.1. Coupled Enzyme–DNAzyme Processes	2921
5.2. Controlling Enzyme Functions on Nucleic Acid Scaffolds	2922
6. Conclusions and Perspectives	2929
Author Information	2930
Corresponding Author	2930
Author Contributions	2930
Notes	2930
Biographies	2930
Acknowledgments	2931
References	2931

1. INTRODUCTION

DNA is one of the most fascinating biopolymers. Besides its central role as carrier of genetic information and translation of the genetic code into proteins, DNA holds great promise as a functional material for bioanalysis, DNA computing, DNA nanotechnology, and nanomedicine. The two purine bases adenine (A) and guanine (G) and the two pyrimidine bases thymine (T) and cytosine (C) provide the “vocabulary” to construct and encode the base sequence information into the biopolymers. The basic Watson–Crick complementary base pairing yields the double-helix duplex DNA consisting of A–T and C–G hydrogen-bonded base pairs.^{1,2} Self-assembly of single-stranded DNA chains into supramolecular nanostructures and metal-ion-assisted cooperative stabilization of DNA duplexes are further structural motives characterizing the DNA biopolymers, Figure 1A. Self-assembly of G-rich sequences into G-quadruplexes,^{3,4} pH-stimulated transformation of C-rich chains into i-motif^{5,6} and ion-bridged complexes formed between bases, such as T–Hg²⁺–T^{7,8} or C–Ag⁺–C^{9,10} bridges, represent frequently encountered supramolecular nanostructures in the DNA polymer chains. Furthermore, incorporation of non-native nucleic acid bases into DNA chains leads to new “ligandosides”^{11,12} acting as chelators for association of ions and bridging of DNA chains to yield catalytic nucleic acid nanostructures.^{13,14} Supramolecular complexes between proteins and sequence-specific domains of DNA play a central role in signal transduction and in the activation of cellular

Received: July 4, 2013

Published: February 27, 2014



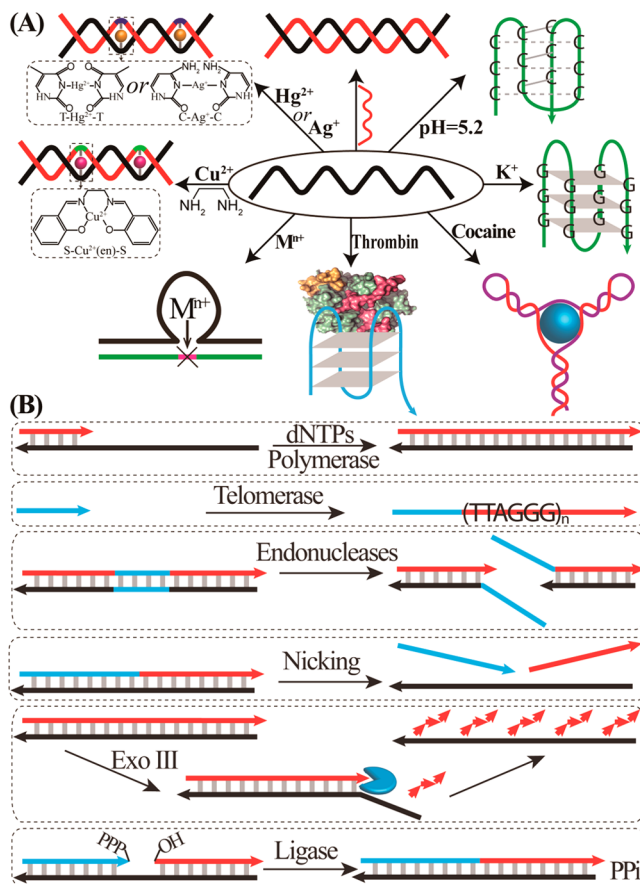


Figure 1. (A) Schematic structural transitions of DNA triggered by external stimuli. (B) Examples of biocatalyzed transformations on DNA nanostructures.

processes,^{15–20} for example, the oriC replication region in bacteria,¹⁸ the TATA box in eukaryotes transcription machinery,¹⁹ or the aminoacyl tRNA synthetase that recognizes different tRNAs during the translation process.²⁰ Furthermore, ingenious methods to select and amplify sequence-specific nucleic acids, exhibiting specific recognition sites (aptamers) for low-molecular-weight substrates, macromolecules and even cells,^{21–23} and development of catalytic nucleic acids (DNAzymes or ribozymes)^{24–26} provide new functional materials. The systematic evolution of ligands by exponential enrichment, the SELEX procedure,²⁷ and further developments of this process^{28,29} introduced versatile methods to prepare indispensable quantities of specific receptors and new catalysts.

Besides the unique properties of nucleic acids, numerous native biocatalysts catalyze chemical transformations utilizing DNA as substrate. Polymerase replicates nucleic acids in the presence of the nucleotides mixture, dNTPs, and a template as initiator,^{30–32} and telomerase catalyzes elongation of the telomer chains.^{33–35} Endonucleases are sequence-specific biocatalysts cleaving duplex DNA structures,^{36,37} exonucleases (e.g., Exo III) act as digestive biocatalysts that cleave specific ends of duplex DNA domains,^{38,39} and nicking enzymes are sequence-specific catalysts cleaving one strand of duplex DNA structures. Similarly, ligase acts as biocatalyst for ligating two (or more) nucleic acid strands,^{40,41} and helicase catalyzes separation of duplex oligonucleotides into single strands by a ATP-dependent reaction,^{42,43} Figure 1B.

These unique structural and functional properties of DNA and the availability of a “toolbox” of catalysts for cut-and-paste manipulation of nucleic acids paved the way to develop the area of DNA nanotechnology. Different research disciplines can be identified in the rapidly developing field of DNA nanotechnology, Figure 2. These include application of the unique

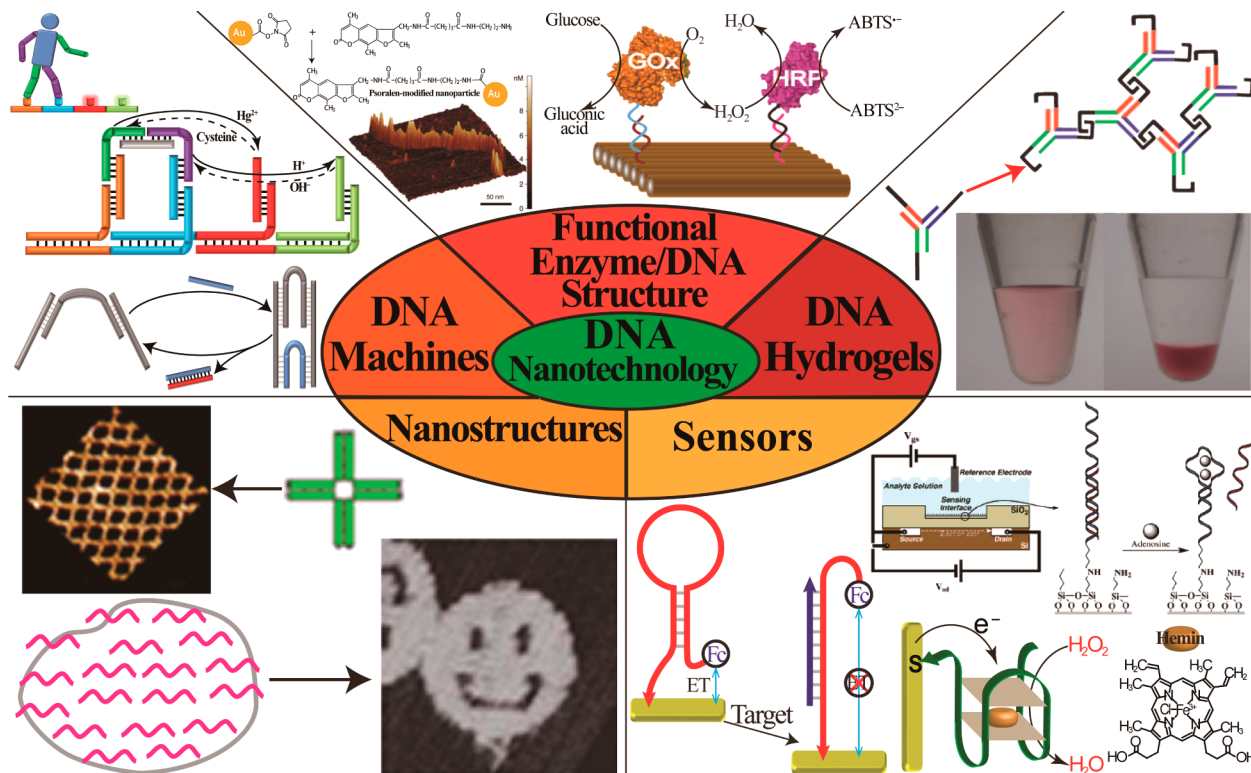


Figure 2. Schematic presentation of different areas associated with DNA nanotechnology.

recognition properties of nucleic acids or aptamers as recognition ligands for sensing events^{44–47} and implementation of catalytic nucleic acids as amplifying labels for sensing processes.^{48–53} Indeed, numerous studies have addressed the use of nucleic acids in developing electrochemical,^{54–59} electronic,^{60–62} optical,^{63–68} microgravimetric,^{69–71} and mechanical sensors,^{72–75} and different methods to amplify the readout signals and to increase the sensitivity of the sensing platforms by catalytic labels^{76,77} or target regeneration^{47,78–80} schemes were demonstrated. A further discipline in DNA nanotechnology involves controlled self-assembly of DNA subunits into one-dimensional (1D) templates, two-dimensional (2D) lattices, and three-dimensional (3D) nanostructures.^{81–84} Ingenious DNA subunits (tiles) consisting of pretailored hybridization arms^{85–87} or nucleic acid chains exhibiting geometrical complementarity^{88–93} were used to assemble programmed DNA nanostructures. Alternatively, short nucleic acids with complementarity features to domains of large viral DNA rings were used as stapler units for construction of origami-type 2D and 3D nanostructures.^{94–99} Different self-assembled nanostructures provided templates for the spatial, ordered, positioning of enzymes for activation of enzyme cascades^{90–93,100–105} and “bottom-up” construction of nanostructures and nanoscale devices.^{106–108} Also, the tailored “engineering” of the base sequences in DNA provided means to encode information that activates molecular “DNA machines”.^{109–112} Various triggering fuels such as DNA strands,^{113–115} pH,^{116–119} ions,¹²⁰ light,^{121–125} and chemical reactions^{126–132} were used as “fuels” for activation of DNA machines. Different DNA machines, such as “tweezers”,^{114,119–121,132,133} “walkers”,^{115–117,125–130,134,135} “steppers”,¹¹⁷ “cranes”,¹³⁶ “rotors”,¹³⁷ “rotating rings”,¹³⁸ and more,^{139,140} were activated by the different fuels, and programmed assembly of nanoparticles by DNA machines^{141–145} or the programmed “walking” of nucleic acids on DNA templates or DNA nanostructures were demonstrated.^{146,147} In addition, self-assembly and cross-linking of DNA may lead to formation of hydrogels,^{148,149} and specifically to stimuli-responsive DNA hydrogels.^{150,151} Finally, the information encoded in DNA has been extensively implemented to develop DNA computing systems.^{47a,152–155} Different DNA nanostructures were used to perform logic gate operations,^{25a,156–161} and three different strategies addressed the use of DNA as a functional material for activation of gate cascades and assembly of computing circuits and computing devices. These included the cascaded generation of computing circuits using the strand-displacement mechanism,^{162–167} use of DNAzymes for activating logic gate cascades^{168–172} and pH-programmable computing circuits,¹⁷³ and programmed cleavage of DNA templates by enzymes as computing devices.^{174,175} Advances in DNA nanotechnology hold great promise in different disciplines, including bioanalysis and sensor applications,^{176–181} controlled delivery and release of materials,^{182–184} and fabrication of nanoscale devices.^{106–108,185–188} In particular, use of “smart” functional DNA nanostructures for controlling intracellular processes is of substantial interest for future nanomedicine.¹⁸⁹ Although this research area is at its infancy, recent studies demonstrated the incorporation of functional DNA nanostructures into cells and the logic activation of autonomous “sense-and-treat” biological transformations.¹⁹⁰

Despite the progress in DNA nanotechnology, challenging issues are still ahead of us. Methods to amplify DNA

recognition events are essential to develop “living” DNA technologies and complex DNA computing circuits and to design ultrasensitive sensing platforms. Such amplification paths could involve the coupling of catalytic processes in response to an input or analyte or development of feedback cycles that regenerate the input. Furthermore, systems that translate a recognition event into new functional entities, and eventually, catalytic entities, could provide new dimensions in the area of DNA nanotechnology. The present review sheds light on different recent approaches to tailor “smart” DNA nanostructures for autonomous activation of catalytic DNA cascades and their use for sensing, logic operations, and assembly of complex nanostructures.

2. ENZYME-FREE NUCLEIC ACID-ACTIVATED CHAIN REACTIONS

The thermodynamics associated with formation of stable DNA duplexes have been extensively studied, and the effects of the number of base pairs, nature of base pairing, salt concentrations, shape of the resulting duplexes, and cooperative effects on duplex stabilities were extensively characterized.¹⁹¹ The relative stabilities of duplex DNA nanostructures provide instructive information for dynamic transitions within duplex DNA systems. One of these dynamic transformations is the DNA strand-displacement process, Figure 3A. In this process,¹⁹² one (or more) DNA strand(s) hybridized with a nucleic acid template, which includes an exposed single-stranded domain (“toehold”), is being displaced by an auxiliary DNA strand exhibiting complementarity to the “toehold”

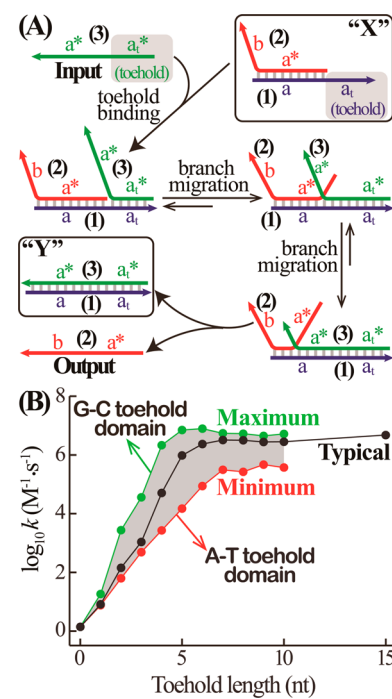


Figure 3. (A) DNA strand-displacement principle that involves a toehold tether binding domain that stimulates branch migration and formation of energetically stabilized duplex DNA nanostructures. (B) Theoretical modeling of the kinetics of the DNA strand-displacement process as a function of the number of bases in the toehold domains and the secondary influence of the base composition of the toehold regions. Reprinted with permission from ref 192c. Copyright 2011 Nature Publishing Group.

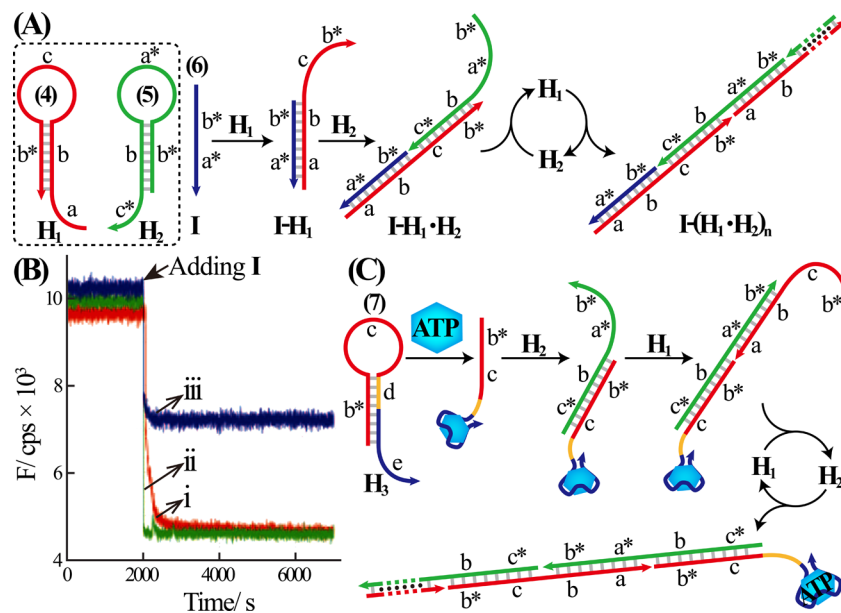


Figure 4. (A) Target-triggered isothermal autonomous hybridization chain reaction (HCR) using the cross-opening of two hairpin structures. (B) Fluorescence monitoring of the HCR by labeling domain a of hairpin H₁ with the 2-amino purine unit. This fluorophore exhibits high fluorescence in a single-stranded structure, and it is being quenched due to stacking in a duplex DNA structure: (i) Time-dependent decrease of fluorescence upon initiation of the hybridization chain reaction between hairpins H₁ and H₂ by the initiator DNA, I. Molar ratio of components I:H₁:H₂ = 0.5:1:1.2. (ii) Opening of hairpin H₁ only by an excess of the initiator, I. Molar ratio H₁:I = 1:4. (iii) Opening of only hairpin H₁ by the initiator, I, at a molar ratio of H₁:I = 1:0.5. (C) Activation of the autonomous HCR-based cross-opening of two hairpins H₁ and H₂ by the single-stranded nucleic acid tethered aptamer–ATP complex generated upon opening of hairpin H₃ by ATP. Reprinted with permission from ref 195. Copyright 2004 National Academy of Sciences.

domain and partial, or full, complementarity to the template DNA sequence, which yields a new DNA duplex structure of enhanced stability. This principle is displayed in Figure 3A, where the DNA complex “X” consisting of the hybrid (a–a_t)/(a^{*}–b) (1/2) interacts with the auxiliary strand a_t*–a^{*} (3), leading to the DNA strand-displacement reaction. DNA strands are designed to include the appropriate sequences, where domain x is complementary to domain x*. In this process the auxiliary input DNA strand (3) hybridizes with the toehold region a_t of the DNA complex “X”, and sequential branch migration yields the fully hybridized DNA complex “Y” (1/3) and generation of the output DNA strand (2). The kinetics of the strand-displacement process was modeled and found to depend on the number of DNA bases associated with the toehold domains (nt) and the relative stability of the toehold complex (region a_t/a_t^{*}),^{192c,193} Figure 3B. It was found that the rate constant for the strand-displacement reaction ranged from 1.0 to $6.0 \times 10^6 \text{ M}^{-1} \text{ s}^{-1}$ depending on the number of toehold bases, and these rate constants revealed boundary values for A–T toehold domains (low) and G–C toehold domains (high). Numerous studies have addressed the strand-displacement process and its possible implications.¹⁹⁴ Here, the strand-displacement principle, especially the autonomous hybridization chain reaction (HCR) and the autonomous catalytic hairpin assembly (CHA), will be discussed within the context of amplified sensing, autonomous formation of functional DNA nanostructures, and DNA computing circuits.

2.1. Hybridization Chain Reactions (HCR) for Sensing and Tailoring Nanostructures

The analyte-triggered isothermal autonomous hybridization chain reaction (HCR) provides a general principle to stimulate formation of DNA polymeric nanowires as a result of the primary recognition event. According to this principle,¹⁹⁵

Figure 4A, the system consists of two hairpins, H₁ (4) and H₂ (5), where the stem sequence of H₁ (4) includes domain b, complementary to region b* of the target DNA, I (6), and the single-stranded domain a, tethered to sequence b is complementary to region a* of the target DNA (6). The loop of hairpin H₁ is composed of sequence c. The second hairpin H₂ (5) consists of the stem duplex b/b*, the corresponding loop region a*, and the single-stranded domain c* complementary to loop region c of hairpin H₁. In the presence of analyte (6), a toehold-mediated displacement of regions a and b yields a DNA duplex of enhanced stability, which opens hairpin H₁ and forms structure I–H₁. In the resulting I–H₁ structure, the single-stranded domain c–b* opens hairpin H₂ while generating the structure I–H₁·H₂, where the single-stranded domain a*–b* opens hairpin H₁. Thus, the recognition event between hairpin H₁ and the target DNA (6) initiates an isothermal autonomous polymerization process that involves the cross-opening of hairpins H₂ and H₁ while forming a polymeric nanowire consisting of I–(H₁·H₂)_n. Formation of the polymeric nanowire was followed by gel electrophoresis and fluorescence measurements. Upon labeling the 5'-adenine residue of H₁ with the 2-amino-purine fluorophore that exhibits high fluorescence in the single-stranded configuration and quenched fluorescence in a duplex DNA configuration, due to stacking of the fluorophore in between the bases, the transition of the single-stranded tether associated with hairpin H₁ into a fluorophore-quenched duplex polymeric configuration I–(H₁·H₂)_n was demonstrated, Figure 4B. Gel electrophoresis experiments revealed that no polymerization reaction (through cross-opening of H₁ and H₂) was observed in the absence of the analyte. Interestingly, the resulting polymeric nanowires were longer as the analyte concentration was lower, consistent with the fact that only

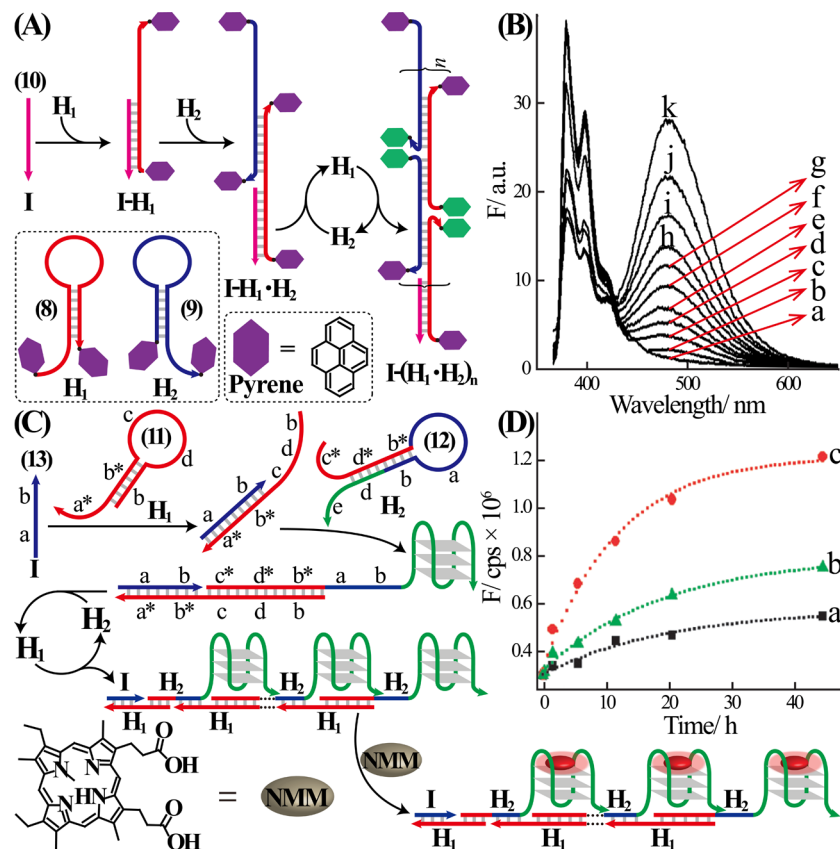


Figure 5. (A) Target I-induced activation of the isothermal autonomous HCR reaction involving cross-opening of two hairpins H₁ and H₂ functionalized at their 3'- and 5'-ends with pyrene units and following the hybridization-based polymerization process through exciplex emission of pyrene. (B) Fluorescence intensities of the exciplexes generated upon analyzing different concentrations of the target DNA by the HCR principle: (a) 0, (b) 2.56×10^{-13} , (c) 1.28×10^{-12} , (d) 6.4×10^{-12} , (e) 3.2×10^{-11} , (f) 1.6×10^{-10} , (g) 8×10^{-10} , (h) 4×10^{-9} , (i) 2×10^{-8} , (j) 1×10^{-7} , and (k) 5×10^{-7} M. Reprinted with permission from ref 196. Copyright 2011 Wiley-VCH. (C) Analyzing a target DNA I by analyte-triggered activation of HCR involving isothermal autonomous cross-opening of two hairpins H₁ and H₂ that yields a NMM/G-quadruplex 1D nanowires. The process is monitored by the fluorescence intensities of the resulting polymeric DNA nanostructures. (D) Fluorescence intensities generated by the NMM/G-quadruplex structures formed in the presence of different concentrations of the target DNA: (a) 0, (b) 2.5×10^{-8} , and (c) 5.0×10^{-8} M. Reprinted with permission from ref 197. Copyright 2011 Royal Society of Chemistry.

small amounts of hairpin H₁ are opened, and these initiate the kinetically favored polymerization process. The isothermal autonomous HCR process was further implemented to amplify formation of aptamer–substrate complexes,¹⁹⁵ Figure 4C. According to this method, a third hairpin, H₃ (7), was introduced into the DNA mixture consisting of the functional hairpins H₁ and H₂. The hairpin H₃ included in its stem region sequence e representing the aptamer sequence (aptamer against ATP). In the presence of the ATP analyte, formation of the ATP/aptamer complex is energetically favored, leading to release of the single-stranded DNA chain comprising domain b*-c. The released single-stranded chain acted, then, as an initiator for the opening of hairpin H₂ and for activation of the HCR process that leads to the DNA polymeric nanowires. Similarly to the amplified fluorescence detection of DNA, the resulting DNA polymeric nanowires enabled amplified optical analysis of ATP with good selectivity.

The optical readout of the target-activated isothermal autonomous HCR process and, particularly, the conjugation of catalytic labels for optical transduction of the HCR mechanism are important issues for practical application of HCR for sensing. The transition of the pyrene monomer into the pyrene excimer was implemented to follow the DNA target-stimulated HCR process,¹⁹⁶ Figure 5A. The two hairpins, H₁

(8) and H₂ (9), were functionalized at their 3'- and 5'-ends with pyrene residues. Since the pyrene units are spatially separated from each other, the two hairpins reveal strong monomer emissions. The target DNA I (10) opening of hairpins H₁ and H₂ and activation of the HCR process lead to polymeric nanowires, where two pyrene units are in close spatial positions in each repeated subunit of the DNA polymer wires. This leads to depletion of the monomer emission and to the enhanced excimer emission, Figure 5B. The method enabled analysis of the target DNA with a detection limit corresponding to 256 fM. A different fluorescence analysis of a target DNA, by the target-stimulated initiation of the isothermal HCR process, and formation of G-quadruplex chain nanostructures were demonstrated. Incorporation of N-methyl mesoporphyrin IX (NMM), as fluorescent labels, into the resulting G-quadruplex units enables the optical readout for the sensing process,¹⁹⁷ Figure 5C. The two hairpins, H₁ (11) and H₂ (12), and the target DNA, I (13), were used to stimulate the isothermal HCR process. The hairpin H₂ includes in its stem region the “caged” sequence of the G-quadruplex (domains d and e). The target-induced cross-opening of the two hairpins generated polymeric nanowires consisting of repeated, tethered G-quadruplexes. Intercalation of the NMM into the resulting G-quadruplex led to generation of high

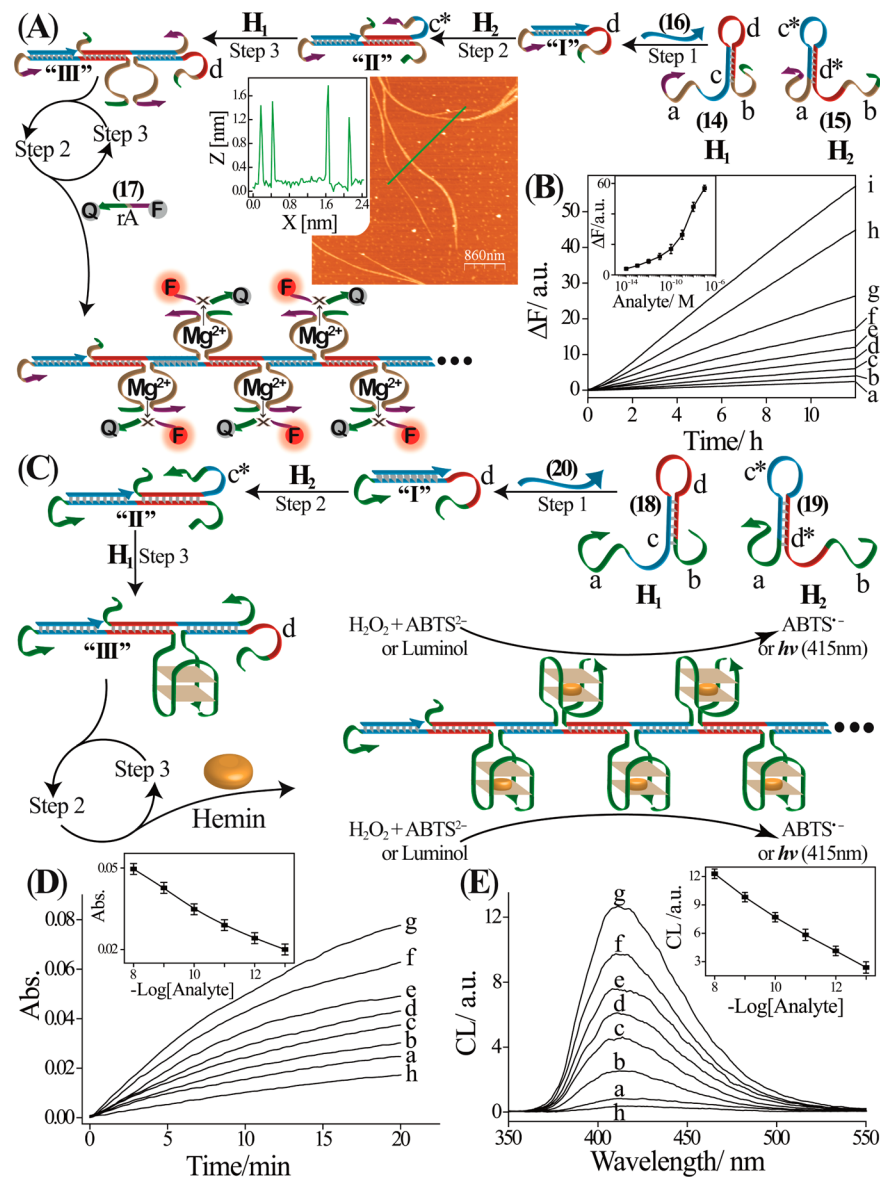


Figure 6. (A) Analysis of a target DNA by the HCR-triggered isothermal autonomous cross-opening of two hairpins H_1 and H_2 that generates supramolecular polymeric nanowires consisting of the Mg^{2+} -dependent DNAzyme units. (Inset) AFM image and cross-section analysis of the resulting polymer nanowires. Analysis of the target through the HCR process is followed by the Mg^{2+} -dependent DNAzyme cleavage of a F/Q-functionalized substrate that leads to generation of fluorescence. (B) Time-dependent fluorescence changes upon analyzing different concentrations of the target DNA according to A: (a) 0, (b) 1×10^{-14} , (c) 1×10^{-13} , (d) 1×10^{-12} , (e) 1×10^{-11} , (f) 1×10^{-10} , (g) 1×10^{-9} , (h) 4×10^{-8} , and (i) 2×10^{-7} M. (Inset) Derived calibration curve. Reprinted with permission from ref 48a. Copyright 2011 American Chemical Society. (C) Analysis of a target DNA by autonomous HCR-triggered cross-opening of two hairpins H_1 and H_2 that yield hemin/G-quadruplex DNAzyme-functionalized supramolecular nanowires. Analysis of the target DNA through HCR-initiated formation of the hemin/G-quadruplex HRP-mimicking DNAzyme nanowires is followed either by the colorimetric DNAzyme-catalyzed oxidation of $ABTS^{2-}$ by H_2O_2 to $ABTS^{\bullet-}$ or by the DNAzyme-catalyzed generation of chemiluminescence in the presence of H_2O_2 /luminol. (D) Time-dependent absorbance changes of $ABTS^{\bullet-}$ and (E) chemiluminescence spectra formed upon analyzing different concentrations of the target DNA according to C: (a) 0, (b) 1×10^{-13} , (c) 1×10^{-12} , (d) 1×10^{-11} , (e) 1×10^{-10} , (f) 1×10^{-9} , and (g) 1×10^{-8} M and (h) hemin only. (Inset) Resulting calibration curves. Reprinted with permission from ref 49a. Copyright 2012 American Chemical Society.

fluorescence. As the concentration of the analyte increased, the resulting fluorescence was enhanced, Figure 5D, thus enabling analysis of the analyte with a detection limit of 25 nM.

Catalytic units coupled to the HCR products were used for amplified detection of DNA. Specifically, DNAzymes were tethered to the HCR products, and these acted as catalysts for amplified fluorescence, colorimetric, or chemiluminescence detection of the respective target DNA. In one system,^{48a} Figure 6A, the two hairpin structures, H_1 (14) and H_2 (15),

and the DNA analyte (16) were used as components for activation of the isothermal autonomous HCR process. The two hairpins H_1 (14) and H_2 (15) included at their 3'- and 5'-ends the sequences corresponding to the subunits of the Mg^{2+} -dependent DNAzyme.¹⁹⁸ These DNAzyme subunits are partially "caged" by the stem regions of the two hairpins, thus prohibiting random self-assembly of the catalytically active Mg^{2+} -dependent supramolecular DNAzyme nanostructures, in the absence of the analyte DNA. In the presence of the DNA

target (**16**), the cross-opening of the hairpins H_1 and H_2 is activated, and the HCR-generated polymeric DNA nanowires are decorated by catalytically active Mg^{2+} -dependent DNAzyme units. Formation of the HCR-generated DNA nanowires was followed by AFM characterization (12 μm -long wires, 1.8 nm height), Figure 6A (inset). In the presence of the Mg^{2+} -dependent DNAzyme substrate (**17**), which was labeled with a fluorophore/quencher (F/Q) pair at its 5'- and 3'-ends, catalytic cleavage of substrate (**17**) by the polymer-assembled repeated DNAzyme units proceeded, leading to generation of fluorescence, Figure 6B. As the concentration of the analyte increased, the fluorescence generated by the system was intensified, thus allowing sensitive detection of the analyte DNA. The system was successfully implemented to analyze the BRCA1 oncogene with a detection limit corresponding to 10 fM. In a related system,^{49a} the hairpins H_1 (**18**) and H_2 (**19**) included in their stem regions the sequences of the horseradish peroxidase (HRP)-mimicking DNAzyme subunits in an inactive “caged” structure. In the presence of the analyte (**20**), the isothermal autonomous HCR process was activated, and cross-opening of hairpins H_1 and H_2 led to formation of DNA polymeric nanowires to which the respective self-assembled hemin/G-quadruplex HRP-mimicking DNAzyme units were tethered, Figure 6C. The resulting active DNAzyme nanostructures catalyzed the H_2O_2 -mediated oxidation of 2,2'-azino-bis(3-ethylbenzothiazoline-6-sulfonic acid), ABTS²⁻, to the colored product ABTS^{•+} ($\lambda_{\text{max}} = 415 \text{ nm}$) or to the catalyzed generation of chemiluminescence in the presence of luminol/ H_2O_2 ,^{199–201} thus providing colorimetric or chemiluminescence detection of the DNA analyte, Figures 6D and 6E, respectively. These schemes enabled selective analysis of the target DNA. The method was implemented to analyze the BRCA1 oncogene with a detection limit of 100 fM.

The isothermal autonomous HCR process was further used to develop sensing platforms on surfaces. The HCR process was implemented for amplified detection of the p53 oncogene using a microgravimetric quartz crystal microbalance (QCM) as readout method,⁷¹ Figure 7A. The hairpin structure H_{cp} (**21**) was immobilized on a Au/quartz piezoelectric crystal. The opening of the hairpin H_{cp} by the p53 oncogene, I (**22**), released a single-stranded tether that initiated, in the presence of hairpins H_1 (**23**) and H_2 (**24**), the HCR-based polymerization path. The mass associated with the polymeric DNA nanochains was reflected by substantial, time-dependent, resonance frequency changes associated with the crystal, Figure 7B. While the oncogene itself led to minute frequency changes, the HCR process amplified the resonance frequency changes, and these were controlled by the concentrations of the target DNA. In a related study,²⁰² an electrode surface was functionalized with a probe nucleic acid that, upon capturing the analyte, yielded a duplex with a free nucleic acid tether. This tether activated, in the presence of two tailored hairpins, the isothermal autonomous HCR process, which provided polymeric DNA nanochains for association of Ru(II) trisphenanthroline. The resulting electrogenerated chemiluminescence, in the presence of tripropylamine (TPA), provided then the readout signal for amplified detection of the analyte DNA. The isothermal autonomous HCR process was also applied to amplify aptamer–substrate or antigen–antibody recognition events on surfaces,²⁰³ Figure 8A. The antiplatelet-derived growth factor B-chain (anti-PDGF-BB) antibody (Ab) was assembled on enzyme-linked immunosorbent assay (ELISA) plate wells, and the anti-PDGF-BB aptamer (**25**) that included

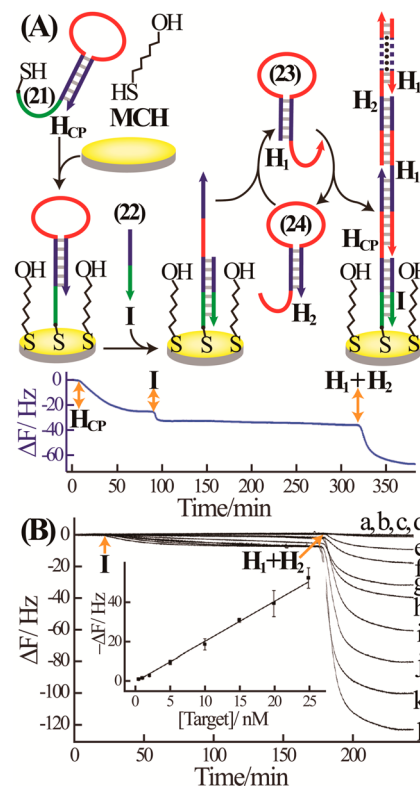


Figure 7. (A) Amplified microgravimetric quartz crystal microbalance (QCM) analysis of the p53 BRCA1 oncogene I (**22**) by HCR-mediated cross-opening of two hairpins, H_1 and H_2 , and generation of supramolecular DNA polymer chains on piezoelectric crystal. The figure shows the time-dependent frequency changes upon assembly of the probe hairpin structure on the surface, subsequent opening of the hairpin by the target DNA, and further cross-opening of the two hairpins, H_1 and H_2 , and generation of the supramolecular polymeric DNA chains (events are marked with the respective arrows). (B) Time-dependent frequency changes observed upon analyzing different concentrations of the oncogene target I by the isothermal autonomous HCR amplification process shown in A: (a) 0, (b) 5.0×10^{-10} , (c) 1.0×10^{-9} , (d) 2.0×10^{-9} , (e) 5.0×10^{-9} , (f) 1.0×10^{-8} , (g) 1.5×10^{-8} , (h) 2.0×10^{-8} , (i) 2.5×10^{-8} , (j) 5.0×10^{-8} , (k) 1.0×10^{-7} , and (l) $2.0 \times 10^{-7} \text{ M}$. (Inset) Derived calibration curve. Reprinted with permission from ref 71. Copyright 2012 Royal Society of Chemistry.

the HCR initiation nucleic acid tether was subsequently linked to the surface-confined immuno-complex. The resulting aptamer–substrate complex hybrid initiated then isothermal autonomous cross-opening of the two hairpins H_1 (**26**) and H_2 (**27**), labeled each with biotins. Subsequent binding of streptavidin-modified quantum dots (SA-QDs) to the biotin-labeled HCR-generated polymeric DNA nanowires enabled luminescence imaging of the formation of the immuno-complexes, Figure 8A. Similarly, formation of immuno-complexes was amplified by the isothermal autonomous HCR process,²⁰⁴ Figure 8B. Antibodies against cytokine-secreting human peripheral mononuclear cells (Ab_1) were immobilized on a glass surface using microcontact soft lithography printing. The surface-confined antigen–antibody complex was further functionalized with another antibody, Ab_2 , modified with nucleic acid initiator units, I (**28**). HCR-activated cross-opening of two fluorophore-labeled hairpin nanostructures H_1 (**29**) and H_2 (**30**) by the initiator-functionalized “sandwich assay,” consisting of the antibody–antigen immuno-complex, led to

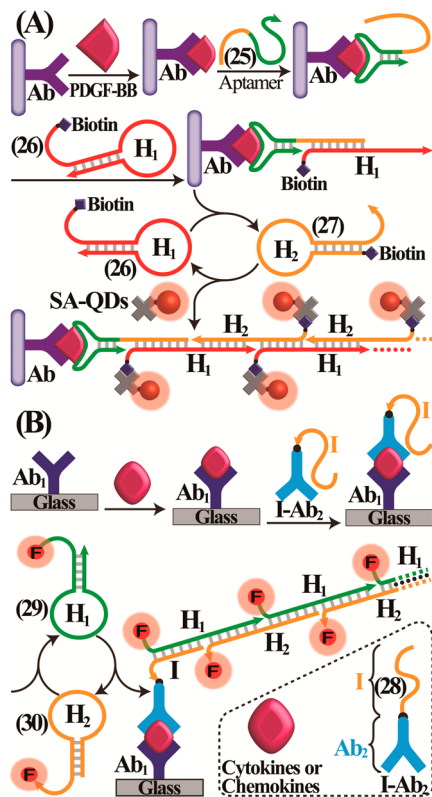


Figure 8. Amplified detection of antigen–antibody complexes using the isothermal autonomous HCR scheme: (A) Analysis of the platelet-derived growth factor B-chain (PDGF-BB) antigen by primary formation of the antigen–antibody immuno-complex on the surface, and subsequent attachment of a tethered nucleic acid aptamer to the immuno-complex. Free single-stranded aptamer tether triggers a HCR-mediated cross-opening of the two biotinylated hairpins H_1 and H_2 . Association of streptavidin-quantum dots (SA-QDs) conjugates to the resulting biotinylated DNA nanochains enables then luminescence detection of the primary antigen–antibody recognition event. (B) Analysis of the antigen–antibody complex formed on a surface through the secondary binding of a nucleic acid-functionalized antibody (I - Ab_2) to the antigen unit associated with the surface to yield a “sandwich-type” immuno-complex. Nucleic acid tethers trigger on a HCR-mediated cross-opening of the two fluorophore-functionalized hairpins, resulting in fluorophore-labeled DNA nanowire wires that enable optical readout of the primary formation of the antigen–antibody complex. Reprinted with permission from ref 204. Copyright 2011 American Chemical Society.

formation of long fluorescent polymeric DNA nanochains that amplified the primary antigen–antibody recognition events.

The isothermal autonomous cross-opening chain reaction of predesigned DNA hairpin nanostructures has been advanced to construct an autonomous polymerization locomotion motor that is powered by free-energy-driven DNA hybridization.¹¹³ The system mimics the *Rickettsia* bacterial pathogen that polymerizes multiple actin filaments capable of locomotion. In contrast to the protein-based native motor, the synthetic locomotion motor analog is all-DNA-based, Figure 9A. The system consists of two hairpins, H_1 (31) and H_2 (32), where H_1 is functionalized with tether sequences a and x^* , and H_2 is modified at its tethers with sequences c^* and y^* . The single-stranded loops of H_1 and H_2 are composed of domains c and a^* , respectively. The DNA duplex (33/34) consists of an anchoring strand A (33) and a *Rickettsia* strand R (34). While DNA regions b^* and b components of A and R are

complementary, the tether sequence a^* is linked to the anchoring strand A, whereas tethers x and y are associated with the *Rickettsia* strand R. The A/R duplex (33/34) introduced into the composite system, consisting of hairpins H_1 and H_2 , initiates the isothermal autonomous living polymerization motor that results in locomotion of strand R at the end of the polymeric nanowires. Figure 9A depicts the dynamic stepwise living polymerization motor powered by free-energy-powered DNA hybridization, which results in the autonomous locomotion process. In the first step, hairpin H_1 binds to the DNA A/R duplex (33/34), leading to structure “I”. The resulting structure rearranges into the energetically favored duplex structure “II”. The single-stranded tethers associated with structure “II” bind to the free complementary tethers of hairpin H_2 , resulting in structure “III”, which rearranges into the energetically favored structure “IV” that further isomerizes to stable structure “V”. The free tethers of structure “V” bind then to hairpin H_1 , leading to structure “VI”. The cyclic autonomous living polymerization that continuously cross-opens hairpins H_1 and H_2 , while rearranging the DNA adducts into energetically favored duplex structures, linear DNA polymeric nanowires “VII” carrying at their two ends the DNA strands A and R are formed. The polymerization reactions were followed by gel electrophoresis experiments, fluorescence quenching measurements, and microscopy imaging characterization. Figures 9B and 9C depict the AFM images of two different DNA origami nanostructures “A” and “R” that include at their edges eight protruding anchoring strands (A) and eight protruding *Rickettsia* strands (R) (Strands are at positions marked with full circles). In the presence of the respective A/R duplexes (33/34) at the edges of the respective DNA origami structures and, in the presence of hairpins H_1 and H_2 , living polymerization at the anchoring sites of the DNA origami is initiated, leading to long DNA polymeric chain nanowires.

2.2. Catalytic Hairpin Assembly (CHA) Reactions for Amplified Sensing and Programmed Nanostructuring

Nucleic acid hairpin structures might act as catalytic energetic traps that may be activated by an initiator strand to yield complex nanostructures through a free-energy-driven isothermal autonomous catalytic hairpin assembly (CHA) process, leading to stable duplex DNA nanoscale assemblies.²⁰⁵ This is exemplified²⁰⁶ in Figure 10A with the application of an initiator strand T (35) and two hairpins H_A (36) and H_B (37). The initiator DNA strand includes segments a_t^* and a^* . The DNA hairpins, H_A and H_B , are designed to include the appropriate sequences (where domain x is complementary to domain x^*). The initiator T triggers the opening of hairpin H_A to yield the DNA assembly “I”. The resulting single-stranded tether of “I” opens hairpin H_B to yield the intermediate structure “II” that includes two duplex DNA domains. The exposed free tether a^*-a_t stimulates, however, strand displacement of the initiator strand T to yield the energetically favored linear duplex DNA “III”. Release of the initiator strand leads to secondary activation of the cascade reaction that stimulates hybridization of hairpins H_A and H_B . The isothermal autonomous programmed regeneration of the initiator nucleic acid, through cross-opening of hairpins H_A and H_B , represents an enzyme-free amplification means for detection of the initiator strand through its catalytic regeneration/recycling. The value of the programmed initiator-induced opening of the nucleic acid hairpins rests not only on the amplified sensing of a target

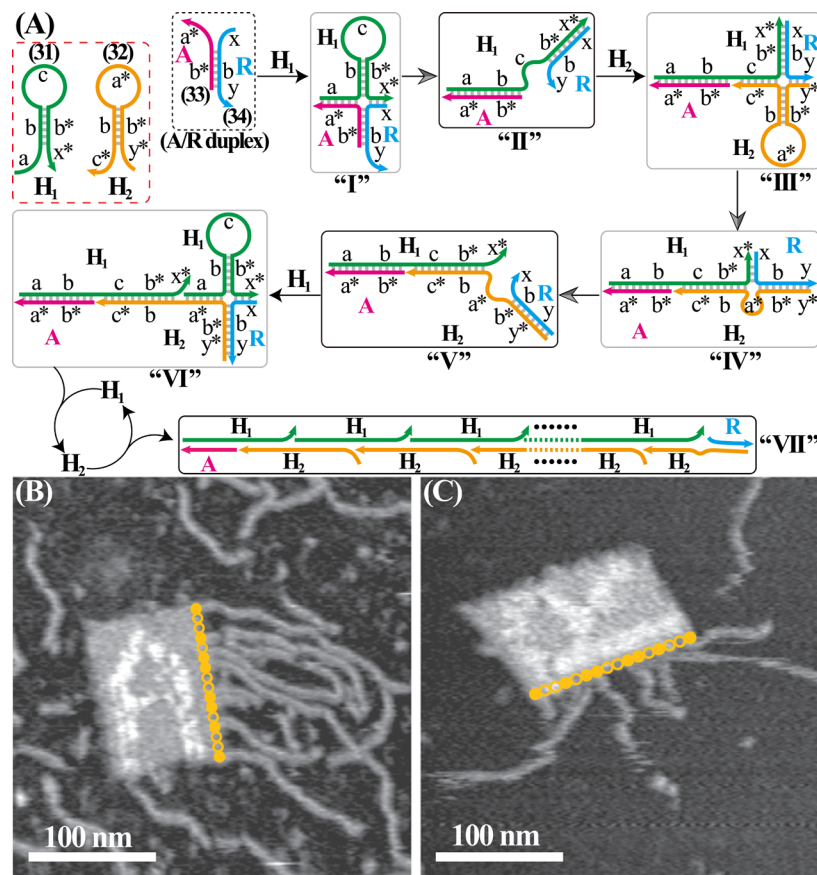


Figure 9. (A) Generation of 1D DNA nanowires through the cross-opening of two DNA hairpins triggered-on by the DNA duplex (33/34) that initiates an isothermal autonomous living polymerization locomotion motor that is powered by free-energy-driven hybridization chain reactions. (B) DNA origami nanostructure demonstrating the growth of the supramolecular DNA chains on the rectangular origami units substituted at their edges with the A/R duplex. A is a protruding tether that initiates autonomous cross-opening of the hairpins and subsequent locomotion of the structure as described in A. (C) DNA origami nanostructure demonstrating growth of the DNA nanowires on rectangular origami units functionalized at their edges with the R/A initiator duplex (R acts as protruding tether). Locomotion motor proceeds by isothermal autonomous cross-opening of the hairpins and is powered by the free-energy-driven hybridization reactions, as described in A. Reprinted with permission from ref 113. Copyright 2007 Nature Publishing Group.

DNA, but also on the possibility to include additional hairpin structures that, upon CHA reactions, lead to nanostructures of enhanced complexities.²⁰⁶ Figure 10B exemplifies the initiator-induced cascaded opening of three different caged DNA hairpin structures H_A (38), H_B (39), and H_C (40). The initiator strand T (41) opens hairpin H_A to yield nanostructure “I”, and the free single-stranded tether in structure “I” opens hairpin H_B to form structure “II”. The latter single-stranded tether in “II” opens hairpin H_C to generate the quasi-stabilized structure “III”. The latter single-stranded tether displaces the primary initiator unit T to yield the energetically favored Y-shaped DNA structure “IV”. The isothermal autonomous formation of the programmed Y-shaped nanostructure was imaged by AFM, Figure 10C. Similarly, using four functional DNA hairpins system nanostructures composed of “cross”-geometries were demonstrated.

The programming of self-assembly pathways through the initiator-driven CHA was extended to activate an isothermal autonomous cross-catalytic hairpin-mediated hybridization reaction involving intercommunicating two pairs of DNA hairpins that results in the amplified exponential growth of two different programmed DNA duplexes,²⁰⁶ Figure 11. The system consists of two metastable DNA hairpin pairs H_A, H_B (42 and 43) and H_C, H_D (44 and 45). In the presence of the initiator

DNA, T (46), hairpin H_A is opened to yield structure T·H_A, and the free single-stranded sequence of T·H_A opens hairpin H_B to yield intermediate structure T·H_A–H_B that undergoes an internal strand-displacement process that releases the initiator nucleic acid T and yields the DNA duplex product H_A–H_B. The single-stranded DNA tether associated with H_A–H_B activates the cross-opening of hairpin H_C to yield the intermediate DNA structure H_A–H_B–H_C, and the single-stranded tether of the opened hairpin H_C opens hairpin H_D while forming the DNA duplex H_C–H_D and recycling the duplex structure H_A–H_B. The released H_C–H_D nanostructure includes, however, the free single-stranded tether that opens hairpin H_A and yields the intermediate structure H_C–H_D–H_A. The latter product reacts with hairpin H_B to yield the DNA duplex structure H_A–H_B while recycling the original duplex structure H_C–H_D, that is, the initiator-driven intercommunication of the mixture of two hairpin pairs H_A/H_B and H_C/H_D leads to exponential amplified autonomous growth of the DNA duplex products H_A–H_B and H_C–H_D.

The initiator-driven isothermal autonomous CHA process has been implemented for development of amplified DNA detection schemes,²⁰⁷ Figure 12. The initiator strand may act as the DNA analyte. Accordingly, by one approach, Figure 12A, the two hairpins H_A (47) and H_B (48) acted as kinetic

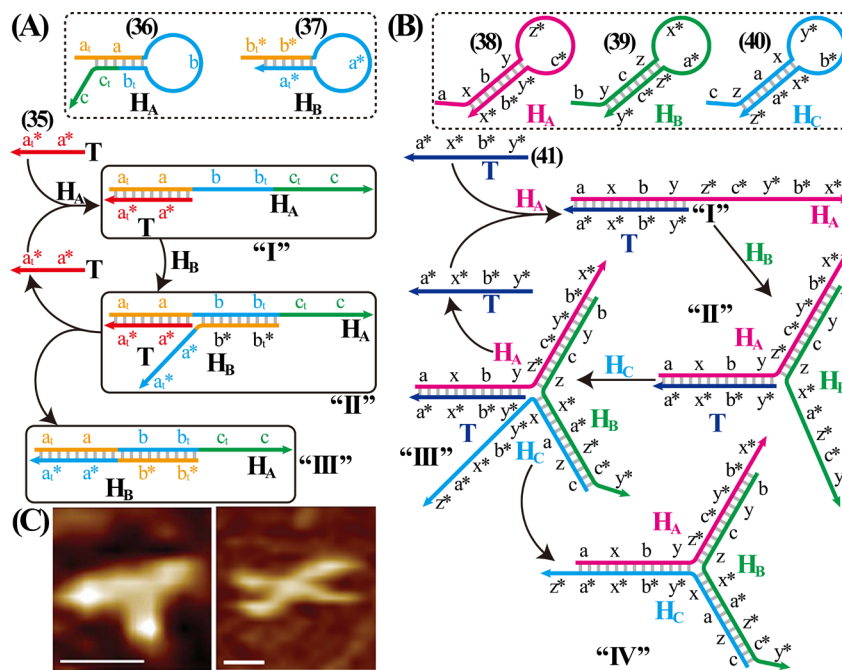


Figure 10. (A) Catalytic formation of a 1D DNA nanostructure through the initiator-driven isothermal catalytic hairpin assembly (CHA) of hairpins H_A and H_B that regenerates the initiator T and the autonomous sequential cross-opening of hairpins H_A and H_B. (B) Catalytic initiator-induced generation of branched DNA nanostructures by sequential opening of three hairpins H_A, H_B, and H_C using the CHA process and the programmed sequential opening of the three hairpins. (C) AFM images corresponding to the initiator-induced catalytic formation of branched DNA nanostructures using three hairpins (left) or four hairpins (right). Scale bar: 10 nm. Reprinted with permission from ref 206. Copyright 2008 Nature Publishing Group.

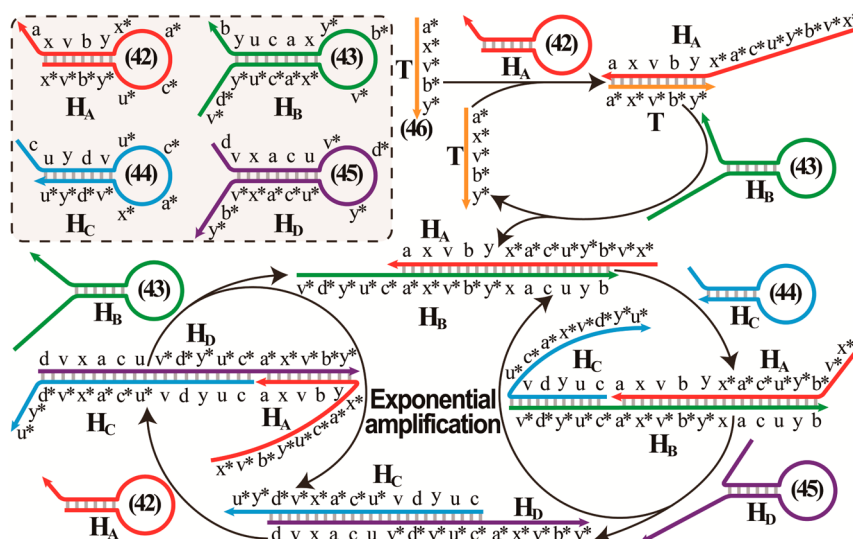


Figure 11. Initiator-driven isothermal autonomous cross-CHA process: cross-catalytic opening of two pairs of intercommunicating hairpins H_A and H_B, and H_C and H_D that leads to the amplified, exponential growth of two different programmed DNA duplexes. Reprinted with permission from ref 206. Copyright 2008 Nature Publishing Group.

energetic traps that regenerate the target analyte, T (49), through the catalytic hairpin-mediated hybridization of the two hairpins. Hairpin H_A included, however, in addition to the encoded information to displace the initiator-analyte, the caged sequence of the hemin/G-quadruplex HRP-mimicking DNAzyme. Thus, the target DNA, T (49), opens hairpin H_A to yield intermediate nanostructure T·H_A that includes the HRP-mimicking DNAzyme sequence a and the toehold sequence c that hybridizes with the complementary stem region c* of hairpin H_B to yield the quasi-stabilized complex T·H_A–H_B. The

intrastucture strand-displacement reaction recycles the initiator analyte strand while forming the energetically stabilized DNA duplex H_A–H_B and self-assembly of the catalytically active hemin/G-quadruplex DNAzyme supramolecular nanostructure that acts as colorimetric or chemiluminescence transducer of the DNA recognition event. Thus, the process includes two complementary amplification paths consisting of the recycling of the target analyte and catalytic colorimetric or chemiluminescence readout of the recognition event through the

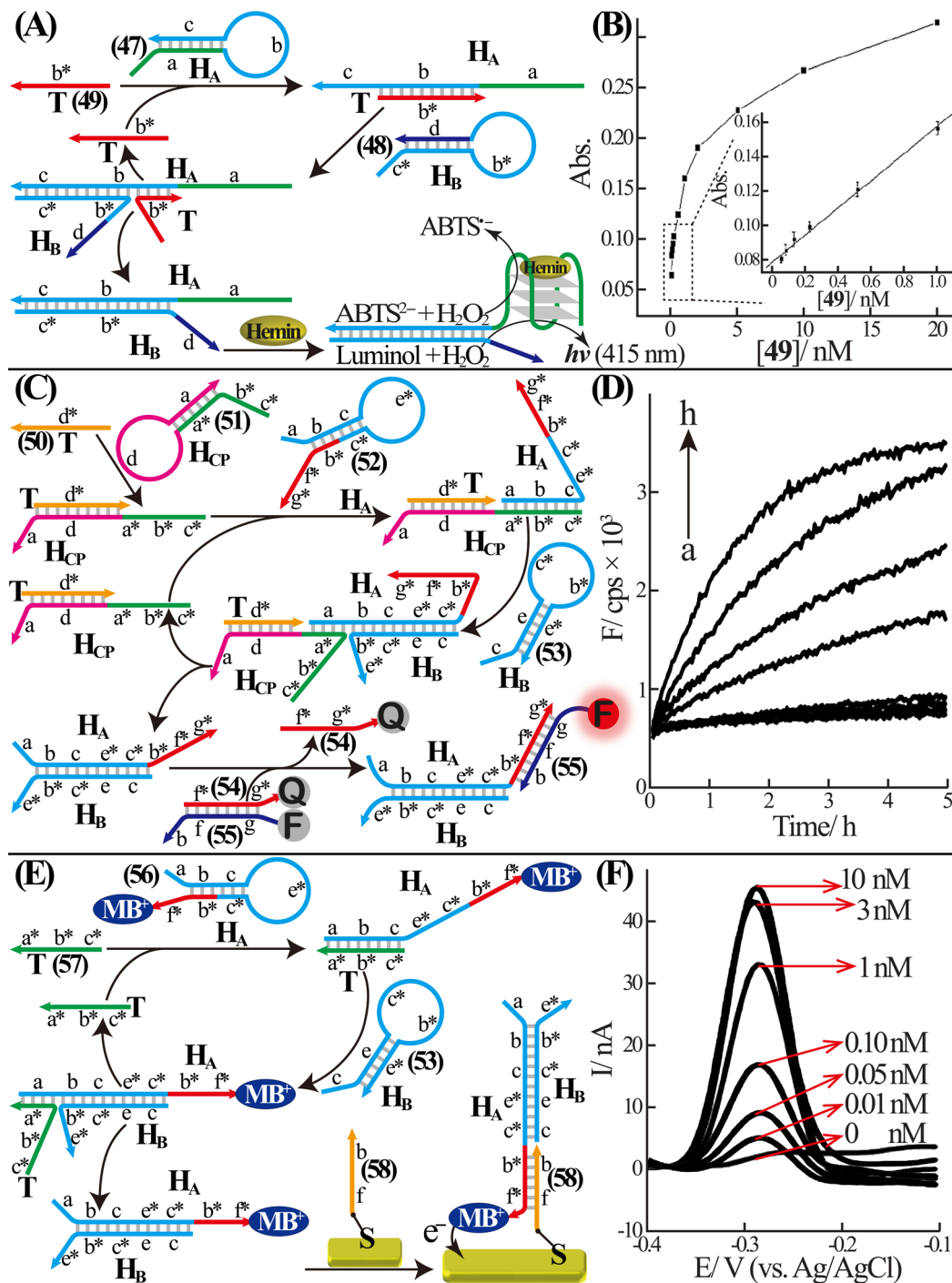


Figure 12. Analysis of a target DNA acting as catalyst for the programmed sequential opening of two hairpins that regenerates the target DNA by an isothermal autonomous CHA mechanism: (A) Application of a hairpin H_A that yields the hemin/G-quadruplex HRP-mimicking DNAzyme for amplified colorimetric or chemiluminescence detection of the analyte through H_2O_2 -mediated oxidation of ABTS²⁻ to the colored product ABTS^{•-} ($\lambda_{\text{max}} = 415$ nm) or the generation of chemiluminescence. (B) Calibration curve corresponding to absorbance changes upon analyzing different concentrations of the target DNA according to A for a fixed time interval of 10 min. (Inset) Enlargement of the low-concentration region. Reprinted with permission from ref 207. Copyright 2012 Royal Society of Chemistry. (C) Target-induced sequential opening of hairpins that regenerates the target by an isothermal autonomous CHA mechanism and concomitant toehold-based strand-displacement separation of a F/Q-modified reporter duplex that leads to a fluorescence signal. (D) Time-dependent fluorescence changes upon analyzing different concentrations of the target DNA according to C: (a) 0, (b) 2.0×10^{-11} , (c) 5.0×10^{-11} , (d) 1.0×10^{-10} , (e) 5.0×10^{-10} , (f) 1.0×10^{-9} , (g) 2.0×10^{-9} , and (h) 5.0×10^{-9} M. (E) Catalytic target-induced programmed sequential opening of two hairpins that regenerates the target DNA through the isothermal autonomous CHA process where hairpin H_A is modified with the redox-active methylene blue (MB⁺) group. Resulting nanostructure is hybridized with a complementary probe nucleic acid associated with an electrode, and the voltammetric signal of the MB⁺ units provides the readout signal. (F) Voltammetric responses observed upon analyzing different concentrations of the target DNA according to E. Reprinted with permission from ref 208. Copyright 2011 Oxford University Press.

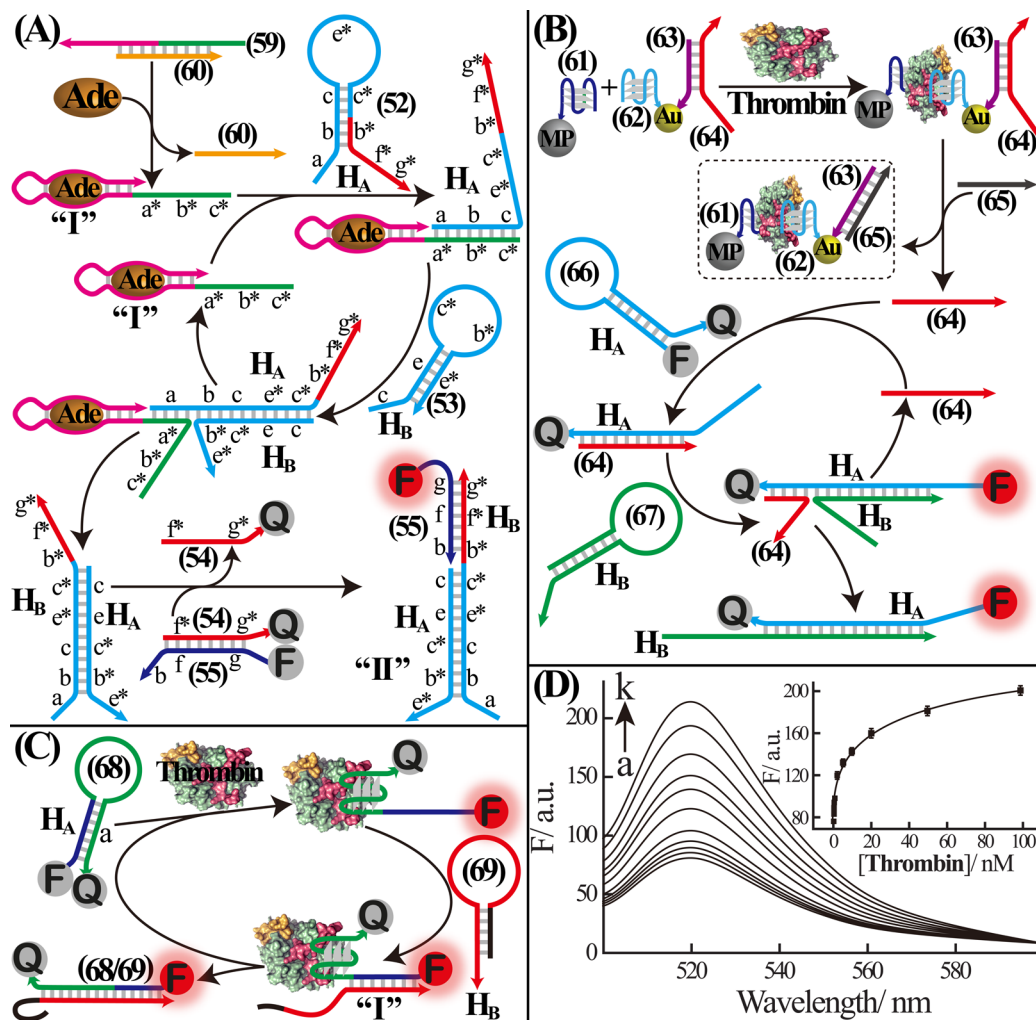


Figure 13. (A) Amplified fluorescence adenosine aptasensor using the isothermal catalytic sequential opening of two hairpins using the autonomous CHA mechanism. Blocked antiadenosine aptamer sequence is separated in the presence of adenosine to form the respective adenosine-aptamer complex “I”. Single-strand tether of “I” catalyzes sequential opening of hairpins H_A and H_B to yield the duplex structure $H_A - H_B$ using the toehold-initiated branch-migration displacement reaction. Product structure $H_A - H_B$ separates a F/Q-modified duplex reporter unit to yield the fluorescent product “II”. Reprinted with permission from ref 208. Copyright 2011 Oxford University Press. (B) Amplified detection of thrombin through the thrombin-aptamer complex-initiated isothermal autonomous CHA reaction, leading to a fluorescence signal. Reprinted with permission from ref 209. Copyright 2012 Elsevier. (C) Amplified fluorescence aptamer sensor of thrombin implementing the isothermal autonomous CHA-activated sequential opening of two hairpins H_A and H_B . Resulting intermediate structure “I” includes the encoded sequence to displace the thrombin while generating an energetically stabilized DNA duplex and regenerating the thrombin analyte. (D) Fluorescence spectra corresponding to analysis of different concentrations of thrombin according to scheme C upon operating the CHA reaction for a fixed time interval of 2 h: (a) 0, (b) 2.0×10^{-11} , (c) 5.0×10^{-11} , (d) 2.0×10^{-10} , (e) 5.0×10^{-10} , (f) 2.0×10^{-9} , (g) 5.0×10^{-9} , (h) 1.0×10^{-8} , (i) 2.0×10^{-8} , (j) 5.0×10^{-8} , and (k) 1.0×10^{-7} M. (Inset) Derived calibration curve. Reprinted with permission from ref 210. Copyright 2012 Elsevier.

DNAzyme-mediated reaction. The system enabled detection of the target DNA with a detection limit of 20 pM, Figure 12B.

The analyte initiator-triggered isothermal autonomous CHA process was further applied for fluorescence detection of DNA or RNA analytes,²⁰⁸ Figure 12C. The target (50)-induced opening of the capture probe DNA (51) released a sequence $a^* - b^* - c^*$ that initiated sequential catalytic cross-opening of hairpins H_A (52) and H_B (53), resulting in a duplex structure with a single-stranded tether consisting of sequence $b^* - f^* - g^*$. This tether stimulated strand displacement of a coadded F/Q-modified duplex (54/55) transducing element. This secondary strand-displacement process enabled fluorescence detection of the target DNA with a sensitivity corresponding to 20 pM, Figure 12D. A related method for fluorescence detection of the target DNA by the CHA process used a caged G-quadruplex

sequence in one of the hairpin structures as optical transducing elements.¹⁹⁷

The analyte-triggered isothermal autonomous CHA process, for amplified detection of DNA, was further modified and allowed quantitative electrochemical readout of the DNA-analyte,²⁰⁸ Figure 12E. In this system, hairpin H_A (56) was functionalized at its 3'-end of the tether nucleic acid f^* with the redox-active methylene blue (MB^+) unit. The opening of hairpin H_A by the analyte, T (57), yielded the duplex structure T- H_A . Subsequently, the single-stranded domain c^* of T- H_A bound hairpin H_B (53) and opened H_B through strand displacement to form the structure $H_A - H_B$ while displacing the analyte T. The free single-stranded tether $b^* - f^*$, associated with $H_A - H_B$, was then hybridized with the thiolated complementary capture nucleic acid (58), assembled on a Au

electrode. The electrical responses of the captured, redox-labeled DNA duplexes H_A-H_B , linked to the electrode, Figure 12F, provided a quantitative electronic signal related to the concentration of the analyte DNA. The method enabled analysis of the target DNA with a detection limit corresponding to 10 pM.

The paradigm of amplified sensing through the target-induced isothermal autonomous CHA process was further extended to analyze aptamer–substrate complexes,²⁰⁸ Figure 13A. The nucleic acid (59) that included the anti-ATP aptamer sequence and the initiator sequence was blocked with the nucleic acid (60). Blocking of the initiator sequence prohibited activation of the two-hairpin-mediated catalytic hybridization machinery. In the presence of ATP, formation of the energetically stabilized aptamer–ATP complex released the blocker DNA (60) and the free initiator, consisting of sequence $a^*-b^*-c^*$, activated the catalytic hairpin-mediated successive opening of hairpins H_A (52) and H_B (53) to form duplex DNA assembly H_A-H_B , while recycling the aptamer–ATP complex linked to the initiator strand. Secondary displacement of the fluorophore/quencher-functionalized duplex (54/55) by the H_A-H_B DNA hybrid structure led to generation of fluorescence and quantitative analysis of ATP. In a related study, amplified detection of thrombin, through its aptamers, was demonstrated,²⁰⁹ Figure 13B. The availability of two different aptamers that bind to different sites of thrombin provided a means to develop the amplified detection scheme. One aptamer (61) was linked to magnetic particles (MP), whereas the second aptamer (62) was linked to Au nanoparticles (AuNPs) modified with the DNA duplex (63/64). In the presence of thrombin, the respective bis-aptamer/thrombin “sandwich” complex was separated by an external magnetic field. Subsequent displacement of the blocker strand (63) by the antiblocker strand (65) yielded the initiator strand (64), which activated the isothermal autonomous catalytic hairpin-mediated hybridization process of hairpins H_A (66) and H_B (67). As hairpin H_A (66) was labeled with a fluorophore/quencher pair, the initial detection of thrombin could be followed by switching on of the fluorescence, resulting in the isothermal autonomous CHA reactions.

In a related study,²¹⁰ Figure 13C, a hairpin structure H_A (68) modified with a fluorophore/quencher pair was used to initiate the isothermal autonomous CHA reaction upon analyzing thrombin. The loop region of the hairpin H_A (68) includes the antithrombin sequence a , and thus, opening of the hairpin H_A through formation of the thrombin–aptamer complex leads to a free exposed single-stranded tether nucleic acid that opens hairpin H_B (69) to yield the intermediate complex “I”. The free tether of hairpin H_B is designed, however, to have the complementary sequence for binding the aptamer domain associated with thrombin, thus leading to regeneration of the thrombin analyte and formation of the stabilized DNA duplex H_A-H_B (68/69) that yields fluorescence as reporting signal, Figure 13D. The method enabled analysis of thrombin with a sensitivity corresponding to 20 pM.

An interesting approach for amplified detection of a target DNA has implemented coupled isothermal catalytic hybridization reaction processes consisting of the autonomous HCR and the CHA reaction,²¹¹ Figure 14. In this system the primary target (70)-induced opening of hairpin H_1 (71) triggers the autonomous HCR between hairpin H_1 (71) and hairpin H_2 (72) to yield a linear DNA chain nanostructure, which includes as protruding tethers the repeated single-stranded units L ,

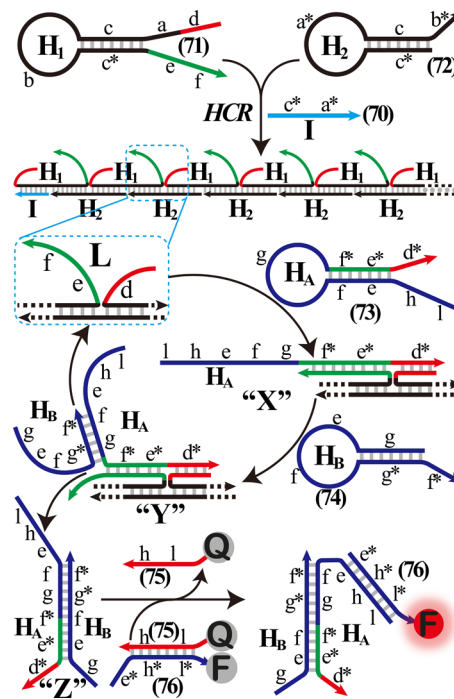


Figure 14. Amplified fluorescence detection of a target DNA by an isothermal autonomous cascaded process involving the HCR that is coupled to the CHA-activated sequential opening of two functional hairpins, H_A and H_B . In the primary step, the target-triggered HCR process between hairpins H_1 and H_2 yields polymeric nanowires consisting of subunits L . Single-stranded overhangs associated with L stimulate the catalytic sequential opening of hairpins H_A and H_B . Primary opening of hairpin H_A yields “tile” units “X”, and this opens H_B to yield the intermediary structure “Y” that undergoes toehold-based branch migration hybridization to regenerate the subunits L . This yields the energetically stabilized DNA duplex “Z” that separates a F/Q -modified DNA duplex reporter unit to yield a fluorescence readout signal. Reprinted with permission from ref 211. Copyright 2012 American Chemical Society.

consisting of components d and $e-f$. These elements activate the autonomous CHA process, in the presence of the two hairpins H_A (73) and H_B (74). The opening of hairpin H_A (73) by the protruding tether units L yields a linear tile construct “X” that includes the single-stranded domain $f-g$ of hairpin H_A (73) as a functional toehold unit to open hairpin H_B (74), a process that leads to an intermediate nanostructure “Y”. Formation of structure “Y” induces the energetically driven strand displacement of the tile while regenerating the original HCR-generated DNA nanowire and concomitant formation of the DNA duplex “Z”. In the presence of an auxiliary F/Q -modified DNA duplex structure (75/76) the structure “Z” displaces the fluorophore-labeled nucleic acid strand, leading to a fluorescence signal that reports the coupled nonenzymatic catalytic amplification process.

2.3. Cascaded Strand-Displacement Processes for Logic Gates and DNA Machines

The strand-displacement principle has been implemented to construct a digital computing circuit by cascaded logic gates.¹⁶⁶ One of the interesting principles to assemble the logic gates is depicted in Figure 15A, where the system is composed of a threshold duplex element $Th_{2,5;5}$, a fuel strand unit $w_{5,7}$, an input strand $w_{2,5}$, and a DNA duplex structure gate $G_{5,5;6}$. The system also includes a reporter element Rep_6 , consisting of a

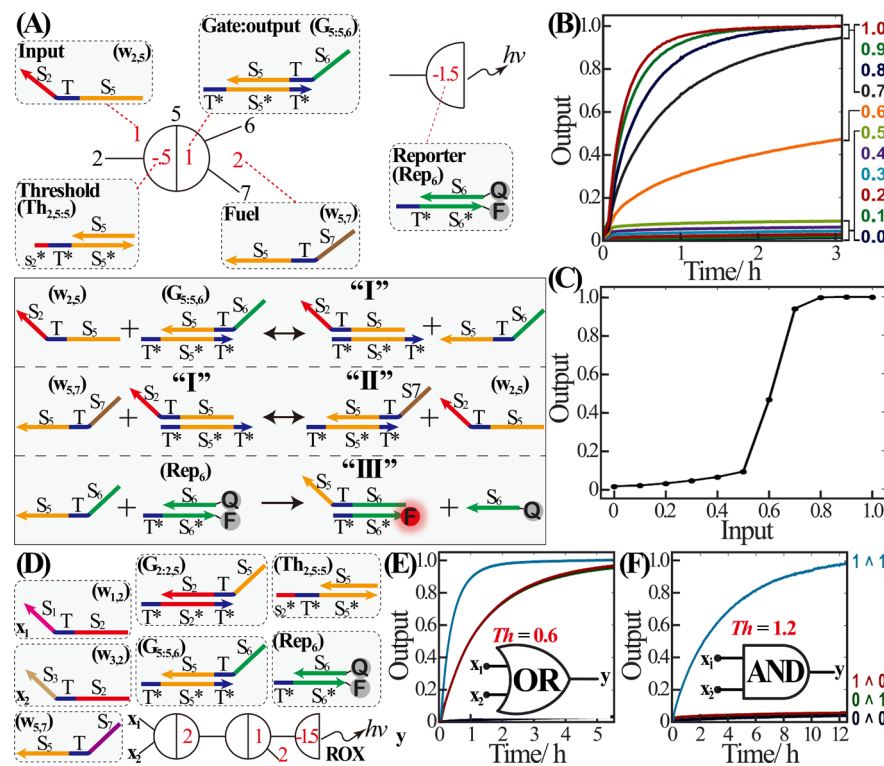


Figure 15. Assembly of digital computing circuits of logic gate cascades by implementing the toehold-based strand-displacement mechanism and a computation module consisting of an input $w_{2,5}$, gate output units $G_{5,5,6}$ being guided by a threshold control unit $Th_{2,5,5}$, and a fuel strand $w_{5,7}$. (A) Principle for controlling the gate output by the input, fuel, and threshold control units. Output strand displaces a fluorophore/quencher-functionalized nucleic acid duplex Rep_6 that provides the readout for the gate. (B) Time-dependent fluorescence intensity changes of the logic gate by variable concentrations of the threshold unit. (C) Demonstration of the effect of threshold composition on the gate fluorescence performance. (D) Schematic application of the threshold/fuel-guided activation of OR or AND logic gate cascades using two inputs x_1 and x_2 . (E) Fluorescence readout signals of the OR gate. (F) Fluorescence readout signals of the AND gate. Reprinted with permission from ref 166. Copyright 2011 American Association for the Advancement of Science.

DNA duplex structure modified with a fluorophore/quencher pair. The input strand $w_{2,5}$ includes complementarities to the gate duplex unit $G_{5,5,6}$ and is capable of displacing the strand S_6-T-S_5 and similarly is capable to displace the strand S_5 from the threshold duplex $Th_{2,5,5}$. The strand displacement of the strand S_5 from threshold unit $Th_{2,5,5}$ is, however, energetically favored, due to an additional partial hybridization, of part of S_2 , of the input to the toehold domain s_2^* of the threshold system. That is, displacement of the gate duplex $G_{5,5,6}$ proceeds only when the molar ratio between the input and the threshold unit is >1 . Accordingly, the input displaces the strand S_6-T-S_5 while forming the duplex structure “I”. Under these conditions, the fuel strand $w_{5,7}$ displaces the input strand $w_{2,5}$ while generating structure “II,” acting as waste product. The released input strand $w_{2,5}$ proceeds, however, with the autonomous displacement processes and the fuel-driven separation of the gate duplex unit $G_{5,5,6}$. The released strand S_6-T-S_5 from the gate duplex unit $G_{5,5,6}$ displaces the reporter duplex Rep_6 to yield the fluorescent DNA duplex structure “III” that acts as readout signal. Thus, the molar ratio between the input and the threshold unit controls the operation of the system. While at a molar ratio of input/threshold corresponding to ≤ 1 the system is mute, due to the blocking of the input by the threshold unit, at an input/threshold ratio > 1 , the cyclic, fuel-driven activation of the gate is triggered on, leading to displacement of the output S_6-T-S_5 and subsequent formation of the fluorescence signal, Figure 15B and 15C. The fuel-driven and threshold-controlled release of the output strand S_6-T-S_5 can then be

triggered by two inputs, x_1 and x_2 , to yield a digital output from the system, Figure 15D. When the molar ratio of the inputs x_1/Th or x_2/Th is >1 , the system activates an “OR” gate, Figure 15E. When the ratio corresponds to $(x_1/Th + x_2/Th) > 1$ ($x_1/Th < 1$ and $x_2/Th < 1$), the system acts as an “AND” gate, Figure 15F. With this fundamental paradigm the released output strand S_6-T-S_5 could act as input for a variety of cascaded gates, and the scale-up of multilayer digital computing circuits was demonstrated. This concept was further developed to transform arbitrary linear threshold circuits into nucleic acid strand-displacement cascades that function as neural networks.¹⁶⁷

The strand-displacement principle was further implemented to trigger various DNA machines. This is exemplified in Figure 16A with the assembly of DNA tweezers.¹¹⁴ The DNA construct “I” includes the nucleic acid chain (77) hybridized with the DNA units (78 and 79) that include single-stranded tethers a and b, respectively. The fuel strand Fu (80) is complementary to regions a and b, thus leading to closure of the open structure “I” to the closed tweezers configuration “II”. Since the fuel strand Fu includes a toehold tether c*, treatment of configuration “II” with the antifuel strand aFu (81) leads to strand displacement of Fu to form the energetically stable “waste” DNA duplex Fu/aFu (80/81) and to recovery of the open tweezers structure “I”. By the labeling of the 5'- and 3'-ends of nucleic acid (77) with a F/Q pair, the dynamic Fu/aFu-triggered transitions of the DNA machine between the open “I” and the closed “II” states could be followed by the

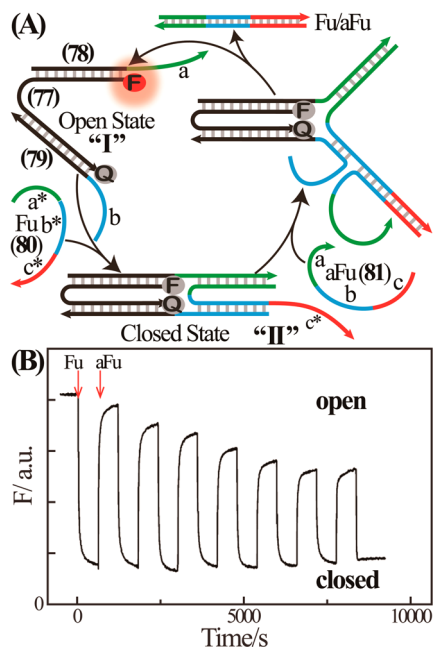


Figure 16. (A) Cyclic strand-displacement-based tweezers DNA machine being activated by a fuel strand (Fu) to close the device and an antifuel strand (aFu) to open the device. (B) Switchable fluorescence intensities upon cyclic closure and opening of the DNA device by the fuel/antifuel (Fu/aFu) strands. Reprinted with permission from ref 114. Copyright 2000 Nature Publishing Group.

intramolecular fluorescence resonance energy transfer (FRET) process, Figure 16B. While the open molecular device revealed high fluorescence, due to the spatial separation of the

fluorophore from the quencher, the close proximity between the fluorophore and the quencher in the closed state led to effective quenching and low fluorescence. A variety of other DNA machines, such as walkers,¹³⁵ a crane,¹³⁶ and dynamic programmed swinging of catenated DNA rings,¹³⁸ have implemented the strand-displacement principle to drive the mechanical operations of DNA machines.

Isothermal cascaded hybridization chain reactions were also implemented to drive directional autonomous DNA machines, e.g., bipedal walkers. This is exemplified¹¹⁵ with the design of a three-step bipedal walker driven by two hairpin fuels, H₁ and H₂, Figure 17. In this system, a DNA track consisting of nine footholds I–IX with programmed sequences and partial complementarities between the footholds and the walker unit was designed. The bipedal walker was hybridized in the primary position onto footholds I and III through pedals L₁ and L₂ that included foothold II as a central statue. The hairpin H₁ includes complementary regions to the central statue II (domain a^{*}–d^{*}) as well as to the foothold I (domain a–b–c). Opening of the hairpin fuel H₁ by the statue II released the sequence a–b–c that displaces the pedal L₁ from foothold I, due to the enhanced stabilization of the displaced foothold I. The released pedal L₁ strand displaces the partially hybridized footholds IV/V through formation of the energetically favored duplex with foothold V, leading to the first pedal walkover that generates foothold IV as the central statue between pedals L₂ and L₁. The subsequent isothermal autonomous hybridization reaction of the product with hairpin H₂ leads to opening of H₂ by the central statue IV (domain a–g) while releasing the sequence a–e–f that displaces pedal L₂ from foothold III. The released pedal L₂ then binds to the partially hybridized footholds VI/VII, a process that leads to the second step of walkover, where

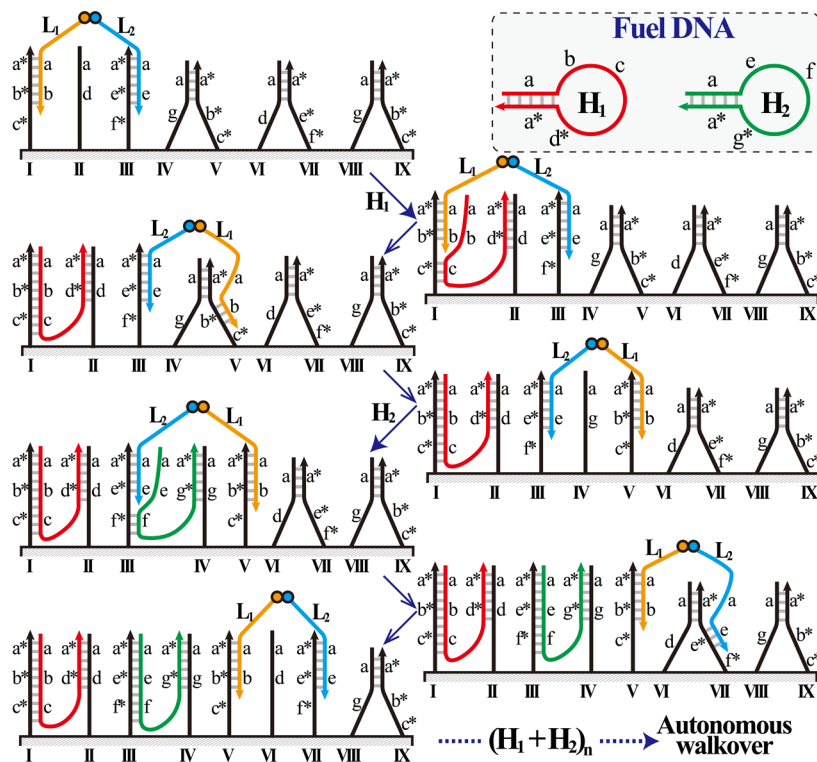


Figure 17. Directional isothermal autonomous tristep bipedal DNA walker using two hairpins, H₁ and H₂, as fuels that stimulate the mechanical walkover process by cascaded hybridization chain reactions. Reprinted with permission from ref 115. Copyright 2009 American Association for the Advancement of Science.

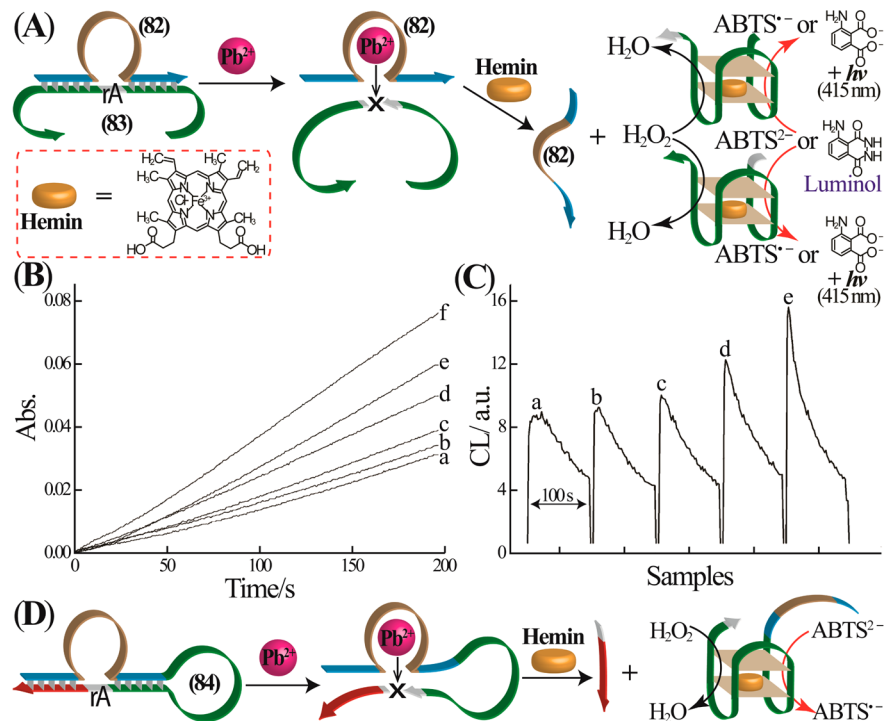


Figure 18. (A) DNAzyme chain reaction for detection of Pb^{2+} ions. Pb^{2+} -dependent DNAzyme cleaves a substrate that leads to two nucleic acid fragments that self-assemble into the hemin/G-quadruplex DNAzyme for colorimetric or chemiluminescence detection of Pb^{2+} ions: (B) Absorbance changes of ABTS^{•-} and (C) chemiluminescence intensities generated by the system described in A upon analyzing different concentrations of Pb^{2+} ions: (a) 0, (b) 1×10^{-8} , (c) 1×10^{-7} , (d) 5×10^{-7} , (e) 1×10^{-6} , and (f) 1×10^{-5} M. Reprinted with permission from ref 237a. Copyright 2008 Royal Society of Chemistry. (D) Bis-functional hairpin structure consisting of the Pb^{2+} -dependent DNAzyme, a caged G-quadruplex sequence, and the ribonucleobase-containing substrate of the DNAzyme. Pb^{2+} -stimulated cleavage of the substrate releases the hemin/G-quadruplex DNAzyme as a catalytic label for colorimetric detection of Pb^{2+} ions.

foothold VI (domain a–d) acts as central single-stranded statue. The subsequent stepwise interaction of the statue with hairpins H₁ and H₂, respectively, leads then to the autonomous directional bipedal walking over on the DNA track. Formation of the different structures on the DNA tracks through sequential binding of the two fuel DNA hairpins was followed by gel electrophoresis.

3. DNAZYME-ACTIVATED CHAIN REACTIONS

DNAzymes or ribozymes are catalytic nucleic acids.^{24–26} Numerous non-natural catalytic nucleic acids were developed in the past decade, including metal-ion-dependent DNAzymes, e.g., Mg^{2+} ,¹⁹⁸ Cu^{2+} ,²¹² Ni^{2+} ,²¹³ Hg^{2+} ,²¹⁴ Zn^{2+} ,²¹⁵ Pb^{2+} ,^{24,216,217} Ca^{2+} ,²¹⁸ and UO_2^{2+} -dependent²¹⁹ DNAzymes, or cofactor-dependent DNAzymes, e.g., histidine-dependent DNAzyme²²⁰ that catalyzes hydrolytic cleavage of oligonucleotides or ligation of oligonucleotide subunits, also, DNAzymes mimicking the functions of native enzymes, such as the hemin/G-quadruplex HRP-mimicking DNAzyme,^{199,221–223} or DNAzymes that catalyze various chemical transformations, such as hydrolysis of phosphonate esters,²²⁴ ligation,²²⁵ phosphorylation,²²⁶ polymerization,²²⁷ peptide bond formation,²²⁸ aldehyde reduction,²²⁹ alcohol dehydrogenation,²³⁰ aldol reaction,²³¹ Michael addition,²³² porphyrin metalation,²³³ acyl transfer,²³⁴ aminoacylation,²³⁵ and Diels–Alder cycloaddition.²³⁶ These catalytic nucleic acids (DNAzymes) were extensively used as amplifying labels for optical^{48–52,237–242} or electrochemical^{53,243–245} sensing platforms, and different DNA, aptamer substrate, and metal-ion sensors were developed. Also, DNAzymes were implemented to stimulate various DNA

machines^{127,147,246–248} and design different logic gate systems.^{155–158,168–171,249} The following section will address the activation of DNAzyme-based isothermal catalytic cascades and discuss their use for the amplified sensing, autonomous synthesis of functional nanostructures, and construction of DNA logic gate cascades and computing circuits.

3.1. Isothermal DNAzyme-Activated Catalytic Cascades

The metal-ion-dependent DNAzymes consist, usually, of a conserved sequence that includes a loop region for binding the respective metal cation and tethered domains that hybridize with a sequence-specific domain of an oligonucleotide substrate that yields the DNAzyme–substrate complex. The substrates of the hydrolytic cleavage DNAzymes usually include a ribonucleobase site, and the DNAzyme-catalyzed cleavage of the substrates proceeds at this conserved site.^{198–220} The metal-ion-dependent DNAzymes have been implemented to develop different electrical or optical metal-ion sensors,^{48–53,237–245} such as aggregation or deaggregation of metallic nanoparticles.^{250–252} The coupling of the metal-ion-induced activation of the DNAzymes to yield secondary, cascaded, catalytic nucleic acids that provide electrochemical or optical readout signals was used for amplified detection of various metal ions. For example, amplified detection of Pb^{2+} ions was demonstrated by designing a loop-containing duplex structure between DNAzyme sequence (82) and the ribonucleobase-containing substrate strand (83),^{237a} Figure 18A. While the loop region of 82 contained the DNAzyme sequence for binding of Pb^{2+} ions, the ribonucleobase-modified sequence (83) provided the substrate for the Pb^{2+} -ion-dependent DNAzyme, and included in the duplex structure two caged

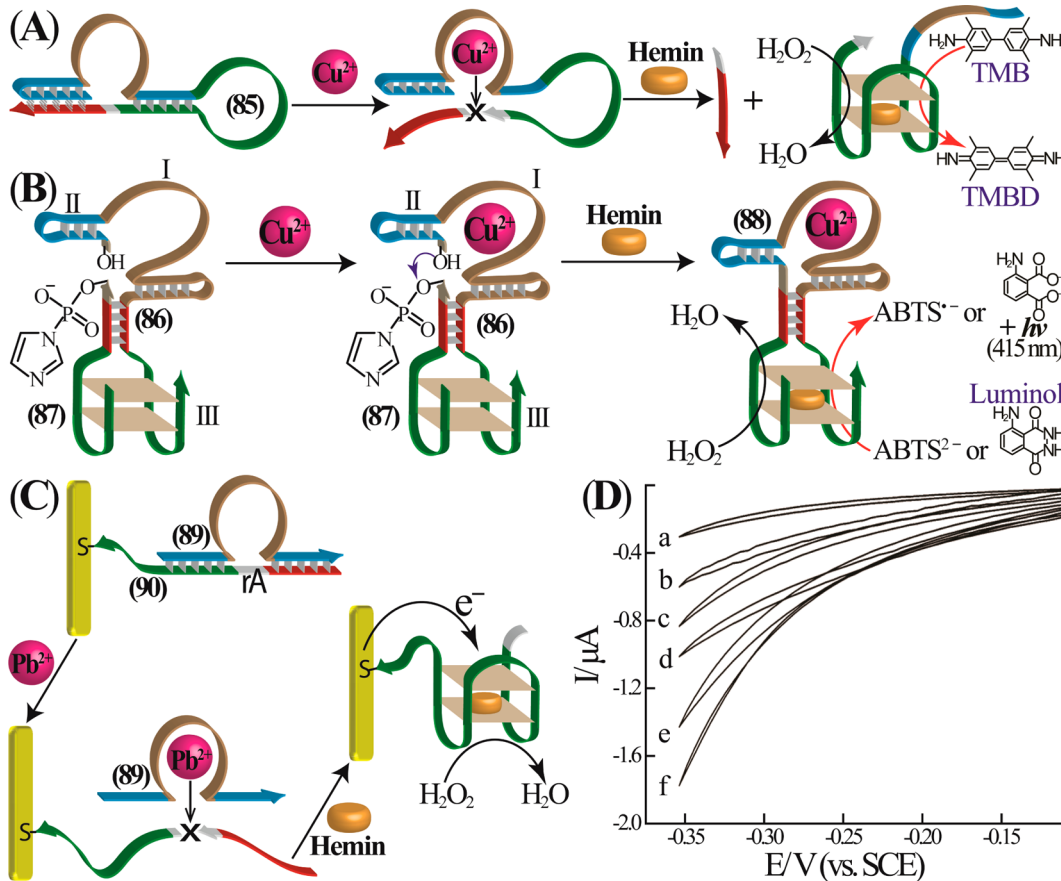


Figure 19. (A) Colorimetric detection of Cu²⁺ ions using a bis-functional hairpin structure consisting of the Cu²⁺-dependent hydrolytic cleavage DNAzyme, a caged G-quadruplex sequence, and the ribonucleobase-containing sequence acting as substrate of the Cu²⁺-dependent DNAzyme. Reprinted with permission from ref 239a. Copyright 2009 American Chemical Society. (B) Analysis of Cu²⁺ ions by the DNAzyme cascade that involves the Cu²⁺-dependent ligation DNAzyme coupled to the hemin/G-quadruplex DNAzyme. Reprinted with permission from ref 240. Copyright 2012 Wiley-VCH. (C) Electrocatalytic detection of Pb²⁺ ions by coupling the Pb²⁺-dependent cleavage of the substrate (90) that releases the hemin/G-quadruplex electrocatalyst for reduction of H₂O₂. (D) Electrocatalytic cathodic currents observed upon analyzing different concentrations of Pb²⁺ ions by the sensing platform outlined in C: (a) 0, (b) 1 × 10⁻¹⁰, (c) 1 × 10⁻⁹, (d) 1 × 10⁻⁸, (e) 1 × 10⁻⁷, and (f) 1 × 10⁻⁶ M. Reprinted with permission from ref 53a. Copyright 2012 American Chemical Society.

sequences of the hemin/G-quadruplex HRP-mimicking DNAzyme unit. In the presence of Pb²⁺ ions, the Pb²⁺-ion-dependent DNAzyme was activated, resulting in cleavage of the substrate (83) and self-assembly of the fragmented substrate units into the hemin/G-quadruplex HRP-mimicking DNAzyme units. The latter DNAzyme provided a biocatalytic label for amplified colorimetric or chemiluminescence detection of the formation of the primary Pb²⁺-ion-dependent DNAzyme. The colorimetric assay has involved the hemin/G-quadruplex DNAzyme-catalyzed oxidation of ABTS²⁻ by H₂O₂ to form the colored product ABTS^{•-} ($\lambda_{\text{max}} = 415 \text{ nm}$), Figure 18B. In addition, the chemiluminescence assay^{199–201} included the hemin/G-quadruplex DNAzyme-catalyzed oxidation of luminol by H₂O₂, Figure 18C. The system revealed selectivity toward analysis of Pb²⁺ ions, and the detection limit for analyzing Pb²⁺ ion corresponded to 10 nM. A similar approach to analyze Pb²⁺ ion was demonstrated by applying a hairpin DNA structure (84) that included in its stem region the catalytically active Pb²⁺-dependent DNAzyme sequence and in the loop region the caged hemin/G-quadruplex HRP-mimicking DNAzyme sequence.^{238a} Cleavage of the stem region of the hairpin structure (84), in the presence of Pb²⁺ ions, resulted in the cleaving and opening of the hairpin and self-assembly of the fragmented substrate units into catalytically active hemin/G-quadruplex

HRP-mimicking DNAzyme units that provided the colorimetric output signal, Figure 18D.

Similarly, the Cu²⁺-ion-dependent hydrolytic cleavage DNAzyme has been applied to activate a DNAzyme cascade for amplified detection of Cu²⁺ ions,^{239a} Figure 19A. A loop-modified DNA sequence (85) that included the triplex-Cu²⁺-dependent DNAzyme domain, its substrate domain, and a caged HRP-mimicking DNAzyme sequence was designed. In the presence of Cu²⁺ ions, the substrate domain was cleaved off, resulting in self-assembly of the hemin/G-quadruplex HRP-mimicking DNAzyme catalyzed the H₂O₂-mediated oxidation of TMB to the colored TMBD, thus providing the readout signal for amplified colorimetric detection of Cu²⁺ ions (detection limit, 1 μM). Also, the Cu²⁺-dependent ligation DNAzyme^{225a} was implemented to detect Cu²⁺ ions,²⁴⁰ Figure 19B. The Cu²⁺-dependent DNAzyme sequence I was tethered to a duplex domain II consisting of the hydroxyl-functionalized substrate of the ligation DNAzyme and to a G-quadruplex subunit III to yield the nucleic acid structure (86). This unit was coupled to a second single-stranded nucleic acid (87) composed of the imidazole-modified cosubstrate of the ligation DNAzyme conjugated to the second subunit of the G-quadruplex. In the presence of the Cu²⁺ ions, ligation of the subunits proceeds to yield nucleic acid structure (88), and the

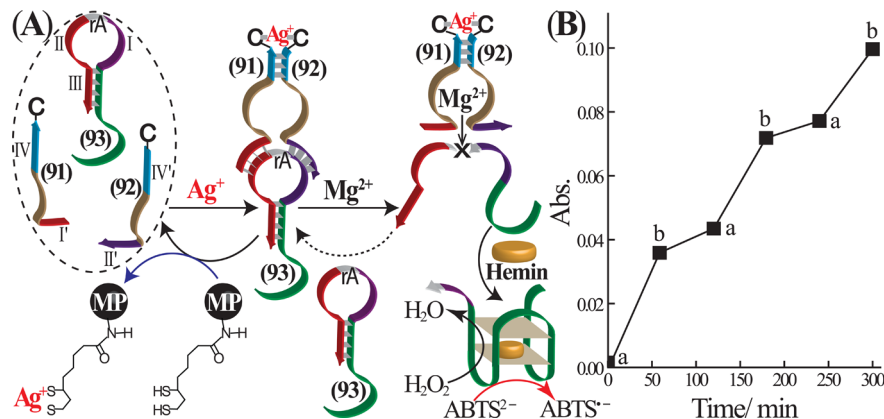


Figure 20. (A) Ag^+ -ion-triggered activation of a DNAzyme cascade consisting of the Mg^{2+} -dependent hydrolytic cleavage DNAzyme and the hemin/G-quadruplex DNAzyme and switchable activation of the DNAzyme cascade by lipoic acid ligand-functionalized magnetic particles (MP) that remove the Ag^+ ions. (B) Time-dependent switchable activation of the DNAzyme cascade by cyclic addition of Ag^+ ions to the system, points a, and their removal by the ligand-modified magnetic particles (MP), points b. Reprinted with permission from ref 50a. Copyright 2010 Royal Society of Chemistry.

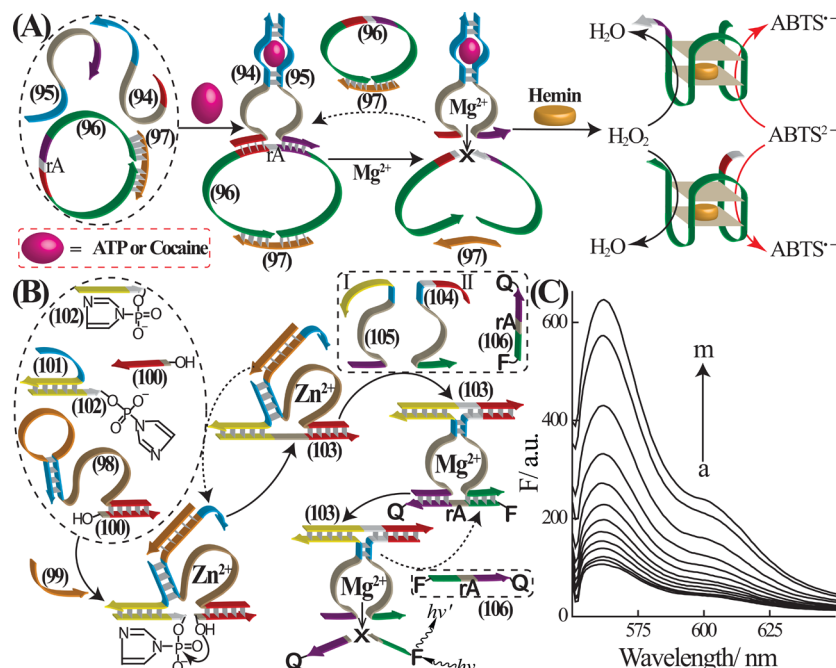


Figure 21. (A) Activation of a DNAzyme cascade by cooperative stabilization of the Mg^{2+} -dependent DNAzyme using an aptamer-substrate (ATP or cocaine) complex. Cooperatively stabilized Mg^{2+} -dependent DNAzyme cleaves a blocked quasi-circular DNA to yield the hemin/G-quadruplex DNAzyme. Reprinted with permission from ref 51a. Copyright 2009 Wiley-VCH. (B) Activation of a bi-DNAzyme cascade for amplified analysis of a target DNA. Analyte activates the Zn^{2+} -dependent ligation DNAzyme and ligated product-induced assembly of the Mg^{2+} -dependent DNAzyme. Resulting Mg^{2+} -dependent DNAzyme cleaves a fluorophore/quencher-functionalized substrate to yield fluorescence by a fluorophore-labeled fragment. (C) Fluorescence spectra upon analyzing different concentrations of the target DNA by the scheme outlined in B: (a) 0, (b) 1×10^{-11} , (c) 2×10^{-11} , (d) 5×10^{-11} , (e) 1×10^{-10} , (f) 2×10^{-10} , (g) 5×10^{-10} , (h) 1×10^{-9} , (i) 5×10^{-9} , (j) 1×10^{-8} , (k) 5×10^{-8} , (l) 1×10^{-7} , and (m) 2×10^{-7} M. Reprinted with permission from ref 241. Copyright 2012 American Chemical Society.

ligated domain stabilizes the cooperative formation of the catalytically active hemin/G-quadruplex HRP-mimicking DNAzyme. The later DNAzyme generates a colorimetric signal by the H_2O_2 -mediated oxidation of ABTS^{2-} to the colored product $\text{ABTS}^{\bullet-}$ or yields a chemiluminescence signal through the DNAzyme-catalyzed oxidation of luminol by H_2O_2 . As the ligation process is controlled by the concentration of the Cu^{2+} ions, the resulting color or chemiluminescence signals provide a quantitative readout signal for detection of different concentrations of Cu^{2+} ions. The system enabled selective analysis of Cu^{2+} ions with a sensitivity corresponding to 1 nM. By

modification of domain II, associated with the Cu^{2+} -dependent ligation DNAzyme, cascaded catalytic systems composed of the functional nanostructures for analysis of Hg^{2+} ions or aptamer–cocaine complexes were developed.²⁴⁰

The metal-ion-dependent DNAzyme-induced release and activation of the hemin/G-quadruplex electrocatalytic DNAzyme^{53,245} was also applied for electrochemical analysis of Pb^{2+} ions.^{53a} A nucleic acid duplex structure (89/90) was assembled on a Au electrode surface, Figure 19C. The loop-containing nucleic acid (89) included the Pb^{2+} -recognition DNAzyme sequence, whereas the ribonucleobase-containing strand (90)

acted as substrate for hydrolytic cleavage DNAzyme and included the caged sequence of the hemin/G-quadruplex HRP-mimicking DNAzyme. In the presence of Pb^{2+} ions, the substrate strand (**90**) was cleaved, resulting in dissociation of DNAzyme-containing sequence (**89**) and self-assembly of the hemin/G-quadruplex DNAzyme on the electrode surface. This acted as an electrocatalyst for reduction of H_2O_2 at the electrode surface. The resulting electrocatalytic currents are related to the concentration of the Pb^{2+} ions, Figure 19D. This enabled selective electrochemical detection of Pb^{2+} ions with a detection limit corresponding to 100 pM.

An interesting metal-ion-activated ON-OFF switchable DNAzyme cascade was demonstrated by applying the Mg^{2+} -dependent hydrolytic cleavage DNAzyme coupled to the hemin/G-quadruplex HRP-mimicking DNAzyme,^{50a} Figure 20A. The DNA strands (**91** and **92**) provide two subunits of the Mg^{2+} -dependent DNAzyme, and these are terminated at their 3'- and 5'-ends, respectively, with coadded cytosine bases. The DNA hairpin structure (**93**) includes in its loop region the ribonucleobase-containing sequence acting as substrate for the Mg^{2+} -dependent DNAzyme and in the stem region the hemin/G-quadruplex DNAzyme sequence in a "caged" catalytically inactive nanostructure. While the Mg^{2+} -dependent DNAzyme subunits cannot assemble into a catalytically active hydrolytic cleavage DNAzyme nanostructure, addition of Ag^+ ions bridge the two cytosine bases through a C– Ag^+ –C bridge, stabilizing the active Mg^{2+} -dependent DNAzyme/substrate complex. In this structure, the autonomous cleavage of the hairpin DNA substrate (**93**) proceeds, leading to formation of the hemin/G-quadruplex HRP-mimicking DNAzyme that provides the colorimetric transduction for formation of the primary Mg^{2+} -dependent hydrolytic cleavage DNAzyme. Addition of magnetic particles (MP)-functionalized with the lipoic acid ligands allowed magnetic separation of the Ag^+ ions and eliminated the Ag^+ ions from the bridged DNAzyme subunits (**91** and **92**), through formation of Ag^+ –lipoic acid complexes. This results in dissociation of the Mg^{2+} -dependent DNAzyme subunits and switching off cleavage of the G-quadruplex-caged hairpin substrate (**93**) and activation of the catalytic activity of hemin/G-quadruplex HRP-mimicking DNAzyme. Readdition of Ag^+ ions reactivated the Mg^{2+} -dependent DNAzyme nanostructure and the subsequent biocatalytic cascade, Figure 20B.

Other stimuli for activation of DNAzyme cascades include the use of aptamer–substrate complexes as driving force for the catalytic cascade reaction.^{51a} For example, the two DNA strands (**94** and **95**) include, each, subunits of the Mg^{2+} -dependent hydrolytic cleavage DNAzyme and the anti-ATP or anticocaine aptamers, Figure 21A. While in the absence of ATP or cocaine the aptamer subunit-functionalized DNAzyme subunits do not form a stable DNAzyme structure, in the presence of ATP or cocaine, the respective aptamer–substrate complexes are formed, and these cooperatively stabilize the DNAzyme structures, hybridized with the quasi-circular ribonucleobase-containing substrate strand (**96**), blocked by the DNA strand (**97**). The quasi-circular substrate (**96/97**) includes, however, two caged sequences of the hemin/G-quadruplex HRP-mimicking DNAzyme. Accordingly, in the presence of Mg^{2+} ions, cleavage of the functional DNAzyme substrate (**96/97**) proceeds, resulting in separation of two catalytically active hemin/G-quadruplex DNAzyme nanostructures. The hemin/G-quadruplex DNAzyme catalyzed oxidation of ABTS²⁻ by H_2O_2 and provided an optical path for amplified colorimetric

detection of ATP or cocaine. This aptamer/substrate-complex-driven DNAzyme cascade enabled analysis of ATP or cocaine with detection limits corresponding to 5 and 1 μM , respectively. Nucleic acids have been, similarly, implemented to cooperatively stabilize the Mg^{2+} -dependent hydrolytic cleavage DNAzyme subunits and their hybridization with the functional hybrid substrate units (**96/97**).^{51a} Cleavage of the substrate by the Mg^{2+} -dependent DNAzyme units resulted in separation and self-assembly of the hemin/G-quadruplex HRP-mimicking DNAzymes, and this provided the catalytic label for amplified detection of the DNA target by the DNAzyme cascades.

An interesting DNAzyme-activated cascade that was implemented for amplified detection of DNA has involved the DNA target-stimulated activation of a DNAzyme cascade using the Zn^{2+} -dependent ligation DNAzyme as a catalytic promoter,²⁴¹ Figure 21B. The nucleic acid (**98**) includes a modified subunit sequence of the Zn^{2+} -dependent ligation DNAzyme^{225a} that is partially caged in a hairpin domain acting as recognition site for the target DNA (**99**). It also includes a recognition arm for the DNAzyme substrate subunit (**100**). The second ligation DNAzyme subunit (**101**) binds to the imidazolyl substituted nucleic acid (**102**), acting as cosubstrate subunit. While in the absence of a triggering DNA target the composite system is catalytically inactive, addition of the target DNA (**99**) opens the hairpin structure associated with the DNA strand (**98**), allowing self-organization of the cooperatively stabilized Zn^{2+} -dependent ligation DNAzyme that binds the two DNAzyme substrate subunits strands (**100** and **102**). The DNAzyme-promoted ligation process leads to the ligated product (**103**). The system includes also two separated Mg^{2+} -dependent hydrolytic cleavage DNAzyme subunit strands (**104** and **105**) that include tethered arms I and II, complementary to the ligated product (**103**). Strand displacement of the ligated product by the Mg^{2+} -dependent DNAzyme subunits leads to stabilization of the DNAzyme supramolecular structure, consisting of the Mg^{2+} -dependent DNAzyme subunits bridged by the ligation product (**103**) and the fluorophore/quencher-labeled substrate (**106**) of the Mg^{2+} -dependent DNAzyme. The strand displacement of the ligated product (**103**) by the Mg^{2+} -dependent DNAzyme subunits (**104** and **105**), subsequent cleavage of the DNAzyme substrate (**106**), and separation of the Mg^{2+} -dependent DNAzyme units (**103/104/105**) provide an isothermal autonomous cycle to regenerate the Zn^{2+} -dependent ligation DNAzyme and the Mg^{2+} -dependent hydrolytic cleavage DNAzyme while generating fluorescence of the cleaved-off substrate strand (**106**). Thus, the ligation/cleavage DNAzyme cascade enables amplified detection of the primary target DNA (**99**). Figure 21C depicts the fluorescence spectra generated by the DNAzyme cascade upon analyzing different concentrations of the genetic disorder Tay-Sachs mutated gene. The system enabled analysis of the mutant gene with a detection limit corresponding to 10 pM.

3.2. Isothermal Autonomous DNAzyme-Activated Catalytic Cascades

Isothermal replication of molecular components is one of the most fundamental reactions in nature. The most simple isothermal autonomous replication process, Figure 22A, involves a template molecule, T, that binds two substrate subunits, A and B, that are complementary to the template. The chemical linkage between substrate subunits A and B yields a product molecule identical to the template T. Thus, the

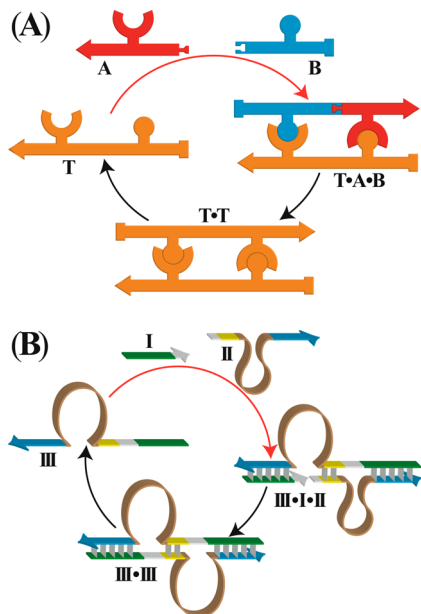


Figure 22. (A) General scheme for an isothermal autonomous self-replication machinery that uses a template T and two template subunits A and B . (B) Self-replication machinery that uses the ligase ribozyme III as catalytic template and its two ribozyme subunits I and II as substrates.

template-assisted linkage between A and B generates a second template molecule, thus providing exponential growth of the product (template) units in the system. The kinetics of the isothermal autonomous replication of a template structure using molecular ligation has been theoretically^{253–255} and experimentally modeled.^{256–258} While the isothermal replication path seems simple, it suffers from some basic limitations. As the ligated product reveals enhanced binding affinity to the template molecule, as compared to the binding affinity of the substrate subunits, effective displacement of the product molecule by the substrate subunits occurs only in early stages of the reaction (where the concentrations of the substrate subunits are high), and the self-inhibition process by the product is enhanced, as the isothermal autonomous replication reaction proceeds. One method to enhance autonomous replication may involve generation of catalytic units, such as ribozymes or DNAzymes as catalytic templates. For example, Figure 22B uses a catalytic nucleic acid strand, III , that ligates two partially complementary nucleic acid substrate strands, I and II , that hybridize with the catalytic nucleic acid template. Separation of the ligated product strand yields two catalytic nucleic acid template units.²⁵⁹

The isothermal autonomous ribozyme- or DNAzyme-activated catalytic cascades may proceed by two fundamental paths: (i) Ribozyme- or DNAzyme-mediated catabolic cleavage of substrates to assemble ribozyme or DNAzyme subunits into new catalytically active ribozyme or DNAzyme nanostructures; (ii) Ribozyme- or DNAzyme-mediated anabolic replication through catalyzed ligation reactions. Figure 23A depicts the isothermal autonomous catabolic cross-cleavage of two circular DNAzyme substrates that include caged sequences of catalytically inactive DNAzyme units by two 10–23 RNA-cleaving DNAzymes L_A and L_B .²⁶⁰ The substrates of the two different DNAzymes are C_A for L_B and C_B for L_A . In the presence of any of the two DNAzymes, cross-cleavage of substrates C_A and C_B proceeds, leading to formation of L_A by the L_B -catalyzed

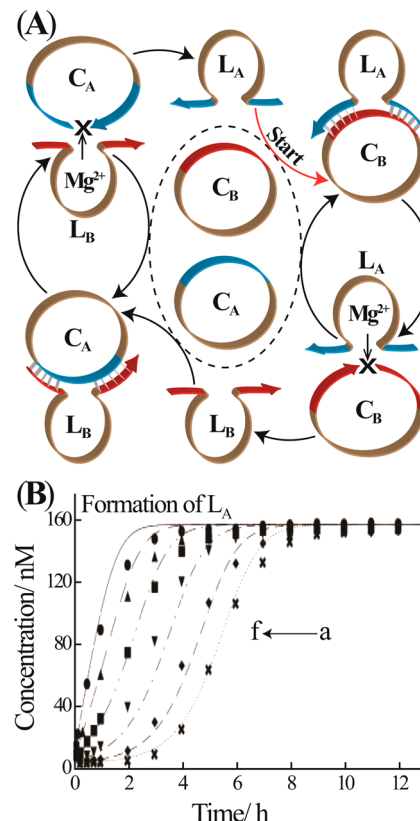
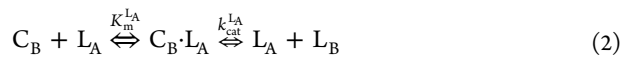
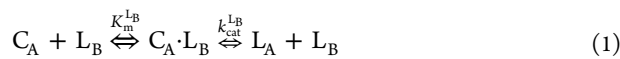
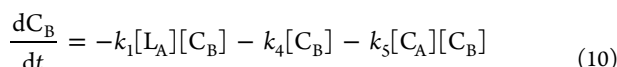
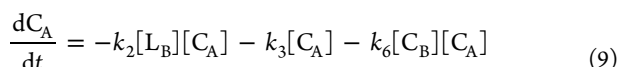
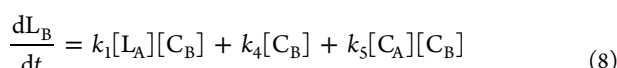
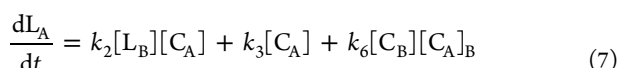


Figure 23. (A) Isothermal autonomous catabolic cross-cleavage of two circular substrates that include caged, inactive DNAzyme units by two different 10–23 RNA-cleaving DNAzymes L_A and L_B , leading to exponential growth of the two DNAzyme structures. (B) Exponential growth of DNAzyme L_A at different concentrations of DNAzyme L_B : (a) 0, (b) 1.0×10^{-9} , (c) 5.0×10^{-9} , (d) 2.0×10^{-8} , (e) 5.0×10^{-8} , and (f) 1.0×10^{-7} M. Reprinted with permission from ref 260. Copyright 2003 National Academy of Sciences.

cleavage of substrate C_A and formation of L_B through the L_A -catalyzed cleavage of substrate C_B . The process leads to exponential growth of the two DNAzyme nanostructures. Figure 23B depicts the exponential growth of DNAzyme L_A at different concentrations of DNAzyme trigger L_B . The kinetics of exponential formation of the DNAzymes L_A and L_B has been simulated using the set of DNAzyme-driven autonomous cascade reactions outlined in eqs 1–6 and the set of differential eqs 7–10 where k_1 and k_2 are given by eqs 11 and 12. From this theoretical modeling the kinetic parameters K_m and k_{cat} for L_A and L_B were evaluated to be $K_m = 260 \pm 9$ nM, $k_{cat} = 2.4 \pm 0.03$ min⁻¹ and $K_m = 320 \pm 7$ nM, $k_{cat} = 3.6 \pm 0.03$ min⁻¹, respectively.





$$k_1 = \frac{k_{cat}^{L_A}}{K_M^{L_A} + [C_B]} \quad (11)$$

$$k_2 = \frac{k_{cat}^{L_B}}{K_M^{L_B} + [C_A]} \quad (12)$$

In a series of studies,^{261,262} the isothermal autonomous ribozyme template-induced replication of ligation ribozymes through the coupling of complementary ribozyme subunits to the ribozyme template was demonstrated, Figure 24A. The ligation ribozyme sequence (107) exhibits a catalytically active secondary structure, and the substrate subunit strand (108) and 5'-triphosphorylated substrate subunit strand (109) were hybridized with the ribozyme template. Ligation of the 3'-end of substrate subunit (108) to the 5'-triphosphate substrate subunit strand (109) yielded the replicated ribozyme strand (107). Thus, the primary ligation-ribozyme-initiated catalytic ligation process replicates the catalytically active ribozyme template structure for subsequent isothermal autonomous replication reactions. The secondary hairpin structure of the ribozyme is essential to retain the active site microenvironment of the ligation ribozyme. Indeed, mutation of the hairpin duplex structure with the antiflavin mononucleotide, anti-FMN, or antitheophylline, anti-Theo, aptamer sequences, resulted in catalytically inactive ribozyme nanostructures. In the presence of FMN or Theo, Figure 24B, the aptamer–substrate complexes stabilized the duplex domain of the secondary structure of the ribozyme using cooperative interactions, resulting in the catalytically active microenvironment of the ribozyme. The aptamer–substrate complex-stimulated isothermal autonomous replication of a ligation ribozyme sequence was further coupled to the autonomous cross-ligation of two ligation ribozyme nanostructures, thus providing an amplification route for detection of the aptamer substrate (e.g., theophylline).²⁶²

The sensing of a target DNA (110) by isothermal activation of a catabolic process, which autonomously regenerates the target DNA-activated DNAzyme structure and synthesizes an amplifying DNAzyme unit, was demonstrated using the Mg²⁺-dependent hydrolytic cleavage DNAzyme.^{52a} The isothermal activation system, Figure 25A, consisted of the nucleic acids (111 and 112), where the domain I of strand 111 corresponds to a subunit of the Mg²⁺-dependent DNAzyme and nucleic acid 112 includes in domain II the caged sequence of the second subunit of the DNAzyme. Also, hairpin structure 113 included in its single-stranded ribonucleobase (rA)-containing loop domains III and IV, the substrate sequences for the Mg²⁺-dependent DNAzyme, and in the stem region V, the target sequence in a caged inactive configuration. The hairpin

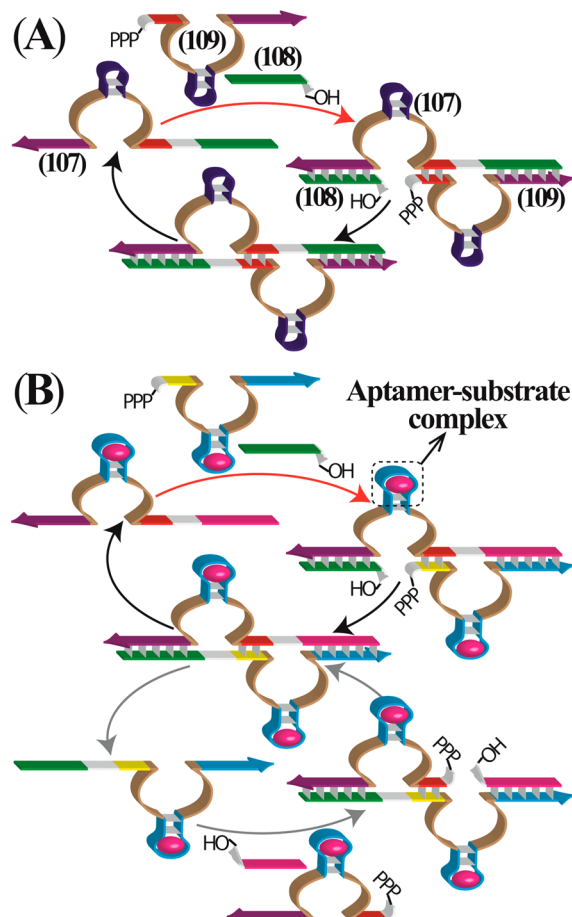


Figure 24. (A) Schematic template-induced isothermal autonomous replication of the ligation ribozyme by coupling of two complementary subunits acting as cosubstrates for the ribozyme. Reprinted with permission from ref 261. Copyright 2009 American Association for the Advancement of Science. (B) Template-induced autonomous replication of the ligation ribozyme through the aptamer–substrate complex-assisted formation of an active ligation ribozyme nanostructure and ligation of the ribozyme subunits by the catalytic ribozyme. Reprinted with permission from ref 262. Copyright 2009 Nature Publishing Group.

structure (113) was modified at its 5'- and 3'-ends with a F/Q pair as reporter units. In the presence of the analyte target (110), DNA hairpin 111 opened, resulting in the uncaging of the corresponding DNAzyme subunits and assembly of the Mg²⁺-dependent DNAzyme units. Subsequent cleavage of the hairpin substrate strand (113) separated the fluorophore-labeled reporter unit (114) and released a new target analog sequence (115) for a secondary cyclic activation of the Mg²⁺-dependent DNAzyme structure. That is, in the presence of the target DNA (110), the isothermal autonomous catabolic replication of the target sequence and the secondary assembly of DNAzyme units for capturing the substrate strand (113) were achieved. The time-dependent fluorescence changes of the system, upon analyzing different concentrations of the target DNA, are depicted in Figure 25B. The system enabled detection of the target DNA with a detection limit corresponding to 1 pM. The disadvantage associated with application of the amplified detection scheme outlined in Figure 25A for analyzing a target DNA is, however, the need to optimize the sequences associated with the different nucleic acid components to prevent cross-interactions, thereby

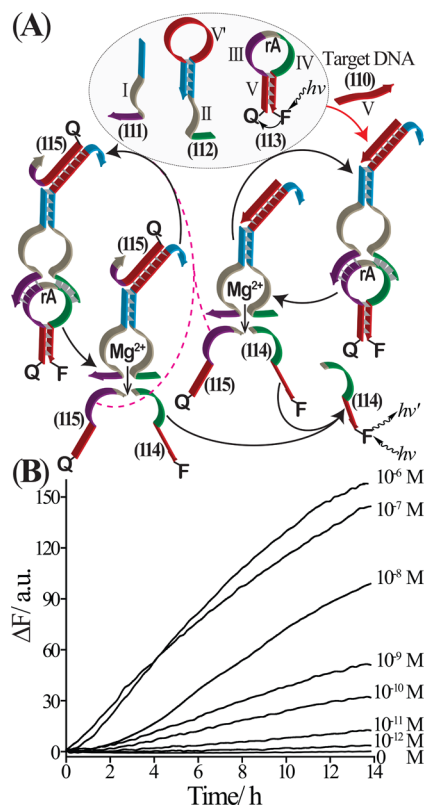


Figure 25. (A) Amplified detection of a target DNA through the target-induced assembly of the Mg^{2+} -dependent cleavage DNAzyme and isothermal autonomous catabolic replication of the target sequence through the DNAzyme-stimulated cleavage of the fluorophore/quencher-labeled hairpin substrate (113). Fluorophore-labeled strand (114) provides the readout signal for the sensing process. (B) Time-dependent fluorescence changes upon analyzing different concentrations of the target (110) according to the scheme outlined in A. Reprinted with permission from ref 52a. Copyright 2011 Wiley-VCH.

minimizing the background signal in the absence of the target. This apparent disadvantage was, however, resolved by adding one additional “helper” hairpin structure to the optimized sensing module. Opening of the “helper” hairpin yields a nucleic acid tether that activates the isothermal autonomous catabolic DNAzyme reaction cycle. This has been demonstrated with the analysis of the Tay-Sachs genetic disorder mutated gene with a detection limit corresponding to 1 pM.

Isothermal cascaded generation of the Zn^{2+} -dependent ligation DNAzyme was demonstrated and implemented for amplified detection of a target-analyte DNA,²⁴² Figure 26A. The system consists of a nucleic acid strand (117) that includes a subunit of the Zn^{2+} -dependent ligation DNAzyme sequence, a hairpin domain that provides the recognition sequence for the target DNA (116), and a stem region that cages the subunit of the ligation DNAzyme. Also, the system consists of a second subunit of the ligation DNAzyme (118), the hydroxylated substrate subunit (119), and the imidazole phosphate-modified cosubstrate subunit (120), acting as the components to be ligated. The caged DNAzyme subunit structure prohibits self-assembly of the functional ligation DNAzyme structure. In the presence of the analyte DNA (116), however, opening of the hairpin 117 results in self-assembly of the ligation DNAzyme structure, and this yields, in the presence of Zn^{2+} ions, the ligated DNA product (121). The latter product was, however,

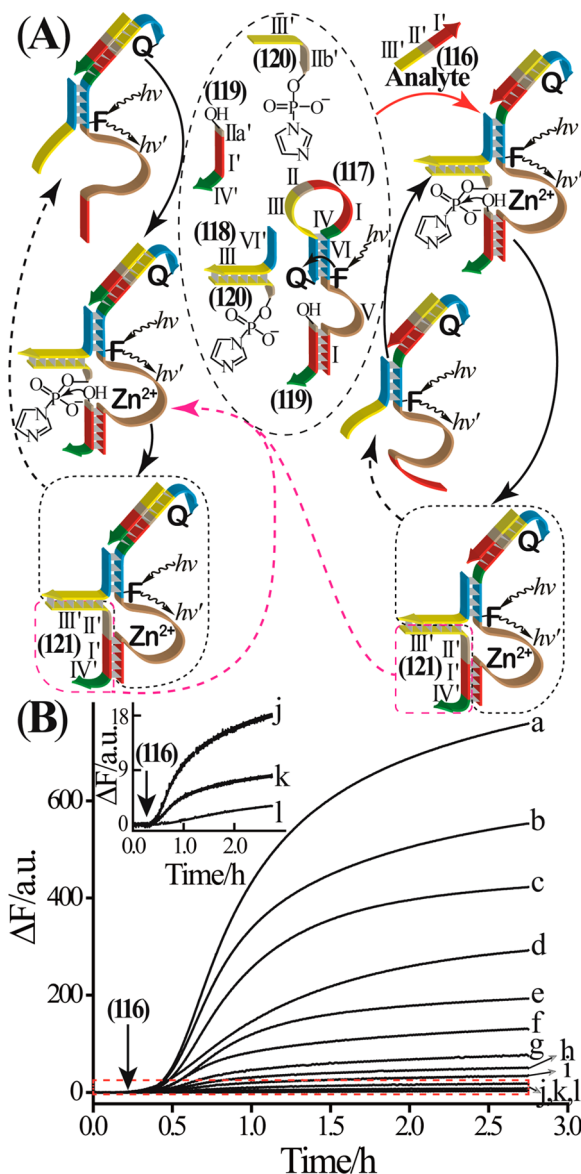


Figure 26. (A) Amplified analysis of a target DNA by the Zn^{2+} -dependent ligation DNAzyme-mediated autonomous synthesis of an analog sequence to the target. Target 116 triggers hairpin 117 to form the catalytically active ligation DNAzyme. Resulting ligated product 121 includes the target sequence and further opens hairpin 117 to yield another ligation DNAzyme unit. As hairpin 117 is labeled with a F/Q pair, its opening by the target or replicated target sequence leads to a fluorescence readout signal. (B) Time-dependent fluorescence changes upon analyzing different concentrations of the target 116 according to the scheme outlined in A: (a) 4.0×10^{-7} , (b) 2.0×10^{-7} , (c) 1.0×10^{-7} , (d) 4.0×10^{-8} , (e) 2.0×10^{-8} , (f) 1.0×10^{-8} , (g) 4.0×10^{-9} , (h) 2.0×10^{-9} , (i) 1.0×10^{-9} , (j) 1.0×10^{-10} , (k) 1.0×10^{-11} , and (l) 0 M. Reprinted with permission from ref 242. Copyright 2012 American Chemical Society.

designed to include the target sequence, and hence, its displacement by the loop region of strand 117 regenerates the primary-formed DNAzyme unit and forms the second catalytically active DNAzyme structure. Thus, the Zn^{2+} -dependent ligation DNAzyme activated by the target DNA leads to the isothermal autonomous replication of the functional DNAzyme structure. By labeling of nucleic acid 117 with a F/Q pair, the opening of the DNAzyme subunit-encoded hairpin strand (117) by the target-analyte (or the

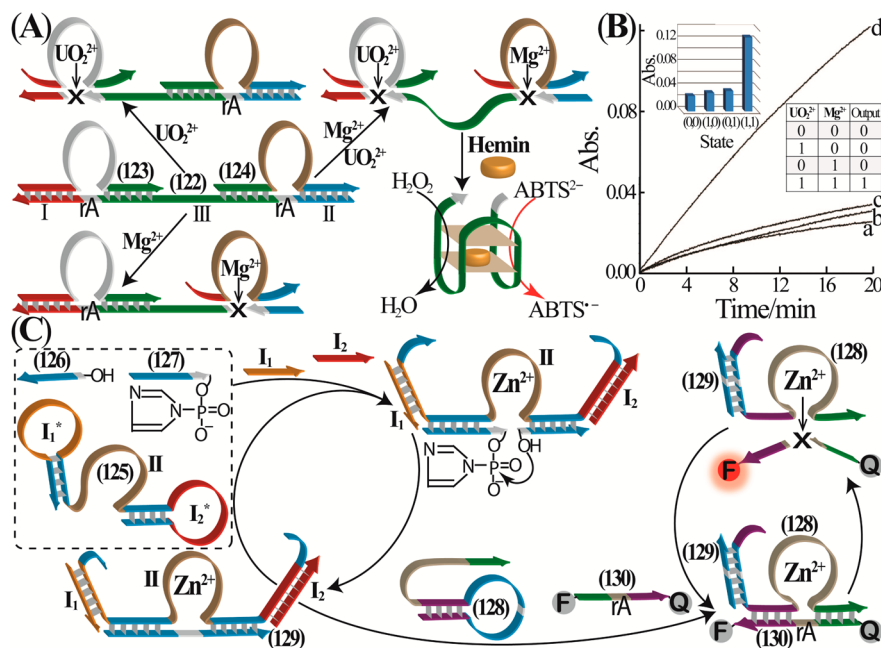


Figure 27. (A) Assembly of an AND logic gate based on the UO₂²⁺- and Mg²⁺-dependent DNAzymes. In the presence of UO₂²⁺ and Mg²⁺ ions as inputs, the substrate (122) is cleaved to yield the hemin/G-quadruplex DNAzyme as output. “Output” DNAzyme mediates catalyzed oxidation of ABTS²⁻ to ABTS^{•-} by H₂O₂. (B) Time-dependent absorbance changes as a result of formation of ABTS^{•-} using the inputs: (a) 0, 0 (b) 1, 0 (c) 0, 1 (d) 1, 1. (Inset) Bar presentation of the output signals in the presence of the different inputs. (Right) Derived truth table of the AND gate. Reprinted with permission from ref 168. Copyright 2009 American Chemical Society. (C) Assembly of an AND logic gate based on the Zn²⁺-dependent ligation DNAzyme coupled to the Zn²⁺-dependent hydrolytic cleavage DNAzyme. Zn²⁺-dependent ligation DNAzyme blocked by two hairpin structures. Only upon treatment of DNA (125) with the two inputs, I₁ and I₂, the Zn²⁺-ligation DNAzyme is released and activated. Resulting ligated product 129 opens hairpin 128 that includes the caged sequence of the Zn²⁺-dependent cleavage DNAzyme. Cleavage of the DNAzyme substrate (130) leads to the fluorophore-labeled DNA fragment product that acts as output for the logic gate. Reprinted with permission from ref 169. Copyright 2005 American Chemical Society.

ligated product) leads to activation of the fluorescence of the fluorophore. Figure 26B depicts the time-dependent fluorescence changes upon analyzing different concentrations of the target DNA (116) by isothermal autonomous replication of the ligation DNAzyme. The composition of the nucleic acid sequences, included in the system, needs to be optimized to yield a minimal background signal and allow effective displacement of the ligated product, thus facilitating the autonomous replication process. This reflects a possible disadvantage of the system as a sensing platform, as it would require tedious optimization of the system for any specific target analyte. This apparent disadvantage was, however, resolved by introduction of an additional hairpin structure that, upon opening by the respective analyte, yields a tandem sequence that activates the optimized isothermal autonomous DNAzyme replication machinery. This has been demonstrated with the analysis of the Tay-Sachs mutated gene with a sensitivity that corresponded to 10 pM.

3.3. DNAzyme-Activated Autonomous Cascaded Logic Gates and DNA Machines

Manipulation of nucleic acids by hydrolytic cleavage of DNAzymes allowed the design of logic gate systems and digital computing logic circuits. Besides the amplification of the output signals by means of the DNAzymes, the output of one DNAzyme operation unit might act as input for a second DNAzyme logic gate unit, thus allowing isothermal autonomous assembly of fan-out or cascaded DNAzyme computing logic gate circuits.

Use of metal-ion-dependent hydrolytic cleavage DNAzyme and the hemin/G-quadruplex HRP-mimicking DNAzyme for

assembly of AND or OR logic gate systems was demonstrated.¹⁶⁸ In one system, Figure 27A, the AND logic gate was constructed by using the bis-functionalized ribonucleobase-containing nucleic acid template (122) and the Mg²⁺- and UO₂²⁺-dependent DNAzyme sequences 123 and 124, respectively. The DNA template strand 122 includes substrate domains I and II for the UO₂²⁺- and Mg²⁺-dependent DNAzymes, and these are separated by the oligonucleotide region III that includes the G-quadruplex sequence. In the presence of Mg²⁺ or UO₂²⁺ ions as inputs, only parts of the DNA template (122) are cleaved off and separated, leaving the G-quadruplex sequence in an intact, caged, duplex structure with one of the DNAzyme sequences (123 or 124), leading to a “0” output. In turn, in the presence of Mg²⁺ and UO₂²⁺ ions as inputs, the two DNAzymes are activated, leading to fragmentation of the template nucleic acid (122) into three pieces, allowing self-assembly of the released DNA domain III into the catalytically active hemin/G-quadruplex HRP-mimicking DNAzyme nanostructure. The latter DNAzyme catalyzes the H₂O₂-mediated oxidation of ABTS²⁻ to the colored product ABTS^{•-} ($\lambda_{\text{max}} = 415 \text{ nm}$) that provides the output signal for the logic gate system. As an intense output signal of ABTS^{•-} is observed (“1”) only in the presence of Mg²⁺ and UO₂²⁺ ions as inputs, Figure 27B, the system represents an AND logic gate. Using a similar approach, an OR logic gate was constructed.¹⁶⁸

A related approach to tailor a computing logic gate circuit by a cascade of DNAzyme reactions was demonstrated by implementation of functional DNA hairpin structures¹⁶⁹ and using the Zn²⁺-dependent ligation and hydrolytic DNAzymes as

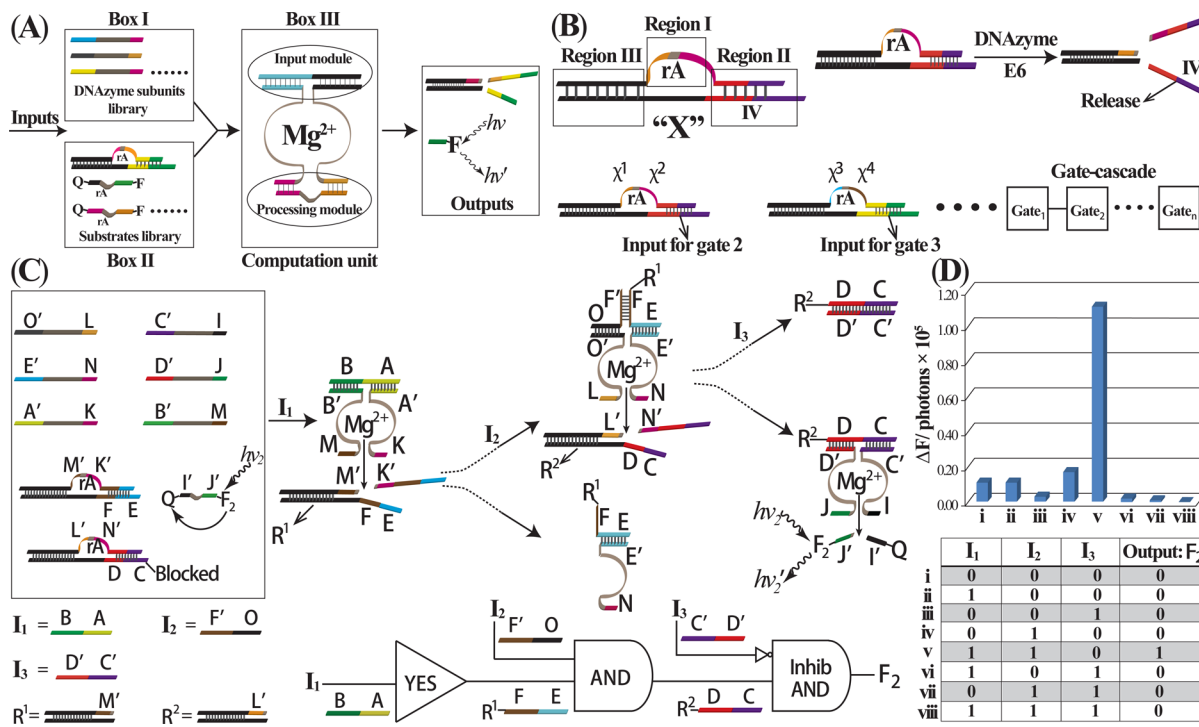


Figure 28. (A) Application of a computational module consisting of a library of the Mg^{2+} -dependent DNAzyme subunits, inputs, DNAzyme substrates, and F/Q-functionalized substrates for input-guided activation of the DNAzyme cascade. (B) Structure of a caged ribonucleobase-containing substrate that upon cleavage by the input-guided Mg^{2+} -dependent DNAzyme releases a single-stranded DNA (IV) acting as input for a second logic gate. By application of different caged ribonucleobase-containing substrates a gate cascade is activated. (C) Composition of a computational module for activation of a YES-AND-Inhib AND gate cascade. Terminal cleavage of the fluorophore/quencher-labeled substrate leads to a fluorophore-labeled fragment acting as output. (D) Fluorescence intensity changes of the gate cascade triggered by inputs I_1 , I_2 , and I_3 defined in the resulting truth table (bottom) according to the scheme shown in C. Reprinted with permission from ref 170. Copyright 2010 Nature Publishing Group.

output signal generators. This is exemplified in Figure 27C with the construction of an AND logic gate. The DNA structure (125) includes two hairpin subdomains, where the sequence region II, marked in brown, corresponds to the ligation DNAzyme, while the hairpin loops I_1^* and I_2^* include the recognition sequences for inputs I_1 and I_2 , respectively. In this DNA structure, the ligation DNAzyme sequence is caged in a catalytically inactive configuration by the two hairpin subdomains. The two substrate subunits (126 and 127) of the ligation DNAzyme and the reporter hairpin structure (128) are also included in the system. Inputs I_1 or I_2 open only the hairpins I_1^* or I_2^* , respectively, processes that do not lead to activation of the ligation DNAzyme nanostructure. Subjecting the functional DNA structure (125) to both inputs, I_1 and I_2 , opens the two hairpins while releasing a free, catalytically active, ligation DNAzyme unit that acts as output catalyst for reporting the logic gate operation. Binding of the ligation DNAzyme substrate subunits (126 and 127) to the activated ligation DNAzyme results in their catalyzed ligation to yield ligated DNA product (129). The reporter hairpin strand (128) includes in its loop region a recognition sequence for the ligated DNA product (129) and in its stem region a caged catalytically inactive configuration of the Zn^{2+} -dependent hydrolytic cleavage DNAzyme. The resulting ligated product (129) leads then to opening of the reporter hairpin structure (128), a process that activates the Zn^{2+} -dependent hydrolytic cleavage DNAzyme unit. Binding of the fluorophore/quencher-modified DNAzyme substrate (130) to the corresponding DNAzyme results in cleavage of the substrate, and the

fluorescence generated by the fluorophore-labeled fragmented substrate provides the output signal of the isothermal autonomous DNAzyme cascaded system. As the output is generated only in the presence of the two inputs I_1 and I_2 that open, as the primary step, the hairpins I_1^* and I_2^* , respectively, an AND logic gate is demonstrated by the system.

A different approach to construct isothermal autonomous DNAzyme-based logic gate circuits implemented the Mg^{2+} -dependent hydrolytic cleavage DNAzyme as biocatalyst.¹⁷⁰ The concept is based on construction of a computing unit that includes a library of the Mg^{2+} -dependent DNAzyme subunits and the substrates for the different Mg^{2+} -dependent DNAzyme units formed by the corresponding DNAzyme subunits, Figure 28A. In the presence of the appropriate nucleic acid inputs, the input-guided assembly of the respective DNAzyme subunits form the corresponding DNAzyme unit that binds the respective substrate. As the different substrates include different recognition arms and different fluorophore/quencher pairs, cleavage of the substrate by the respective DNAzyme structure yields a fluorescence signal that reflects the input that triggers on the DNA computational unit. Using this approach, a universal set of logic gates was demonstrated. This basic concept was further extended to develop computational logic gate circuits using the Mg^{2+} -dependent DNAzyme subunits library as processing module, Figure 28B. Toward this goal, a modified DNAzyme hybrid substrate structure "X", consisting of the single-stranded loop domain, region I, and two duplex regions II and III, was designed. Region I provides the substrate sequence for the respective DNAzyme unit, and upon cleavage

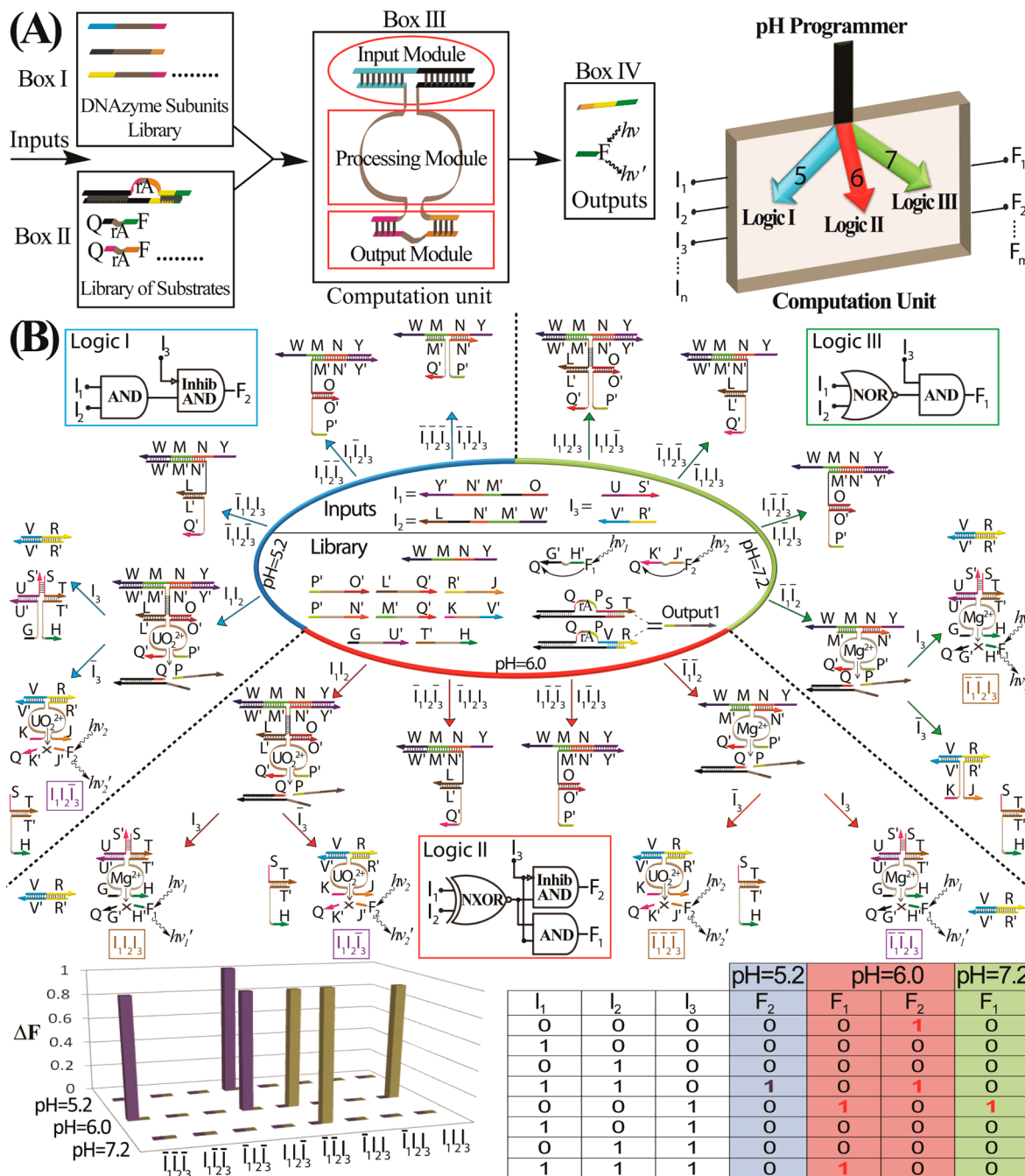


Figure 29. (A) Computational module consisting of modular UO_2^{2+} - and Mg^{2+} -dependent DNAzyme subunits for powering of pH-programmable logic arrays. At pH = 5.2, only the UO_2^{2+} -DNAzyme is active, at pH = 7.2, only the Mg^{2+} -DNAzyme is active, whereas at pH = 6.0, both the UO_2^{2+} - and the Mg^{2+} -dependent DNAzymes are active. (B) pH-programmed logic arrays driven by the computational module. Scheme shows the pH-stimulated interconversion between programs and the resetting of the programs to the original computational module. (Bottom) Fluorescence outputs corresponding to the different logic arrays associated with the different programs and the respective truth table. Reprinted with permission from ref 173. Copyright 2012 American Chemical Society.

of the hybrid substrate the single-stranded domain IV is formed and released from hybrid substrate "X". This may then act as input for the cascaded DNAzyme chain reactions: accordingly, by designing a set of DNAzyme substrates, where regions x^1/x^2 , x^3/x^4 , ..., provide the diversity of the formation of different DNAzyme nanostructures and sequential formation of input DNA strands for activation of the logic gate cascade. Using this concept construction of a computing module that performs the logic gate chain YES-AND-Inhib AND is demonstrated using a library of DNAzyme subunits, DNAzyme substrates, and inputs,

as displayed in Figure 28C. The fluorescence transduction of this input-guided logic gate cascade and the respective truth table are displayed in Figure 28D. This concept was extended to construct pH-programmed logic gate cascades.¹⁷³ Toward this goal, the computing module includes DNAzyme subunits of two different metal-ion-dependent DNAzymes, the Mg^{2+} -dependent DNAzyme subunits, and the UO_2^{2+} -dependent DNAzyme subunits. While the Mg^{2+} -dependent DNAzyme is catalytically active at pH = 7.2 and inactive at pH = 5.2, the UO_2^{2+} -dependent DNAzyme is catalytically active at pH = 5.2

and inactive at pH = 7.2. At pH = 6.0, the two DNAzymes reveal, however, partial activities. This enables the use of common inputs, I₁, I₂, I₃, and activation of three different computing circuits at pH = 5.2, 6.0, and 7.2, as depicted in Figure 29A. Three different logic gate cascades were activated by subjecting the computation unit to the different pH environments, and by changing the pH of the system, the interconversion between different programs was demonstrated. Using substrates labeled with appropriate fluorophore/quencher pairs for the catalytically active DNAzymes in the different computing circuit programs, the fluorescence output identified the respective programs as shown in Figure 29B and the respective truth table.

An isothermal autonomous multistep nucleic acid "walker" system was developed using a DNA template scaffold, S, as the walker track, and a DNAzyme unit as a driving force of the machine,¹²⁷ Figure 30. The DNA track consists of the "track"

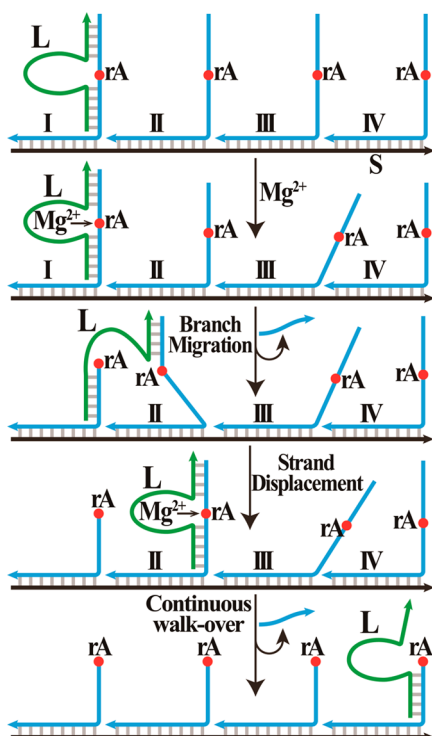


Figure 30. Isothermal autonomous multistep DNA walker driven by cascaded Mg^{2+} -dependent DNAzyme catalytic transformations. Reprinted with permission from ref 127. Copyright 2005 Wiley-VCH.

template S on which four footholds I, II, III, and IV were constructed through specific hybridization. Each of these footholds included the specific ribonucleobase-containing sequence of the Mg^{2+} -dependent 10–23-type DNAzyme (ribonucleobase marked with red color). The walker unit, L, includes the Mg^{2+} -dependent DNAzyme sequence and appropriate overhangs to bind to the different single-stranded domains of the footholds. In the primary step of the molecular device, the walker unit L is stabilized on foothold I. Cleavage of the foothold I by the DNAzyme sequence of the walker cleaves off a part of the foothold, thus releasing a single-stranded overhang on the walker L that favors walkover to foothold II. Hybridization of the overhang with foothold II via a branch migration strand-displacement mechanism yields a duplex structure of superior stability. Subsequent cleavage of foothold

II by the Mg^{2+} -dependent DNAzyme stimulates the subsequent walkover of the walker unit L to foothold III by branch migration and strand-displacement processes. Finally, cleavage of foothold III by the DNAzyme results in the final step of transition of the walker strand L to foothold IV, that is, gradual destabilization of the duplex between the DNAzyme-containing sequence of the walker L with the different footholds dictates the autonomous unidirectional "walking" process, which is associated with constant fragmentation of the supramolecular DNA device composed of the scaffold and footholds. The walking process was imaged by electrophoretic analysis of the fragmented products of the device.

Stepwise cleavage of DNA footholds associated with a surface by a Zn^{2+} -dependent DNAzyme "spider" construct was reported.²⁶³ This concept was implemented for the ingenious, programmed activation of the isothermal autonomous walking process of a nanoscale DNA spider robot on a predicated path associated with a DNA origami landscape,¹⁴⁷ Figure 31A. A DNA spider robot nanostructure that includes "three legs," I, II, and III, composed of the Zn^{2+} -dependent 8–17 type DNAzyme sequence with appropriate overhangs, and a capture arm L is linked to the DNA origami template, which includes complementary protruding nucleic acids I*, II*, III*, and L*. The nucleic acid L* acts as an anchoring site for precise deposition of the "three-leg" spider robot on the DNA origami template. The origami template includes additional dictated binding sites in the form of protruding nucleic acid I*, II*, and III*, complementary to the three legs I, II, and III, respectively. These sites are, however, nonpopulated due to the locking of the spider robot to the anchoring site L*. Treatment of the system with the trigger strand T unlocks the capture arm L, and in the presence of the Zn^{2+} ions as DNAzyme cofactors, the stepwise cleavage of the protruding footholds proceeds, leading to the walkover of the legs to the next binding sites (footholds). Thus, the walking spider robot at different time intervals of operation can occupy different predicted sites a, b, c, and d on the DNA origami template. By labeling the functional DNA origami with two coordinate labels, the motility of the spider robot on the DNA origami template could be followed by atomic force microscopy (AFM), Figure 31B.

4. ENZYME/DNAZYME COUPLED CATALYTIC CASCADES

Different enzymes catalyze a variety of transformations on DNA templates. These include the replication of DNA, the ligation of nucleic acid units, the specific nicking of one strand of a DNA duplex structure, or the symmetrical or nonsymmetrical cleavage of duplex DNA structures. The enzymes provide a rich "toolbox" for manipulation of DNA nanostructures. Specifically, this arsenal of enzymes enables the synthesis and subsequent separation of catalytic nucleic acid sequences (DNAzymes). This subsection will address the different applications of coupled catalytic cascades that combine naturally occurring enzymes and DNAzymes.

4.1. Biocatalytic Cascades Driven by Coupled DNAzymes and Rolling Circle Amplification (RCA) Processes

The rolling circle amplification (RCA) process consists of the isothermal continuous lengthening of a short DNA strand (primer) hybridized with the circular DNA template in the presence of polymerase/dNTPs mixture, Figure 32. Circular replication of the DNA template proceeds hundreds and even thousands of times, leading to micrometer-long DNA chains

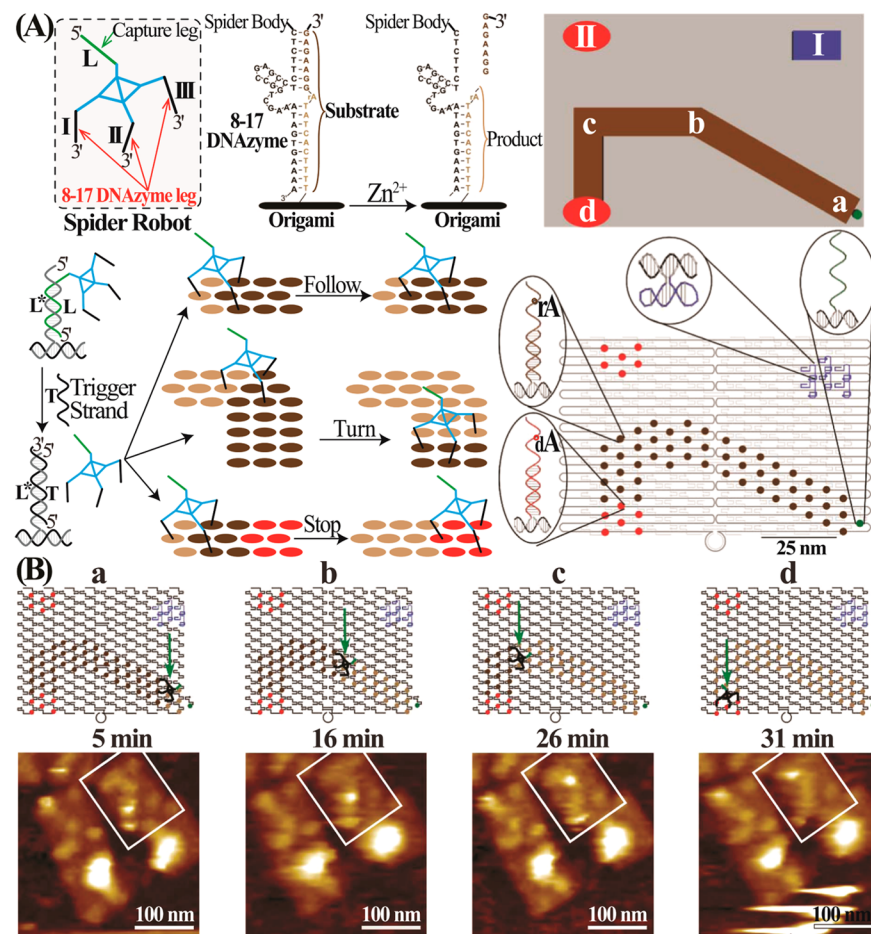


Figure 31. Isothermal autonomous programmed DNA “walking robot” activated on a tailored DNA origami template and driven by sequential cleavage of dictated foothold strands by the Mg²⁺-dependent DNAzyme “spider” machine. Reprinted with permission from ref 147. Copyright 2010 Nature Publishing Group.

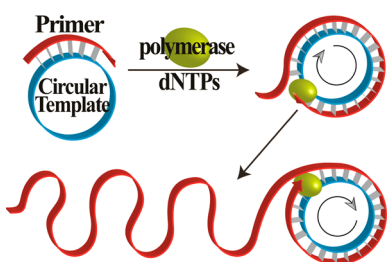


Figure 32. Schematic presentation of the isothermal rolling circle amplification (RCA) process.

that include tandem repeat units of the replicated circular template.^{264–266} The RCA process has been extensively used for amplified biosensing applications. The 3'- and 5'-ends of DNA padlock probes were hybridized with the target DNA and ligated by DNA ligase. The subsequent Phi29 DNA polymerase-stimulated RCA process was then followed by molecular beacons,^{267,268} fluorophores,^{269,270} or molecular zippers.²⁷¹ The RCA process was further implemented to amplify antigen–antibody recognition complexes^{272,273} and follow formation of aptamer–substrate complexes.^{274–278} Also, the RCA process was used to generate periodic templates for programmed assembly of metallic nanoparticles²⁷⁹ or proteins,²⁸⁰ thus providing new means for the bottom-up synthesis of functional nanostructures. The coupling between the RCA-mediated

generation of chains consisting of tandem repeated catalytic nucleic acids (DNAzymes) units provided an important venue to generate functional nanostructures, a topic that will be addressed in this subsection.

The biocatalytic activities of DNAzymes together with the specific recognition properties of aptamers were coupled with the isothermal RCA process to develop various amplified aptamer-based sensing platforms (aptasensors). Aptamer-functionalized DNAzyme can be used to activate the RCA process and construct various amplified aptasensors. This has been demonstrated with the development of an amplified fluorescence aptasensor for ATP using an anti-ATP aptamer-functionalized ligation DNAzyme sequence that conjugates the 3'-phosphorothioate and 5'-ido residue of the DNAzyme substrate or circular padlock probe,²⁷⁴ Figure 33A. The system consisted of the ligation DNAzyme sequence (**131**) that was elongated by the anti-ATP aptamer sequence and a DNAzyme substrate sequence (**132**) that binds through its 3'- and 5'-ends to the functionalized DNAzyme sequence (**131**). The anti-ATP aptamer-functionalized ligation DNAzyme was labeled with biotin at its 5'-end and immobilized on a streptavidin-coated glass slide. While in the absence of ATP, formation of the catalytically active DNAzyme nanostructure was prohibited due to insufficient intramolecular DNA hybridization, binding of ATP to the aptamer domain cooperatively stabilized the tertiary structure of the ligation DNAzyme, leading to intramolecular ligation of the 3'- and 5'-ends of the DNAzyme substrate

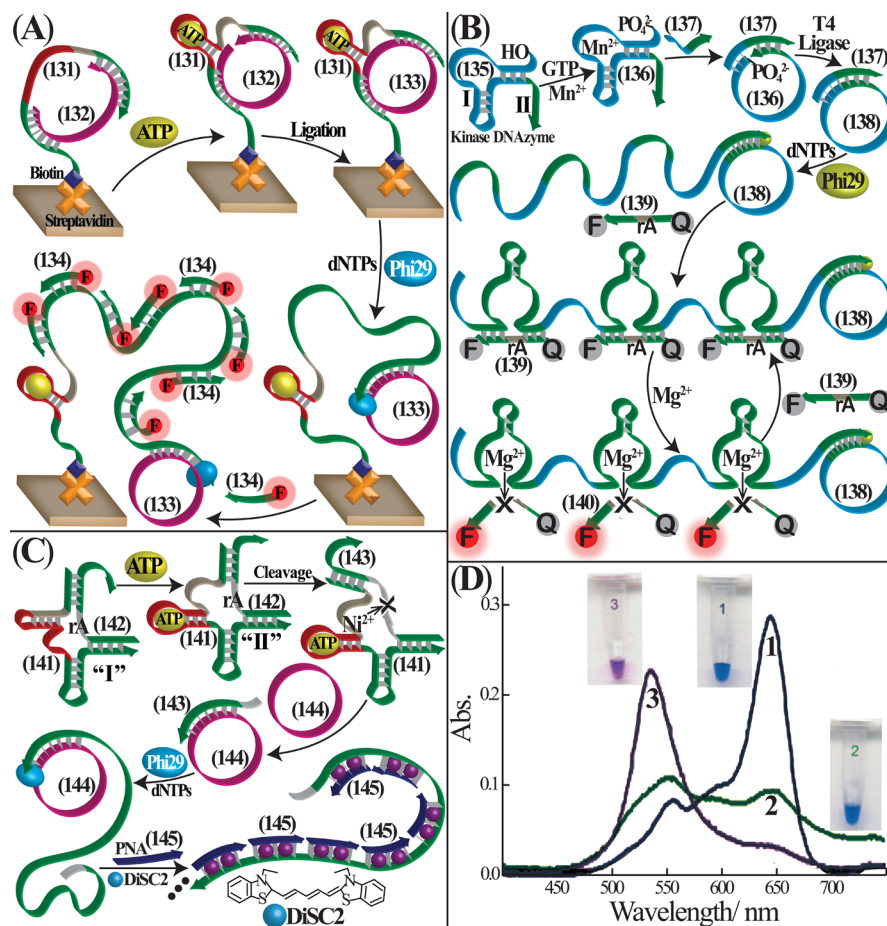


Figure 33. (A) Amplified fluorescence ATP–aptasensor based on the isothermal RCA process. Probe containing the aptamer sequence is immobilized on the surface and bridged by a template nucleic acid. Formation of the ATP–aptamer complex triggers on the RCA process, and binding of a fluorophore-labeled nucleic acid to the constant repeat units of the RCA product provides the readout signal. Reprinted with permission from ref 274. Copyright 2005 American Chemical Society. (B) Amplified fluorescence detection of GTP by the kinase DNAzyme-catalyzed phosphorylation of a functional nucleic acid structure that is coupled to the ligase-induced formation of a circular DNA that acts as a template for activation of the polymerase/dNTPs-stimulated RCA process. This leads to DNA wires consisting of the Mg^{2+} -dependent DNAzyme units, and their catalytic activity provides the fluorescence readout signal. Reprinted with permission from ref 275a. Copyright 2013 American Chemical Society. (C) ATP–aptamer complex-induced formation of the Ni^{2+} -dependent DNAzyme that cleaves the substrate and yields a fragment initiating the RCA process. Amplified detection of ATP is achieved by monitoring the color of DiSC2 associated to the duplex between peptide nucleic acid (PNA) units hybridized with the constant repeat units of the RCA product. (D) Spectra and color images corresponding to (1) Only DiSC2, (2) DiSC2 and RCA product, and (3) DiSC2, PNA, and the RCA product. Analysis of ATP according to the scheme shown in C. Reprinted with permission from ref 275b. Copyright 2009 Wiley-VCH.

(132). The resulting DNAzyme stimulated the ligation reaction and yielded a circular DNA template (133) that is associated with the anti-ATP aptamer-functionalized ligation DNAzyme sequence (131). Subsequent activation of the RCA process, using Phi29 DNA polymerase and dNTPs mixture, generated DNA chains consisting of constant repeat units replicating the circular DNA template (133). Hybridization of fluorophore-labeled probe nucleic acid (134) with the sequence-specific replication units enabled the fluorescence detection of ATP, with a detection limit corresponding to $1 \mu\text{M}$. In a related system, the kinase deoxyribozyme^{275a} was coupled to the RCA process to yield a DNAzyme/enzyme cascade for sensing of guanosine triphosphate, GTP, Figure 33B. The nucleic acid structure (135) included the kinase-specific DNAzyme sequence (domain I) for the phosphorylation of the 5'-end by GTP. The programmed sequence included also a tethered domain II that is complementary to the Mg^{2+} -dependent DNAzyme. Intramolecular ligation of the 3'- and 5'-ends of the phosphorylated product (136) that is capped by strand (137)

yielded a circular DNA template (138) that, in the presence of Phi29 polymerase/dNTPs mixture, triggered on the RCA process. This resulted in formation of long wires composed of the Mg^{2+} -dependent DNAzyme. In the presence of Mg^{2+} ions and the F/Q-modified substrate (139) the substrate was fragmented to the fluorophore-functionalized product (140) that provided the optical readout signal for GTP. The system revealed selectivity for analyzing GTP, and GTP could be analyzed with a detection limit of $1 \mu\text{M}$. In a further study, the Ni^{2+} -dependent hydrolytic RNA-cleavage DNAzyme was conjugated to the isothermal RCA process to develop an optical colorimetric ATP aptasensor in solution,^{275b} Figure 33C. The functionalized DNA sequence (141) consisted of the Ni^{2+} -dependent RNA-cleavage DNAzyme sequence and the anti-ATP aptamer sequence, and this was hybridized with the DNAzyme substrate strand (142), which included the ribonucleobase cleavage site. While in the absence of ATP, the DNA sequence (141) folded into a catalytically inactive DNA configuration “I”, in the presence of ATP, it folded into

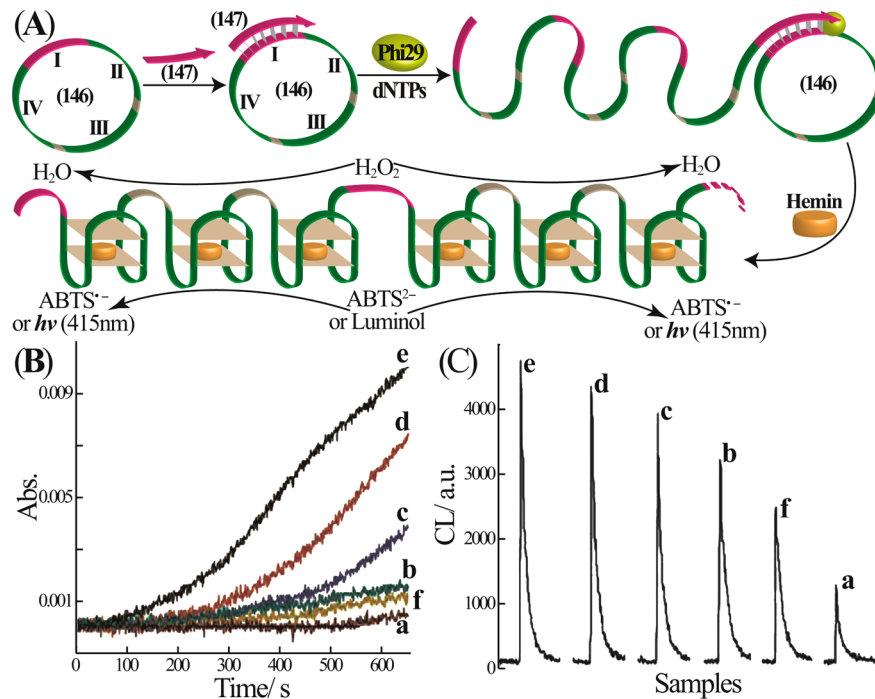


Figure 34. (A) Amplified analysis of a target DNA by the isothermal RCA process that synthesizes nanowires of the hemin/G-quadruplex HRP-mimicking DNAzyme. (B) Time-dependent absorbance changes of ABTS^{•-} and (C) chemiluminescence intensities generated by the hemin/G-quadruplex DNAzyme nanowires described in A upon analyzing different concentrations of the target DNA: (a) 0, (b) 1×10^{-14} , (c) 1×10^{-12} , (d) 1×10^{-11} , and (e) 1×10^{-9} M target and (f) 1×10^{-8} M foreign calf thymus ssDNA. Reprinted with permission from ref 281b. Copyright 2007 Royal Society of Chemistry.

the catalytically active DNAzyme structure “II,” leading to cleavage of the DNAzyme substrate nucleic acid (142). The released substrate fragment (143) activated, in the presence of the predesigned circular DNA template (144) and Phi29 polymerase/dNTPs mixture, the corresponding RCA process. Hybridization with the peptide nucleic acid (PNA, (145)), complementary to the RCA-generated DNA chains, resulted in tandem repeated DNA/PNA duplex regions that specifically bind the 3,3'-diethylthiocarbocyanine dye (DiSC2) that changes its color from blue to purple, Figure 33D. The method enabled analysis of ATP with a detection limit of $50 \mu\text{M}$.

An alternative approach for amplified bioanalysis involved the primary activation of the isothermal RCA process and its coupling to DNAzymes to yield an amplification cascade for ultrasensitive biosensing applications. This has been demonstrated, Figure 34A, with the use of a circular nucleic acid template (146), which includes a recognition region I for the target DNA and three functional DNA domains II, III, and IV complementary to the sequence of the hemin/G-quadruplex HRP-mimicking DNAzyme. Binding of the target DNA (147) to circular DNA template (146) initiated, in the presence of Phi29 polymerase/dNTPs mixture, the corresponding RCA process, giving rise to the DNA chains comprising of the tandem hemin/G-quadruplex HRP-mimicking DNAzyme repeat units.²⁸¹ The latter DNAzyme biocatalysts activated the catalyzed oxidation of ABTS²⁻ by H₂O₂ to the colored ABTS^{•-} product ($\lambda_{\text{max}} = 415 \text{ nm}$) or catalyzed generation of chemiluminescence in the presence of luminol/H₂O₂. In order to utilize the method as a general detection system for analyzing any target DNA, a specific DNA hairpin nanostructure that recognizes the corresponding target DNA was introduced into the system. The opening of the probe DNA hairpin structure by the target DNA released a stem-caged,

tandem sequence that activated, in the presence of Phi29 polymerase/dNTPs mixture, the RCA process and subsequent generation of the hemin/G-quadruplex HRP-mimicking DNAzyme nanochains. Using this method the colorimetric or chemiluminescence detection of M13 phage DNA was demonstrated,^{281b} Figure 34B and 34C. The analyte DNA was sensed with a detection limit corresponding to 10 fM. This analytical platform was further extended to a fluorescence assay by implementing the RCA-generated hemin/G-quadruplex HRP-mimicking DNAzyme chains to catalyze oxidation of Amplex Red by H₂O₂ to the fluorescent dye product, Resorufin.²⁸²

The coupled isothermal RCA-activated hemin/G-quadruplex HRP-mimicking DNAzyme cascade was further applied to amplify detection of aptamer–substrate complexes, e.g., analysis of PDGF-BB,^{276a} Figure 35A. Two anti-PDGF-BB aptamers that bind to different domains of the PDGF-BB are well known.²⁸³ Accordingly, magnetic particles (MP) were modified with one of the anti-PDGF-BB aptamers strand (148). The binding of PDGF-BB to the aptamer-containing strand (148) and subsequent association of the second functional anti-PDGF-BB aptamer sequence (149) to the analyte led to the bi-functional aptamer–analyte complex that was separated by an external magnetic field. The single-strand tether associated with the second anti-PDGF-BB aptamer strand (149) hybridized with a circular DNA template (150). The RCA process initiated in the presence of Phi29 polymerase/dNTPs mixture led to generation of the hemin/G-quadruplex DNAzyme nanochains that provided catalysts for H₂O₂-mediated oxidation of ABTS²⁻ to the colored product ABTS^{•-} ($\lambda_{\text{max}} = 415 \text{ nm}$) and to amplified detection of PDGF-BB target, Figure 35B. The method enabled the colorimetric detection of the target PDGF-BB with a detection limit corresponding to $0.2 \text{ pg}\cdot\text{mL}^{-1}$.

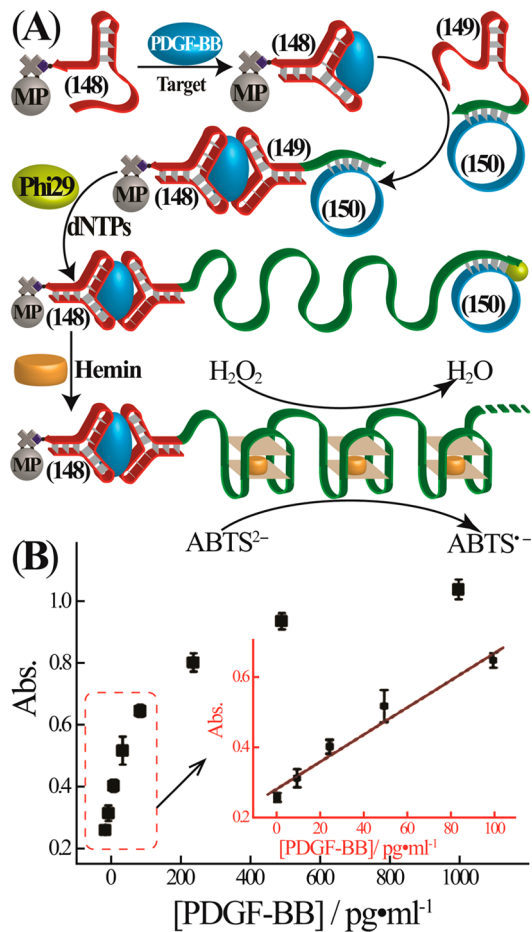


Figure 35. (A) Magnetic particles (MP)-assisted amplified detection of PDGF-BB by a sandwich aptamer assay coupled to the isothermal RCA process. Magnetic field separated magnetic beads functionalized with the PDGF-BP aptamers “sandwich” initiate RCA synthesis of hemin/G-quadruplex DNAzyme wires that catalyze oxidation of ABTS²⁻ by H₂O₂ to form the colored ABTS^{•-} product. (B) Resulting calibration curve corresponding to analysis of different concentrations of PDGF-BB according to A. (Inset) Calibration curve of the lower concentration range of PDGF-BB. Reprinted with permission from ref 276a. Copyright 2012 American Chemical Society.

4.2. Biocatalytic Cascades Driven by Coupled DNAzymes and Endonucleases/Nicking Enzymes

Cleavage of duplex DNA strands by sequence-specific endonucleases or the sequence-specific nicking of one nucleic acid strand associated with duplex DNA strands provides general means to fragment DNA nanostructures. Thus, by nanoengineering of the DNA sequences “smart” nucleic acid structures that respond to an external trigger (analyte) and activate endonucleases/nicking enzymes may be designed. Such enzymes may fragment the DNA nanostructures into new functional DNA units acting as DNAzymes yielding “activator” elements that duplicate the analyte nanostructure, or activate isothermal autonomous catalytic reactions, that lead to continuous generation of replicated DNAzyme units. Accordingly, coupling of biocatalytic cascades that involve DNAzymes and endonucleases/nicking enzymes provides important means to amplify recognition events.

Conjugation of the nicking enzyme (N.BstNB I) with the hemin/G-quadruplex HRP-mimicking DNAzyme was used to develop an isothermal ultrasensitive colorimetric detection

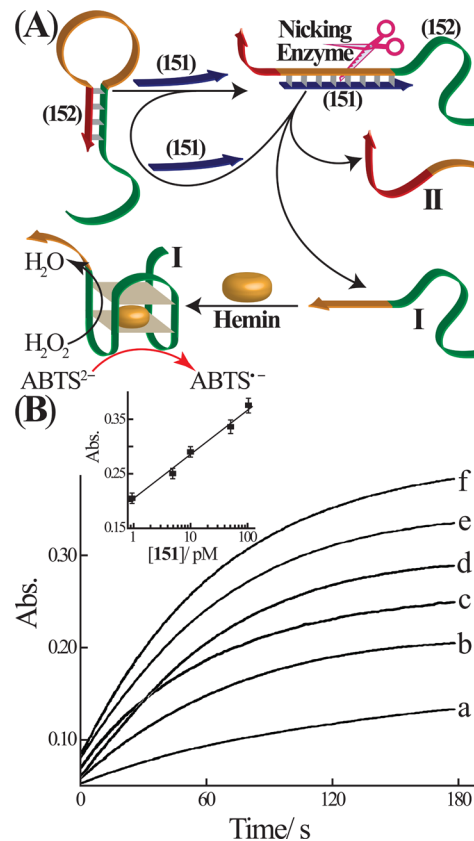


Figure 36. (A) Amplified sensing of a target DNA by the target-induced opening of a functional DNA hairpin structure that leads upon nicking to isothermal autonomous regeneration of the target and to formation of the hemin/G-quadruplex DNAzyme. (B) Time-dependent absorbance changes upon analyzing different concentrations of the target DNA using the hemin/G-quadruplex DNAzyme-catalyzed oxidation of ABTS²⁻ by H₂O₂ as colorimetric readout signal: (a) 0, (b) 1×10^{-12} , (c) 5×10^{-12} , (d) 1×10^{-11} , (e) 5×10^{-11} , and (f) 1×10^{-10} M. (Inset) Resulting calibration curve. Reprinted with permission from ref 284a. Copyright 2011 Royal Society of Chemistry.

system for the p53 tumor-promoting gene target, (151)^{284a} Figure 36A. The functional DNA hairpin sequence (152) included the recognition sequence for the target DNA (151) in the loop region and the DNAzyme sequence in a caged catalytically inactive configuration in the stem region. Opening of the functional DNA hairpin strand (152) by the p53 gene target (151) was followed by the N.BstNB I-stimulated nicking of the duplex DNA structure (151/152). This led to fragmentation of the original hairpin strand (152) into fragment I consisting of the self-assembled HRP-mimicking hemin/G-quadruplex DNAzyme, to generation of a “waste” product II of the nicked hairpin sequence (152), and to separation and recycling of the DNA target sequence (151). Thus, the nicking of the target-hairpin complex (151/152) leads to isothermal autonomous generation of the hemin/G-quadruplex DNAzyme that catalyzes oxidation of ABTS²⁻ by H₂O₂ to the colored product, ABTS^{•-}, Figure 36B. The method enabled detection of the p53 gene with a detection limit corresponding to 1.0 pM. Similarly, sensitive detection of miRNAs was achieved using a cascaded amplification strategy that combines duplex-specific endonuclease amplification with either the hemin/G-quadruplex DNAzyme or the 8–17 DNAzyme biocatalytic labels.^{284b} A related approach^{285a} has implemented an engineered DNA hairpin structure that

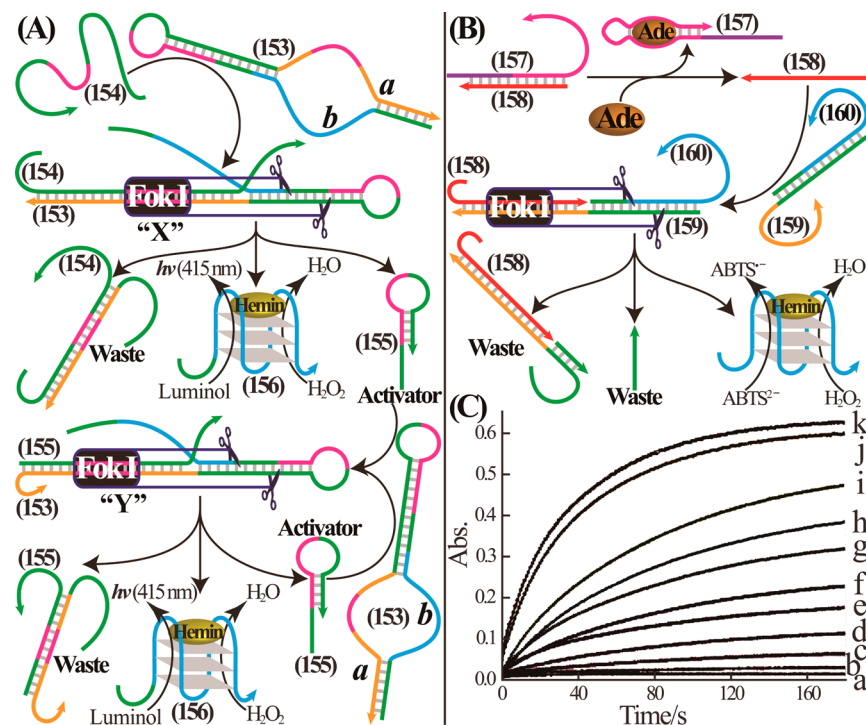


Figure 37. (A) Amplified analysis of DNA using the coupled Fok I and hemin/G-quadruplex DNAzyme as an amplifying catalytic cascade: DNA target rearranges a functional hairpin to structure “X” that is cleaved by Fok I to yield the hemin/G-quadruplex DNAzyme and an activator unit that triggers isothermal autonomous and synthetic hemin/G-quadruplex DNAzyme that provides the chemiluminescence readout signal for the sensing event. Reprinted with permission from ref 286. Copyright 208 American Chemical Society. (B) Amplified adenine-aptamer sensing platform implementing the Fok I and hemin/G-quadruplex DNAzyme cascade as amplification platform. Hemin/G-quadruplex DNAzyme catalyzes H₂O₂-mediated oxidation of ABTS²⁺ to the colored product ABTS^{•-}. (C) Time-dependent absorbance changes upon analyzing different concentrations of adenine by the system shown in B: (a) hemin alone, (b) 0.2 μM without Folk I, (c) 0 μM, (d) 0.5 μM, (e) 2 μM, (f) 5 μM, (g) 20 μM, (h) 50 μM, (i) 200 μM, and (j) 2 mM. Reprinted with permission from ref 287. Copyright 2009 Wiley-VCH.

included two caged G-quadruplex domains in the stem region and a single-stranded recognition sequence for the target in the loop region, where the functional hairpin strand was immobilized on the magnetic beads. The association of the target DNA with the functional hairpin structure was followed by a magnetic separation process and subsequent nicking of the hairpin, a process that led to formation of two HRP-mimicking hemin/G-quadruplex DNAzyme nanostructures. These catalyzed generation of chemiluminescence in the presence of luminol/H₂O₂, and this provided readout signal for the recognition event. Also, a related study has implemented a hairpin structure that includes an aptamer sequence, a quasi-circular probe that includes caged catalytically inactive G-quadruplex sequences, and the nicking enzyme Nb.BbvCI as an isothermal aptasensor machinery for amplified detection of thrombin.^{285b} Opening of the hairpin by the thrombin analyte, by formation of the aptamer–thrombin complex, released the stem sequence that hybridized with the quasi-circular probe. Subsequent nicking of the quasi-circle regenerated the aptamer–thrombin complex and released two active units of the hemin/G-quadruplex HRP-mimicking DNAzyme that provided a catalytic label for amplified detection of thrombin by the H₂O₂-mediated oxidation of ABTS²⁺ to the colored product ABTS^{•-}. The detection limit for analyzing thrombin corresponded to 2.5 pM.

Alternatively, the Fok I endonuclease was coupled to the HRP-mimicking hemin/G-quadruplex DNAzyme for amplified analysis of target DNA,²⁸⁶ Figure 37A. The nanoengineered hairpin structure DNA (153) included in domain *a* the

recognition sequence for the hepatitis B gene target (154) and a caged hemin/G-quadruplex DNAzyme sequence in domain *b*. In the presence of the DNA target (154), strand displacement of the functional DNA hairpin strand (153) proceeds, leading to formation of a supramolecular structure “X”, consisting of the DNA complex (153/154). The resulting complex includes the specific DNA duplex region for the binding of Fok I, thus activating sequence-specific fragmentation of the supramolecular structure “X”. This leads to a waste DNA product, to generation of an activator DNA strand (155), and to formation of the HRP-mimicking hemin/G-quadruplex DNAzyme unit (156) that catalyzes generation of chemiluminescence in the presence of H₂O₂/luminol. Since the activator DNA strand (155) includes the analyte sequence, it displaces the DNA hairpin substrate strand (153) to form the supramolecular structure “Y” (153/155) complex, which is further recognized and cleaved by the Fok I endonuclease. Thus, interaction of the functional hairpin strand (153) with the analyte DNA (154) leads to the Fok I-stimulated, isothermal, autonomous, catalytic cleavage of the DNA hairpin sequence (153) into a fragment activator unit (155) and a separated catalytically active HRP-mimicking hemin/G-quadruplex DNAzyme unit that optically transduces the recognition event via chemiluminescence signals. The method enabled detection of the hepatitis B gene target with a detection limit corresponding to 10 fM.

A related system has implemented the Fok I endonuclease/hemin/G-quadruplex HRP-mimicking DNAzyme cascade to develop an amplified aptasensor for adenine,²⁸⁷ Figure 37B. The functionalized aptamer strand (157) was used to block the

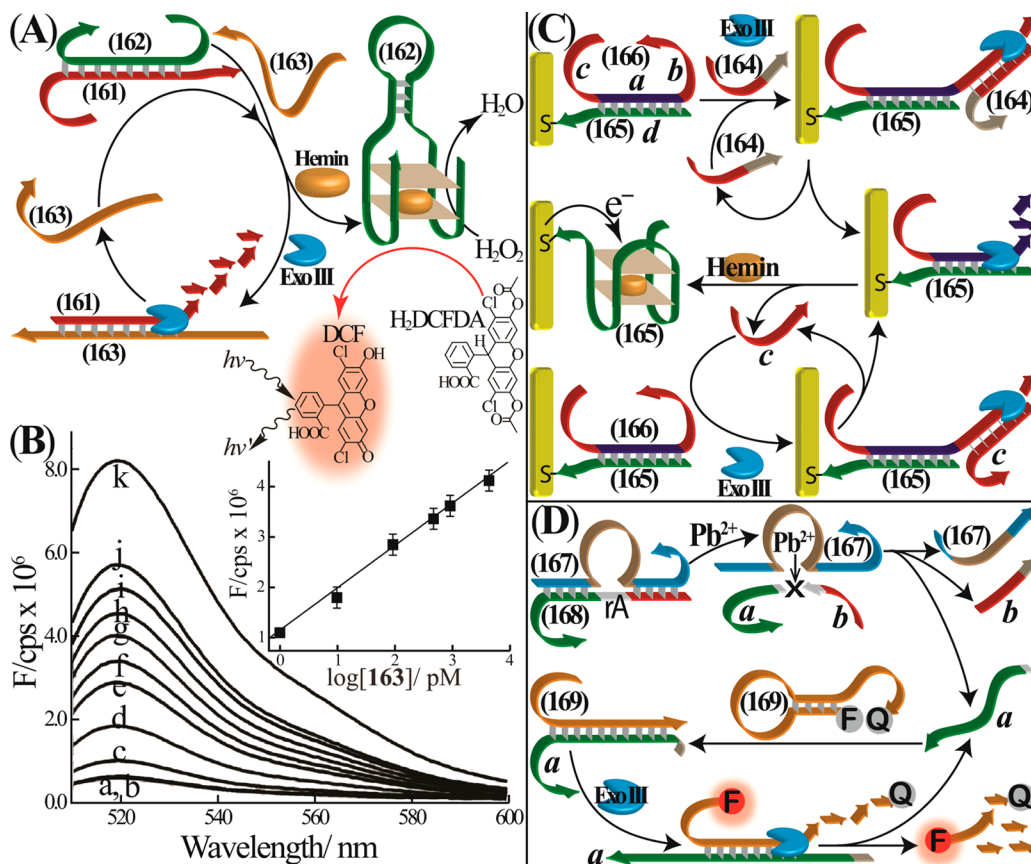


Figure 38. (A) Amplified analysis of a target DNA by the coupled Exonuclease III (Exo III) and hemin/G-quadruplex DNAzyme as catalytic cascade. Target-induced separation of the functional duplex (**161/162**) leads to formation of the hemin/G-quadruplex DNAzyme and a duplex structure (**161/163**) being “digested” by Exo III to regenerate the free analyte. DNAzyme-catalyzed oxidation of dihydro dichlorofluoresceine (H₂DCFDA) to the fluorescent fluoresceine (DCF) provides the readout signal for the sensing platform. (B) Fluorescence spectra corresponding to analysis of different concentrations of the target DNA according to A: (a) 0 M, (b) 0.1 pM, (c) 1 pM, (d) 10 pM, (e) 100 pM, (f) 500 pM, (g) 1 nM, (h) 5 nM, (i) 10 nM, (j) 50 nM, and (k) 100 nM. (Inset) Derived calibration curve. Reprinted with permission from ref 288a. Copyright 2012 Elsevier. (C) Amplified electrochemical detection of an analyte DNA using a blocked nucleic acid G-quadruplex sequence and Exo III as analyte regeneration catalyst. Blocker units include a single-stranded tether **b** for binding the analyte and a single-stranded tether **c** consisting of an analog sequence to the target. Recognition of the target DNA activates the Exo III “digestion” of tether **b** and sequence **a** of the blocker. This process leads to regeneration of the target, uncaging of the G-quadruplex sequence, and release of the analog sequence **c** to the target. Resulting hemin/G-quadruplex provides the readout signal for the sensing event. Reprinted with permission from ref 78e. Copyright 2013 American Chemical Society. (D) Amplified fluorescence analysis of Pb²⁺ ions by the Pb²⁺-dependent DNAzyme. Cleavage of the DNAzyme substrate leads to a functional strand that opens a fluorophore/quencher-modified hairpin and is being regenerated by Exo III. Reprinted with permission from ref 288b. Copyright 2013 Elsevier.

DNA primer sequence (**158**). In the presence of adenosine, the DNA duplex (**157/158**) was separated to yield the aptamer–substrate complex, and this released the DNA primer strand (**158**). The latter product hybridized with the toehold of a predesigned DNA duplex structure (**159/160**) substrate, where the predesigned DNA strand (**160**) included the HRP-mimicking hemin/G-quadruplex DNAzyme sequence in a caged, catalytically inactive configuration. Formation of the **158/159/160** supramolecular structure generated the Fok I endonuclease binding site on the duplex region of **158/159**, and this resulted in the sequence-specific cleavage of the duplex region of the **159/160** complex and uncaging of the G-quadruplex sequence that self-assembled into the HRP-mimicking DNAzyme, which catalyzed oxidation of ABTS²⁻ by H₂O₂ to form the colored product, ABTS^{•+}, Figure 37C. The method allowed detection of adenosine with a detection limit corresponding to 2 μM.

Exonuclease III, Exo III, is a versatile catalyst for isothermal hydrolytic digestion of the 3'-end of duplex nucleic acid structure. Since the 3'-end of single-stranded nucleic acids or

the 5'-end of duplex nucleic acids are nonreactive to Exo III, the enzyme is an effective catalytic tool to manipulate DNA structures. Indeed, ingenious amplified sensing platforms that implement Exo III-mediated regeneration of the target analyte for amplified detection of DNA or aptamer–substrate complexes were reported.^{47,78–80} Coupling of the Exo III-stimulated regeneration of the analyte with concomitant formation of a DNAzyme provides a dual-amplification path where the DNAzyme label transduces the sensing events. The coupling between the enzyme Exo III and the HRP-mimicking hemin/G-quadruplex DNAzyme enabled amplified detection of DNA through isothermal recycling of the DNA target and autonomous cascaded activation of the HRP-mimicking DNAzyme,^{288a} Figure 38A. The system consists of a blocked DNA primer sequence (**161**) and a functionalized DNA blocker strand (**162**). Treatment of the blocked DNA assembly (**161/162**) with the target DNA (**163**) releases the functional DNA blocker unit (**162**) by a strand-displacement reaction while generating the DNA duplex (**161/163**) and concomitant assembly of the DNA blocker unit (**162**) into a DNA hairpin

structure that includes the catalytically active hemin/G-quadruplex HRP-mimicking DNAzyme as a biocatalytic label. The Exo III-stimulated “digestion” of the 3'-end of the DNA duplex (**161/163**) resulted in regeneration of the target DNA (**163**), which initiated autonomous separation of the DNA duplex assembly (**161/162**) and the continuous generation of the HRP-mimicking DNAzyme units. The later DNAzyme catalyzed the H_2O_2 -mediated oxidation of 2',7'-dichlorodihydrofluorescein diacetate (H_2DCFDA) to the fluorescent dye, 2',7'-dichlorofluorescein (DCF), and provided a fluorescence readout signal for the sensing process, Figure 38B. The method enabled detection of a target DNA (**163**) with a detection limit corresponding to 100 fM. The isothermal Exo III-stimulated regeneration of the target DNA was further implemented for amplified electrochemical analysis of a nucleic acid target on the surface,^{78e} Figure 38C. A functional thiolated nucleic acid (**165**) was assembled on a Au electrode, and the blocker units (**166**) that included a complementary sequence (domain *a*) to **165** and two single-stranded tethers *b* and *c* were hybridized to **165**. The domain *d* in **165** included the G-quadruplex sequence in a caged catalytically inactive configuration. The target nucleic acid (**164**) hybridized with the tether sequence *b* of blocker (**166**), leading to a complete 3'/5' duplex end. In the presence of Exo III, hydrolytic cleavage of blocker (**166**) proceeds, leading to release (regeneration) of the target (**164**), digestion of domain *a* of blocker (**166**), and release of the tether *c* that is an analog of the target. This process uncages the G-quadruplex sequence of blocker (**166**). The regenerated target and released target analog provide then a cyclic amplification for autonomous cleavage of the DNA duplexes (**165/166**) associated with the Au surface. The binding of hemin to the resulting surface-bound G-quadruplexes and the electrical response of the resulting hemin/G-quadruplexes provide the readout signal for the sensing events. The method enabled analysis of the target DNA with a detection limit corresponding to 0.5 pM.

While the previous examples demonstrated enzyme-mediated generation of the catalytic DNAzyme, the opposite activation of an enzyme by a DNAzyme is also possible. A Pb^{2+} -ion detection platform made use of the Pb^{2+} -dependent DNAzyme that was coupled to the isothermal Exo III regeneration process,^{288b} Figure 38D. The Pb^{2+} -dependent DNAzyme sequence (**167**) cleaved the substrate (**168**) to fragments *a* and *b*. The F/Q-functionalized hairpin structure (**169**) included a recognition sequence for fragment *a*. Opening of the hairpin (**169**) by fragment *a* yielded duplex *a/169*, where the 3'-end of **169** and the 5'-end of *a* generated an intact duplex. The Exo III-stimulated selective digestion of the strand (**169**) recycled strand *a* that further opened the hairpin probe, thus providing an amplification path for sensing Pb^{2+} . The system enabled analysis of Pb^{2+} with a detection limit corresponding to 2.0 pM.

Also, the isothermal amplified detection of histidine using the L-histidine-dependent RNA-cleavage DNAzyme for activation of a nicking enzyme as a secondary amplification path,²⁸⁹ Figure 39A. The functionalized DNAzyme structure (**170**) is cleaved in the presence of L-histidine to the DNA subunits (**171** and **172**). The DNA fragment (**172**) opens a F/Q-functionalized DNA hairpin strand (**173**), which forms the DNA duplex structure (**172/173**). Nicking of the DNA strand (**173**) by the endonuclease (Nt.BbvC1) results in regeneration of DNA fragment (**172**) and autonomous generation of fluorescence as readout signal for the L-histidine analyte, Figure 39B. The

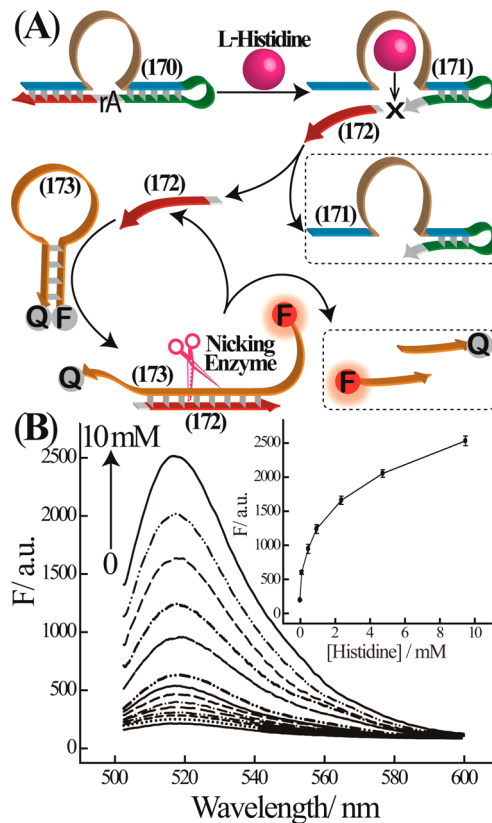


Figure 39. (A) Amplified fluorescence analysis of L-histidine by the coupled histidine-dependent DNAzyme and a nicking enzyme cascade. DNAzyme yields a fragment unit to open a F/Q-modified DNA hairpin structure that yields a functional duplex being cleaved to a fluorescent strand while releasing the fragment strand (**172**) for autonomous opening of hairpin **173**. (b) Fluorescence spectra upon analyzing different concentrations of histidine. (Inset) Derived calibration curve. Reprinted with permission from ref 289. Copyright 2011 American Chemical Society.

system enabled detection of L-histidine with a detection limit corresponding to 200 nM.

4.3. Biocatalytic Transformations Driven by Coupled Polymerase/Nicking Enzyme DNAzyme Cascades

A versatile method for amplified detection of different analytes (DNA, proteins, or ions) was developed using the coupled polymerase/nicking enzymes-stimulated generation of DNAzymes that provide the readout signal for the cascaded biocatalytic processes.^{290–293} This is exemplified in Figure 40A, with analysis of the DNA target (**174**). The sequence of the DNA scaffold (**175**) includes the recognition region *a* for DNA target (**174**), a sequence-specific domain *b*, which upon replication yields a nicking site for endonuclease (N.BbvC IA), and a domain *c* that is complementary to the G-quadruplex sequence and yields, in the presence of DNA polymerase/dNTPs/hemin, the biocatalytically active hemin/G-quadruplex HRP-mimicking DNAzyme. In the presence of the DNA target (**174**), the DNA polymerase/dNTPs mixture, replication of the DNA template (**175**) proceeds. The nicking sequence in the replicated domain *b'* is cleaved by the endonuclease (N.BbvC IA). The cleaved site initiates the secondary replication of the DNA template (**175**) while displacing and releasing the replicated HRP-mimicking DNAzyme sequence. As a result, the isothermal autonomous replication/nicking and displacement of the DNAzyme unit proceeds, leading to colorimetric

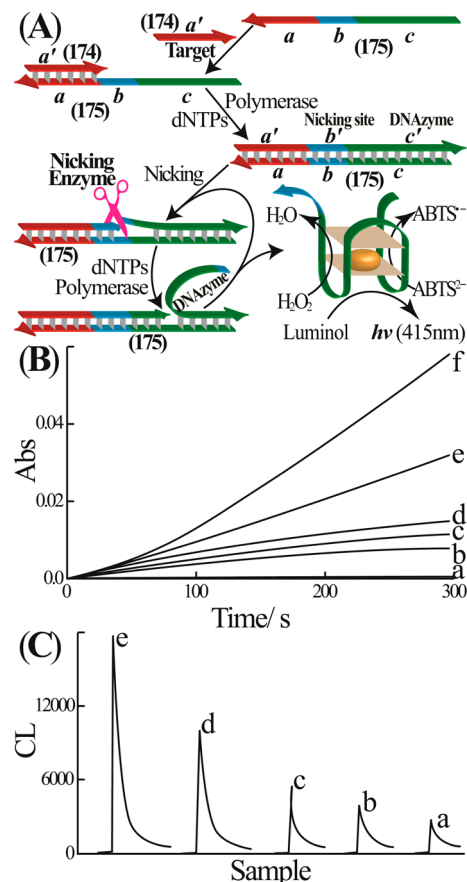


Figure 40. (A) Colorimetric or chemiluminescence amplified detection of a target DNA by the isothermal autonomous polymerization/nicking machinery and displacement of the hemin/G-quadruplex DNAzyme as readout biocatalyst. (B) Time-dependent absorbance changes upon analyzing different concentrations of a target DNA according to A through the DNAzyme-catalyzed oxidation of ABTS²⁻ by H₂O₂. (C) Chemiluminescence intensities generated upon analyzing different concentrations of the target DNA according to A using the DNAzyme-catalyzed oxidation of luminol by H₂O₂. Concentrations of the target DNA for B and C correspond to (a) 1×10^{-8} M foreign calf thymus ssDNA and (b) 1×10^{-14} , (c) 1×10^{-12} , (d) 1×10^{-10} , (e) 1×10^{-8} , and (f) 1×10^{-6} M. Reprinted with permission from ref 290. Copyright 2006 Wiley-VCH.

detection of the target DNA (174) through the DNAzyme-catalyzed oxidation of ABTS²⁻ by H₂O₂ to the colored product ABTS^{•-} ($\lambda_{\text{max}} = 415$ nm), Figure 40B, or through DNAzyme-catalyzed oxidation of luminol by H₂O₂ and generation of chemiluminescence,²⁹⁰ Figure 40C. Amplified detection of a DNA target through the isothermal autonomous replication DNAzyme machinery displayed in Figure 40A was further extended to a versatile sensing configuration, where the DNA template of the DNA machine is retained constant and includes a tandem recognition sequence. A coadded DNA hairpin structure that includes in its loop domain a target-specific recognition probe sequence and in its stem a conserved sequence complementary to the tandem region, *a*, of the machinery template activates the isothermal autonomous replication/nicking of DNAzyme machinery. Thus, opening of the coadded tailored DNA hairpin structure by the respective analyte target triggered on the autonomous amplification DNA machinery and the cascaded DNAzyme catalytic reaction, and yielded the colorimetric/chemiluminescence readout signals for

detection of the respective targets. The method enabled analysis of a DNA target (M13 phage) with a sensitivity corresponding to 10 fM.²⁹⁰

The isothermal autonomous replication/nicking machinery that synthesizes the DNAzyme reporting units suffers, however, from a basic limitation. Since the concentration of the sensing DNA template is substantially higher than that of the analyte, the displaced DNAzyme sequences may bind to “empty” template units rather than assembling into the catalytically active DNAzyme reporter nanostructures. This leads to long detection time intervals that require accumulation of “free” catalytically active DNAzyme nanostructures. This limitation as well as the improvement of the sensitivity of the sensing machinery were addressed by modifying the DNA template structure and using DNA blocker units that prohibit undesired binding of the displaced DNAzyme sequences,²⁹¹ Figure 41. Region *c* of the template DNA (176) was elongated with the sequence *a* complementary to the analyte DNA. The resulting domain *c-a* of template strand 176 was blocked with the nucleic acid (177), where the complementary domain *c'* consists of the Mg²⁺-dependent DNAzyme. In the presence of the target analyte (178), the isothermal autonomous polymerization/nicking machinery and subsequent release of the unperturbed Mg²⁺-dependent DNAzyme nanostructures (177) was activated. The generated Mg²⁺-dependent DNAzyme cleaved the fluorophore/quencher-functionalized substrate (179), resulting in a fluorophore-labeled fragmented nucleic acid that provides a fluorescence signal. The displaced Mg²⁺-dependent DNAzyme unit includes, however, following the design of the blocker units, a tether sequence consisting of *a'* (the target sequence). This process replicates the DNA target sequence, thus activating the exponential, isothermal, autonomous, synthesis of the Mg²⁺-dependent DNAzyme units for amplified detection of the target DNA. This amplification machinery enabled detection of the target DNA with a detection limit that corresponded to 1.0 aM. This one-pot amplification machinery was generic and further adapted to construct the amplified aptamer sensing schemes, e.g., for cocaine, by introducing an additional aptamer-functionalized template into the present system.²⁹¹

The polymerization/nicking machinery generating a DNAzyme unit on tailored DNA scaffolds, as an isothermal amplification scheme, was extended to follow the DNA-methylation enzyme, methyltransferase (MTase),^{294a} Figure 42. MTase catalyzes methylation of cytosine bases in sequence-specific DNA domains, and it is important in controlling epigenetic processes that regulate cell functions by altering gene expression.²⁹⁵ The DNA machinery template strand (180) was hybridized with a reporter DNA hairpin nanostructure (181) that included the MTase-specific methylation sequence. The resulting methylated DNA sequence was then cleaved off by the endonuclease (DpnI) to yield the fragmented product strand (182) that hybridized with the scaffold DNA (180). The DNA polymerase/dNTPs-mediated replication of the DNA template (180) yielded the nicking domain, thus triggering on the replication/nicking DNA machinery and isothermal autonomous replication/displacement of the HRP-mimicking hemin/G-quadruplex DNAzyme sequence. The DNAzyme-catalyzed oxidation of ABTS²⁻ by H₂O₂ yields the colored product ABTS^{•-} that enabled quantitative colorimetric detection of MTase. The method enables analysis of MTase with a detection limit corresponding to 0.25 units·mL⁻¹. A related system that combines the endonuclease/RCA polymerization/nicking

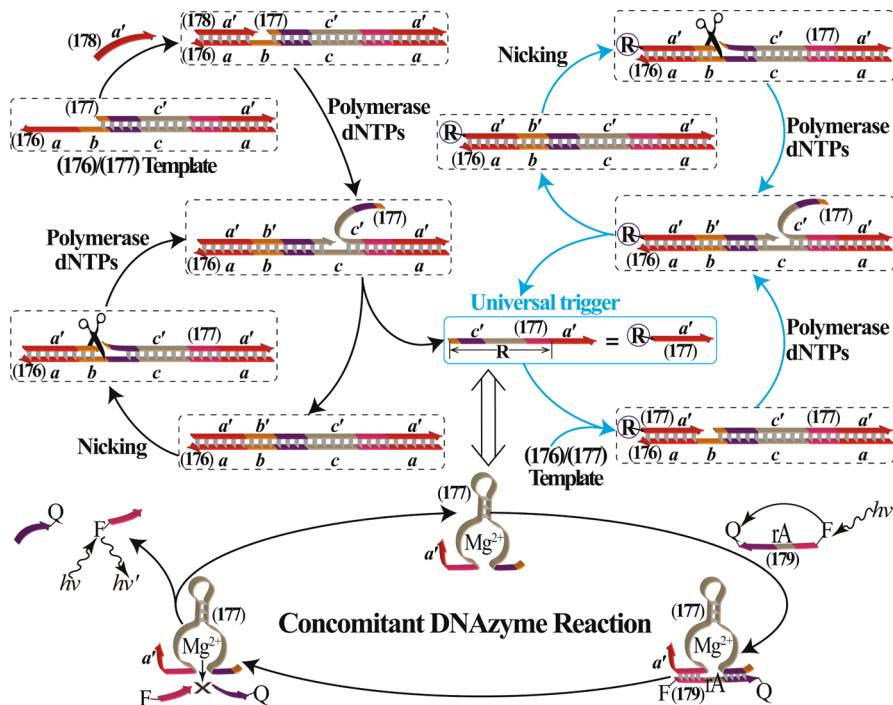


Figure 41. Autonomous, isothermal, amplified detection of DNA using a blocked nanoengineered DNA template and the polymerization/nicking enzyme/DNAzyme machinery as amplification route. Replication/nicking machinery displaces the blocker sequence, resulting in activation of the Mg^{2+} -dependent DNAzyme that cleaves the fluorophore/quencher-functionalized substrate to a fluorophore-labeled nucleic acid fragment that provides a fluorescence readout signal for the one-pot sensing process. Displaced nucleic acid includes, besides the DNAzyme sequence, a tethered domain *a'* that is identical to the analyte sequence. As a result, exponential activation of the synthesis of the reporting DNAzyme units is demonstrated. Reprinted with permission from ref 291. Copyright 2013 American Chemical Society.

cascade and the HRP-mimicking DNAzyme was applied as biocatalytic series of reactions for amplified detection of MTase,^{294b} Figure 42B. The hairpin probe H_p (183) underwent methylation by MTase to yield the methylated product H_M (184), and this was subsequently cleaved, in the stem region, by the endonuclease, Dpn I, to fragment the hairpin to three units I, II, and III. The single-stranded, methyl-substituted strand I triggered on the RCA process on a circular template (185) that included the complementary sequence to yield a replicated chain consisting of the G-quadruplex sequence and a nicking domain for Nb.BsmI enzyme. Thus, the isothermal RCA process led to autonomous self-assembly of the hemin/G-quadruplex DNAzyme as chemiluminescence reporting units in the presence of luminol/ H_2O_2 and to the nucleic acid fragments that continuously activated the RCA process on the circular template units. The method enabled amplified detection of the MTase activity with a detection limit of $130 \mu\text{U}\cdot\text{mL}^{-1}$.

Systems consisting of isothermal autonomous polymerase/endonuclease-stimulated replication/nicking of the HRP-mimicking DNAzyme machinery were also applied to develop a sensitive amplified detection platform for Hg^{2+} ions.²⁹³ Mercury ions act as common environmental pollutants, and their accumulation in the human body through the food chains causes brain damage and other chronic diseases.²⁹⁶ Hence, the rapid and sensitive detection of Hg^{2+} ions in water, food, or human fluids has substantial significance. Figure 43A depicts the Hg^{2+} ions sensing platform using the functional nucleic acid template (186). This includes the Hg^{2+} ions recognition sequence *a* and the functional DNA domains *b* and *c* that yield upon replication the nicking site and the HRP-mimicking DNAzyme sequence, respectively. In the presence of Hg^{2+} ions,

the DNA domain *a* folds into an intramolecular T– Hg^{2+} –T bridged DNA hairpin structure that provides the active 3'-end site for replication of the scaffold in the presence of DNA polymerase/dNTPs mixture. Replication of the DNA template (186) yields the N.BbVC IA nicking site *b'*, which upon cleavage provides the opening for the secondary continuous replication of the template, with concomitant displacement and release of the G-quadruplex sequence, which in the presence of hemin self-assembles into the catalytically active hemin/G-quadruplex HRP-mimicking DNAzyme. Isothermal autonomous synthesis of the HRP-mimicking DNAzyme and subsequent DNAzyme-catalyzed oxidation of ABTS²⁻ by H_2O_2 to the colored product ABTS^{•+} ($\lambda_{\max} = 415 \text{ nm}$) provide two complementary amplification paths for colorimetric detection of Hg^{2+} ions, Figure 43B. The method enabled selective analysis of Hg^{2+} ions with a detection limit corresponding to 1.0 nM.

4.4. Coupled Ligation-Triggered DNAzyme Cascades

While previous sections have implemented the cleavage enzymes for isothermal autonomous synthesis of DNAzymes for amplified detection of DNA targets, proteins, or small molecules, one may apply the ligase-stimulated coupling of nucleic acid subunits as a means to synthesize DNAzyme structures and to apply the ligase/DNAzyme coupled biocatalytic cascades for developing amplified sensing platforms.²⁹⁷ This has been exemplified with the development of an amplified ATP sensing platform, Figure 44A. The nucleic acid (187) acts as a template for the association of two functionalized oligonucleotides 188 and 189. In the presence of the ATP-dependent ligase, coupling of the two DNA subunits to the ligated DNA product (190) occurred. Strand

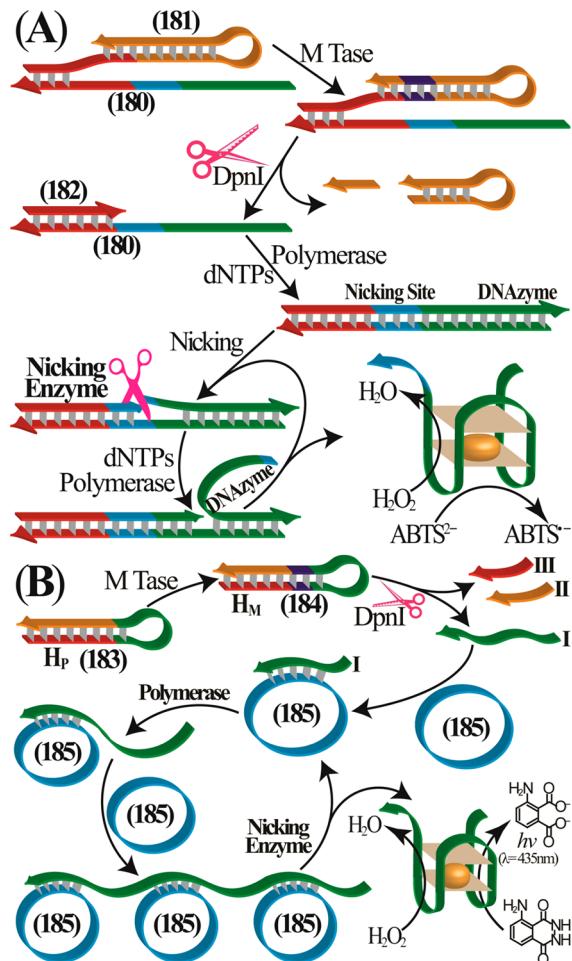


Figure 42. (A) Following the activity of MTase by a coupled endonuclease (DpnI)-polymerase/nicking enzyme-hemin/G-quadruplex DNAzyme cascade. Reprinted with permission from ref 294a. Copyright 2010 American Chemical Society. (B) Amplified analysis of MTase by methylation of hairpin H_P and its fragmentation by the DpnI endonuclease. The resulting fragment acts as an initiator for isothermal autonomous activation of the RCA process that lead to recycling of the RCA initiator and formation of the hemin/G-quadruplex DNAzyme as chemiluminescence reporter units. Reprinted with permission from ref 294b. Copyright 2013 American Chemical Society.

displacement of the template DNA strand (187) by the “helper” strand (191) releases the ligated DNA sequence (190) that corresponds to the Zn²⁺-dependent RNA-cleavage DNAzyme. In the presence of a fluorophore/quencher-modified DNA beacon nanostructure (192) that includes in its loop domain the ribonucleotide-containing substrate sequence of the Zn²⁺-dependent hydrolytic cleavage DNAzyme, the DNAzyme (190) catalyzed cleavage of functional DNA hairpin substrate structure (192). This enabled the separation of the fluorophore- and quencher-labeled DNA hairpin fragments of the DNA beacon probe (192) and provided fluorescence readout of the released ligated DNAzyme product. As the DNA ligation process is controlled by the concentration of ATP, generation of the Zn²⁺-dependent DNAzyme and thus cleavage of the DNA hairpin substrates (192) are related to the concentration of ATP. The resulting fluorescence intensities provide then a quantitative signal for analysis of ATP (detection limit 100 pM). A related ligase/DNAzyme cascade was also implemented to follow the activity of ligase,²⁹⁸ Figure 44B. A

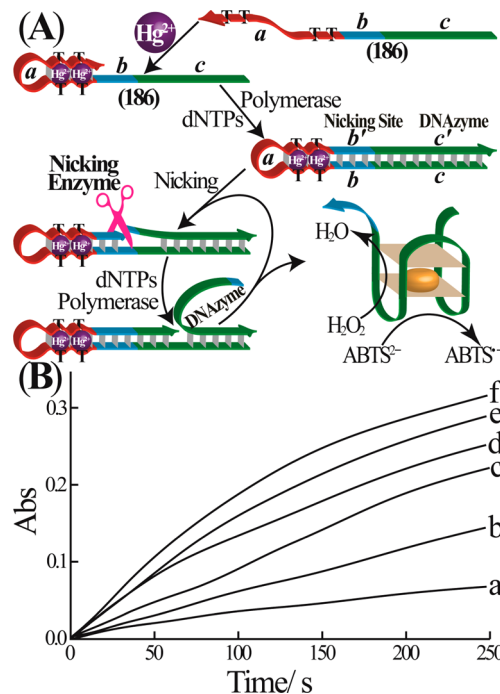


Figure 43. (A) Detection of Hg²⁺ ions through activation of an isothermal autonomous polymerization/nicking enzyme cascade that synthesizes the hemin/G-quadruplex DNAzyme. (B) Time-dependent absorbance changes resulting from the hemin/G-quadruplex DNAzyme-catalyzed oxidation of ABTS²⁻ by H₂O₂ to yield ABTS⁻ using different concentrations of Hg²⁺ ions: (a) hemin only and (b) 0, (c) 1 × 10⁻⁹, (d) 1 × 10⁻⁸, (e) 1 × 10⁻⁷, and (f) 5 × 10⁻⁷ M. Reprinted with permission from ref 293. Copyright 2008 Wiley-VCH.

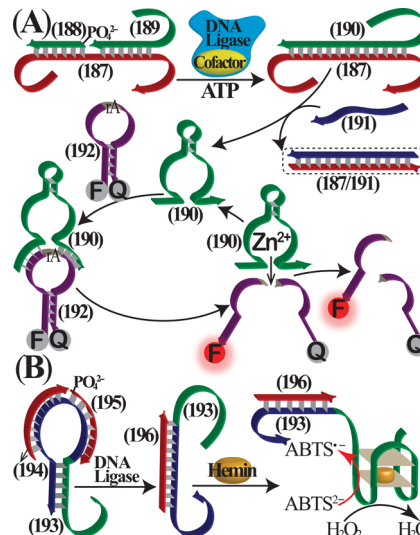


Figure 44. (A) Analysis of ATP through a coupled ligase/Zn²⁺-dependent DNAzyme cascade leading to cleavage of a fluorophore/quencher-modified DNA hairpin (192) that generates a fluorophore reporter unit. Reprinted with permission from ref 297. Copyright 2011 American Chemical Society. (B) Analysis of DNA ligase activity through ligation of two nucleic acids (194 and 195), and opening of the hairpin structure by the ligated product to yield the hemin/G-quadruplex DNAzyme as catalytic label. Reprinted with permission from ref 298. Copyright 2012 Wiley-VCH.

hairpin DNA nanostructure (193) that includes in its stem region the caged sequence of the hemin/G-quadruplex HRP-

mimicking DNAzyme was used as a functional nanostructure for probing the activity of ligase. The two nucleic acid subunits (**194** and **195**) hybridized with the single-stranded loop of the DNA hairpin probe (**193**). The ligase-induced conjugation of the two DNA strands (**194** and **195**) resulted in a complementary DNA strand (**196**) that opened the hairpin DNA structure (**193**), thus allowing self-assembly of the catalytically active hemin/G-quadruplex HRP-mimicking DNAzyme. This enabled colorimetric analysis of the activity of ligase through the DNAzyme-catalyzed oxidation of ABTS²⁻ by H₂O₂ to the colored product ABTS^{•+}. The system enabled quantitative assay of ligase with a detection limit of 0.2 units mL⁻¹.

A coupled ligation DNAzyme/nicking enzyme sensing platform for amplified detection of DNA was developed,²⁴¹ Figure 45A. The system consisted of the Zn²⁺-dependent ligation DNAzyme subunits (**98** and **101**) and the respective substrate subunits (**102** and **100**). The system also included the fluorophore/quencher-functionalized hairpin (**197**), which acts

as activator and reporter element. In the presence of the DNA analyte (**99**), the DNAzyme subunits and substrates self-assemble into structure “I”, where DNAzyme-catalyzed ligation reaction proceeds. As the reporter hairpin structure (**197**) is designed to include a complementary domain to the ligated product, strand displacement of the ligated product (**103**) proceeds, leading to the duplex structure “II” that is tailored to include the Nt.BspQI nicking domain. The nicking process leads to separation of the fluorophore-functionalized nucleic acid fragment that provides the readout signal for the sensing process, Figure 45B. The target-stimulated regeneration of the ligation DNAzyme and subsequent cleavage of the duplex DNA structure “II” by the nicking reaction provide the catalytic cascade for amplified detection of the target DNA.

4.5. DNAzyme-Amplified Detection of Telomerase Activity

The telomeres caps protect eukaryotic chromosome ends against degradation or fusion.²⁹⁹ They consist of short tandem repeat units (TTAGGG), and in human somatic cells the telomeres undergo progressive shortening during cell proliferation. At a certain length of the telomeres, the cell is signaled to terminate the cell life cycle and undergoes apoptosis.^{300,301} Telomerase is a ribonucleoprotein that binds to the telomer chains while elongating the telomeres. This biocatalytic process proceeds oppositely to the natural shortening of the telomer chains, thus leading to immortal or malignant cells.^{301,302} Indeed, in over 85% of different cancer cells, elevated amounts of telomerase were detected, and it provides a versatile biomarker for cancer cells.^{303,304} Coupling of telomerase with DNAzymes provides a general means to detect telomerase extracted from cancer cells.

Figure 46A shows the chemiluminescence detection of telomerase using the hemin/G-quadruplex HRP-mimicking DNAzyme as catalytic reporting unit.¹⁹⁹ The primer DNA strand (**198**), recognized by telomerase, was assembled on a Au surface. In the presence of telomerase and the dNTPs mixture, telomerization of the primer DNA units (**198**) on the surface occurred. Hybridization of a functional nucleic acid strand (**199**), consisting of the G-quadruplex sequence and the complementary sequence to the tandem telomer repeat units, leads to a hybrid DNA nanostructure composed of the repeated telomer/G-quadruplex HRP-mimicking DNAzyme units associated with the Au surface, Figure 46A. The surface-anchored G-quadruplex sequence yields in the presence of hemin the catalytically active G-quadruplex/hemin DNAzyme structure, which catalyzes generation of chemiluminescence through oxidation of luminol by H₂O₂. As the content of telomeres and their lengths are controlled by the amount of telomerase, the coverage of the surface by the hemin/G-quadruplex HRP-mimicking DNAzyme units and the resulting chemiluminescence intensities are controlled by the content of telomerase. The method enabled detection of telomerase extracted from 1000 HeLa cancer cells, Figure 46B. The analytical platform was further amplified using AuNPs functionalized with nucleic acid chains, composed of DNA sequences complementary to the telomer repeat units, and the tethering of hemin/G-quadruplex HRP-mimicking DNAzyme catalytic reporting units.³⁰⁵

The telomer chains themselves are G-rich DNA sequences, and under appropriate conditions, the chains self-assemble into G-quadruplex nanostructures.^{306,307} The binding of hemin to these telomer G-quadruplexes resulted in catalytically active

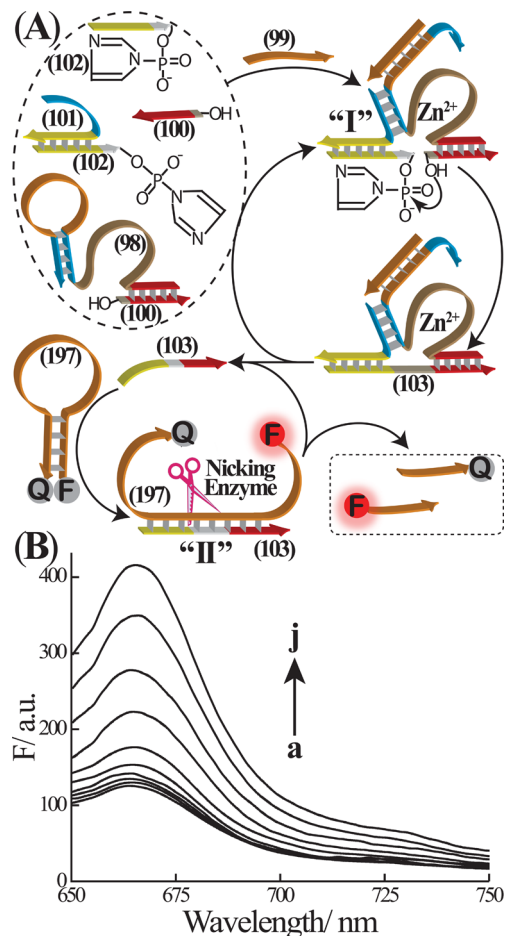


Figure 45. (A) Analysis of a target DNA through the self-assembly of the Zn²⁺-dependent ligation DNAzyme. Strand displacement of the ligated product by a fluorophore/quencher-labeled hairpin leads to a duplex structure that is nicked to regenerate the ligated product and yield a fluorophore-labeled nucleic acid fragment acting as readout signal. (B) Fluorescence spectra generated upon analyzing different concentrations of the target DNA by the system shown in A for a fixed time interval of 2 h: (a) 0, (b) 0.5, (c) 1, (d) 2, (e) 5, (f) 10, (g) 20, (h) 50, (i) 100, and (j) 200 nM. Reprinted with permission from ref 241. Copyright 2012 American Chemical Society.

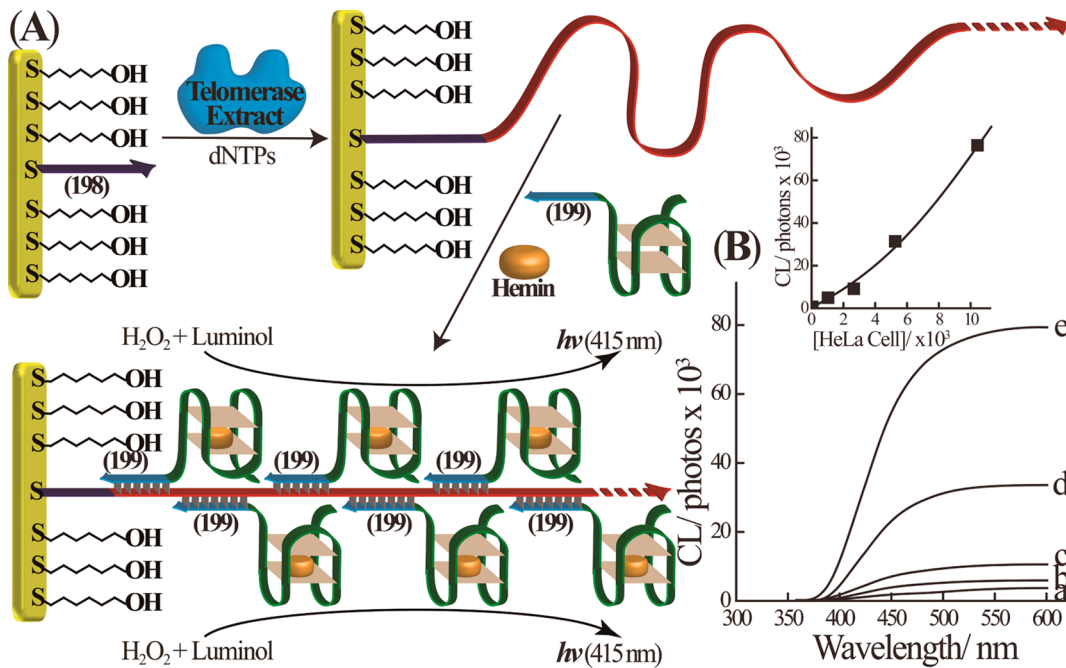


Figure 46. (A) Analysis of telomerase extracted from cancer cells through the telomerase-induced telomerization of DNA primer on a Au surface and binding of hemin/G-quadruplex DNAzyme labels to the telomer repeat units, leading to DNAzyme-catalyzed generation of chemiluminescence. (B) Chemiluminescence intensities upon analyzing telomerase extracted from different numbers of HeLa cancer cells: (a) 10 000 cells without DNAzyme labels, (b) 1000 cells, (c) 2500 cells, (d) 5000 cells, and (e) 10 000 cells. (Inset) Derived calibration curve. Reprinted with permission from ref 199. Copyright 2004 American Chemical Society.

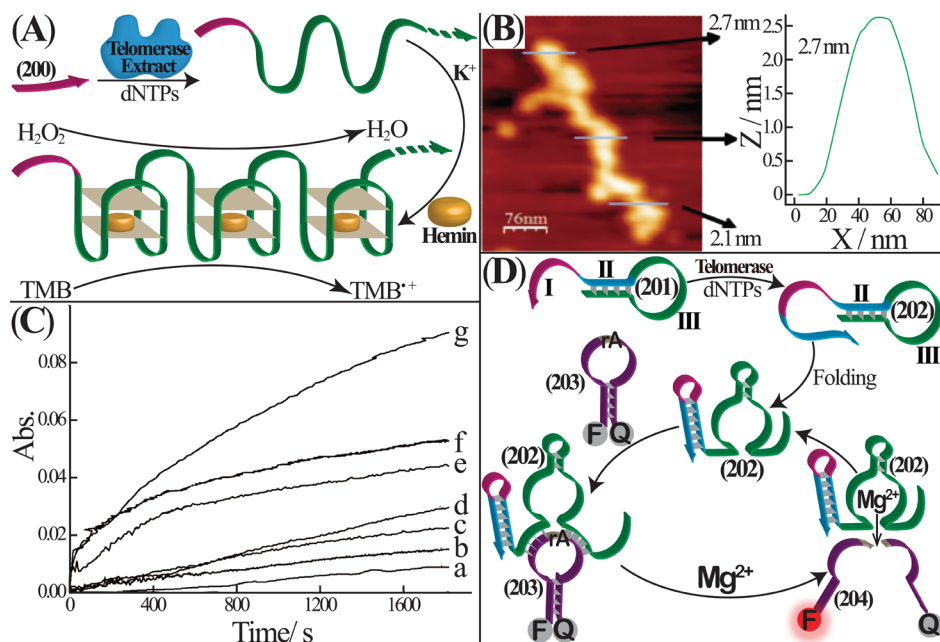


Figure 47. (A) Analysis of telomerase extracted from 293T cancer cells through telomerase-induced telomerization of a primer and self-assembly of the telomer repeat units into hemin/G-quadruplex DNAzyme catalytic units that catalyze the H₂O₂-mediated oxidation of TMB to the colored product, TMB⁺. (B) AFM image of the resulting G-quadruplex telomer nanochains. (C) Time-dependent absorbance changes upon analyzing telomerase extracted from different numbers of 293T cancer cells: (a) 200, (b) 400, (c) 800, (d) 1200, (e) 1600, (f) 2000, and (g) 3000 cells/μL. Reprinted with permission from ref 308a. Copyright 2010 Wiley-VCH. (D) Amplified fluorescence detection of telomerase activity using a telomerase-probe-modified functional hairpin structure and the Mg²⁺-dependent DNAzyme as fluorescence-generation catalyst. Telomerization process leads to the telomer chain that opens the loop region of hairpin 202 and unlocks the “caged” Mg²⁺-dependent DNAzyme sequence. Resulting DNAzyme cleaves the fluorophore/quencher-modified hairpin substrate 203, leading to the readout signal.

DNAzyme nanostructures that mimic the functions of HRP enzyme.^{308a} This feature enabled colorimetric detection of telomerase, Figure 47A. The primer DNA strand (200) was

elongated in the presence of telomerase and the dNTPs mixture to yield the telomeric chains composed of tandem repeated hemin/G-quadruplex HRP-mimicking DNAzyme

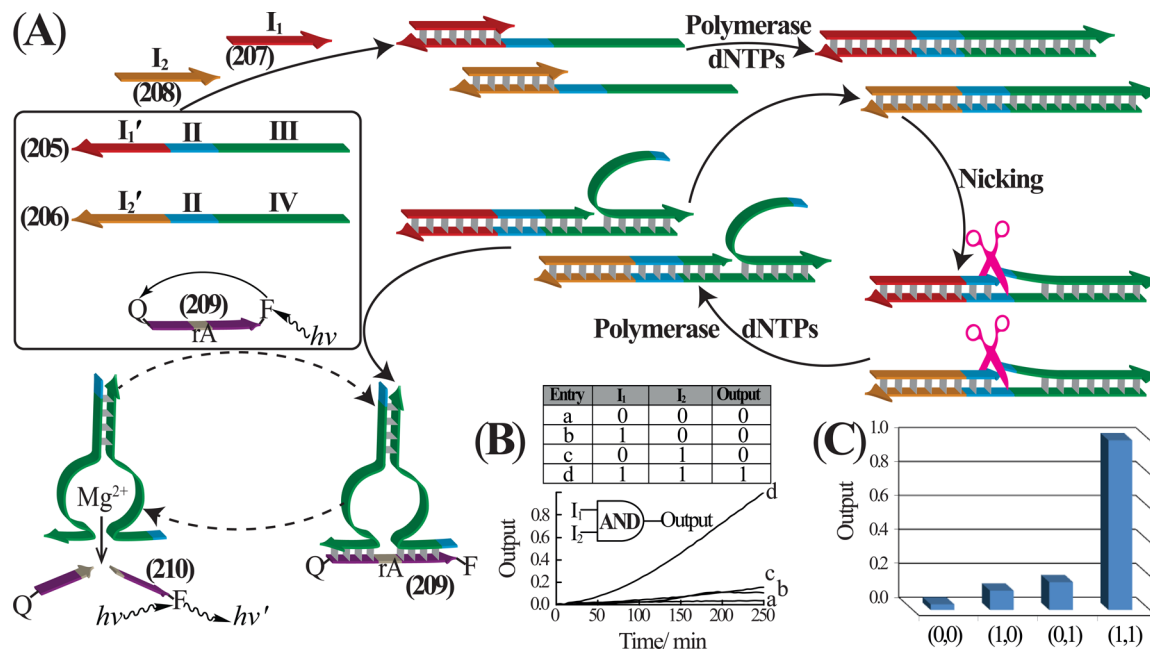


Figure 48. (A) Design of an AND logic gate by polymerase/nicking machineries activated by two inputs I_1 and I_2 that lead to displacement of the Mg^{2+} -dependent DNAzyme subunits. Cleavage of the fluorophore/quencher-labeled substrate by the self-assembled Mg^{2+} -dependent DNAzyme leads to a fluorescence output. (B) Time-dependent fluorescence changes upon activation of the system by (a) no input, (b) only I_1 , (c) only I_2 , (d) I_1 and I_2 . (Inset) Resulting truth table of the AND logic gate. (C) Fluorescence intensities generated by the AND logic gate in the form of a “bar” presentation. Reprinted with permission from ref 171. Copyright 2012 Wiley-VCH.

units. In the presence of H_2O_2 and 3,3',5,5'-tetramethylbenzidine, TMB, the DNAzyme-catalyzed oxidation of TMB by H_2O_2 to the colored product 3,3',5,5'-tetramethylbenzidine diimine, $TMB^{\bullet+}$ occurred, Figure 47A. As the concentration of the biocatalytic telomeric hemin/G-quadruplex HRP-mimicking DNAzyme units is controlled by the content of telomerase, the resulting colored oxidized product provides a quantitative readout signal for detection of telomerase. Figure 47B depicts the AFM image of the telomeric hemin/G-quadruplex DNAzyme chains, demonstrating a height of ca. 2.7 nm (as compared to the height of 1.2 nm for regular duplex DNA). Figure 47C shows the time-dependent absorbance changes upon analyzing the telomerase extracted from different numbers of HeLa cancer cells. The system enabled detection of telomerase originating from 200 HeLa cancer cells. A different approach to follow telomerase activity by a DNAzyme as amplifying label is depicted in Figure 47D.^{308b} The hairpin structure (201) includes in domain I the primer sequence recognized by telomerase and in region II a tailored sequence that is complementary to the telomer repeat units. The domain III in 201 includes the caged sequence of the Mg^{2+} -dependent DNAzyme. In the presence of telomerase/dNTPs mixture the single-stranded domain I was elongated, leading to formation of the telomer chain, and this reconfigured the hairpin structure to form, through strand displacement, the energetically stabilized hairpin (202). In the reconfigured structure (202), the Mg^{2+} -dependent DNAzyme sequence was uncaged. This led to formation of the active Mg^{2+} -dependent DNAzyme that cleaved the fluorophore/quencher-modified hairpin (203) that included in its loop region the ribonucleobase-containing substrate of the DNAzyme. The resulting fragmented fluorophore-modified substrate (204) provided the readout signal for the activity of telomerase. The method enabled analysis of telomerase from 200 HeLa cancer cells as a lower limit.

4.6. Logic Gates with Cascaded Enzyme/DNAzyme Systems

The DNA machineries that produce DNAzymes by a probe-activated isothermal autonomous replication/nicking process on DNA templates¹⁷¹ were further implemented to tailor logic gates by cascaded enzyme/DNAzyme systems, Figure 48. This is exemplified with the construction of the AND logic gate, Figure 48A. The two nucleic acid templates (205 and 206) included the recognition domains I'_1 and I'_2 for the input strands I_1 (207) and I_2 (208), respectively. Domains II in the two DNA templates were designed to generate upon replication a nicking site for Nt.BbvCI nicking enzyme. Domains III and IV of the two DNA templates included tailored sequences that upon replication generate, each, a subunit of the Mg^{2+} -dependent DNAzyme. In the presence of the two inputs, I_1 and I_2 , polymerase/dNTPs mixture and nicking enzyme (Nt.BbvCI), the DNA machinery was activated, resulting in displacement of the Mg^{2+} -dependent DNAzyme subunits. The supramolecular assembly of the DNAzyme subunits into the catalytically active DNAzyme nanostructure resulted in catalytic cleavage of a F/Q-labeled substrate (209), where the resulting fluorophore (F)-labeled DNA fragment (210) provided the output signal for the AND gate, Figure 48B. Using a similar approach, an OR gate and a controlled AND gate were designed.¹⁷¹

5. ENZYME–NUCLEIC ACID SYSTEMS FOR CONTROLLED CHEMICAL PROCESSES

Intracellular multienzyme biocatalytic or biosynthetic pathways reveal unique features reflected by efficient reaction yields, elimination of cross-talks between signaling pathways, and programmed sequential cascaded chemical transformations that are often accompanied by thresholding or feedback mechanisms.³⁰⁹ These unique features originate from the physical and spatial ordering of the biocatalysts in confined regions of the

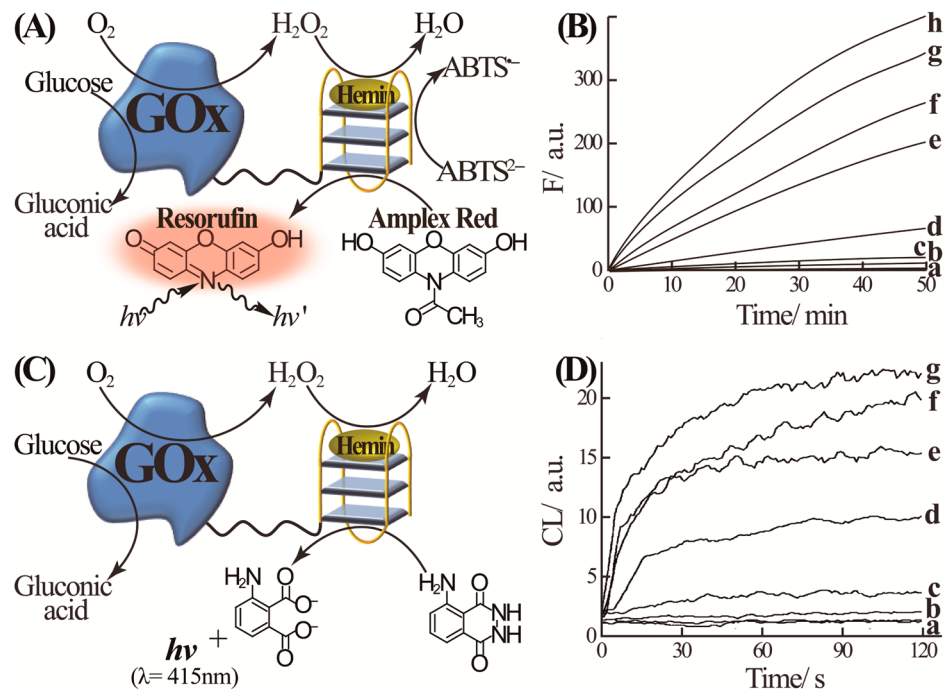


Figure 49. (A) Glucose oxidase (GOx)/hemin/G-quadruplex DNAzyme catalytic cascade. (B) Time-dependent fluorescence changes upon DNAzyme-catalyzed oxidation of Amplex Red to Resorufin by the catalytic cascade shown in A using different concentrations of glucose: (a) 0, (b) 5, (c) 15, (d) 25, (e) 75, (f) 100, (g) 150, and (h) 200 μM . Reprinted with permission from ref 104. Copyright 2011 Royal Society of Chemistry. (C) Generation of chemiluminescence by the GOx/hemin/G-quadruplex DNAzyme catalytic cascade. (D) Time-dependent chemiluminescence changes generated by the GOx/hemin/G-quadruplex DNAzyme cascade in the presence of different concentrations of glucose: (a) 0 μM , (b) 5 μM , (c) 50 μM , (d) 0.5 mM, (e) 5 mM, (f) 10 mM, and (g) 20 mM. Reprinted with permission from ref 105. Copyright 2007 Elsevier.

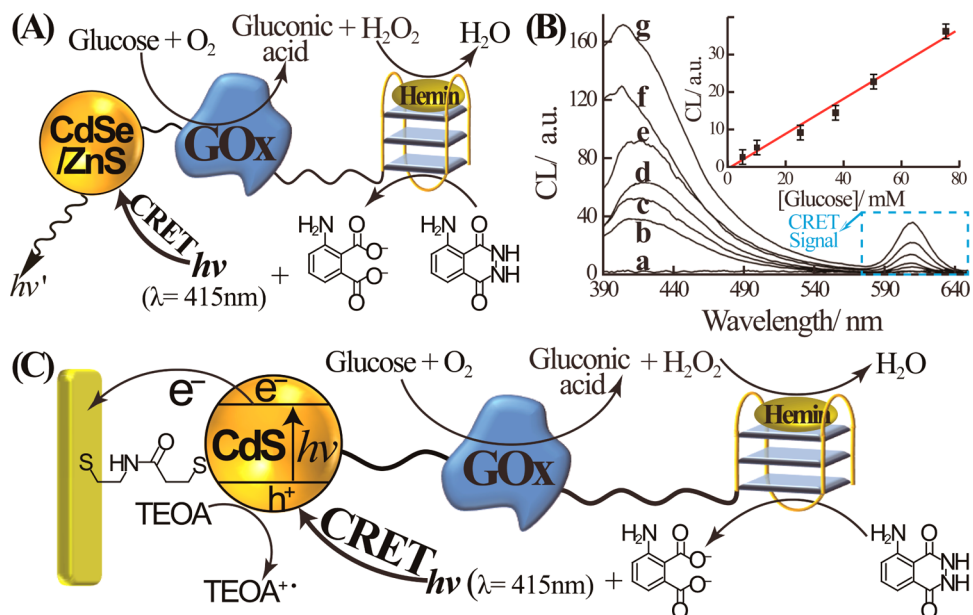


Figure 50. (A) Analysis of glucose by a GOx/hemin/G-quadruplex assembled on CdSe/ZnS quantum dots (QDs). Glucose-mediated generation of chemiluminescence by the GOx/DNAzyme cascade stimulates a chemiluminescence resonance energy transfer (CRET) process that triggers luminescence of the quantum dots. (B) CRET-stimulated luminescence of the QDs upon analyzing different concentrations of glucose according to A: (a) 0 μM , (b) 5 mM, (c) 10 mM, (d) 25 mM, (e) 37 mM, (f) 50 mM, and (g) 75 mM. (Inset) Resulting calibration curve. Reproduced with permission from ref 312. (C) Photoelectrochemical detection of glucose by the CRET-stimulated excitation of Cds QDs by the GOx/hemin/G-quadruplex DNAzyme biocatalytic cascade. Reprinted with permission from ref 313. Copyright 2012 American Chemical Society.

cell compartments. Thus, efforts to mimic intracellular biocatalytic processes should spatially organize the biocatalysts on nanoengineered scaffolds that enable intercatalyst communication and cascaded biotransformations.³¹⁰ In this section we

will discuss the programmed positioning of enzymes or enzymes/DNAzymes on nucleic acid scaffolds that act as organizing matrices for controlled sequential biocatalytic cascades.

5.1. Coupled Enzyme–DNAzyme Processes

Coupling of DNAzymes with enzymes yields hybrid systems that may combine the functionalities of both components. Specifically, covalent attachment of a DNAzyme to a protein–enzyme may lead to chemical communication between the biocatalytic units, that is, the product of one catalyst unit may act as the substrate of the second catalytic unit, thus activating a catalytic cascade. The linkage of the enzyme/DNAzyme pairs might provide an organized nanostructure where localized concentrations of the intercommunicating product/substrate are present. This has been demonstrated by the covalent linkage of the hemin/G-quadruplex HRP-mimicking DNAzyme to glucose oxidase (GOx),¹⁰⁴ Figure 49A. Biocatalyzed oxidation of glucose yielded gluconic acid and H₂O₂, and the resulting H₂O₂ acted as substrate for the hemin/G-quadruplex DNAzyme-catalyzed oxidation of Amplex Red to the fluorescent product, Resorufin. Also, the glucose/GOx-generated H₂O₂ provided the H₂O₂ for the hemin/G-quadruplex DNAzyme-catalyzed oxidation of ABTS^{•-} to the colored product ABTS^{•+} ($\lambda_{\text{max}} = 415 \text{ nm}$). These cascades enabled fluorescence or colorimetric detection of glucose, Figure 49B. Alternatively, the GOx-generated H₂O₂ provided a cosubstrate for activation of the hemin/G-quadruplex DNAzyme-catalyzed generation of chemiluminescence in the presence of luminol,¹⁰⁵ Figure 49C. As the concentration of H₂O₂ was controlled by the concentration of glucose, the resulting chemiluminescence intensities were related to the concentration of glucose, Figure 49D. The system enabled analysis of glucose with a detection limit corresponding to 5 μM .

The chemiluminescence generated by the hemin/G-quadruplex HRP-mimicking DNAzyme linked to semiconductor quantum dots (QDs), such as CdSe/ZnS QDs, was found to stimulate a chemiluminescence resonance energy transfer (CRET) process to the QDs, resulting in the luminescence of the QDs without external irradiation.^{135,311} This property was used to develop functionalized QDs for the CRET-based detection of glucose,³¹² Figure 50A. The hemin/G-quadruplex DNAzyme was covalently tethered to GOx, and the biocatalytic hybrid was covalently linked to the CdSe/ZnS QDs. The GOx-catalyzed oxidation of glucose generated gluconic acid and H₂O₂. The latter product acted as cosubstrate for the DNAzyme-catalyzed oxidation of luminol, leading to generation of chemiluminescence. The resulting CRET process to the QDs triggered on the luminescence of the QDs. As the concentration of H₂O₂ is controlled by the concentration of glucose, the resulting CRET signal provided a quantitative readout signal of the glucose concentrations, Figure 50B. The CRET process was further implemented for development of a photoelectrochemical glucose biosensor, with no external irradiation,³¹³ Figure 50C. The GOx/hemin/G-quadruplex hybrid was covalently linked to CdS QDs associated with a Au electrode. The GOx-catalyzed oxidation of glucose by O₂ yields gluconic acid and H₂O₂, and the resulting hemin/G-quadruplex DNAzyme-catalyzed generation of chemiluminescence activates the CRET process to the QDs. The internal photoexcitation of the QDs resulted in ejection of the conduction-band electrons to the electrode, while the valence-band holes were scavenged by the sacrificial triethanolamine, TEOA, electron donor. This sequence of electron-transfer steps resulted in formation of a steady-state photocurrent without external irradiation. The intensities of the photocurrents were related to the intensities of the

chemiluminescence signals, and these were controlled by the concentrations of glucose.

The hemin/G-quadruplex DNAzyme was found not only to act as a HRP-mimicking DNAzyme but also to function as a NADH oxidase DNAzyme and as a NADH peroxidase DNAzyme.^{222a} Under anaerobic conditions, the hemin/G-quadruplex DNAzyme catalyzed the oxidation of NADH to NAD⁺ by H₂O₂. Accordingly, the hemin/G-quadruplex DNAzyme could be coupled to the NAD⁺-dependent enzyme alcohol dehydrogenase (AlcDH) to trigger the biocatalytic NAD⁺-mediated oxidation of ethanol to acetaldehyde using H₂O₂ as oxidant, Figure 51A. Under aerobic conditions the hemin/G-quadruplex demonstrated NADH oxidase activities

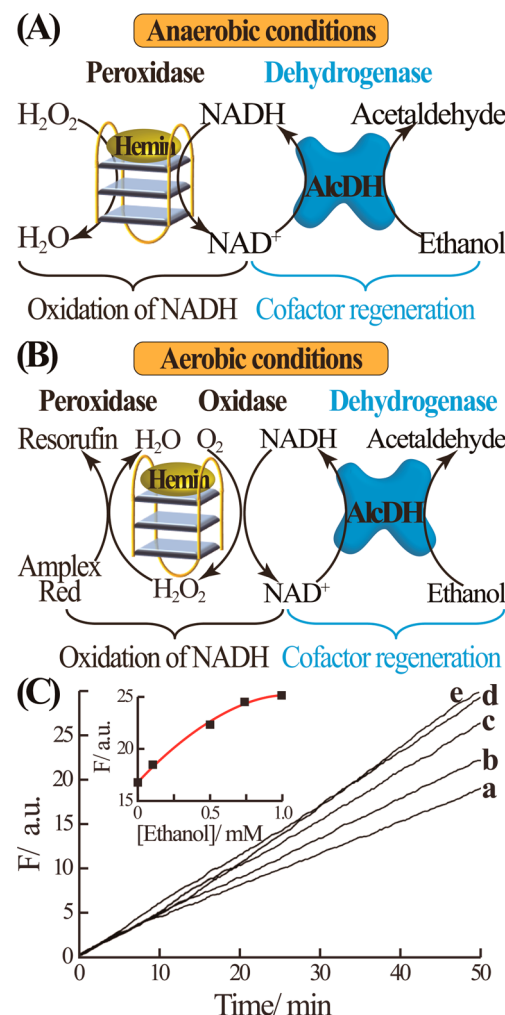


Figure 51. (A) Activation of a hemin/G-quadruplex/alcohol dehydrogenase (AlcDH) cascade, under anaerobic conditions, where H₂O₂ oxidizes ethanol to acetaldehyde. Hemin/G-quadruplex acts as DNAzyme-mimicking NADH peroxidase. (B) Activation of a hemin/G-quadruplex/AlcDH cascade under aerobic conditions where the hemin/G-quadruplex acts as a DNAzyme-mimicking NADH oxidase and as a HRP-mimicking DNAzyme. Peroxidase activity of the DNAzyme leads to oxidation of Amplex Red to the fluorescent product Resorufin that provides the readout signal for the biocatalytic cascade. (C) Time-dependent fluorescence changes upon analyzing different concentrations of ethanol by the biocatalytic cascade shown in B: (a) 0, (b) 0.1, (c) 0.5, (d) 0.75, and (e) 1 mM. (Inset) Derived calibration curve. Reprinted with permission from ref 222a. Copyright 2011 Wiley-VCH.

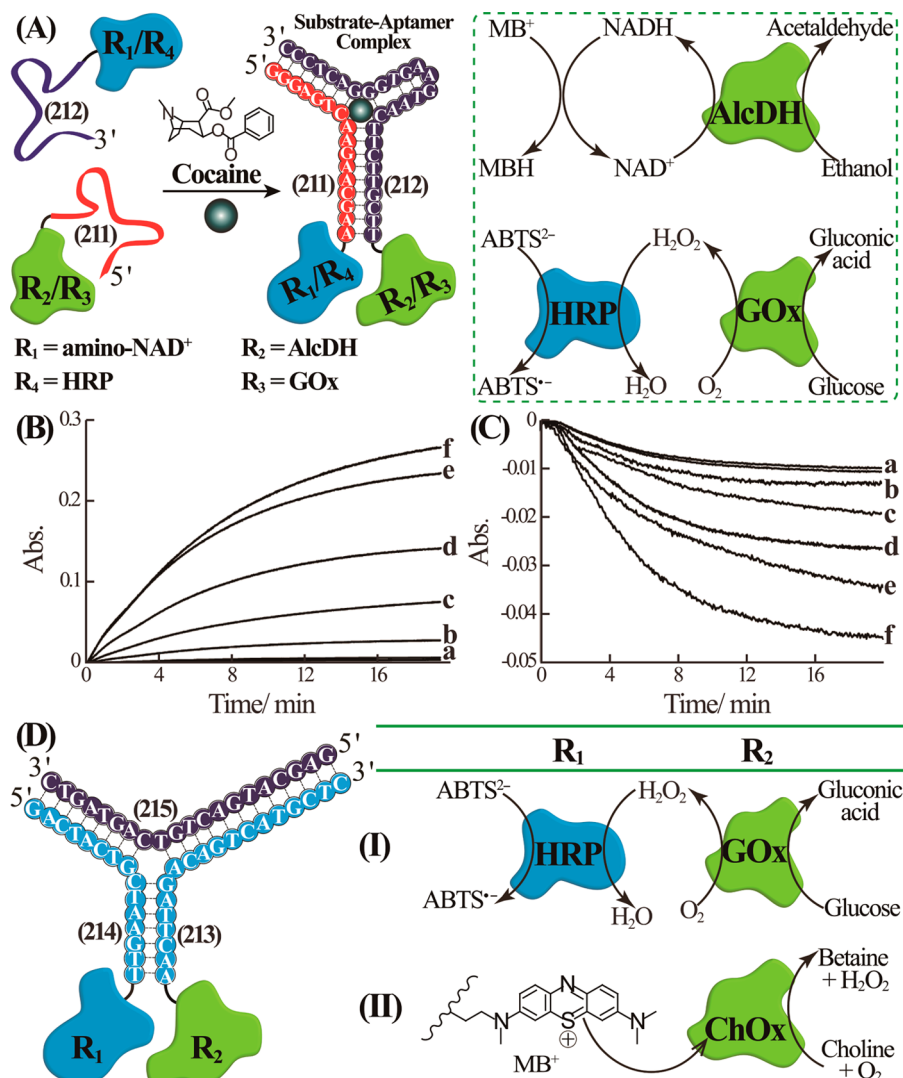


Figure 52. (A) Activation of a bienzyme cascade (glucose oxidase/horseradish peroxidase, GOx/HRP) or an enzyme/cofactor cascade (NAD⁺/alcohol dehydrogenase, NAD⁺/AlcDH) using the cocaine-induced assembly of cocaine–aptamer subunits carrying the components of the catalytic cascades. These cascades are applied for sensing of cocaine. (B) Time-dependent absorbance changes upon analyzing different concentrations of cocaine by the GOx/HRP cascade. (C) Time-dependent absorbance changes upon analyzing different concentrations of cocaine by the NAD⁺/AlcDH cascade. Concentrations of the cocaine for B and C correspond to (a) 0, (b) 5×10^{-7} , (c) 1×10^{-6} , (d) 1×10^{-5} , (e) 1×10^{-4} , and (f) 1×10^{-3} M. Reprinted with permission from ref 102. Copyright 2009 American Chemical Society. (D) (I) Activation of the GOx/HRP cascade by a Y-shaped DNA nanostructure carrying the biocatalysts. (II) Probing the inhibition of choline oxidase (ChOx) by methylene blue (MB⁺) by implementation of a Y-shaped DNA carrying the inhibitor and ChOx. Reprinted with permission from ref 103. Copyright 2010 Wiley-VCH.

and simultaneous HRP activities, Figure 51B. In this system, the hemin/G-quadruplex DNAzyme was coupled to alcohol dehydrogenase, AlcDH, acting as an enzymatic NADH regeneration biocatalyst. In the presence of AlcDH and ethanol biocatalytic oxidation of ethanol to acetaldehyde proceeded while generating the reduced NADH cofactor. The hemin/G-quadruplex catalyzed then oxidation of NADH to NAD⁺ while producing H₂O₂ as coproduct, thus revealing NADH–oxidase activities. The hemin/G-quadruplex acted, further, as the HRP-mimicking DNAzyme that catalyzed the H₂O₂-mediated oxidation of Amplex Red to the fluorescent product Resorufin. As the concentration of H₂O₂ is controlled by the concentration of ethanol, the resulting fluorescence signals are related to the concentrations of ethanol, Figure 51C. The discovery that the hemin/G-quadruplex DNAzyme acts as an effective catalyst for regeneration of the NAD⁺ cofactor has important implications for future implementation of this

DNAzyme in biotechnological biotransformations that involve regeneration of the NAD⁺ cofactor.

5.2. Controlling Enzyme Functions on Nucleic Acid Scaffolds

Hybridization of nucleic acids or the recognition and binding properties of nucleic acids (aptamers) might be used to organize enzymes on DNA scaffolds and thereby control their activities. This might include the spatial organization of enzymes to activate biocatalytic cascades and the structural organization of cofactor–enzyme units or inhibitor–enzyme units for controlling biocatalytic functions. Activation of an enzyme cascade of the two enzymes glucose oxidase, GOx, and horseradish peroxidase, HRP, was demonstrated using an aptamer–substrate (cocaine) complex as template for activation of the biocatalytic cascade,¹⁰² Figure 52A. This biocatalytic cascade was used as a reporter module for the sensing of cocaine. Enzymes GOx and HRP were chemically modified

with the anticocaine aptamer subunits (**211** and **212**), respectively. While in the absence of cocaine, the two biocatalysts are separated and the two enzymes lack interenzyme communication, formation of the cocaine–aptamer subunits complex brings the two enzymes into close proximity. As a result, the GOx-mediated oxidation of glucose by O₂ yields H₂O₂ and gluconic acid. The resulting H₂O₂ acts as cosubstrate for the HRP unit that catalyzes oxidation of ABTS²⁻ by H₂O₂ to yield the colored product ABTS^{•+} ($\lambda_{\text{max}} = 415 \text{ nm}$). The high local concentration of H₂O₂ at the adjacent HRP site leads to effective oxidation of ABTS²⁻ to the colored product ABTS^{•+}. Accordingly, activation of the bienzyme cascade was controlled by the concentration of cocaine that yielded through the cocaine–aptamer complex the programmed nanostructure of the two enzymes, Figure 52B. In a related system, the cocaine–aptamer subunits complex was used to stimulate the NAD⁺-dependent activation of alcohol dehydrogenase, AlcDH.¹⁰² The aptamer subunits (**211** and **212**) were covalently linked to AlcDH and the synthetic N⁶-(2-aminoethyl)-nicotinamide adenine dinucleotide, amino-NAD⁺, cofactor. While the AlcDH-mediated oxidation of ethanol, in the presence of the diffusional cofactor, was inefficient, the organization of the enzyme/cofactor units in close proximity, by means of the cocaine–aptamer subunits complex, led to effective biocatalyzed oxidation of ethanol to acetaldehyde with concomitant generation of the reduced NADH cofactor. The secondary reduction of methylene blue, MB⁺, by the reduced NADH cofactor enabled the cyclic, effective biocatalytic oxidation of ethanol, and it provided a colorimetric readout signal for the aptamer-stimulated biocatalytic reactions, Figure 52C.

The enzyme functions were also controlled by means of the organization of the biocatalytic units on duplex DNA structures. The control of two biocatalytic systems by supramolecular Y-shaped DNA structures was demonstrated.¹⁰³ In one system, I, the two enzymes, GOx and HRP, were modified with the nucleic acids (**213** and **214**), respectively, and the two nucleic acid-functionalized biocatalysts were conjugated by forming a Y-shaped DNA nanostructure with the complementary nucleic acid (**215**), Figure 52D. The spatial proximity between GOx and HRP enables activation of the bienzyme cascade, where the H₂O₂ generated by GOx acted as cosubstrate for the HRP-catalyzed oxidation of ABTS²⁻ to the colored product ABTS^{•+}. In another system, II, the Y-shaped DNA nanostructure was further implemented to inhibit the biocatalytic functions of an enzyme. Methylene Blue, MB⁺, is known to inhibit the enzyme choline oxidase (ChOx).³¹⁴ Accordingly, the nucleic acids (**213** and **214**) were modified with ChOx and MB⁺, respectively. The high local concentration of the inhibitor in steric proximity to the enzyme led to effective inhibition of the enzyme. The degree of inhibition is related to the concentration of the bridging nucleic acid (**215**).

The organization of enzymes on 1D DNA scaffolds provided a means to control enzyme cascades on the surface. The nucleic acids (**216** and **217**) were linked to GOx and HRP, respectively, and the enzymes were arranged on a DNA scaffold (**218**) through hybridization of the tethered nucleic acid, Figure 53A. The GOx-mediated oxidation of glucose yielded gluconic acid and H₂O₂, and the latter product acted as substrate for the HRP-catalyzed oxidation of Amplex Red to Resorufin that provided a fluorescent readout signal for the bienzyme cascade.^{100b} A similar approach was implemented to activate the luciferase-catalyzed generation of bioluminescence.

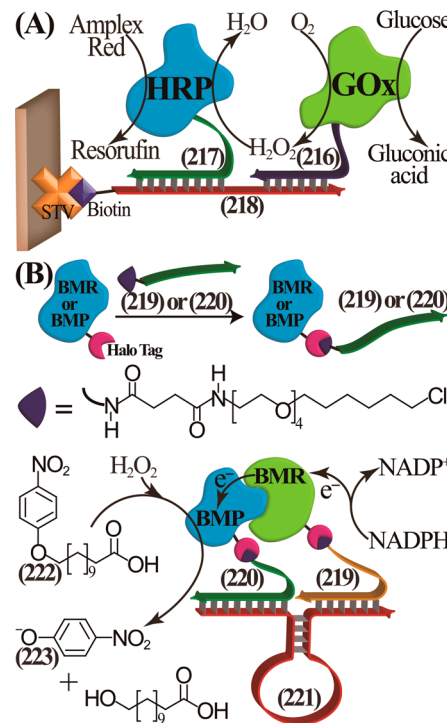


Figure 53. (A) Activation of the GOx/HRP bienzyme cascade on a nucleic acid scaffold associated with a surface. Reprinted with permission from ref 100b. Copyright 2008 Elsevier. (B) Reconstitution of the P-450 BM3 biocatalyst on a nucleic acid scaffold allowing oxidative cleavage of *p*-nitrophenoxyl-oxyethylene carboxylic acid (**222**) to *p*-nitrophenolate (**223**). Subunits of the enzymes BMR and BMP were functionalized with the halo tag protein, and the chloroalkyl-functionalized nucleic acids were linked as tethers to the BMR and BMP subunits. Reconstitution of the subunits on the template (**221**) activate in the presence of NADPH oxidative cleavage of **222**. Reprinted with permission from ref 101. Copyright 2011 American Chemical Society.

The two enzymes NADH oxidoreductase and luciferase were assembled on a nucleic acid scaffold that allowed generation of bioluminescence by the bioluminase cascade. The oxidoreductase-catalyzed reduction of flavin mononucleotide, FMN, by NADH, yielded FMNH₂, and the product acted as cosubstrate for the luciferase-stimulated generation of bioluminescence in the presence of an aldehyde and oxygen.^{100a} The steric proximity of the two enzymes on the DNA scaffold resulted in effective communication between the two biocatalysts. The structural organization of catalytically inactive protein subunits on a nucleic acid scaffold enabled the scaffold-assisted reconstitution of a catalytically active enzyme. This has been demonstrated¹⁰¹ with the reconstitution of the P-450 BM3 biocatalyst. This enzyme is composed of two subunits consisting of the reductase domain, BMR, and the porphyrin active domain, BMP. Using genetic engineering, the Halo Tag protein was fused to each of these domains, and the fused Tag proteins enabled covalent attachment of chloroalkyl-functionalized nucleic acids to each of the enzyme subunits. Hybridization of the **219**-functionalized-BMR unit and **220**-modified BMP unit to the DNA scaffold (**221**) brought the protein subunits into steric proximity that allowed reconstitution of the two subunits into a catalytically active biocatalytic nanostructure, Figure 53B. The self-assembled P-450 BM3 unit catalyzed oxidative cleavage of *p*-nitrophenoxyl-oxyethylene carboxylic acid (**222**) to *p*-nitrophenolate (**223**), occurring in

the resulting reconstituted assembly. The reaction involved primary reduction of the BMR site by NADPH, followed by reduction of the porphyrin site in BMP, leading to oxidative cleavage of 222 in the presence of H_2O_2 .

Multi-bienzyme cascades were also activated on 1D DNA wire nanostructures,^{90–92} Figure 54. A circular DNA template

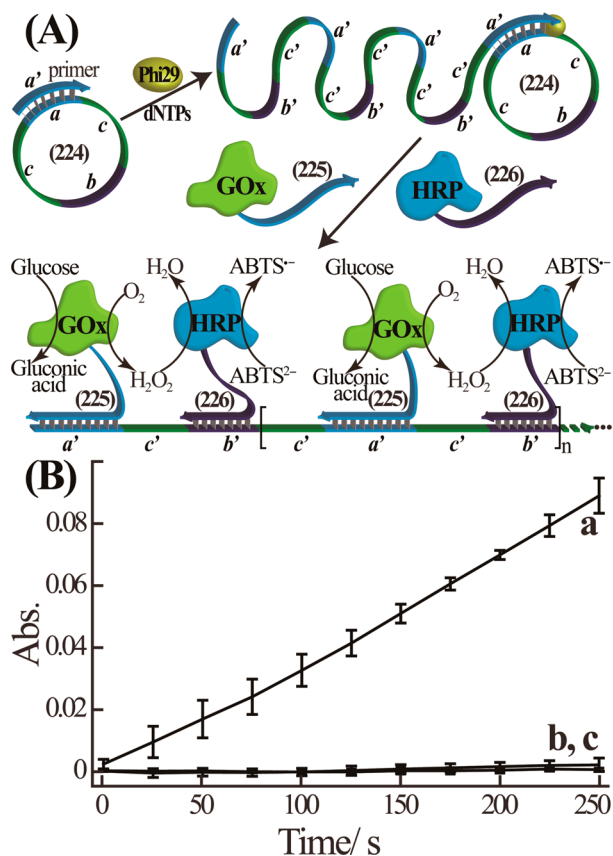


Figure 54. (A) Activation of the GOx/HRP bienzyme cascade by programmed hybridization of nucleic acid-tethered GOx and HRP on the tandem repeat units of an RCA-generated DNA wire. (B) Time-dependent absorbance changes of ABTS^{•⁻} upon (a) activation of the GOx/HRP bienzymes cascade on the RCA template, (b) reaction of GOx and HRP in the absence of the template, and (c) reaction of GOx and HRP in the presence of foreign calf thymus DNA. In all experiments, $[\text{GOx}] = 1.5 \mu\text{M}$ and $[\text{HRP}] = 1.5 \mu\text{M}$. Reprinted with permission from ref 91. Copyright 2009 American Chemical Society.

(224) that includes three domains *a*, *b*, and *c* was used as template for polymerase/dNTPs-mediated activation of the RCA process, leading to formation of micrometer long DNA nanowires consisting of tandem repeat units composed of the complementary nucleic acid sequences *a'*, *b'*, and *c'*. The two enzymes, GOx and HRP, were functionalized with the respective nucleic acid units (225 and 226) that are complementary to sequences *a'* and *b'* associated with the RCA-generated DNA nanowires. This enabled the ordered assembly of the two enzymes on the DNA scaffold, Figure 54A. The steric proximity between the two enzymes on the template DNA enabled activation of the biocatalytic cascade,⁹¹ where the GOx-mediated oxidation of glucose by O_2 yielded gluconic acid and H_2O_2 , and the latter product acted as substrate for HRP that mediated oxidation of ABTS²⁻ to the colored product, ABTS^{•⁻} ($\lambda_{\text{max}} = 415 \text{ nm}$). The resulting colored product enabled the probing of the biocatalytic cascade, Figure 54B.

Control experiments demonstrated that the randomly separated two enzymes in solution or in the presence of a foreign DNA, which does not organize the biocatalysts, failed to activate the bienzyme cascade. These results demonstrated the significance of the spatial ordering of the two biocatalysts on the DNA scaffold as a means to activate enzyme cascade. The close proximity of the two, sterically confined, enzymes permits effective utilization of the product of the first enzyme to act as substrate for the second biocatalyst without diffusion to the bulk solution, where its concentration is low. A related activation of a bienzyme cascade on a 1D DNA scaffold was demonstrated by the assembly of the two enzymes, GOx and HRP, on a DNA template consisting of circular DNA units cross-linked by cocaine–aptamer complexes.⁹⁰

Rapid advances in the design of DNA nanostructures and programmed tethering of proteins to such structures^{81–88,279,280} paved the way to tailor biocatalytic cascades on DNA nanostructures. This has been demonstrated with the self-assembly of micrometer-long 2D DNA subunits and programmed binding of the two enzymes GOx and HRP on the 2D DNA nanostructures.⁹² The single-stranded DNAs (227 and 228 or 229–232) exhibit interstrand complementarities to yield the 2D hexagon-type strip nanostructures “I” or “II”, respectively, Figure 55A. The DNA hexagon units at the edge of the strips include protruding DNA domains L₁ and L₂, and these provide specific tethers for anchoring the enzymes. Accordingly, the GOx was functionalized with the nucleic acid L₁', whereas HRP was modified with the nucleic acid L₂', thus allowing programmed assembly of the two enzymes on the respective DNA strips. AFM images confirmed formation of the conjugated enzymes on the 2D DNA scaffolds, Figure 55B. In the presence of glucose, the bienzyme cascade was activated; GOx mediated oxidation of glucose to gluconic acid and H_2O_2 , and the latter product acted as substrate for HRP that catalyzed oxidation of ABTS²⁻ to the colored product, ABTS^{•⁻}, that provided an optical readout signal for imaging of the bienzyme cascade, Figure 55C. The spatial separation of the two enzymes controlled the rate of the biocatalytic cascade on the two kinds of DNA nanostructures. The bienzyme cascade was found to be faster on the two-hexagon strips than on the four-hexagon nanostructures. This was attributed to the intimate steric contact between the two enzymes on the two-hexagon template that enabled effective uptake of the GOx-generated H_2O_2 by the neighboring HRP catalyst. The spatial separation of the two enzymes by the four-hexagon units allowed partial diffusion of H_2O_2 to the bulk solution, thus reducing the efficiency of the biocatalytic cascade. The two enzymes, GOx and HRP, solubilized in the solution in the absence of the hexagon strips at the same concentrations as on the DNA scaffold did not communicate one with another and did not activate the bienzyme cascade, Figure 55C, curve *c*. These results imply that the spatial confinement of the two enzymes on the DNA templates is essential to communicate the two biocatalysts and drive the biocatalytic chain cascade.

A further development in the activation of enzyme cascades on DNA nanostructures involved programmed positioning of the enzymes GOx and HRP on origami DNA tiles at spatially controlled distances,⁹³ Figure 56A. The origami DNA tiles included protruding nucleic acid strands that enabled the dictated assembly of the enzymes, modified with complementary strands, to the DNA tiles via specific hybridization while retaining predicted distances between the two enzymes. Accordingly, the two enzymes GOx and HRP were assembled

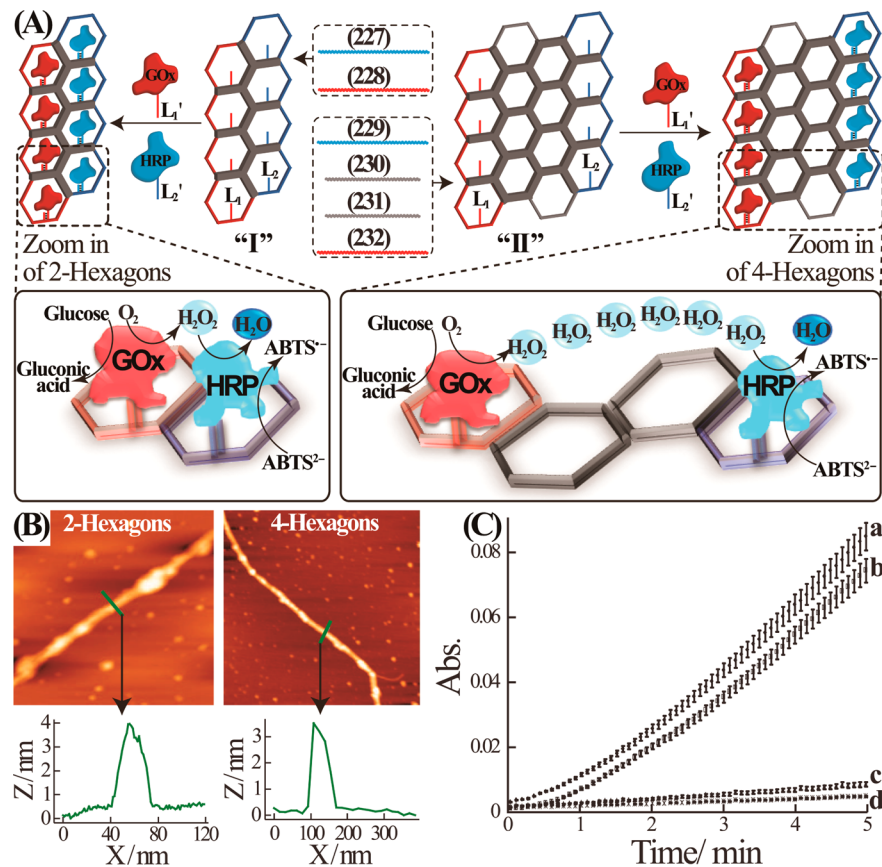


Figure 55. (A) Activation of the GOx/HRP bienzyme cascade on spatially separated “two-hexagon” or “four-hexagon” self-assembled DNA strips. Nucleic acid-functionalized enzymes are positioned on the strips by hybridization with the protruding chains linked to the respective hexagons. (B) AFM images corresponding to the GOx/HRP-functionalized “two-hexagons” and “four-hexagons” strips and the respective cross-sections analyses. (C) Time-dependent absorbance changes of ABTS^{•-} upon activation of the GOx/HRP bienzyme cascade on (a) the “two-hexagon” strips, (b) the “four-hexagon” strips, (c) the two enzymes in the presence of the foreign calf thymus DNA, (d) the two solubilized enzymes without any nucleic acid scaffolds. In all experiments, the content of GOx and HRP corresponded to 1 μ M, each. Reprinted with permission from ref 92. Copyright 2009 Nature Publishing Group.

on the DNA origami tile at separation distances corresponding to 10, 20, 45, and 65 nm. The efficiency of the GOx/HRP biocatalytic cascade, where the H₂O₂ product generated by GOx, was transferred to HRP, and this mediated oxidation of ABTS^{•-} to the colored product ABTS^{•+} was controlled by the spatial distance separating the two enzymes. While the 10 nm separated biocatalysts revealed an efficient cascaded biotransformation that is ca. 2-fold enhanced as compared to the 20 nm separated biocatalytic cascade, the 20–65 nm separated bienzyme cascaded systems revealed very similar cascaded efficiencies as compared to the biocatalytic cascade occurring by the free enzymes in solution, Figure S6B. The similarities in the efficiencies of the bienzyme systems consisting of the 20–65 nm separated biocatalysts were rationalized in terms of a Brownian diffusional model that suggested that at these separation distances, the H₂O₂ generated by GOx mostly diffuses to the bulk solution. The very efficient cascade observed for the 10 nm separated bienzyme cascade system was, however, attributed to the intimate contact between the two enzymes and to the unique properties of the hydration layer of the contacting proteins. As the water molecules associated with the proteins are translationally and rotationally constrained, relative to bulk water molecules, the biocatalytically generated H₂O₂ reveals high affinity to this hydration layer, leading to a dimensionality limited mechanism that favors

transfer of H₂O₂ through the contacted enzyme structure over diffusion to the solution. The effective cascading of the two enzymes by the constrained protein-contacted microenvironment suggested that incorporation of a bridging protein into the origami tile nanostructure, where the two enzymes are spatially separated by a bulk water layer microenvironment, could transform the bienzyme cascade controlled by a Brownian diffusion model into a bienzyme cascade exhibiting dimensional-limited diffusion. Accordingly, the GOx/HRP bienzyme cascaded system separated by an interenzyme distance of 20 nm was bridged by a noncatalytic protein (neuroavidin, NTV, or streptavidine, STV, conjugated to galactosidase, Gal), Figure S6C. AFM images of the separated two-enzyme origami tiles and the Gal-bridged bienzyme tiles revealed that the Gal protein bridges the two enzymes into an intimate contacted protein structure, Figure S6D. Indeed, the efficiency of the bienzyme cascaded process, in the presence of the noncatalytic protein bridge, was substantially enhanced as compared to the nonbridged bienzyme system, Figure S6E, implying that the bridging protein facilitated dimensional-limited diffusion through the hydration layer of the protein-contacted enzyme units.

A significant advance in nucleic acid nanotechnology was demonstrated by the intracellular cascading of two enzymes on a self-assembled two-dimensional scaffold.^{315a} Two fusion

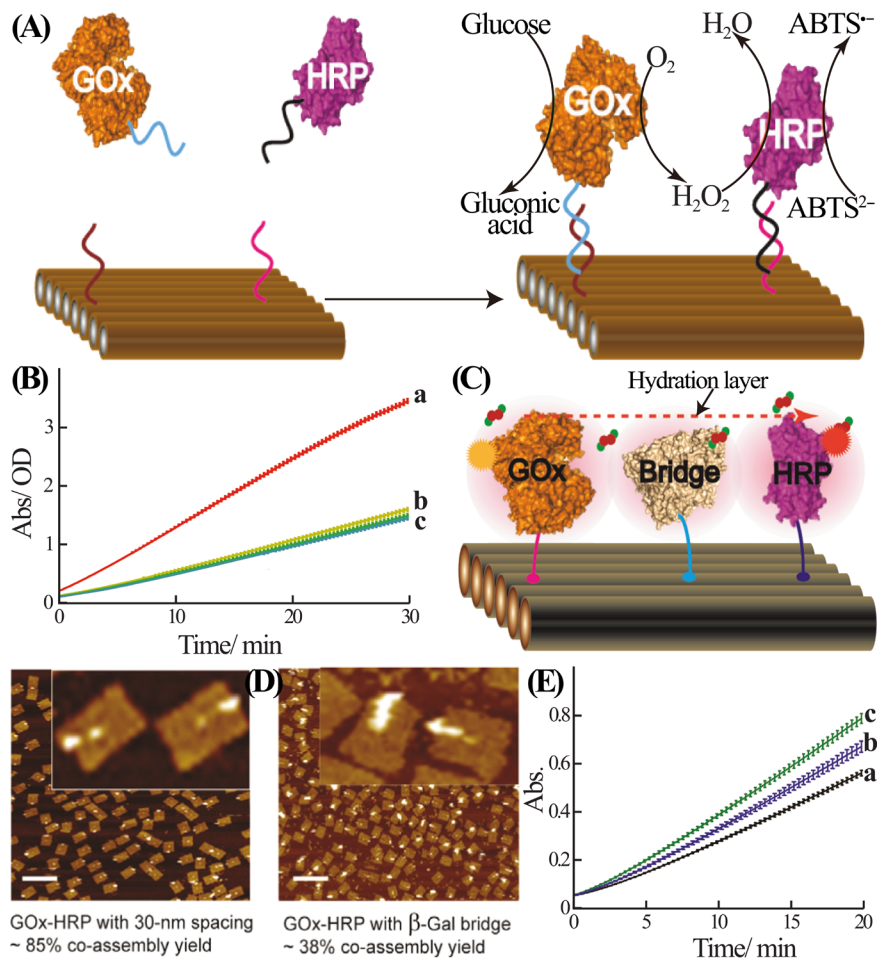


Figure 56. (A) Activation of the GOx/HRP bienzyme cascade using programmed spatially-controlled configurations of the two enzymes on a DNA origami template. Nucleic acid-functionalized GOx and HRP are hybridized with predesigned protruding nucleic acids that dictate the distance between the biocatalysts. (B) Time-dependent absorbance changes of ABTS⁺· generated by the bienzyme cascade where the enzymes are separated by (a) 10 nm, (b) 20 nm, and (c) two solubilized enzymes without any nucleic acid scaffolds. (C) Protein-assisted activation of the GOx/HRP bienzyme cascade on the DNA origami template. (D) AFM images corresponding to the GOx and HRP positioned on the origami template (left) and to the protein (β -galactosidase, β -Gal) bridged GOx-HRP units (right). (E) Time-dependent absorbance changes upon activation of the GOx/HRP bienzyme cascade: (a) no bridge, (b) in the presence of neutravidin (NTV) as bridge; (c) in the presence of β -galactosidase (β -Gal) as bridge. Reprinted with permission from ref 93. Copyright 2012 American Chemical Society.

protein conjugates consisting of the protein adapters F_M (PP7) and H_p (MS2), fused to proteins F (ferredoxin) and H (hydrogenase), respectively, were prepared, Figure 57A, inset. Cells were programmed to generate the RNA units, d2' (233) and d2'' (234), that include, each, the hairpin aptamer domains for F_M and H_p , respectively. The structure d2' includes the encoded complementarities to form a self-dimeric tile, d2-1, and the resulting tile includes the sequence programmed tether to bind d2'' to form the extended tile, d2-2, by genetic engineering. Self-polymerization of this tile element leads to a 2D tile array consisting of adjacent aptamer units against F_M and H_B , Figure 57A. The dictated intracellular binding of the fused proteins to the aptamer units resulted in the spatial confinement of the proteins on the RNA scaffolds, leading to efficient biosynthetic H_2 evolution, Figure 57B. While the unscattered fused proteins generated a negligible amount of H_2 , the protein scaffolded array revealed a 48-fold increase in the evolved hydrogen. This effective H_2 evolution was attributed to the efficient electron-transfer cascade occurring in the spatially confined nanoenvironment of the two proteins.

Photoisomerizable compounds such as azobenzene derivatives reveal switchable binding properties to nucleic acid structures. For example, while *trans*-azobenzene intercalates into duplex DNA structures, the photoisomerized *cis*-azobenzene isomer lacks affinity for its association with duplex DNA structures. Cyclic photoisomerization of *trans*-azobenzene ($\lambda_{\text{max}} = 365 \text{ nm}$) and the reverse recovery of *cis*-azobenzene to *trans*-azobenzene ($\lambda > 450 \text{ nm}$) were then used to control the stability of duplex DNA structures. While intercalation of *trans*-azobenzene into duplex DNA cooperatively stabilized the double-stranded DNA structure, photoisomerization to the *cis*-azobenzene released the intercalator units and weakened the duplex structures. This photostimulated reaction was used to reconfigure nucleic acid nanostructures to ON and OFF catalytic DNAzyme structures³¹⁶ and photonically drive DNA machines.^{123,124,317}

DNA scaffolds were also implemented to switch enzyme cascades activated by external stimuli, such as photonic signals or electrical signals. For example, reversible photoisomerization of *trans*-azobenzene to *cis*-azobenzene ($\lambda_{\text{max}} = 365 \text{ nm}$) and back isomerization of *cis*-azobenzene to *trans*-azobenzene ($\lambda >$

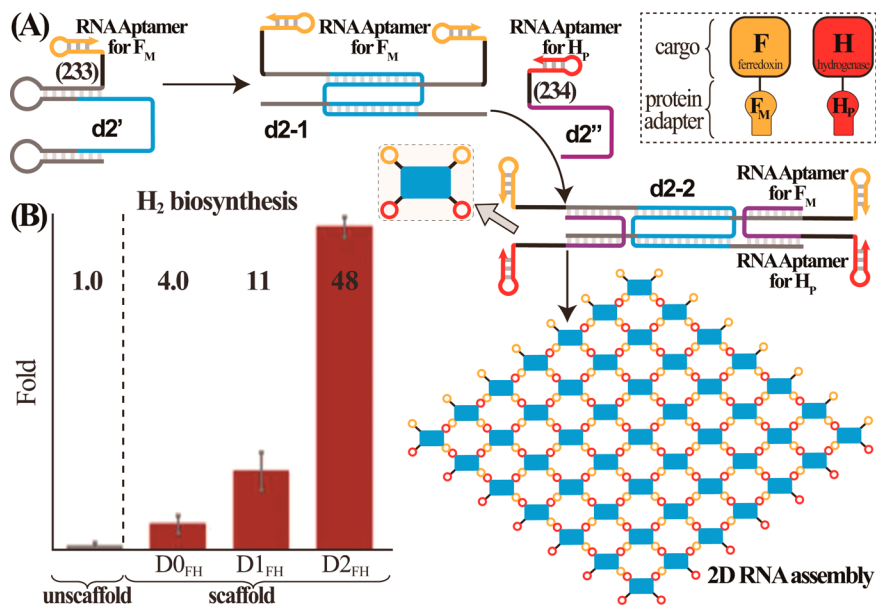


Figure 57. (A) Self-assembly of two-dimensional RNA tiles consisting of the ferredoxin (F) and hydrogenase (H) in close proximity. Engineering of the tile subunit is based on the primary eliciting of aptamer against the fusion protein conjugates F_M (PP7) and H_P (MS2) that are fused to ferredoxin (F) and hydrogenase (H). Anti-F_M aptamer is part of the RNA structure (233) that includes two hairpin units. Structure 233 dimerizes to the energetically stabilized structure d2-1. Nucleic structure 234 that includes the anti-H_P aptamer sequence encodes appropriate base order to interact with d2-1 to structure d2-2. The latter product includes the encoded base sequence to self-assemble into the 2D tile structure. Programmed binding of F and H to the respective protruding aptamer sequences yields a spatially close structure of the two proteins on the RNA scaffold. (B) Relative yield for biosynthesis of hydrogen upon incorporation of the F/H-incorporated two-dimensional RNA assembly structure shown in A into cells, as compared to the reference systems that included unscattered F/H units or spatially separated F/H units on one-dimensional scaffolds. Reprinted with permission from ref 315a. Copyright 2011 American Association for the Advancement of Science.

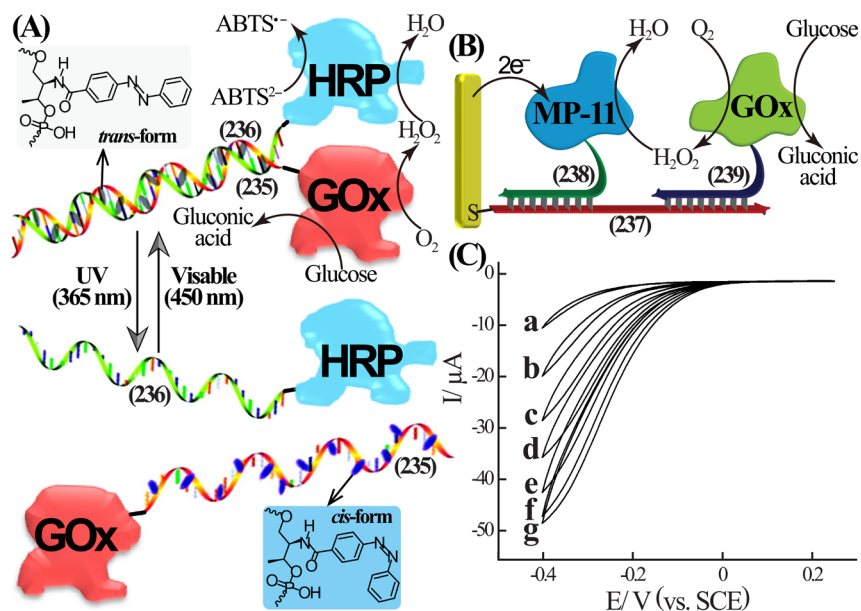


Figure 58. (A) Photochemical switching of the GOx/HRP bienzyme cascade for photoisomerization of azobenzene. Intercalation of *trans*-azobenzene into the duplex of nucleic acid tethers associated with GOx/HRP stabilizes the duplex structure leads to activation of the bienzyme cascade. Photoisomerization of *trans*-azobenzene to *cis*-azobenzene leads to separation of the DNA duplex and blocking of the bienzyme cascade. Reprinted with permission from ref 315b. Copyright 2011 American Chemical Society. (B) Electrocatalytic activation of the microperoxidase-11/glucose oxidase (MP-11/GOx) cascade by positioning of the two proteins on a nucleic acid scaffold associated with an electrode. (C) Electrocatalytic cathodic currents generated by the MP-11/GOx cascade in the presence of different concentrations of glucose: (a) 0, (b) 20, (c) 40, (d) 60, (e) 80, (f) 100, and (g) 120 mM. Reprinted with permission from ref 315c. Copyright 2009 American Chemical Society.

450 nm) were used to photoinitiate the bienzyme cascade consisting of GOx and HRP.^{315b} Figure 58A. Accordingly, GOx was functionalized with nucleic acid chains (235) modified with the *trans*-azobenzene functional groups. In

the presence of HRP, functionalized with the partially complementary strand (236), the duplex DNA stabilized by the intercalated *trans*-azobenzene was formed. This led to spatial organization of the two enzymes GOx and HRP. The

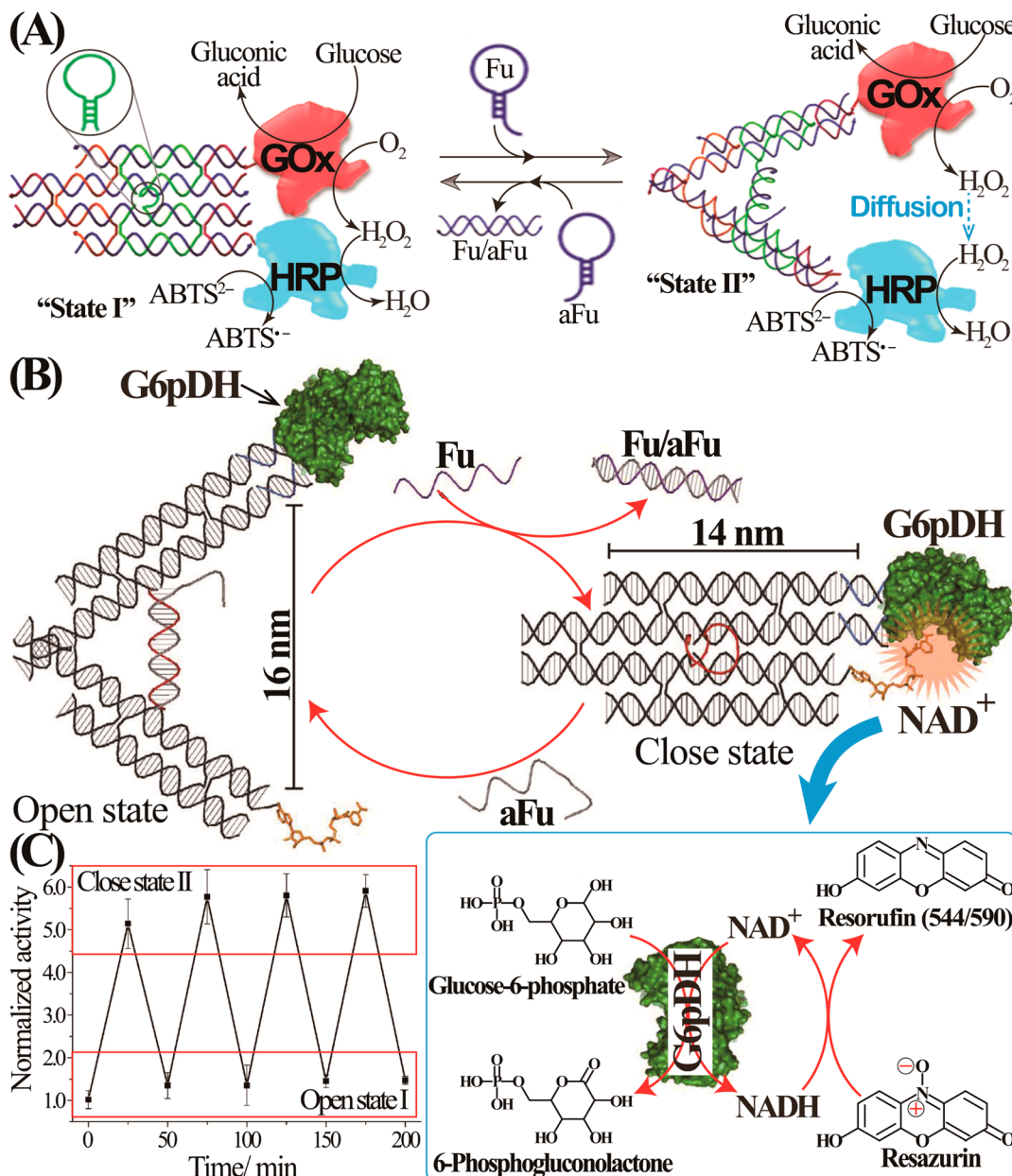


Figure 59. (A) Cyclic activation and deactivation of the bienzyme cascade consisting of glucose oxidase/horseradish peroxidase (GOx/HRP) by the reversible closure (ON) and opening (OFF) of a DNA tweezers structure. Reprinted with permission from ref 315d. Copyright 2013 Wiley-VCH. (B) Cyclic activation and deactivation of the NAD⁺-dependent glucose-6-phosphate dehydrogenase (G6pDH) by the reversible closure (ON) and opening (OFF) of a DNA tweezers structure. (C) Cyclic ON/OFF normalized activities of G6pDH upon switchable oxidation of glucose-6-phosphate, monitored through the fluorescence changes stimulated by the NADH-mediated reduction of Resazurin to Resorufin. Reprinted with permission from ref 315e. Copyright 2013 Nature Publishing Group.

intimate contact between GOx and HRP led to activation of the bienzyme cascade, where GOx-catalyzed oxidation of glucose led to formation of gluconic acid and H_2O_2 product and the resulting H_2O_2 provided the substrate for HRP that stimulated oxidation of ABTS²⁻ to the colored product ABTS^{•-} ($\lambda_{\text{max}} = 415 \text{ nm}$). Photoisomerization of the *trans*-azobenzene units to the *cis*-azobenzene state resulted in destabilization of functional duplex DNA nanostructures, separation of the two conjugated enzymes, and switching off of the biocatalytic cascade. An analogous light-induced switchable catalytic cascade was demonstrated with the photoisomerizable *trans*-azobenzene units and using GOx and the hemin/G-quadruplex HRP-mimicking DNAzyme as catalytic units.^{315b}

Also, a bioelectrocatalytic cascade was activated on a DNA scaffold associated with an electrode.^{315c} The thiolated nucleic acid (237) was assembled on a Au electrode, and micro-peroxidase-11 (MP-11)-modified with the nucleic acid (238) and GOx-functionalized with the nucleic acid (239) were hybridized with the scaffold as footholds, where MP-11 was adjacent to the electrode and GOx occupied the remote position, Figure 58B. GOx-stimulated oxidation of glucose generated gluconic acid and H_2O_2 . The resulting H_2O_2 at the electrode surface enabled the effective bioelectrocatalyzed reduction of H_2O_2 by MP-11, Figure 58C. The ordering of the two biocatalysts on the DNA scaffold was found to play an important role in the efficiency of the bioelectrocatalytic

cascade, and exchanging the positions of GOx and MP-11 on the DNA scaffold led to lower electrocatalytic responses that corresponded only to 10% of the magnitudes of the system shown in Figure 5B.

DNA tweezers machines were used to control the bienzyme cascade consisting of GOx and HRP,^{315d} Figure S9 A. The arms of the tweezers were each functionalized with GOx and HRP, respectively. The tweezers arms were linked into a closed structure through an interarm hairpin structure, state I. In the presence of a DNA fuel, (Fu), the interbridging hairpin structure was opened to yield the duplex nucleic acid-stabilized arms of the opened tweezers, state II. The proximity between GOx and HRP in the closed state of the tweezers led to effective activation of the bienzyme cascade resulting in effective formation of ABTS^{•+}. Opening of the tweezers spatially separated the two enzymes, resulting in diffusion of the H₂O₂ product generated by GOx into the bulk solution and to inefficient communication between the two enzymes. By applying an antifuel hairpin (aFu), the added fuel strand (Fu) that opened the tweezers was removed by generating an energetically stabilized Fu/aFu duplex, leading to closure of the tweezers. By cyclic addition of the Fu and aFu strands, the reversible “mechanical” activation of the bienzyme cascade was switched between OFF and ON states, respectively. A related study has implemented the DNA tweezers device to switch the biocatalytic oxidation of glucose-6-phosphate by the NAD⁺-dependent glucose-6-phosphate dehydrogenase (G6pDH),^{315e} Figure S9B. The ends of the tweezers arms were modified with G6pDH and the NAD⁺ cofactor, respectively. While in the open structure of the tweezers, inefficient NAD⁺-mediated oxidation of glucose-6-phosphate occurred, closure of the tweezers by the fuel strand (Fu) resulted in an intimate contact between the NAD⁺ cofactor and G6pDH. This allowed effective oxidation of glucose-6-phosphate with concomitant formation of NADH. The secondary NADH-mediated reduction of Resazurin to the fluorescent Resorufin product regenerated the cofactor, and it provided the readout signal for the biocatalytic process. By the cyclic closure of the tweezers with the fuel strand (Fu) and opening of the closed tweezers with the antifuel strand (aFu), the reversible and switchable activation/deactivation of the biocatalytic process to ON and OFF states was demonstrated, Figure S9C.

6. CONCLUSIONS AND PERSPECTIVES

The present review has discussed different methods to use the information encoded in DNA to drive integrated nonenzymatic and enzymatic cascaded catalytic transformations. Nonenzymatic reactions combined the strand-displacement concept, branch migration, and the autonomous hybridization chain reactions with the catalytic functions of nucleic acids (DNAzymes). This led to unique transformations where reactions at the molecular level were translated into autonomous processes that yielded nanostructures exhibiting emerging functionalities. Synthesis of DNAzyme nanowires,^{48a,49a} triggering of nonenzymatic ligation²⁴¹ and replication reactions,²⁴² and programmed synthesis of nanostructures^{113,206} represent such emerging functions.

Enzymatic-driven cascades have implemented well-established and specific biocatalytic reactions on DNA, such as polymerization, ligation, nicking, hydrolytic scission, and more, as basic tools that were coupled to nonenzymatic processes, such as DNAzyme-catalyzed transformations, or isothermal autonomous hybridization chain reactions. These combined

enzymatic/nonenzymatic processes have established new paradigms for autonomous isothermal replication of catalytic nanostructures^{290,291} and regeneration of molecular components.²⁸⁸ All of these biocatalytic cascades are triggered by primary nucleic acid recognition complexes. Furthermore, the discovery of the selection method of aptamers that bind low molecular weight substrates, proteins, and cells and the availability of specific metal-ion-bridged duplex DNA nanostructures allowed development of new chemical paradigms where specific recognition complexes trigger complex non-enzymatic or enzymatic cascades. Naturally, extensive efforts were directed to application of the enzymatic and non-enzymatic nucleic acid cascades for amplified sensing of DNA, aptamer–substrate complexes, and metal ions. Unprecedented sensitivities for detection of the various analytes were demonstrated. Several of the nonenzymatic or enzymatic cascades were suggested as potential alternatives for the legendary polymerase chain reaction (PCR) as amplification means. The analytical advantages of such cascaded amplification sensing cycles are obvious, since these processes proceed under isothermal conditions, do not require special instrumentation, can be imaged by the naked eye, and can be adapted for field tests or point-of-case applications. Albeit substantial progress was accomplished by applying nonenzymatic or enzymatic catalytic cascades in bioanalysis, important challenges are still ahead of us. Most of these bioanalytical platforms were implemented in “clean” chemical environments, and their application in “real” biological environments, such as serum, urine, or saliva, is required. Furthermore, substantial progress in applying nanomaterials, such as metal nanoparticles,³¹⁸ nanoclusters,³¹⁹ semiconductor quantum dots,³²⁰ carbon nanotubes,³²¹ and graphene oxide³²² for biosensing has been accomplished. Conjugation of DNA-based catalytic cascades to nanomaterials might yield biohybrid systems revealing new properties and functions. Also, development of multiplexed amplified analytical assays using cascaded catalytic machineries for parallel analysis of several targets is an interesting path to follow.³¹¹ For example, the ability to trigger dictated replication/nicking machineries on nucleic acid templates while synthesizing programmed sequences of DNAAzymes¹⁷¹ paves the way to use a combination of DNA templates being triggered by a collection of different targets, thus leading to different DNAAzymes as reporter units.

Design of autonomous programmed catalytic cascades based on nucleic acids has, however, significant scientific implications, far beyond sensing. In cells, multicatalytic reactions are often proceeding in spatially organized and microcompartmentalized microenvironments.^{309a} The spatial organization of the molecular components in cells permits effective directional flow of the respective substrate/products, and activation of catalytic cascades allows controlled signal transfer, facilitates complex catalytic pathways involving selective branching and feedback mechanism, triggers threshold-controlled transformations, and prohibits cross-talks between signaling pathways.^{309b} The ability to use DNA as template or scaffold for precise positioning of enzymes or DNAzymes paves the way to develop complex *in vitro* catalytic networks mimicking cellular functions. Such systems hold great promise for programmed synthesis^{248a,323} and selective synthesis.³²⁴ Substantial progress has been accomplished in recent years by activation of enzyme cascades on nucleic acid templates,⁹² and new phenomena such as the unique functions of localized water molecules associated with the template proteins were discovered.⁹³ Nonetheless,

challenging goals are still ahead of us: Activation of replication cascades on DNA scaffolds, leading to products with emerging catalytic properties, programmed separation of the products and their dictated transfer to other scaffolds for chain reactions, and triggering of the chemical transformations by means of external stimuli, such as light, electrical, or chemical signals, represent important topics for development of “living technologies” mimicking cellular processes.

Programmed polymerization of monomer nucleic acid units through nonenzymatic processes, such as the HCR process, or by enzymatic reactions, such as the RCA process, may lead to polymer chains that include predesigned protruding tethers or predesigned hybridization domains that enable the dictated assembly of metallic nanoparticles,²⁷⁹ metallic NPs, and fluorophores or ordered binding of proteins.⁹⁰ Such functional nanostructures are anticipated to reveal unique plasmonic properties^{144,325} or allow activation of enzymatic cascades. Also, the conjugation of nucleic acids to nanomaterials could provide future “smart materials” for controlled drug release. For example, the loading of drugs in the pores of mesoporous nanoparticles and their locking in the pores by predesigned functional nucleic acid nanostructures might lead to “smart materials” where biomarker-induced activation of biocatalytic reactions on the nucleic acid capping units unlocks the pores and releases the loaded materials. This concept was recently implemented to load the mesoporous SiO₂ pores with the anticancer drug doxorubicin by locking the pores with the Mg²⁺-dependent DNAzyme sequences.^{184a} In the presence of Mg²⁺ ions, the pores were unlocked and the drug was released. By the engineering of the nucleic acid capping units modified gating units where aptamer–biomarker recognition complexes triggered the DNAzyme catalytic process and released the drugs were developed.^{184a} By coupling mesoporous materials capped with different signal triggered gates, activation of dictated and ordered cascaded biocatalytic reactions, opening the pores, may be envisaged. Such smart materials might provide matrices for controlled release of drugs or programmed synthesis.

Incorporation of nucleic acid machineries into cells has utmost implications for the engineering of cells and for future nanomedicine. Although these research activities are at their infancy, several scientific breakthroughs were already demonstrated, highlighting the future perspectives of the field. Assembly of ordered 2D and 3D nanoscale structures consisting of RNA has been reported,³²⁶ and integration of such man-made nanostructures with the cellular transcription machinery could yield engineered cells with new functionalities. The possibility to genetically engineer cells for synthesis of nucleic acids that are programmed to position proteins for cascaded biocatalytic reactions by means of aptamer units provides new means to synthesize cells with new functionalities. Successful genetic engineering of cells that synthesize RNA scaffolds for spatial confinement of fused proteins and their activation toward effective biosynthetic hydrogen evolution³¹⁵ represents exciting opportunities to harness nanoengineered cells for synthesis of feedstocks or for energy conversion and fuel production. Also, the recently reported, and related, stimulation of cell signaling by means of nanoscale nucleic acid robots¹⁹⁰ highlights the future possible applications of intracellular DNA/proteins scaffolds for nanomedicine. In this study, two clasps made of origami units were modified with protruding nucleic acids and used as functional units to form a reservoir for the binding of molecular payloads that bind to the reservoir and lock it by complementary base pairing. By

designing the lock duplex DNA units to act as recognition aptamers for specific cellular biomarkers, programmed opening of the DNA container and release of payloads was demonstrated.¹⁸² Thus, such DNA nanorobots may be used as future nanotools for biomarker-induced release of enzymes or of molecular triggers that activate intracellular catalytic cascades.

Finally, cascaded nonenzymatic- or enzymatic-nucleic-acid-driven processes may provide scaffolds for secondary synthesis of new nanoscale materials. For example, the HCR process that leads to polymer chains of functional repeat units may be designed to generate tether-functionalized polymer wires for deposition of metallic NPs.³²⁷ Such metal NPs/DNA hybrids are anticipated to yield materials exhibiting new optical properties such as plasmonic coupling or dichroic functions.³²⁸ Alternatively, HCR-mediated synthesis of DNAzyme wires, such as G-quadruplex wires,^{49a} may lead to templates for secondary synthesis of polymers, e.g., nanowires of conductive polymers.

To conclude, the structural and functional information encoded in DNA has been extensively used to develop cascaded chemical transformations. Although, significant advances of such autonomous catalytic processes were accomplished, important future challenges are in front of us, and bright implications of these processes for sensing, nanomedicine, material science, and living technologies may be envisaged.

AUTHOR INFORMATION

Corresponding Author

*E-mail: willnea@vms.huji.ac.il.

Author Contributions

[‡]These authors contributed equally. This manuscript was written through contributions of all authors. All authors have given approval to the final version of the manuscript.

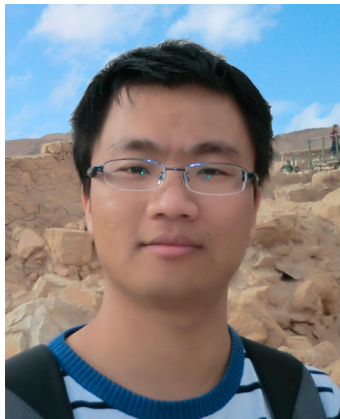
Notes

The authors declare no competing financial interest.

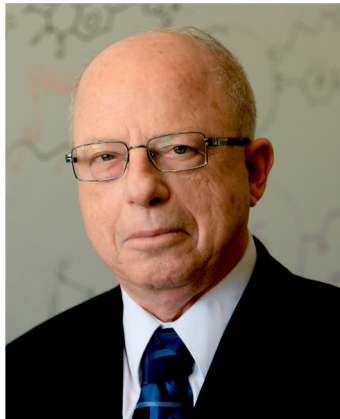
Biographies



Fuan Wang is currently a postdoctoral research fellow in the laboratory of Professor Itamar Willner, Institute of Chemistry, The Hebrew University of Jerusalem. He received his B.S. degree from Zhengzhou University, China (2003), and completed his Ph.D. research at Changchun Institute of Applied Chemistry, Chinese Academy of Sciences (2008). His research interests focus on DNA nanotechnology including development of DNA sensing and amplification schemes, DNA computing, and DNA machines.



Chun-Hua Lu is currently a postdoctoral research associate in the laboratory of Professor Itamar Willner, Institute of Chemistry, The Hebrew University of Jerusalem. He received his B.S (2005) and Ph.D. (2011) degrees from the College of Chemistry and Chemical Engineering, Fuzhou University, China. His research interests address topics of DNA nanotechnology including DNA machines, plasmonic effects using DNA/metal nanoparticle structures, and DNA hydrogels.



Itamar Willner completed his Ph.D. studies at The Hebrew University of Jerusalem in 1978. After postdoctoral research (1978–1981) at U.C. Berkeley, he joined the Institute of Chemistry at The Hebrew University of Jerusalem, where he was appointed Professor in 1986. He coauthored over 670 research papers and monographs, and he serves on many editorial boards of journals. He holds over 39 000 citations, H-index 102. His research interests include bioelectronics and molecular electronics, nanobiotechnology, and, specifically, DNA-based nanotechnology, sensors, and biosensors, application of metal and semiconductor nanoparticles for sensing, functional monolayer and thin film assemblies, light-induced electron-transfer processes, artificial photosynthesis and photobioelectrochemistry cells, supramolecular chemistry, and “smart” stimuli-responsive materials for drug delivery. He is the recipient of the Kolthoff Award, The Max-Planck Research Award for International Cooperation, the Israel Chemical Society Award, the Israel Prize in Chemistry, the Rothschild Prize, and the EMET Prize. He is a member of the Israel Academy of Sciences, the German National Academy of Sciences, Leopoldina, and the European Academy of Sciences and Arts.

ACKNOWLEDGMENTS

Our research on DNA nanotechnology was supported by the Israel Science Foundation, the MULTI and Mireagent FET Open EG Projects, and the Volkswagen Foundation.

REFERENCES

- (1) (a) Watson, J. D.; Crick, F. H. C. *Nature* **1953**, *171*, 737. (b) Sinden, R. R.; Pearson, C. E.; Potaman, V. N.; Ussery, D. W. *Adv. Gen. Biol.* **1998**, *5*, 1. (c) Hannon, M. J. *Chem. Soc. Rev.* **2007**, *36*, 280. (d) Stulz, E.; Clever, G.; Shionoya, M.; Mao, C. *Chem. Soc. Rev.* **2011**, *40*, 5633.
- (2) (a) Wilkins, M. H. F.; Stokes, A. R.; Wilson, H. R. *Nature* **1953**, *171*, 738. (b) Bansal, M. *Curr. Sci.* **2003**, *85*, 1556. (c) Sessler, J. L.; Lawrence, C. M.; Jayawickramarajah, J. *Chem. Soc. Rev.* **2007**, *36*, 314.
- (3) (a) Gellert, M.; Lipsett, M. N.; Davies, D. R. *Proc. Natl. Acad. Sci. U.S.A.* **1962**, *48*, 2013. (b) Simonsson, T. *Biol. Chem.* **2001**, *382*, 621. (c) Collie, G. W.; Parkinson, G. N. *Chem. Soc. Rev.* **2011**, *40*, 5867. (d) Juskowiak, B. *Anal. Chim. Acta* **2006**, *568*, 171.
- (4) (a) Sen, D.; Gilbert, W. *Nature* **1988**, *334*, 364. (b) Burge, S.; Parkinson, G. N.; Hazel, P.; Todd, A. K.; Neidle, S. *Nucleic Acids Res.* **2006**, *34*, 5402. (c) Davis, J. T.; Spada, G. P. *Chem. Soc. Rev.* **2007**, *36*, 296.
- (5) (a) Gehring, K.; Leroy, J. L.; Guérón, M. *Nature* **1993**, *363*, 561. (b) Chen, L.; Cai, L.; Zhang, X.; Rich, A. *Biochemistry* **1994**, *33*, 13540. (c) Collin, D.; Gehring, K. *J. Am. Chem. Soc.* **1998**, *120*, 4069.
- (6) (a) Leroy, J. L.; Guérón, M.; Mergny, J. L.; Helene, C. *Nucleic Acids Res.* **1994**, *22*, 1600. (b) Nonin, S.; Leroy, J. L. *J. Mol. Biol.* **1996**, *261*, 399. (c) Nonin, S.; Phan, A. T.; Leroy, J. L. *Structure* **1997**, *5*, 1231.
- (7) (a) Miyake, Y.; Togashi, H.; Tashiro, M.; Yamaguchi, H.; Oda, S.; Kudo, M.; Tanaka, Y.; Kondo, Y.; Sawa, R.; Fujimoto, T.; Machinami, T.; Ono, A. *J. Am. Chem. Soc.* **2006**, *128*, 2172. (b) Tanaka, Y.; Oda, S.; Yamaguchi, H.; Kondo, Y.; Kojima, C.; Ono, A. *J. Am. Chem. Soc.* **2007**, *129*, 244. (c) He, S.; Li, D.; Zhu, C.; Song, S.; Wang, L.; Long, Y.; Fan, C. *Chem. Commun.* **2008**, 4885. (d) Liu, C. W.; Hsieh, Y. T.; Huang, C. C.; Chang, H. T. *Chem. Commun.* **2008**, 2242. (e) Deng, L.; Zhou, Z.; Li, J.; Li, T.; Dong, S. *Chem. Commun.* **2011**, *47*, 11065.
- (8) (a) Lee, J. S.; Han, M. S.; Mirkin, C. A. *Angew. Chem., Int. Ed.* **2007**, *46*, 4093. (b) Xue, X.; Wang, F.; Liu, X. *J. Am. Chem. Soc.* **2008**, *130*, 3244. (c) Zhu, Z.; Su, Y.; Li, J.; Li, D.; Zhang, J.; Song, S.; Zhao, Y.; Li, G.; Fan, C. *Anal. Chem.* **2009**, *81*, 7660. (d) Li, T.; Dong, S.; Wang, E. *Anal. Chem.* **2009**, *81*, 2144. (e) Zhu, Z.; Su, Y.; Li, J.; Li, D.; Zhang, J.; Song, S.; Zhao, Y.; Li, G.; Fan, C. *Anal. Chem.* **2009**, *81*, 7660.
- (9) (a) Ono, A.; Cao, S. Q.; Togashi, H.; Tashiro, M.; Fujimoto, T.; Machinami, T.; Oda, S.; Miyake, Y.; Okamoto, I.; Tanaka, Y. *Chem. Commun.* **2008**, 4825. (b) Freeman, R.; Finder, T.; Willner, I. *Angew. Chem., Int. Ed.* **2009**, *48*, 7818. (c) Li, T.; Shi, L.; Wang, E.; Dong, S. *Chem.—Eur. J.* **2009**, *15*, 3347. (d) Wen, Y.; Xing, F.; He, S.; Song, S.; Wang, L.; Long, Y.; Li, D.; Fan, C. *Chem. Commun.* **2010**, *46*, 2596.
- (10) (a) Chiang, C. K.; Huang, C. C.; Liu, C. W.; Chang, H. T. *Anal. Chem.* **2008**, *80*, 3716. (b) Park, K. S.; Jung, C.; Park, H. G. *Angew. Chem., Int. Ed.* **2010**, *49*, 9757. (c) Huy, G. D.; Zhang, M.; Zuo, P.; Ye, B. C. *Analyst* **2011**, *136*, 3289.
- (11) (a) Tanaka, K.; Tengeiji, A.; Kato, T.; Toyama, N.; Shiro, M.; Shionoya, M. *J. Am. Chem. Soc.* **2002**, *124*, 12494. (b) Clever, G. H.; Sölti, Y.; Burks, H.; Spahl, W.; Carell, T. *Chem.—Eur. J.* **2006**, *12*, 8708. (c) Tanaka, K.; Clever, G. H.; Takezawa, Y.; Yamada, Y.; Kaul, C.; Shionoya, M.; Carell, T. *Nature Nanotechnol.* **2006**, *1*, 190. (d) Clever, G. H.; Carell, T. *Angew. Chem., Int. Ed.* **2007**, *46*, 250. (e) Clever, G. H.; Shionoya, M. *Coord. Chem. Rev.* **2010**, *254*, 2391. (f) Wojciechowski, F.; Leumann, C. *J. Chem. Soc. Rev.* **2011**, *40*, 5669.
- (12) (a) Meggers, E.; Holland, P. L.; Tolman, W. B.; Romesberg, F. E.; Schultz, P. G. *J. Am. Chem. Soc.* **2000**, *122*, 10714. (b) Atwell, S.; Meggers, E.; Spraggan, G.; Schultz, P. G. *J. Am. Chem. Soc.* **2001**, *123*, 12364. (c) Clever, G. H.; Kaul, C.; Carell, T. *Angew. Chem., Int. Ed.* **2007**, *46*, 6226. (d) Ono, A.; Torigoe, H.; Tanaka, Y.; Okamoto, I. *Chem. Soc. Rev.* **2011**, *40*, 5855. (e) Takezawa, Y.; Shionoya, M. *Acc. Chem. Res.* **2012**, *45*, 2066.
- (13) (a) Schwögl, A.; Carell, T. *Org. Lett.* **2000**, *2*, 1415. (b) Park, S.; Sugiyama, H. *Angew. Chem., Int. Ed.* **2010**, *49*, 3870. (c) Boersma, A. J.; Megens, R. P.; Feringa, B. L.; Roelfes, G. *Chem. Soc. Rev.* **2010**, *39*, 2083.

- (14) (a) Erkkila, K. E.; Odom, D. T.; Barton, J. K. *Chem. Rev.* **1999**, 99, 2777. (b) Xu, Y.; Zhang, Y. X.; Sugiyama, H.; Umano, T.; Osuga, H.; Tanaka, K. *J. Am. Chem. Soc.* **2004**, 126, 6566.
- (15) (a) Mitchell, P. J.; Tjian, R. *Science* **1989**, 245, 371. (b) Lee, T. I.; Young, R. A. *Annu. Rev. Genet.* **2000**, 34, 77. (c) Brivanlou, A. H.; Darnell, J. E. *Science* **2002**, 295, 813. (d) van Nimwegen, E. *Trends Genet.* **2003**, 19, 479.
- (16) (a) Meyyappan, M.; Atadja, P. W.; Riabowol, K. T. *Biol. Signals* **1996**, 5, 130. (b) Thomas, M. C.; Chiang, C. M. *Crit. Rev. Biochem. Mol. Biol.* **2006**, 41, 105. (c) Moscou, M. J.; Bogdanove, A. J. *Science* **2009**, 326, 1501.
- (17) (a) Libermann, T. A.; Zerbini, L. F. *Curr. Gene Ther.* **2006**, 6, 17. (b) Boch, J.; Scholze, H.; Schornack, S.; Landgraf, A.; Hahn, S.; Kay, S.; Lahaye, T.; Nickstadt, A.; Bonas, U. *Science* **2009**, 326, 1509. (c) Teif, V. B.; Rippe, K. *Nucleic Acids Res.* **2009**, 37, 5641.
- (18) (a) Zyskind, J. W.; Cleary, J. M.; Brusilow, W. S.; Harding, N. E.; Smith, D. W. *Proc. Natl. Acad. Sci. U.S.A.* **1983**, 80, 1164. (b) Kornberg, A. *Trends Biochem. Sci.* **1984**, 9, 122.
- (19) Wefald, F. C.; Devlin, B. H.; Williams, R. S. *Nature* **1990**, 344, 260.
- (20) Cusack, S. *Curr. Opin. Struct. Biol.* **1997**, 7, 881.
- (21) (a) Osborne, S. E.; Matsumura, I.; Ellington, A. D. *Curr. Opin. Chem. Biol.* **1997**, 1, 5. (b) Chang, K. Y.; Varani, G. *Nat. Struct. Biol.* **1997**, 4, 854. (c) Potyrailo, R. A.; Conrad, R. C.; Ellington, A. D.; Hieftje, G. M. *Anal. Chem.* **1998**, 70, 3419. (d) Hermann, T.; Patel, D. J. *Science* **2000**, 287, 820.
- (22) (a) Lee, J. F.; Stovall, G. M.; Ellington, A. D. *Curr. Opin. Struct. Biol.* **2006**, 10, 282. (b) Willner, I.; Zayats, M. *Angew. Chem., Int. Ed.* **2007**, 46, 6408. (c) Goulko, A. A.; Li, F.; Le, X. C. *Trends Anal. Chem.* **2009**, 28, 878.
- (23) (a) Zhou, J.; Battig, M. R.; Wang, Y. *Anal. Bioanal. Chem.* **2010**, 398, 2471. (b) Iliuk, A. B.; Hu, L.; Tao, W. A. *Anal. Chem.* **2011**, 83, 4440. (c) Famulok, M.; Mayer, G. *Acc. Chem. Res.* **2011**, 44, 1349.
- (24) Breaker, R. R.; Joyce, G. F. *Chem. Biol.* **1994**, 1, 223.
- (25) (a) Willner, I.; Shlyahovsky, B.; Zayats, M.; Willner, B. *Chem. Soc. Rev.* **2008**, 37, 1153. (b) Famulok, M.; Hartig, J. S.; Mayer, G. *Chem. Rev.* **2007**, 107, 3715. (c) Pan, W.; Clawson, G. A. *Expert Opin. Biol. Ther.* **2008**, 8, 1071. (d) Silverman, S. K. *Chem. Commun.* **2008**, 3467.
- (26) (a) Achenbach, J. C.; Chiuman, W.; Cruz, R. P. G.; Li, Y. *Curr. Pharm. Biotechnol.* **2004**, 5, 321. (b) Joyce, G. F. *Annu. Rev. Biochem.* **2004**, 73, 791. (c) Sando, S.; Sasaki, T.; Kanatani, K.; Aoyama, Y. *J. Am. Chem. Soc.* **2003**, 125, 15720. (d) Joyce, G. F. *Angew. Chem., Int. Ed.* **2007**, 46, 6420.
- (27) (a) Tuerk, C.; Gold, L. *Science* **1990**, 249, 505. (b) Ellington, A. D.; Szostak, J. W. *Nature* **1990**, 346, 818. (c) Osborn, S. E.; Ellington, A. D. *Chem. Rev.* **1997**, 97, 349. (d) Robertson, M. P.; Ellington, A. D. *Nat. Biotechnol.* **2001**, 19, 650. (e) Mendonsa, S. D.; Bowser, M. T. *Anal. Chem.* **2004**, 76, 5387.
- (28) (a) Gopinath, S. C. *Anal. Bioanal. Chem.* **2007**, 387, 171. (b) Sefah, K.; Shangguan, D.; Xiong, X.; O'Donoghue, M. B.; Tan, W. *Nat. Protoc.* **2010**, 5, 1169. (c) Waybrant, B.; Pearce, T. R.; Wang, P.; Sreevatsan, S.; Kokkoli, E. *Chem. Commun.* **2012**, 48, 10043.
- (29) (a) Yamamoto, R.; Murakami, K.; Taira, K.; Kumar, P. K. R. *Gene Ther. Mol. Biol.* **1998**, 1, 451. (b) Cox, J. C.; Ellington, A. D. *Bioorg. Med. Chem.* **2001**, 9, 2525. (c) Shamah, S. M.; Healy, J. M.; Cload, S. T. *Acc. Chem. Res.* **2008**, 41, 130.
- (30) (a) Sethi, V. S. *Prog. Biophys. Mol. Biol.* **1971**, 23, 67. (b) Johnne, R.; Müller, H.; Rector, A.; van Ranst, M.; Stevens, H. *Trends Microbiol.* **2009**, 17, 205. (c) Gill, J. P.; Wang, J.; Millar, D. P. *Biochem. Soc. Trans.* **2011**, 39, 595.
- (31) (a) Kornberg, A. *Science* **1960**, 131, 1503. (b) Lehman, I. R. *J. Biol. Chem.* **2003**, 278, 34743. (c) Friedberg, E. C. *Nat. Rev. Mol. Cell Biol.* **2006**, 7, 143.
- (32) (a) Kornberg, T.; Gefter, M. L. *Proc. Natl. Acad. Sci. U.S.A.* **1971**, 68, 761. (b) Ohmori, H.; Friedberg, E. C.; Fuchs, R. P.; Goodman, M. F.; Hanaoka, F.; Hinkle, D.; Kunkel, T. A.; Lawrence, C. W.; Livneh, Z.; Nohmi, T.; Prakash, L.; Prakash, S.; Todo, T.; Walker, G. C.; Wang, Z.; Woodgate, R. *Mol. Cell* **2001**, 8, 7. (c) Hubscher, U.; Maga, G.; Spadari, S. *Annu. Rev. Biochem.* **2002**, 71, 133.
- (33) (a) Gomez, D. E.; Armando, R. G.; Farina, H. G.; Menna, P. L.; Cerrudo, C. S.; Ghiringhelli, P. D.; Alonso, D. F. *Int. J. Oncol.* **2012**, 41, 1561. (b) Zhou, X.; Xing, D. *Chem. Soc. Rev.* **2012**, 41, 4643. (c) Günes, C.; Rudolph, K. L. *Cell* **2013**, 152, 390. (d) Xu, Y. *Chem. Soc. Rev.* **2011**, 40, 2719.
- (34) (a) Nicholls, C.; Li, H.; Wang, J. Q.; Liu, J. P. *Protein Cell* **2011**, 2, 726. (b) Gladych, M.; Wojtyla, A.; Rubis, B. *Biochem. Cell Biol.* **2011**, 89, 359. (c) Wojtyla, A.; Gladych, M.; Rubis, B. *Mol. Biol. Rep.* **2011**, 38, 3339.
- (35) (a) Martinez, P.; Blasco, M. A. *Nat. Rev. Cancer.* **2011**, 11, 161. (b) Mason, M.; Schuller, A.; Skordalakes, E. *Curr. Opin. Struct. Biol.* **2011**, 21, 92. (c) Lu, W.; Zhang, Y.; Liu, D.; Songyang, Z.; Wan, M. *Exp. Cell Res.* **2013**, 319, 133.
- (36) (a) Widlak, P.; Garrard, W. T. *J. Cell. Biochem.* **2005**, 94, 1078. (b) Calvin, K.; Li, H. *Cell. Mol. Life Sci.* **2008**, 65, 1176. (c) Fagbemi, A. F.; Orelli, B.; Schaerer, O. D. *DNA Repair* **2011**, 10, 722.
- (37) (a) Low, R. L. *Mitochondrion* **2003**, 2, 225. (b) Stoddard, B. L. Q. *Rev. Biophys.* **2005**, 38, 49. (c) Gupta, R.; Capalash, N.; Sharma, P. *Appl. Microbiol. Biotechnol.* **2012**, 94, 583.
- (38) (a) Rogers, S. G.; Weiss, B. *Methods Enzymol.* **1980**, 65, 201. (b) Mukherjee, D.; Fritz, D. T.; Kilpatrick, W. J.; Gao, M.; Wilusz, J. *Methods Mol. Biol.* **2004**, 257, 193. (c) West, S.; Gromak, N.; Proudfoot, N. J. *Nature* **2004**, 432, 522.
- (39) (a) Guo, L. H.; Wu, R. *Methods Enzymol.* **1983**, 100, 60. (b) Geerlings, T. H.; Vos, J. C.; Raué, H. A. *RNA* **2004**, 6, 1698. (c) Kaetzel, D. M.; Zhang, Q.; Yang, M.; McCorkle, J. R.; Ma, D.; Craven, R. J. *J. Bioenerg. Biomembr.* **2006**, 38, 163.
- (40) (a) Weiss, B.; Richardson, C. C. *Proc. Natl. Acad. Sci. U.S.A.* **1967**, 57, 1021. (b) Lehnman, I. R. *Science* **1974**, 186, 790. (c) Johnson, A.; O'Donnell, M. *Curr. Biol.* **2005**, 15, R90.
- (41) (a) Shuman, S.; Schwer, B. *Mol. Microbiol.* **1995**, 17, 405. (b) Shuman, S. *Structure* **1996**, 4, 653. (c) Dwivedi, N.; Dubre, D.; Pandey, J.; Singh, B.; Kukshal, V.; Ramachandran, R.; Tripathi, R. P. *Med. Res. Rev.* **2008**, 28, 545.
- (42) (a) Mohaghegh, P.; Hickson, I. D. *Hum. Mol. Genet.* **2001**, 10, 741. (b) Plank, J.; Hsieh, T. S. *J. Biol. Chem.* **2009**, 284, 30737. (c) Suhasini, A. N.; Brosh, R. M., Jr. *Cell Cycle* **2010**, 9, 2317.
- (43) (a) Patel, S. S.; Pandey, M.; Nandakumar, D. *Curr. Opin. Chem. Biol.* **2011**, 15, 595. (b) Wu, Y.; Brosh, R. M., Jr. *Nucleic Acids Res.* **2012**, 40, 4247. (c) Boos, D.; Frigola, J.; Diffley, J. F. *Curr. Opin. Cell Biol.* **2012**, 24, 423.
- (44) (a) Pavlov, V.; Shlyahovsky, B.; Willner, I. *J. Am. Chem. Soc.* **2005**, 127, 6522. (b) Ferguson, B. S.; Buchsbaum, S. F.; Swensen, J. S.; Hsieh, K.; Lou, X.; Soh, H. T. *Anal. Chem.* **2009**, 81, 6503. (c) Baur, J.; Gondran, C.; Holzinger, M.; Defrancq, E.; Perrot, H.; Cosnier, S. *Anal. Chem.* **2010**, 82, 1066. (d) Freeman, R.; Girsh, J.; Willner, I. *ACS Appl. Mater. Interfaces* **2013**, 5, 2815.
- (45) (a) Bardea, A.; Patolsky, F.; Dagan, A.; Willner, I. *Chem. Commun.* **1999**, 21. (b) Baker, B. R.; Lai, R. Y.; Wood, M. S.; Doctor, E. H.; Heeger, A. J.; Plaxco, K. W. *J. Am. Chem. Soc.* **2006**, 128, 3138. (c) Kolpashchikov, D. M. *J. Am. Chem. Soc.* **2006**, 128, 10625. (d) Kolpashchikov, D. M. *Chem. Rev.* **2010**, 110, 4709. (e) Yu, Z. G.; Lai, R. Y. *Chem. Commun.* **2012**, 48, 10523.
- (46) (a) Stojanovic, M. N.; de Prada, P.; Landry, D. W. *J. Am. Chem. Soc.* **2001**, 123, 4928. (b) O'Sullivan, C. K. *Anal. Bioanal. Chem.* **2002**, 372, 44. (c) Stojanovic, M. N.; Landry, D. W. *J. Am. Chem. Soc.* **2002**, 124, 9678. (d) Kirby, R.; Cho, E. J.; Gehrke, B.; Bayer, T.; Park, Y. S.; Neikirk, D. P.; McDevitt, J. T.; Ellington, A. D. *Anal. Chem.* **2004**, 76, 4066. (e) Niu, Y.; Zhao, Y.; Fan, A. *Anal. Chem.* **2011**, 83, 7500.
- (47) (a) Liu, X.; Aizen, R.; Freeman, R.; Yehezkel, O.; Willner, I. *ACS Nano* **2012**, 6, 3553. (b) Freeman, R.; Girsh, J.; Jou, A. F.; Ho, J. A.; Hug, T.; Dernedde, J.; Willner, I. *Anal. Chem.* **2012**, 84, 6192. (c) Zhang, Z.; Sharon, E.; Freeman, R.; Liu, X.; Willner, I. *Anal. Chem.* **2012**, 84, 4789. (d) Liu, X.; Freeman, R.; Willner, I. *Chem.—Eur. J.* **2012**, 18, 2207. (e) Lu, C. H.; Li, J.; Lin, M. H.; Wang, Y. W.; Yang, H. H.; Chen, X.; Chen, G. N. *Angew. Chem., Int. Ed.* **2010**, 49, 8454. (f) Hu, P.; Zhu, C.; Jin, L.; Dong, S. *Biosens. Bioelectron.* **2012**, 34, 83.

- (g) Lu, C. H.; Wang, F.; Willner, I. *Chem. Sci.* **2012**, *3*, 2616. (h) Li, J.; Fu, H. E.; Wu, L. J.; Zheng, A. X.; Chen, G. N.; Yang, H. H. *Anal. Chem.* **2012**, *84*, 5309.
- (48) (a) Wang, F.; Elbaz, J.; Orbach, R.; Magen, N.; Willner, I. *J. Am. Chem. Soc.* **2011**, *133*, 17149. (b) Xiao, Y.; Pavlov, V.; Niazov, T.; Dishon, A.; Kotler, M.; Willner, I. *J. Am. Chem. Soc.* **2004**, *126*, 7430. (c) Du, Y.; Li, B.; Wang, E. *Acc. Chem. Res.* **2013**, *46*, 203.
- (49) (a) Shimron, S.; Wang, F.; Orbach, R.; Willner, I. *Anal. Chem.* **2012**, *84*, 1042. (b) Zhou, W. H.; Zhu, C. L.; Lu, C. H.; Guo, X.; Chen, F.; Yang, H. H.; Wang, X. *Chem. Commun.* **2009**, 6845. (c) Gerasimova, Y. V.; Kolpashchikov, D. M. *Chem. Biol.* **2010**, *17*, 104.
- (50) (a) Shimron, S.; Elbaz, J.; Henning, A.; Willner, I. *Chem. Commun.* **2010**, *46*, 3250. (b) Kolpashchikov, D. M. *ChemBioChem* **2007**, *8*, 2039. (c) Kolpashchikov, D. M. *J. Am. Chem. Soc.* **2008**, *130*, 2934. (d) Li, T.; Shi, L.; Wang, E.; Dong, S. *Chem.—Eur. J.* **2009**, *15*, 1036.
- (51) (a) Elbaz, J.; Moshe, M.; Shlyahovsky, B.; Willner, I. *Chem.—Eur. J.* **2009**, *15*, 3411. (b) Liu, J.; Lu, Y. *J. Am. Chem. Soc.* **2007**, *129*, 9838. (c) Li, T.; Wang, E.; Dong, S. *Chem. Commun.* **2008**, 3654.
- (52) (a) Wang, F.; Elbaz, J.; Teller, C.; Willner, I. *Angew. Chem., Int. Ed.* **2011**, *50*, 295. (b) Liu, J.; Cao, Z.; Lu, Y. *Chem. Rev.* **2009**, *109*, 1948. (c) Zhang, X. B.; Kong, R. M.; Lu, Y. *Annu. Rev. Anal. Chem.* **2011**, *4*, 105.
- (53) (a) Pelossof, G.; Tel-Vered, R.; Willner, I. *Anal. Chem.* **2012**, *84*, 3703. (b) Shen, L.; Chen, Z.; Li, Y.; He, S.; Xie, S.; Xu, X.; Liang, Z.; Meng, X.; Li, Q.; Zhu, Z.; Li, M.; Le, X. C.; Shao, Y. *Anal. Chem.* **2008**, *80*, 6323. (c) Dong, X. Y.; Mi, X. N.; Zhang, L.; Liang, T. M.; Xu, J. J.; Chen, H. Y. *Biosens. Bioelectron.* **2012**, *38*, 337.
- (54) (a) Ronkainen, N. J.; Halsall, H. B.; Heineman, W. R. *Chem. Soc. Rev.* **2010**, *39*, 1747. (b) Liu, G.; Sun, C.; Li, D.; Song, S.; Mao, B.; Fan, C.; Tian, Z. *Adv. Mater.* **2010**, *22*, 2148. (c) Hocek, M.; Fojta, M. *Chem. Soc. Rev.* **2011**, *40*, 5802. (d) Wu, Y.; Lai, R. Y. *Chem. Commun.* **2013**, *49*, 3422. (e) Yu, Z. G.; Lai, R. Y. *Anal. Chem.* **2013**, *85*, 3340.
- (55) (a) Patolsky, F.; Lichtenstein, A.; Willner, I. *Angew. Chem., Int. Ed.* **2000**, *39*, 940. (b) Wang, J.; Wang, F.; Dong, S. *J. Electroanal. Chem.* **2009**, *626*, 1. (c) Yang, W.; Lai, R. Y. *Chem. Commun.* **2012**, *48*, 8703. (d) Yin, B. C.; Guan, Y. M.; Ye, B. C. *Chem. Commun.* **2012**, *48*, 4208. (e) Xuan, F.; Luo, X.; Hsing, I. M. *Biosens. Bioelectron.* **2012**, *35*, 230.
- (56) (a) Patolsky, F.; Weizmann, Y.; Willner, I. *J. Am. Chem. Soc.* **2002**, *124*, 770. (b) Drummond, T. G.; Hill, M. G.; Barton, J. K. *Nat. Biotechnol.* **2003**, *21*, 1192. (c) Li, D.; Yan, Y.; Wieckowska, A.; Willner, I. *Chem. Commun.* **2007**, 3544. (d) Cafete, S. J.; Lai, R. Y. *Chem. Commun.* **2010**, *46*, 3941. (e) Shiddiky, M. J.; Torriero, A. A.; Zeng, Z.; Spiccia, L.; Bond, A. M. *J. Am. Chem. Soc.* **2010**, *132*, 10053.
- (57) (a) Patolsky, F.; Lichtenstein, A.; Willner, I. *J. Am. Chem. Soc.* **2001**, *123*, 5194. (b) Lai, R. Y.; Plaxco, K. W.; Heeger, A. J. *Anal. Chem.* **2007**, *79*, 229. (c) Ikebukuro, K.; Kiyoohara, C.; Sode, K. *Biosens. Bioelectron.* **2005**, *20*, 2168. (d) Golub, E.; Pelossof, G.; Freeman, R.; Zhang, H.; Willner, I. *Anal. Chem.* **2009**, *81*, 9291. (e) Du, Y.; Chen, C.; Yin, J.; Li, B.; Zhou, M.; Dong, S.; Wang, E. *Anal. Chem.* **2010**, *82*, 1556.
- (58) (a) Fan, C. H.; Plaxco, K. W.; Heeger, A. J. *Proc. Natl. Acad. Sci. U.S.A.* **2003**, *100*, 9134. (b) Hansen, J. A.; Wang, J.; Kawde, A. N.; Xiang, Y.; Gothelf, K. V.; Collins, G. *J. Am. Chem. Soc.* **2006**, *128*, 2228. (c) Du, Y.; Li, B.; Wei, H.; Wang, Y.; Wang, E. *Anal. Chem.* **2008**, *80*, 5110. (d) Kannan, B.; Williams, D. E.; Booth, M. A.; Travas-Sejdic, J. *Anal. Chem.* **2011**, *83*, 3415. (e) Wang, L.; Xu, M.; Han, L.; Zhou, M.; Zhu, C.; Dong, S. *Anal. Chem.* **2012**, *84*, 7301.
- (59) (a) Patolsky, F.; Katz, E.; Willner, I. *Angew. Chem., Int. Ed.* **2002**, *41*, 3398. (b) Patolsky, F.; Lichtenstein, A.; Willner, I. *Chemistry* **2003**, *9*, 1137. (c) Castaneda, M. T.; Alegret, S.; Merkoci, A. *Methods Mol. Biol.* **2009**, *504*, 127. (d) Du, Y.; Li, B.; Wang, F.; Dong, S. *Biosens. Bioelectron.* **2009**, *24*, 1979.
- (60) (a) Zayats, M.; Huang, Y.; Gill, R.; Ma, C. A.; Willner, I. *J. Am. Chem. Soc.* **2006**, *128*, 13666. (b) Sharon, E.; Freeman, R.; Tel-Vered, R.; Willner, I. *Electroanalysis* **2009**, *21*, 1291. (c) Thomas, J. M.; Chakraborty, B.; Sen, D.; Yu, H. Z. *J. Am. Chem. Soc.* **2012**, *134*, 13823.
- (d) Kulkarni, A.; Xu, Y.; Ahn, C.; Amin, R.; Park, S. H.; Kim, T.; Lee, M. *J. Biotechnol.* **2012**, *160*, 91.
- (61) (a) Park, S. J.; Taton, T. A.; Mirkin, C. A. *Science* **2002**, *295*, 1503. (b) Sharon, E.; Freeman, R.; Riskin, M.; Gil, N.; Tzafati, Y.; Willner, I. *Anal. Chem.* **2010**, *82*, 8390. (c) Wenga, G.; Jacques, E.; Salaün, A. C.; Rogel, R.; Pichon, L.; Geneste, F. *Biosens. Bioelectron.* **2013**, *40*, 141. (d) Gonçalves, D.; Prazeres, D. M.; Chu, V.; Conde, J. P. *Biosens. Bioelectron.* **2008**, *24*, 545.
- (62) (a) Bardea, A.; Dagan, A.; Willner, I. *Anal. Chim. Acta* **1999**, *385*, 33. (b) Uslu, F.; Ingebrandt, S.; Mayer, D.; Böcker-Meffert, S.; Odenthal, M.; Offenhäusser, A. *Biosens. Bioelectron.* **2004**, *19*, 1723. (c) Kim, D. S.; Jeong, Y. T.; Park, H. J.; Shin, J. K.; Choi, P.; Lee, J. H.; Lim, G. *Biosens. Bioelectron.* **2004**, *20*, 69. (d) Uno, T.; Tabata, H.; Kawai, T. *Anal. Chem.* **2007**, *79*, 52.
- (63) (a) Piunno, P. A.; Krull, U. J.; Hudson, R. H.; Damha, M. J.; Cohen, H. *Anal. Chem.* **1995**, *67*, 2635. (b) Balakin, K. V.; Korshun, V. A.; Mikhalev, I. I.; Maleev, G. V.; Malakhov, A. D.; Prokhorenko, I. A.; Berlin, Yu. A. *Biosens. Bioelectron.* **1998**, *13*, 771. (c) Gaylord, B. S.; Heeger, A. J.; Bazan, G. C. *J. Am. Chem. Soc.* **2003**, *125*, 896. (d) Kwakye, S.; Baeumner, A. *Anal. Bioanal. Chem.* **2003**, *376*, 1062. (e) Krishnamoorthy, K.; Gokhale, R. S.; Contractor, A. Q.; Kumar, A. *Chem. Commun.* **2004**, 820. (f) Socher, E.; Bethge, L.; Knoll, A.; Jungnick, N.; Herrmann, A.; Seitz, O. *Angew. Chem., Int. Ed.* **2008**, *47*, 9555.
- (64) (a) Robelek, R.; Niu, L.; Schmid, E. L.; Knoll, W. *Anal. Chem.* **2004**, *76*, 6160. (b) Gaylord, B. S.; Massie, M. R.; Feinstein, S. C.; Bazan, G. C. *Proc. Natl. Acad. Sci. U.S.A.* **2005**, *102*, 34. (c) Liu, G. L.; Rodriguez, V. B.; Lee, L. P. *J. Nanosci. Nanotechnol.* **2005**, *5*, 1933. (d) Ho, H. A.; Doré, K.; Boissinot, M.; Bergeron, M. G.; Tanguay, R. M.; Boudreau, D.; Leclerc, M. *J. Am. Chem. Soc.* **2005**, *127*, 12673. (e) Pu, K. Y.; Liu, B. *Biosens. Bioelectron.* **2009**, *24*, 1067.
- (65) (a) Elghanian, R.; Storhoff, J. J.; Mucic, R. C.; Letsinger, R. L.; Mirkin, C. A. *Science* **1997**, *277*, 1078. (b) Storhoff, J. J.; Elghanian, R.; Mucic, R. C.; Mirkin, C. A.; Letsinger, R. L. *J. Am. Chem. Soc.* **1998**, *120*, 1959. (c) Massey, M.; Krull, U. J. *Anal. Bioanal. Chem.* **2010**, *398*, 1605. (d) Srinivas, A. R.; Peng, H.; Barker, D.; Travas-Sejdic, J. *Biosens. Bioelectron.* **2012**, *35*, 498. (e) Xing, X. J.; Liu, X. G.; He, Y.; Lin, Y.; Zhang, C. L.; Tang, H. W.; Pang, D. W. *Biomacromolecules* **2013**, *14*, 117.
- (66) (a) Tyagi, S.; Kramer, F. R. *Nat. Biotechnol.* **1996**, *4*, 303. (b) Giesendorf, B. A. J.; Vet, J. A. M.; Tyagi, S.; Mensink, E. J.; Trijbels, F. J.; Blom, H. *J. Clin. Chem.* **1998**, *44*, 482. (c) Patolsky, F.; Gill, R.; Weizmann, Y.; Mokari, T.; Banin, U.; Willner, I. *J. Am. Chem. Soc.* **2003**, *125*, 13918. (d) Sharon, E.; Freeman, R.; Willner, I. *Anal. Chem.* **2010**, *82*, 7073. (e) Wang, R. E.; Zhang, Y.; Cai, J.; Cai, W.; Gao, T. *Curr. Med. Chem.* **2011**, *18*, 4175.
- (67) (a) Marras, S. A. E.; Kramer, F. R.; Tyagi, S. *Genet. Anal.* **1999**, *14*, 151. (b) Nilsson, K. P. R.; Inganäs, O. *Nat. Mater.* **2003**, *2*, 419. (c) Tan, W. H.; Wang, K. M.; Drake, T. J. *Curr. Opin. Chem. Biol.* **2004**, *8*, 547. (d) Du, H.; Strohsahl, C. M.; Camera, J.; Miller, B. L.; Krauss, T. D. *J. Am. Chem. Soc.* **2005**, *127*, 7932. (e) Wang, K.; Tang, Z.; Yang, C. J.; Kim, Y.; Fang, X.; Li, W.; Wu, Y.; Medley, C. D.; Cao, Z.; Li, J.; Colon, P.; Lin, H.; Tan, W. *Angew. Chem., Int. Ed.* **2009**, *48*, 856.
- (68) (a) Ho, H. A.; Boissinot, M.; Bergeron, M. G.; Corbeil, G.; Doré, K.; Boudreau, D.; Leclerc, M. *Angew. Chem., Int. Ed.* **2002**, *41*, 1548. (b) Ho, H. A.; Leclerc, M. *J. Am. Chem. Soc.* **2004**, *126*, 1384. (c) Wang, S.; Gaylord, B. S.; Bazan, G. C. *J. Am. Chem. Soc.* **2004**, *126*, 5446. (d) Liu, B.; Bazan, G. C. *Chem. Mater.* **2004**, *16*, 4467. (e) Pelossof, G.; Tel-Vered, R.; Liu, X. Q.; Willner, I. *Chem.—Eur. J.* **2011**, *17*, 8904.
- (69) (a) Nicolini, C.; Erokhin, V.; Facci, P.; Guerzoni, S.; Ross, A.; Paschkevitsch, P. *Biosens. Bioelectron.* **1997**, *12*, 613. (b) Matsumo, H.; Niikura, K.; Okahata, Y. *Chem.—Eur. J.* **2001**, *7*, 3305. (c) Prakrankamanant, P.; Leelayuwat, C.; Promptmas, C.; Limpaiboon, T.; Wanram, S.; Prasongdee, P.; Pientong, C.; Daduang, J.; Jearanaikoon, P. *Biosens. Bioelectron.* **2013**, *40*, 252.
- (70) (a) Caruso, F.; Rodda, E.; Furlong, D. N.; Niikura, K.; Okahata, Y. *Anal. Chem.* **1997**, *69*, 2043. (b) Patolsky, F.; Lichtenstein, A.;

- Willner, I. *J. Am. Chem. Soc.* **2000**, *122*, 418. (c) Willner, I.; Patolsky, F.; Weizmann, Y.; Willner, B. *Talanta* **2002**, *56*, 847.
- (71) Tang, W.; Wang, D. Z.; Xu, Y.; Li, N.; Liu, F. *Chem. Commun.* **2012**, *48*, 6678.
- (72) (a) Fritz, J.; Baller, M. K.; Lang, H. P.; Rothuizen, H.; Vettiger, P.; Meyer, E.; Güntherodt, H.; Gerber, C.; Gimzewski, J. K. *Science* **2000**, *288*, 316. (b) Wu, G.; Ji, H.; Hansen, K.; Thundat, T.; Datar, R.; Cote, R.; Hagan, M. F.; Chakraborty, A. K.; Majumdar, A. *Proc. Natl. Acad. Sci. U.S.A.* **2001**, *98*, 1560. (c) Yang, S. M.; Chang, C.; Yin, T. I.; Kuo, P. L. *Sens. Actuators B Chem.* **2008**, *130*, 674.
- (73) (a) Albrecht, C.; Blank, K.; Lalic-Müllthaler, M.; Hirler, S.; Mai, T.; Gilbert, I.; Schiffmann, S.; Bayer, T.; Clausen-Schaumann, H.; Gaub, H. E. *Science* **2003**, *301*, 367. (b) Weizmann, Y.; Patolsky, F.; Lioubashevski, O.; Willner, I. *J. Am. Chem. Soc.* **2004**, *126*, 1073. (c) Zhao, Y.; Ganapathy-subramanian, B.; Shrotriya, P. *J. Appl. Phys.* **2012**, *111*, 074310.
- (74) (a) McKendry, R.; Zhang, J.; Arntz, Y.; Strunz, T.; Hegner, M.; Lang, H. P.; Baller, M. K.; Certa, U.; Meyer, E.; Güntherodt, H. J.; Gerber, C. *Proc. Natl. Acad. Sci. U.S.A.* **2002**, *99*, 9783. (b) Zhang, N. H.; Tan, Z. Q.; Li, J. J.; Meng, W. L.; Xu, L. W. *Curr. Opin. Colloid Interface Sci.* **2011**, *16*, 592.
- (75) (a) Ho, D.; Falter, K.; Severin, P.; Gaub, H. E. *Anal. Chem.* **2009**, *81*, 3159. (b) Choi, J. M.; Hwang, S. U.; Kim, C. H.; Yang, H. H.; Jung, C.; Gyu Park, H.; Yoon, J. B.; Choi, Y. K. *Appl. Phys. Lett.* **2012**, *100*, 163701.
- (76) (a) Kim, E.; Kim, K.; Yang, H.; Kim, Y. T.; Kwak, J. *Anal. Chem.* **2003**, *75*, 5665. (b) Gill, R.; Polksky, R.; Willner, I. *Small* **2006**, *2*, 1037. (c) Polksky, R.; Gill, R.; Kaganovsky, L.; Willner, I. *Anal. Chem.* **2006**, *78*, 2268. (d) Shiddiky, M. J.; Rahman, M. A.; Shim, Y. B. *Anal. Chem.* **2007**, *79*, 6886. (e) Wang, G.; Wang, Y.; Chen, L.; Choo, J. *Biosens. Bioelectron.* **2010**, *25*, 1859. (f) Prusty, D. K.; Herrmann, A. *J. Am. Chem. Soc.* **2010**, *132*, 12197.
- (77) (a) Caruana, D. J.; Heller, A. *J. Am. Chem. Soc.* **1999**, *121*, 769. (b) Patolsky, F.; Lichtenstein, A.; Willner, I. *Nat. Biotechnol.* **2001**, *19*, 253. (c) Das, J.; Aziz, M. A.; Yang, H. *J. Am. Chem. Soc.* **2006**, *128*, 16022. (d) Wang, Z.; Hu, J.; Jin, Y.; Yao, X.; Li, J. *Clin. Chem.* **2006**, *52*, 1958. (e) Liu, G.; Wan, Y.; Gau, V.; Zhang, J.; Wang, L.; Song, S.; Fan, C. *J. Am. Chem. Soc.* **2008**, *130*, 6820. (f) Prusty, D. K.; Kwak, M.; Wildeman, J.; Herrmann, A. *Angew. Chem., Int. Ed.* **2012**, *51*, 11894.
- (78) (a) Zuo, X.; Xia, F.; Xiao, Y.; Plaxco, K. W. *J. Am. Chem. Soc.* **2010**, *132*, 1816. (b) Li, X.; Ding, T.; Sun, L.; Mao, C. *Biosens. Bioelectron.* **2011**, *30*, 241. (c) Zhu, Z.; Gao, F.; Lei, J.; Dong, H.; Ju, H. *Chem.—Eur. J.* **2012**, *18*, 13871. (d) Luo, M.; Xiang, X.; Xiang, D.; Yang, S.; Ji, X.; He, Z. *Chem. Commun.* **2012**, *48*, 7416. (e) Liu, S.; Wang, C.; Zhang, C.; Wang, Y.; Tang, B. *Anal. Chem.* **2013**, *85*, 2282.
- (79) (a) Hsieh, K.; Xiao, Y.; Tom Soh, H. *Langmuir* **2010**, *26*, 10392. (b) Xuan, F.; Luo, X.; Hsing, I. M. *Anal. Chem.* **2012**, *84*, 5216. (c) Wu, D.; Yin, B. C.; Ye, B. C. *Biosens. Bioelectron.* **2011**, *28*, 232. (d) Xu, Q.; Cao, A.; Zhang, L. F.; Zhang, C. Y. *Anal. Chem.* **2012**, *84*, 10845. (e) Ju, E.; Yang, X.; Lin, Y.; Pu, F.; Ren, J.; Qu, X. *Chem. Commun.* **2012**, *48*, 11662.
- (80) (a) Liu, Z.; Zhang, W.; Zhu, S.; Zhang, L.; Hu, L.; Parveen, S.; Xu, G. *Biosens. Bioelectron.* **2011**, *29*, 215. (b) Freeman, R.; Liu, X.; Willner, I. *Nano Lett.* **2011**, *11*, 4456. (c) Zhao, C.; Wu, L.; Ren, J.; Qu, X. *Chem. Commun.* **2011**, *47*, 5461. (d) Yang, C. J.; Cui, L.; Huang, J.; Yan, L.; Lin, X.; Wang, C.; Zhang, W. Y.; Kang, H. *Biosens. Bioelectron.* **2011**, *27*, 119. (e) Miranda-Castro, R.; Marchal, D.; Limoges, B.; Mavré, F. *Chem. Commun.* **2012**, *48*, 8772.
- (81) (a) Lin, C.; Liu, Y.; Rinker, S.; Yan, H. *ChemPhysChem* **2006**, *7*, 1641. (b) Niemeyer, C. M. *Angew. Chem., Int. Ed.* **2010**, *49*, 1200. (c) Lin, C.; Ke, Y.; Chhabra, R.; Sharma, J.; Liu, Y.; Yan, H. *Methods Mol. Biol.* **2011**, *749*, 1. (d) Wilner, O. I.; Willner, I. *Chem. Rev.* **2012**, *112*, 2528. (e) Wang, F.; Willner, B.; Willner, I. *Curr. Opin. Biotechnol.* **2013**, *24*, 562.
- (82) (a) Winfree, E.; Liu, F.; Wenzler, L. A.; Seeman, N. C. *Nature* **1998**, *394*, 539. (b) Aldaye, F. A.; Palmer, A. L.; Sleiman, H. F. *Science* **2008**, *321*, 1795. (c) Teller, C.; Willner, I. *Trends Biotechnol.* **2010**, *28*, 619. (d) Ke, Y.; Voigt, N. V.; Gothelf, K. V.; Shih, W. M. *J. Am. Chem. Soc.* **2012**, *134*, 1770.
- (83) (a) Mao, C.; Sun, W.; Seeman, N. C. *J. Am. Chem. Soc.* **1999**, *121*, 5437. (b) Chelyapov, N.; Brun, Y.; Gopalkrishnan, M.; Reishus, D.; Shaw, B.; Adleman, L. *J. Am. Chem. Soc.* **2004**, *126*, 13924. (c) Sharma, J.; Chhabra, R.; Liu, Y.; Ke, Y.; Yan, H. *Angew. Chem., Int. Ed.* **2006**, *45*, 730. (d) Gothelf, K. V. *Science* **2012**, *338*, 1159.
- (84) (a) Chen, J.; Seeman, N. C. *Nature* **1991**, *350*, 631. (b) Mitchell, J. C.; Harris, J. R.; Malo, J.; Bath, J.; Turberfield, A. *J. Am. Chem. Soc.* **2004**, *126*, 16342. (c) Aldaye, F. A.; Sleiman, H. F. *J. Am. Chem. Soc.* **2007**, *129*, 4130. (d) Voigt, N. V.; Tørring, T.; Rotaru, A.; Jacobsen, M. F.; Ravnsbaek, J. B.; Subramani, R.; Mamdouh, W.; Kjems, J.; Mokhir, A.; Besenbacher, F.; Gothelf, K. V. *Nat. Nanotechnol.* **2010**, *5*, 200.
- (85) (a) Fu, T. J.; Seeman, N. C. *Biochemistry* **1993**, *32*, 3211. (b) LaBean, T. H.; Yan, H.; Kopatsch, J.; Liu, F.; Winfree, E.; Reif, J. H.; Seeman, N. C. *J. Am. Chem. Soc.* **2000**, *122*, 1848. (c) He, Y.; Chen, Y.; Liu, H.; Ribbe, A. E.; Mao, C. *J. Am. Chem. Soc.* **2005**, *127*, 12202. (d) Ke, Y.; Ong, L.; Shih, W.; Yin, P. *Science* **2012**, *338*, 1177. (e) Liu, Y.; Lin, C.; Li, H.; Yan, H. *Angew. Chem., Int. Ed.* **2005**, *44*, 4333.
- (86) (a) Ding, B.; Sha, R.; Seeman, N. C. *J. Am. Chem. Soc.* **2004**, *126*, 10230. (b) Park, S. H.; Barish, R.; Li, H.; Reif, J. H.; Finkelstein, G.; Yan, H.; LaBean, T. H. *Nano Lett.* **2005**, *5*, 693. (c) Wei, B.; Dai, M.; Yin, P. *Nature* **2012**, *485*, 623. (d) Majumder, U.; Rangnekar, A.; Gothelf, K. V.; Reif, J. H.; LaBean, T. H. *J. Am. Chem. Soc.* **2011**, *133*, 3843. (e) Schnitzler, T.; Herrmann, A. *Acc. Chem. Res.* **2012**, *45*, 1419.
- (87) (a) Mathieu, F.; Liao, S.; Kopatsch, J.; Wang, T.; Mao, C.; Seeman, N. C. *Nano Lett.* **2005**, *5*, 661. (b) Liu, Y.; Ke, Y.; Yan, H. *J. Am. Chem. Soc.* **2005**, *127*, 17140. (c) Ke, Y.; Liu, Y.; Zhang, J.; Yan, H. *J. Am. Chem. Soc.* **2006**, *128*, 4414. (d) McLaughlin, C. K.; Hamblin, G. D.; Sleiman, H. F. *Chem. Soc. Rev.* **2011**, *40*, 5647. (e) Kwak, M.; Herrmann, A. *Chem. Soc. Rev.* **2011**, *40*, 5745.
- (88) (a) Weizmann, Y.; Braunschweig, A. B.; Wilner, O. I.; Cheglakov, Z.; Willner, I. *Proc. Natl. Acad. Sci. U.S.A.* **2008**, *105*, 5289. (b) Wilner, O. I.; Henning, A.; Shlyahovsky, B.; Willner, I. *Nano Lett.* **2010**, *10*, 1458. (c) Wilner, O. I.; Orbach, R.; Henning, A.; Teller, C.; Yehezkel, O.; Mertig, M.; Harries, D.; Willner, I. *Nat. Commun.* **2011**, *2*, 540. (d) Hamblin, G. D.; Hariiri, A. A.; Carneiro, K. M.; Lau, K. L.; Cosa, G.; Sleiman, H. F. *ACS Nano* **2013**, *7*, 3022.
- (89) (a) Rothemund, P. W.; Ekani-Nkodo, A.; Papadakis, N.; Kumar, A.; Fygenson, D. K.; Winfree, E. *J. Am. Chem. Soc.* **2004**, *126*, 16344. (b) Liu, H.; Chen, Y.; He, Y.; Ribbe, A. E.; Mao, C. *Angew. Chem., Int. Ed.* **2006**, *45*, 1942. (c) O'Neill, P.; Rothenmund, P. W.; Kumar, A.; Fygenson, D. K. *Nano Lett.* **2006**, *6*, 1379. (d) Yang, H.; Altvater, F.; de Bruijn, A. D.; McLaughlin, C. K.; Lo, P. K.; Sleiman, H. F. *Angew. Chem., Int. Ed.* **2011**, *50*, 4620.
- (90) Wang, Z. G.; Wilner, O. I.; Willner, I. *Nano Lett.* **2009**, *9*, 4098.
- (91) Wilner, O. I.; Shimron, S.; Weizmann, Y.; Wang, Z. G.; Willner, I. *Nano Lett.* **2009**, *9*, 2040.
- (92) Wilner, O. I.; Weizmann, Y.; Gill, R.; Lioubashevski, O.; Freeman, R.; Willner, I. *Nat. Nanotechnol.* **2009**, *4*, 249.
- (93) Fu, J.; Liu, M.; Liu, Y.; Woodbury, N. W.; Yan, H. *J. Am. Chem. Soc.* **2012**, *134*, 5516.
- (94) (a) Rothenmund, P. W. K. *Nature* **2006**, *440*, 297. (b) Jungmann, R.; Liedl, T.; Sobey, T. L.; Shih, W.; Simmel, F. C. *J. Am. Chem. Soc.* **2008**, *130*, 10062. (c) Ke, Y.; Sharma, J.; Liu, M.; Jahn, K.; Liu, Y.; Yan, H. *Nano Lett.* **2009**, *9*, 2445. (d) Bandy, T. J.; Brewer, A.; Burns, J. R.; Marth, G.; Nguyen, T.; Stulz, E. *Chem. Soc. Rev.* **2011**, *40*, 138.
- (95) (a) Shih, W. M.; Lin, C. *Curr. Opin. Struct. Biol.* **2010**, *20*, 276. (b) Han, D.; Pal, S.; Yang, Y.; Jiang, S.; Nangreave, J.; Liu, Y.; Yan, H. *Science* **2013**, *339*, 1412. (c) Wang, F.; Willner, B.; Willner, I. *Curr. Opin. Chem. Biol.* **2013**, *24*, S62.
- (96) (a) Becerril, H. A.; Woolley, A. T. *Chem. Soc. Rev.* **2009**, *38*, 329. (b) Han, D.; Pal, S.; Liu, Y.; Yan, H. *Nat. Nanotechnol.* **2010**, *5*, 712. (c) Han, D.; Pal, S.; Nangreave, J.; Deng, Z.; Liu, Y.; Yan, H. *Science* **2011**, *332*, 342. (d) Andersen, E. S.; Dong, M.; Nielsen, M. M.; Jahn, K.; Lind-Thomsen, A.; Mamdouh, W.; Gothelf, K. V.; Besenbacher, F.; Kjems, J. *ACS Nano* **2008**, *2*, 1213.
- (97) (a) Pitchaiya, S.; Krishnan, Y. *Chem. Soc. Rev.* **2006**, *35*, 1111. (b) Rinker, S.; Ke, Y.; Liu, Y.; Chhabra, R.; Yan, H. *Nat. Nanotechnol.*

- 2008, 3, 418. (c) Nangreave, J.; Han, D.; Liu, Y.; Yan, H. *Curr. Opin. Chem. Biol.* 2010, 14, 608. (d) Numajiri, K.; Kimura, M.; Kuzuya, A.; Komiyama, M. *Chem. Commun.* 2010, 46, 5127.
- (98) (a) Andersen, E. S.; Dong, M.; Nielsen, M. M.; Jahn, K.; Subramani, R.; Mamdouh, W.; Golas, M. M.; Sander, B.; Stark, H.; Oliveira, C. L. P.; Pedersen, J. S.; Birkedal, V.; Besenbacher, F.; Gothelf, K. V.; Kjems, J. *Nature* 2009, 459, 73. (b) Douglas, S. M.; Dietz, H.; Liedl, T.; Höglberg, B.; Graf, F.; Shih, W. M. *Nature* 2009, 459, 414. (c) Dietz, H.; Douglas, S. M.; Shih, W. M. *Science* 2009, 325, 725.
- (99) (a) Liedl, T.; Höglberg, B.; Tytell, J.; Ingber, D. E.; Shih, W. M. *Nat. Nanotechnol.* 2010, 5, 520. (b) Langecker, M.; Arnaut, V.; Martin, T. G.; List, J.; Renner, S.; Mayer, M.; Dietz, H.; Simmel, F. C. *Science* 2012, 338, 932. (c) Fu, Y.; Zeng, D.; Chao, J.; Jin, Y.; Zhang, Z.; Liu, H.; Li, D.; Ma, H.; Huang, Q.; Gothelf, K. V.; Fan, C. *J. Am. Chem. Soc.* 2013, 135, 696.
- (100) (a) Niemeyer, C. M.; Koehler, J.; Wuerdemann, C. *ChemBioChem* 2002, 3, 242. (b) Müller, J.; Niemeyer, C. M. *Biochem. Biophys. Res. Commun.* 2008, 377, 62. (c) Diezmann, F.; Seitz, O. *Chem. Soc. Rev.* 2011, 40, 5789. (d) Fu, J.; Liu, M.; Liu, Y.; Yan, H. *Acc. Chem. Res.* 2012, 45, 1215.
- (101) Erkelenz, M.; Kuo, C. H.; Niemeyer, C. M. *J. Am. Chem. Soc.* 2011, 133, 16111.
- (102) Freeman, R.; Sharon, E.; Tel-Vered, R.; Willner, I. *J. Am. Chem. Soc.* 2009, 131, 5028.
- (103) Freeman, R.; Sharon, E.; Teller, C.; Willner, I. *Chem.—Eur. J.* 2010, 16, 3690.
- (104) Golub, E.; Freeman, R.; Niazov, A.; Willner, I. *Analyst* 2011, 136, 4397.
- (105) Shlyahovsky, B.; Li, D.; Katz, E.; Willner, I. *Biosens. Bioelectron.* 2007, 22, 2570.
- (106) (a) Liu, D.; Park, S. H.; Reif, J. H.; LaBean, T. H. *Proc. Natl. Acad. Sci. U.S.A.* 2004, 101, 717. (b) Maune, H. T.; Han, S. P.; Barish, R. D.; Bockrath, M.; Goddard, W. A., III; Rothmund, P. W. K.; Winfree, E. *Nat. Nanotechnol.* 2010, 5, 61. (c) Saccà, B.; Niemeyer, C. M. *Chem. Soc. Rev.* 2011, 40, 5910. (d) Yamazaki, T.; Aiba, Y.; Yasuda, K.; Sakai, Y.; Yamanaka, Y.; Kuzuya, A.; Ohya, Y.; Komiyama, M. *Chem. Commun.* 2012, 48, 11361.
- (107) (a) Gothelf, K. V.; LaBean, T. H. *Org. Biomol. Chem.* 2005, 3, 4023. (b) Bell, N. A.; Engst, C. R.; Ablay, M.; Divitini, G.; Ducati, C.; Liedl, T.; Keyser, U. F. *Nano Lett.* 2012, 12, 512. (c) Wei, R.; Martin, T. G.; Rant, U.; Dietz, H. *Angew. Chem., Int. Ed.* 2012, 51, 4864. (d) Wang, R.; Nuckolls, C.; Wind, S. J. *Angew. Chem., Int. Ed.* 2012, 51, 11325.
- (108) (a) Patolsky, F.; Weizmann, Y.; Lioubashevski, O.; Willner, I. *Angew. Chem., Int. Ed.* 2002, 41, 2323. (b) Xiao, Y.; Kharitonov, A. B.; Patolsky, F.; Weizmann, Y.; Willner, I. *Chem. Commun.* 2003, 1540. (c) Weizmann, Y.; Patolsky, F.; Popov, I.; Willner, I. *Nano Lett.* 2004, 4, 787. (d) Gothelf, K. V.; Brown, R. S. *Chem.—Eur. J.* 2005, 11, 1062.
- (109) (a) Yan, H.; Zhang, X.; Shen, Z.; Seeman, N. C. *Nature* 2002, 415, 62. (b) Dittmer, W. U.; Reuter, A.; Simmel, F. C. *Angew. Chem., Int. Ed.* 2004, 43, 3550. (c) Krishnan, Y.; Simmel, F. C. *Angew. Chem., Int. Ed.* 2011, 50, 3124.
- (110) (a) Seeman, N. C. *Trends Biochem. Sci.* 2005, 30, 119. (b) Liu, D. S.; Cheng, E.; Yang, Z. Q. *NPG Asia Mater.* 2011, 3, 109. (c) Pinheiro, A. V.; Han, D.; Shih, W. M.; Yan, H. *Nat. Nanotechnol.* 2011, 6, 763.
- (111) (a) Bath, J.; Turberfield, A. J. *Nat. Biotechnol.* 2007, 2, 275. (b) Goodman, R. P.; Heilemann, M.; Doose, S.; Erben, C. M.; Kapanidis, A. N.; Turberfield, A. J. *Nat. Nanotechnol.* 2008, 3, 93. (c) Liu, H.; Liu, D. *Chem. Commun.* 2009, 2625.
- (112) (a) Simmel, F. C.; Dittmer, W. U. *Small* 2005, 1, 284. (b) Lubrich, D.; Lin, J.; Yan, J. *Angew. Chem., Int. Ed.* 2008, 47, 7026. (c) Teller, C.; Willner, I. *Curr. Opin. Biotechnol.* 2010, 21, 376.
- (113) Venkataraman, S.; Dirks, R. M.; Rothmund, P. W. K.; Winfree, E.; Pierce, N. A. *Nat. Nanotechnol.* 2007, 2, 490.
- (114) Yurke, B.; Turberfield, A. J.; Mills, A. P., Jr.; Simmel, F. C.; Neumann, J. L. *Nature* 2000, 406, 605.
- (115) Omabegho, T.; Sha, R.; Seeman, N. C. *Science* 2009, 324, 67.
- (116) Wang, C.; Ren, J.; Qu, X. *Chem. Commun.* 2011, 47, 1428.
- (117) Wang, Z. G.; Elbaz, J.; Willner, I. *Nano Lett.* 2011, 11, 304.
- (118) (a) Liu, D.; Balasubramanian, S. *Angew. Chem., Int. Ed.* 2003, 42, 5734. (b) Liu, D.; Bruckbauer, A.; Abell, C.; Balasubramanian, S.; Kang, D.; Klenerman, D.; Zhou, D. *J. Am. Chem. Soc.* 2006, 128, 2067. (c) Wang, W.; Yang, Y.; Cheng, E.; Zhao, M.; Meng, H.; Liu, D.; Zhou, D. *Chem. Commun.* 2009, 824. (d) Wang, C.; Huang, Z.; Lin, Y.; Ren, J.; Qu, X. *Adv. Mater.* 2010, 22, 2792. (e) Yang, Y.; Liu, G.; Liu, H.; Li, D.; Fan, C.; Liu, D. *Nano Lett.* 2010, 10, 1393.
- (119) (a) Elbaz, J.; Wang, Z. G.; Orbach, R.; Willner, I. *Nano Lett.* 2009, 9, 4510. (b) Modi, S. M. G. S.; Goswami, D.; Gupta, G. D.; Mayor, S.; Krishnan, Y. *Nat. Nanotechnol.* 2009, 4, 325. (c) Surana, S.; Bhat, J. M.; Koushika, S. P.; Krishnan, Y. *Nat. Commun.* 2011, 2, 340. (d) Qi, X. J.; Lu, C. H.; Liu, X.; Shimron, S.; Yang, H. H.; Willner, I. *Nano Lett.* 2013, 13, 4920.
- (120) Wang, Z. G.; Elbaz, J.; Remacle, F.; Levine, R. D.; Willner, I. *Proc. Natl. Acad. Sci. U.S.A.* 2010, 107, 21996.
- (121) Ogura, Y.; Nishimura, T.; Tanida, J. *Appl. Phys. Exp.* 2009, 2, 025004.
- (122) (a) Liu, H.; Xu, Y.; Li, F.; Yang, Y.; Wang, W.; Song, Y.; Liu, D. *Angew. Chem., Int. Ed.* 2007, 46, 2515. (b) Liu, H.; Zhou, Y.; Yang, Y.; Wang, W.; Qu, L.; Chen, C.; Liu, D.; Zhang, D.; Zhu, D. *J. Phys. Chem. B.* 2008, 112, 6893. (c) Kopelman, R. *ACS Nano* 2012, 6, 7553.
- (123) (a) Kang, H.; Liu, H.; Phillips, J. A.; Cao, Z.; Kim, Y.; Chen, Y.; Yang, Z.; Li, J.; Tan, W. *Nano Lett.* 2009, 9, 2690. (b) Dohno, C.; Nakatani, K. *Chem. Soc. Rev.* 2011, 40, 5718. (c) Lohmann, F.; Ackermann, D.; Famulok, M. *J. Am. Chem. Soc.* 2012, 134, 11884.
- (124) You, M.; Huang, F.; Chen, Z.; Wang, R. W.; Tan, W. *ACS Nano* 2012, 6, 7935.
- (125) You, M.; Chen, Y.; Zhang, X.; Liu, H.; Wang, R.; Wang, K.; Williams, K. R.; Tan, W. *Angew. Chem., Int. Ed.* 2012, 51, 2457.
- (126) Yin, P.; Yan, H.; Daniell, X. G.; Turberfield, A. J.; Reif, J. H. *Angew. Chem., Int. Ed.* 2004, 43, 4906.
- (127) Tian, Y.; He, Y.; Chen, Y.; Yin, P.; Mao, C. *Angew. Chem., Int. Ed.* 2005, 44, 4355.
- (128) (a) Wickham, S. F.; Bath, J.; Katsuda, Y.; Endo, M.; Hidaka, K.; Sugiyama, H.; Turberfield, A. J. *Nat. Nanotechnol.* 2012, 7, 169. (b) Wickham, S. F.; Endo, M.; Katsuda, Y.; Hidaka, K.; Bath, J.; Sugiyama, H.; Turberfield, A. J. *Nat. Nanotechnol.* 2011, 6, 166.
- (129) Bath, J.; Green, S. J.; Turberfield, A. J. *Angew. Chem., Int. Ed.* 2005, 44, 4358.
- (130) (a) Kelly, T. R. *Angew. Chem., Int. Ed.* 2005, 44, 4124. (b) Elbaz, J.; Tel-Vered, R.; Freeman, R.; Yildiz, H. B.; Willner, I. *Angew. Chem., Int. Ed.* 2009, 48, 133.
- (131) (a) Liedl, T.; Simmel, F. C. *Nano Lett.* 2005, 5, 1894. (b) Liedl, T.; Olapinski, M.; Simmel, F. C. *Angew. Chem., Int. Ed.* 2006, 45, 5007.
- (132) Elbaz, J.; Moshe, M.; Willner, I. *Angew. Chem., Int. Ed.* 2009, 48, 3834.
- (133) (a) Dittmer, W. U.; Simmel, F. C. *Nano Lett.* 2004, 4, 689. (b) Chhabra, R.; Sharma, J.; Liu, Y.; Yan, H. *Nano Lett.* 2006, 6, 978. (c) Han, X.; Zhou, Z.; Yang, F.; Deng, Z. *J. Am. Chem. Soc.* 2008, 130, 14414. (d) Zhou, C.; Yang, Z.; Liu, D. *J. Am. Chem. Soc.* 2012, 134, 1416.
- (134) (a) Shin, J. S.; Pierce, N. A. *J. Am. Chem. Soc.* 2004, 126, 10834. (b) Simmel, F. C. *ChemPhysChem* 2009, 10, 2593. (c) Ouldridge, T. E.; Hoare, R. L.; Louis, A. A.; Doye, J. P.; Bath, J.; Turberfield, A. J. *ACS Nano* 2013, 7, 2479.
- (135) Liu, X.; Niazov-Elkan, A.; Wang, F.; Willner, I. *Nano Lett.* 2013, 13, 219.
- (136) (a) Muscat, R. A.; Bath, J.; Turberfield, A. J. *Nano Lett.* 2011, 11, 982. (b) Wang, Z. G.; Elbaz, J.; Willner, I. *Angew. Chem., Int. Ed.* 2012, 51, 4322.
- (137) (a) Klapper, Y.; Sinha, N.; Ng, T. W.; Lubrich, D. *Small* 2010, 6, 44. (b) Lu, C. H.; Cecconello, A.; Elbaz, J.; Credi, A.; Willner, I. *Nano Lett.* 2013, 13, 2303.
- (138) Elbaz, J.; Wang, Z. G.; Wang, F.; Willner, I. *Angew. Chem., Int. Ed.* 2012, 51, 2349.
- (139) (a) Bath, J.; Green, S. J.; Allen, K. E.; Turberfield, A. J. *Small* 2009, 5, 1513. (b) Saccà, B.; Siebers, B.; Meyer, R.; Bayer, M.;

- Niemeyer, C. M. *Small* **2012**, *8*, 3000. (c) Pelossof, G.; Tel-Vered, R.; Liu, X.; Willner, I. *Nanoscale* **2013**, *5*, 8977.
- (140) (a) Tian, Y.; Mao, C. *J. Am. Chem. Soc.* **2004**, *126*, 11410. (b) Bhatia, D.; Sharma, S.; Krishnan, Y. *Curr. Opin. Biotechnol.* **2011**, *22*, 475. (c) Zhang, Z.; Olsen, E. M.; Kryger, M.; Voigt, N. V.; Tørring, T.; Gültæk, E.; Nielsen, M.; MohammadZadegan, R.; Andersen, E. S.; Nielsen, M. M.; Kjems, J.; Birkedal, V.; Gothelf, K. V. *Angew. Chem., Int. Ed.* **2011**, *50*, 3983.
- (141) (a) Sebba, D. S.; Mock, J. J.; Smith, D. R.; Labean, T. H.; Lazarides, A. A. *Nano Lett.* **2008**, *8*, 1803. (b) Maye, M. M.; Kumara, M. T.; Nykypanchuk, D.; Sherman, W. B.; Gang, O. *Nat. Nanotechnol.* **2010**, *5*, 116. (c) Chen, J. I.; Chen, Y.; Ginger, D. S. *J. Am. Chem. Soc.* **2010**, *132*, 9600.
- (142) (a) Lermusiaux, L.; Sereda, A.; Portier, B.; Larquet, E.; Bidault, S. *ACS Nano* **2012**, *6*, 10992. (b) Xu, P. F.; Hung, A. M.; Noh, H.; Cha, J. N. *Small* **2013**, *9*, 228. (c) Guo, L.; Ferhan, A. R.; Chen, H.; Li, C.; Chen, G.; Hong, S.; Kim, D. H. *Small* **2013**, *9*, 234.
- (143) (a) Park, S. Y.; Lytton-Jean, A. K. R.; Lee, B.; Weigand, S.; Schatz, G. C.; Mirkin, C. A. *Nature* **2008**, *451*, 553. (b) Macfarlane, R. J.; Lee, B.; Hill, H. D.; Senesi, A. J.; Seifert, S.; Mirkin, C. A. *Proc. Natl. Acad. Sci. U.S.A.* **2009**, *106*, 10493. (c) Jones, M. R.; Macfarlane, R. J.; Lee, B.; Zhang, J.; Young, K. L.; Senesi, A. J.; Mirkin, C. A. *Nat. Mater.* **2010**, *9*, 913.
- (144) (a) Tan, S. J.; Campolongo, M. J.; Luo, D.; Cheng, W. *Nat. Nanotechnol.* **2011**, *6*, 268. (b) Cheng, W.; Campolongo, M. J.; Cha, J. J.; Tan, S. J.; Umbach, C. C.; Muller, D. A.; Luo, D. *Nat. Mater.* **2009**, *8*, 519. (c) Elbaz, J.; Ceccarello, A.; Fan, Z.; Govorov, A. O.; Willner, I. *Nat. Commun.* **2013**, *4*, 2000. (d) Shimron, S.; Ceccarello, A.; Lu, C. H.; Willner, I. *Nano Lett.* **2013**, *13*, 3791.
- (145) (a) Macfarlane, R.; Lee, B.; Jones, M.; Harris, N.; Schatz, G.; Mirkin, C. A. *Science* **2011**, *334*, 204. (b) Jones, M. R.; Mirkin, C. A. *Angew. Chem., Int. Ed.* **2013**, *52*, 2886. (c) Wen, Y.; Chen, L.; Wang, W.; Xu, L.; Du, H.; Zhang, Z.; Zhang, X.; Song, Y. *Chem. Commun.* **2012**, *48*, 3963.
- (146) Gu, H.; Chao, J.; Xiao, S. J.; Seeman, N. C. *Nature* **2010**, *465*, 202.
- (147) Lund, K.; Manzo, A. J.; Dabby, N.; Michelotti, N.; Johnson-Buck, A.; Nangreave, J.; Taylor, S.; Pei, R.; Stojanovic, M. N.; Walter, N. G.; Winfree, E.; Yan, H. *Nature* **2010**, *465*, 206.
- (148) (a) Lee, J. B.; Roh, Y. H.; Um, S. H.; Funabashi, H.; Cheng, W.; Cha, J. J.; Kiatwuthinon, P.; Muller, D. A.; Luo, D. *Nat. Nanotechnol.* **2009**, *4*, 430. (b) Peng, S.; Lee, J. B.; Yang, D.; Roh, Y. H.; Funabashi, H.; Park, N.; Rice, E. J.; Chen, L.; Long, R.; Wu, M.; Luo, D. *Nat. Nanotechnol.* **2012**, *7*, 816. (c) Guo, W.; Orbach, R.; Mironi-Harpaz, I.; Seliktar, D.; Willner, I. *Small* **2013**, *9*, 3748.
- (149) (a) Um, S. H.; Lee, J. B.; Park, N.; Kwon, S. Y.; Umbach, C. C.; Luo, D. *Nat. Mater.* **2006**, *5*, 797. (b) Park, N. Y.; Um, S. H.; Funabashi, H.; Xu, J.; Luo, D. *Nat. Mater.* **2009**, *8*, 432. (c) Roh, Y. H.; Ruiz, R. C.; Peng, S.; Lee, J. B.; Luo, D. *Chem. Soc. Rev.* **2011**, *40*, 5730.
- (150) (a) Cheng, E.; Xing, Y.; Chen, P.; Yang, Y.; Sun, Y.; Zhou, D.; Xu, L.; Fan, Q.; Liu, D. *Angew. Chem., Int. Ed.* **2009**, *48*, 7660. (b) Xing, Y.; Cheng, E.; Yang, Y.; Chen, P.; Zhang, T.; Sun, Y.; Yang, Z.; Liu, D. *Adv. Mater.* **2011**, *23*, 1117. (c) Peng, L.; You, M.; Yuan, Q.; Wu, C.; Han, D.; Chen, Y.; Zhong, Z.; Xue, J.; Tan, W. *J. Am. Chem. Soc.* **2012**, *134*, 12302. (d) Yang, H.; Liu, H.; Kang, H.; Tan, W. *J. Am. Chem. Soc.* **2008**, *130*, 6320. (e) Yan, L.; Zhu, Z.; Zou, Y.; Huang, Y.; Liu, D.; Jia, S.; Xu, D.; Wu, M.; Zhou, Y.; Zhou, S.; Yang, C. *J. Am. Chem. Soc.* **2013**, *135*, 3748.
- (151) (a) Wei, B.; Cheng, I.; Luo, K. Q.; Mi, Y. *Angew. Chem., Int. Ed.* **2008**, *47*, 331. (b) Zhu, Z.; Wu, C.; Liu, H.; Zou, Y.; Zhang, X.; Kang, H.; Yang, C. J.; Tan, W. *Angew. Chem., Int. Ed.* **2010**, *49*, 1052. (c) Lu, C. H.; Qi, X. J.; Orbach, R.; Yang, H. H.; Mironi-Harpaz, I.; Seliktar, D.; Willner, I. *Nano Lett.* **2013**, *13*, 1298.
- (152) (a) Voelcker, N. H.; Guckian, K. M.; Saghatelyan, A.; Ghadiri, M. R. *Small* **2008**, *4*, 427. (b) Picuri, J. M.; Frezza, B. M.; Ghadiri, M. R. *J. Am. Chem. Soc.* **2009**, *131*, 9368. (c) Gianneschi, N. C.; Ghadiri, M. R. *Angew. Chem., Int. Ed.* **2007**, *46*, 3955.
- (153) (a) Genot, A. J.; Bath, J.; Turberfield, A. J. *J. Am. Chem. Soc.* **2011**, *133*, 20080. (b) Zhou, M.; Dong, S. *Acc. Chem. Res.* **2011**, *44*, 1232. (c) Gerasimova, Y. V.; Kolpashchikov, D. M. *Chem. Asian J.* **2012**, *7*, 534. (d) Wang, L.; Zhu, J.; Han, L.; Jin, L.; Zhu, C.; Wang, E.; Dong, S. *ACS Nano* **2012**, *6*, 6659.
- (154) (a) Xia, F.; Zuo, X.; Yang, R.; White, R. J.; Xiao, Y.; Kang, D.; Gong, X.; Lubin, A. A.; Vallée-Bélisle, A.; Yuen, J. D.; Hsu, B. Y.; Plaxco, K. W. *J. Am. Chem. Soc.* **2010**, *132*, 8557. (b) Xie, Z.; Wroblewska, L.; Prochazka, L.; Weiss, R.; Benenson, Y. *Science* **2011**, *333*, 1307. (c) Bonnet, J.; Yin, P.; Ortiz, M. E.; Subsoontorn, P.; Endy, D. *Science* **2013**, *340*, 599. (d) Shis, D. L.; Bennett, M. R. *Proc. Natl. Acad. Sci. U.S.A.* **2013**, *110*, 5028.
- (155) (a) Margolin, A. A.; Stojanovic, M. N. *Nat. Biotechnol.* **2005**, *23*, 1374. (b) Shlyahovsky, B.; Li, Y.; Lioubashevski, O.; Elbaz, J.; Willner, I. *ACS Nano* **2009**, *3*, 1831. (c) Orbach, R.; Remacle, F.; Levine, R. D.; Willner, I. *Proc. Natl. Acad. Sci. U.S.A.* **2012**, *109*, 21228.
- (156) (a) Stojanovic, M. N.; Mitchell, T. E.; Stefanovic, D. *J. Am. Chem. Soc.* **2002**, *124*, 3555. (b) Stojanović, M. N.; Stefanović, D. *J. Am. Chem. Soc.* **2003**, *125*, 6673. (c) Bi, S.; Yan, Y.; Hao, S.; Zhang, S. *Angew. Chem., Int. Ed.* **2010**, *49*, 4438.
- (157) (a) Stojanovic, M. N.; Stefanovic, D. *Nat. Biotechnol.* **2003**, *21*, 1069. (b) Macdonald, J.; Li, Y.; Sutovic, M.; Lederman, H.; Pendri, K.; Lu, W.; Andrews, B. L.; Stefanovic, D.; Stojanovic, M. N. *Nano Lett.* **2006**, *6*, 2598. (c) Elbaz, J.; Shlyahovsky, B.; Li, D.; Willner, I. *ChemBioChem* **2008**, *9*, 232.
- (158) (a) Stojanovic, M. N.; Nikic, D. B.; Stefanovic, D. *J. Am. Chem. Soc.* **2003**, *125*, 321. (b) Lederman, H.; Macdonald, J.; Stefanovic, D.; Stojanovic, M. N. *Biochemistry* **2006**, *45*, 1194. (c) Pei, R.; Matamoros, E.; Liu, M.; Stefanovic, D.; Stojanovic, M. N. *Nat. Nanotechnol.* **2010**, *5*, 773.
- (159) (a) Saghatelyan, A.; Völcker, N. H.; Guckian, K. M.; Lin, V. S.; Ghadiri, M. R. *J. Am. Chem. Soc.* **2003**, *125*, 346. (b) Okamoto, A.; Tanaka, K.; Saito, I. *J. Am. Chem. Soc.* **2004**, *126*, 9458. (c) Miyoshi, D.; Inoue, M.; Sugimoto, N. *Angew. Chem., Int. Ed.* **2006**, *45*, 7716. (d) Li, T.; Wang, E.; Dong, S. *J. Am. Chem. Soc.* **2009**, *131*, 15082.
- (160) (a) Zhou, M.; Du, Y.; Chen, C.; Li, B.; Wen, D.; Dong, S.; Wang, E. *J. Am. Chem. Soc.* **2010**, *132*, 2172. (b) Li, T.; Zhang, L.; Ai, J.; Dong, S.; Wang, E. *ACS Nano* **2011**, *5*, 6334. (c) Chen, J.; Fang, Z.; Lie, P.; Zeng, L. *Anal. Chem.* **2012**, *84*, 6321. (d) Pei, H.; Liang, L.; Yao, G.; Li, J.; Huang, Q.; Fan, C. *Angew. Chem., Int. Ed.* **2012**, *51*, 9020.
- (161) (a) Park, K. S.; Seo, M. W.; Jung, C.; Lee, J. Y.; Park, H. G. *Small* **2012**, *8*, 2203. (b) Li, T.; Ackermann, D.; Hall, A. M.; Famulok, M. *J. Am. Chem. Soc.* **2012**, *134*, 3508. (c) Prokup, A.; Hemphill, J.; Deiters, A. *J. Am. Chem. Soc.* **2012**, *134*, 3810.
- (162) (a) Seelig, G.; Soloveichik, D.; Zhang, D. Y.; Winfree, E. *Science* **2006**, *314*, 1585. (b) Rodrigo, G.; Landrain, T. E.; Jaramillo, A. *Proc. Natl. Acad. Sci. U.S.A.* **2012**, *109*, 15271.
- (163) (a) Frezza, B. M.; Cockcroft, S. L.; Ghadiri, M. R. *J. Am. Chem. Soc.* **2007**, *129*, 14875. (b) Han, D.; Zhu, Z.; Wu, C.; Peng, L.; Zhou, L.; Gulbakan, B.; Zhu, G.; Williams, K. R.; Tan, W. *J. Am. Chem. Soc.* **2012**, *134*, 20797.
- (164) (a) Ogashawa, S.; Kyoi, Y.; Fujimoto, K. *ChemBioChem* **2007**, *8*, 1520. (b) Chen, X. *J. Am. Chem. Soc.* **2012**, *134*, 263.
- (165) (a) Padirac, A.; Fujii, T.; Rondelez, Y. *Curr. Opin. Biotechnol.* **2013**, *24*, 575. (b) Chen, X.; Briggs, N.; McLain, J. R.; Ellington, A. D. *Proc. Natl. Acad. Sci. U.S.A.* **2013**, *110*, 5386.
- (166) Qian, L.; Winfree, E. *Science* **2011**, *332*, 1196.
- (167) Qian, L.; Winfree, E.; Bruck, J. *Nature* **2011**, *475*, 368.
- (168) Moshe, M.; Elbaz, J.; Willner, I. *Nano Lett.* **2009**, *9*, 1196.
- (169) Stojanovic, M. N.; Semova, S.; Kolpashchikov, D.; Macdonald, J.; Morgan, C.; Stefanovic, D. *J. Am. Chem. Soc.* **2005**, *127*, 6914.
- (170) Elbaz, J.; Lioubashevski, O.; Wang, F.; Remacle, F.; Levine, R. D.; Willner, I. *Nat. Nanotechnol.* **2010**, *5*, 417.
- (171) Orbach, R.; Mostinski, L.; Wang, F.; Willner, I. *Chem.—Eur. J.* **2012**, *18*, 14689.
- (172) (a) Chen, J.; Zhou, X.; Zeng, L. *Chem. Commun.* **2013**, *49*, 984. (b) Zhao, Y.; Zhang, Q.; Wang, W.; Jin, Y. *Biosens. Bioelectron.* **2013**, *43*, 231. (c) Zhu, J.; Zhang, L.; Li, T.; Dong, S.; Wang, E. *Adv. Mater.* **2013**, *25*, 2440. (d) Kahan-Hanum, M.; Douek, Y.; Adar, R.; Shapiro, E. *Sci. Rep.* **2013**, *3*, 1535.

- (173) Elbaz, J.; Wang, F.; Remacle, F.; Willner, I. *Nano Lett.* **2012**, *12*, 6049.
- (174) (a) Benenson, Y.; Paz-Elizur, T.; Adar, R.; Keinan, E.; Livneh, Z.; Shapiro, E. *Nature* **2001**, *414*, 430. (b) Benenson, Y.; Gil, B.; Ben-Dor, U.; Adar, R.; Shapiro, E. *Nature* **2004**, *429*, 423. (c) Adar, R.; Benenson, Y.; Linshiz, G.; Rosner, A.; Tishby, N.; Shapiro, E. *Proc. Natl. Acad. Sci. U.S.A.* **2004**, *101*, 9960. (d) Ran, T.; Kaplan, S.; Shapiro, E. *Nat. Nanotechnol.* **2009**, *4*, 642.
- (175) (a) Benenson, Y.; Adar, R.; Paz-Elizur, T.; Livneh, Z.; Shapiro, E. *Proc. Natl. Acad. Sci. U.S.A.* **2003**, *100*, 2191. (b) Benenson, Y. *Nat. Rev. Genet.* **2012**, *13*, 455. (c) Miyamoto, T.; Razavi, S.; Derose, R.; Inoue, T. *ACS Synth. Biol.* **2013**, *2*, 72.
- (176) (a) Venkatesan, B. M.; Bashir, R. *Nat. Nanotechnol.* **2011**, *6*, 615. (b) Serganov, A.; Patel, D. J. *Curr. Opin. Struct. Biol.* **2012**, *22*, 279. (c) Sontz, P. A.; Muren, N. B.; Barton, J. K. *Acc. Chem. Res.* **2012**, *45*, 1792. (d) Palchetti, I.; Mascini, M. *Anal. Bioanal. Chem.* **2012**, *402*, 3103. (e) Xia, F.; White, R. J.; Zuo, X.; Patterson, A.; Xiao, Y.; Kang, D.; Gong, X.; Plaxco, K. W.; Heeger, A. J. *J. Am. Chem. Soc.* **2010**, *132*, 14346.
- (177) (a) Liu, X.; Fan, Q.; Huang, W. *Biosens. Bioelectron.* **2011**, *26*, 2154. (b) Bonanni, A.; del Valle, M. *Anal. Chim. Acta* **2010**, *678*, 7. (c) Tosar, J. P.; Brañas, G.; Laíz, J. *Biosens. Bioelectron.* **2010**, *26*, 1205. (d) Wen, Y.; Peng, C.; Li, D.; Zhuo, L.; He, S.; Wang, L.; Huang, Q.; Xu, Q. H.; Fan, C. *Chem. Commun.* **2011**, *47*, 6278. (e) Lu, C. H.; Li, J.; Qi, X. J.; Song, X. R.; Yang, H. H.; Chen, X.; Chen, G. N. *J. Mater. Chem.* **2011**, *21*, 10915.
- (178) (a) Cho, E. J.; Lee, J. W.; Ellington, A. D. *Annu. Rev. Anal. Chem.* **2009**, *2*, 241. (b) Merkoçi, A. *Biosens. Bioelectron.* **2010**, *26*, 1164. (c) Hvastkovs, E. G.; Buttry, D. A. *Analyst* **2010**, *135*, 1817. (d) Li, D.; Song, S.; Fan, C. *Acc. Chem. Res.* **2010**, *43*, 631.
- (179) (a) Baron, R.; Willner, B.; Willner, I. *Chem. Commun.* **2007**, *323*. (b) Willner, I.; Willner, B. *Nano Lett.* **2010**, *10*, 3805. (c) Østergaard, M. E.; Hrdlicka, P. J. *Chem. Soc. Rev.* **2011**, *40*, 5771. (d) Ma, D. L.; He, H. Z.; Leung, K. H.; Zhong, H. J.; Chan, D. S.; Leung, C. H. *Chem. Soc. Rev.* **2013**, *42*, 3427.
- (180) (a) Peng, H.; Zhang, L.; Soeller, C.; Travas-Sejdic, J. *Biomaterials* **2009**, *30*, 2132. (b) Xiao, Y.; Plakos, K. J.; Lou, X.; White, R. J.; Qian, J.; Plaxco, K. W.; Soh, H. T. *Angew. Chem., Int. Ed.* **2009**, *48*, 4354. (c) Li, F.; Huang, Y.; Yang, Q.; Zhong, Z.; Li, D.; Wang, L.; Song, S.; Fan, C. *Nanoscale* **2010**, *2*, 1021. (d) Lu, C. H.; Li, J.; Liu, J. J.; Yang, H. H.; Chen, X.; Chen, G. N. *Chem.—Eur. J.* **2010**, *16*, 4889. (e) Zhang, L.; Zhu, J.; Li, T.; Wang, E. *Anal. Chem.* **2011**, *83*, 8871.
- (181) (a) Kricka, L. J. *Clin. Chem.* **1999**, *45*, 453. (b) Ho, H. A.; Béra-Abérem, M.; Leclerc, M. *Chem.—Eur. J.* **2005**, *11*, 1718. (c) Venkatesan, N.; Seo, Y. J.; Kim, B. H. *Chem. Soc. Rev.* **2008**, *37*, 648. (d) Zhou, Z.; Du, Y.; Dong, S. *Anal. Chem.* **2011**, *83*, 5122. (e) Dai, N.; Kool, E. T. *Chem. Soc. Rev.* **2011**, *40*, 5756.
- (182) (a) Xu, C.; Zhao, C.; Ren, J.; Qu, X. *Chem. Commun.* **2011**, *47*, 8043. (b) Kang, H.; Liu, H.; Zhang, X.; Yan, J.; Zhu, Z.; Peng, L.; Yang, H.; Kim, Y.; Tan, W. *Langmuir* **2011**, *27*, 399. (c) Zhu, C. L.; Lu, C. H.; Song, X. Y.; Yang, H. H.; Wang, X. R. *J. Am. Chem. Soc.* **2011**, *133*, 1278. (d) Keum, J. W.; Bermudez, H. *Chem. Commun.* **2012**, *48*, 12118. (e) Rangnekar, A.; Zhang, A. M.; Li, S. S.; Bompiani, K. M.; Hansen, M. N.; Gothelf, K. V.; Sullenger, B. A.; LaBean, T. H. *Nanomedicine* **2012**, *8*, 673. (f) Chen, Z.; Li, Z.; Lin, Y.; Yin, M.; Ren, J.; Qu, X. *Biomaterials* **2013**, *34*, 1364.
- (183) (a) Chen, C.; Geng, J.; Pu, F.; Yang, X.; Ren, J.; Qu, X. *Angew. Chem., Int. Ed.* **2011**, *50*, 882. (b) Chen, C.; Pu, F.; Huang, Z.; Liu, Z.; Ren, J.; Qu, X. *Nucleic Acids Res.* **2011**, *39*, 1638. (c) Li, J.; Pei, H.; Zhu, B.; Liang, L.; Wei, M.; He, Y.; Chen, N.; Li, D.; Huang, Q.; Fan, C. *ACS Nano* **2011**, *5*, 8783. (d) Yang, X.; Liu, X.; Liu, Z.; Pu, F.; Ren, J.; Qu, X. *Adv. Mater.* **2012**, *24*, 2890. (e) Liu, J.; Liu, H.; Kang, H.; Donovan, M.; Zhu, Z.; Tan, W. *Anal. Bioanal. Chem.* **2012**, *402*, 187. (f) Rodríguez-Pulido, A.; Kondrachuk, A. I.; Prusty, D. K.; Gao, J.; Loi, M. A.; Herrmann, A. *Angew. Chem., Int. Ed.* **2013**, *52*, 1008. (g) Lu, C. H.; Zhu, C. L.; Li, J.; Liu, J. J.; Chen, X.; Yang, H. H. *Chem. Commun.* **2010**, *46*, 3116.
- (184) (a) Zhang, Z.; Balogh, D.; Wang, F.; Willner, I. *J. Am. Chem. Soc.* **2013**, *135*, 1934. (b) Simmel, F. C. *Nanomedicine* **2007**, *2*, 817. (c) Chen, L. F.; Wen, Y. Q.; Su, B.; Di, J. C.; Song, Y. L.; Jiang, L. *J. Mater. Chem.* **2011**, *21*, 13811. (d) Zhang, Z.; Balogh, D.; Wang, F.; Sung, S. Y.; Nechushtai, R.; Willner, I. *ACS Nano* **2013**, *7*, 8455. (e) He, X.; Zhao, Y.; He, D.; Wang, K.; Xu, F.; Tang, J. *Langmuir* **2012**, *28*, 12909. (f) Lu, C. H.; Willner, B.; Willner, I. *ACS Nano* **2013**, *7*, 8320. (g) Song, L.; Ho, V. H.; Chen, C.; Yang, Z.; Liu, D.; Chen, R.; Zhou, D. *Adv. Healthcare Mater.* **2013**, *2*, 275.
- (185) (a) Ding, B.; Wu, H.; Xu, W.; Zhao, Z.; Liu, Y.; Yu, H.; Yan, H. *Nano Lett.* **2010**, *10*, 5065. (b) Keller, S.; Marx, A. *Chem. Soc. Rev.* **2011**, *40*, 5690. (c) Zhang, G.; Surwade, S. P.; Zhou, F.; Liu, H. *Chem. Soc. Rev.* **2013**, *42*, 2488.
- (186) (a) Deng, Z.; Mao, C. *Angew. Chem., Int. Ed.* **2004**, *43*, 4068. (b) He, Y.; Ye, T.; Ribbe, A. E.; Mao, C. *J. Am. Chem. Soc.* **2011**, *133*, 1742. (c) Lin, C.; Jungmann, R.; Leifer, A. M.; Li, C.; Levner, D.; Church, G. M.; Shih, W. M.; Yin, P. *Nat. Chem.* **2012**, *4*, 832.
- (187) (a) Keren, K.; Berman, R. S.; Buchstab, E.; Sivan, U.; Braun, E. *Science* **2003**, *302*, 1380. (b) Nishinaka, T.; Takano, A.; Doi, Y.; Hashimoto, M.; Nakamura, A.; Matsushita, Y.; Kumaki, J.; Yamashita, E. *J. Am. Chem. Soc.* **2005**, *127*, 8120. (c) Pilo-Pais, M.; Goldberg, S.; Samano, E.; Labean, T. H.; Finkelstein, G. *Nano Lett.* **2011**, *11*, 3489.
- (188) (a) Dong, L.; Hollis, T.; Connolly, B. A.; Wright, N. G.; Horrocks, B. R.; Houlton, A. *Adv. Mater.* **2007**, *19*, 1748. (b) Tørring, T.; Voigt, N. V.; Nangreave, J.; Yan, H.; Gothelf, K. V. *Chem. Soc. Rev.* **2011**, *40*, 5636. (c) Saccà, B.; Niemeyer, C. M. *Angew. Chem., Int. Ed.* **2012**, *51*, 58.
- (189) (a) Afonin, K. A.; Grabow, W. W.; Walker, F. M.; Bindewald, E.; Dobrovolskaia, M. A.; Shapiro, B. A.; Jaeger, L. *Nat. Protoc.* **2011**, *6*, 2022. (b) Jiang, Q.; Song, C.; Nangreave, J.; Liu, X.; Lin, L.; Qiu, D.; Wang, Z. G.; Zou, G.; Liang, X.; Yan, H.; Ding, B. *J. Am. Chem. Soc.* **2012**, *134*, 13396. (c) Zhao, Y. X.; Shaw, A.; Zeng, X.; Benson, E.; Nyström, A. M.; Höglberg, B. *ACS Nano* **2012**, *6*, 8684. (d) Liu, X.; Xu, Y.; Yu, T.; Clifford, C.; Liu, Y.; Yan, H.; Chang, Y. *Nano Lett.* **2012**, *12*, 4254. (e) Afonin, K. A.; Viard, M.; Martins, A. N.; Lockett, S. J.; Maciag, A. E.; Freed, E. O.; Heldman, E.; Jaeger, L.; Blumenthal, R.; Shapiro, B. A. *Nat. Nanotechnol.* **2013**, *8*, 296.
- (190) (a) Douglas, S. M.; Bachelet, I.; Church, G. M. *Science* **2012**, *335*, 831. (b) Elbaz, J.; Willner, I. *Nat. Mater.* **2012**, *11*, 276. (c) Fu, J.; Yan, H. *Nat. Biotechnol.* **2012**, *30*, 407.
- (191) (a) SantaLucia, J.; Hicks, D. *Annu. Rev. Biochem.* **2004**, *33*, 415. (b) Zhang, D. Y.; Turberfield, A. J.; Yurke, B.; Winfree, E. *Science* **2007**, *318*, 1121. (c) Soloveichik, D.; Seelig, G.; Winfree, E. *Proc. Natl. Acad. Sci. U.S.A.* **2010**, *107*, 5393.
- (192) (a) Yurke, B.; Mills, A. P. *Genet. Program. Evolvable Machines* **2003**, *4*, 111. (b) Li, Q.; Luan, G.; Guo, Q.; Liang, J. *Nucleic Acids Res.* **2002**, *30*, e5. (c) Zhang, D. Y.; Seelig, G. *Nat. Chem.* **2011**, *3*, 103.
- (193) Zhang, D. Y.; Winfree, E. *J. Am. Chem. Soc.* **2009**, *131*, 17303.
- (194) (a) Panyutin, I. G.; Hsieh, P. *Proc. Natl. Acad. Sci. U.S.A.* **1994**, *91*, 2021. (b) Green, C.; Tibbets, C. *Nucleic Acids Res.* **1981**, *9*, 1905. (c) Reynaldo, L. P.; Vologodskii, A. V.; Neri, B. P.; Lyamichev, V. I. *J. Mol. Biol.* **2000**, *297*, 511.
- (195) Dirks, R. M.; Pierce, N. A. *Proc. Natl. Acad. Sci. U.S.A.* **2004**, *101*, 15275.
- (196) Huang, J.; Wu, Y.; Chen, Y.; Zhu, Z.; Yang, X.; Yang, C. J.; Wang, K.; Tan, W. *Angew. Chem., Int. Ed.* **2011**, *50*, 401.
- (197) Ren, J.; Wang, J.; Han, L.; Wang, E.; Wang, J. *Chem. Commun.* **2011**, *47*, 10563.
- (198) Breaker, R. R.; Joyce, G. F. *Chem. Biol.* **1995**, *2*, 655.
- (199) Pavlov, V.; Xiao, Y.; Gill, R.; Dishon, A.; Kotler, M.; Willner, I. *Anal. Chem.* **2004**, *76*, 2152.
- (200) (a) Li, Y.; Li, X.; Ji, X.; Li, X. *Biosens. Bioelectron.* **2011**, *26*, 4095. (b) Luo, M.; Chen, X.; Zhou, G.; Xiang, X.; Chen, L.; Ji, X.; He, Z. *Chem. Commun.* **2012**, *48*, 1126. (c) Zong, C.; Wu, J.; Xu, J.; Ju, H.; Yan, F. *Biosens. Bioelectron.* **2013**, *43*, 372.
- (201) (a) Li, T.; Wang, E.; Dong, S. *Chem. Commun.* **2008**, 5520. (b) Li, T.; Wang, E.; Dong, S. *Anal. Chem.* **2010**, *82*, 1515. (c) Wang, H. Q.; Liu, W. Y.; Wu, Z.; Tang, L. J.; Xu, X. M.; Yu, R. Q.; Jiang, J. H. *Anal. Chem.* **2011**, *83*, 1883.

- (202) Chen, Y.; Xu, J.; Su, J.; Xiang, Y.; Yuan, R.; Chai, Y. *Anal. Chem.* **2012**, *84*, 7750.
- (203) Song, W. Q.; Zhu, K. L.; Cao, Z. J.; Lau, C.; Lu, J. H. *Analyst* **2012**, *137*, 1396.
- (204) Choi, J.; Love, K. R.; Gong, Y.; Gierahn, T. M.; Love, J. C. *Anal. Chem.* **2011**, *83*, 6890.
- (205) (a) Turberfield, A. J.; Mitchell, J. C.; Yurke, B.; Mills, A. P.; Blakey, M. I.; Simmel, F. C. *Phys. Rev. Lett.* **2003**, *90*, 118102. (b) Green, S. J.; Lubrich, D.; Turberfield, A. J. *Biophys. J.* **2006**, *91*, 2966.
- (206) Yin, P.; Choi, H. M. T.; Calvert, C. R.; Pierce, N. A. *Nature* **2008**, *451*, 318.
- (207) Zheng, A. X.; Li, J.; Wang, J. R.; Song, X. R.; Chen, G. N.; Yang, H. H. *Chem. Commun.* **2012**, *48*, 3112.
- (208) Li, B. L.; Ellington, A. D.; Chen, X. *Nucleic Acids Res.* **2011**, *39*, e110.
- (209) Niu, S.; Qu, L.; Zhang, Q.; Lin, J. *Anal. Biochem.* **2012**, *421*, 362.
- (210) Zheng, A. X.; Wang, J. R.; Li, J.; Song, X. R.; Chen, G. N.; Yang, H. H. *Biosens. Bioelectron.* **2012**, *36*, 217.
- (211) Li, B.; Jiang, Y.; Chen, X.; Ellington, A. D. *J. Am. Chem. Soc.* **2012**, *134*, 13918.
- (212) (a) Carmi, N.; Shultz, L. A.; Breaker, R. R. *Chem. Biol.* **1996**, *3*, 1039. (b) Carmi, N.; Balkhi, H. R.; Breaker, R. R. *Proc. Natl. Acad. Sci. U.S.A.* **1998**, *95*, 2233. (c) Carmi, N.; Breaker, R. R. *Bioorg. Med. Chem.* **2001**, *9*, 2589.
- (213) (a) Huizenga, D. E.; Szostak, J. W. *Biochemistry* **1995**, *34*, 656. (b) Liu, Z.; Mei, S. H.; Brennan, J. D.; Li, Y. *J. Am. Chem. Soc.* **2003**, *125*, 7539. (c) Shen, Y.; Brennan, J. D.; Li, Y. *Biochemistry* **2005**, *44*, 12066. (d) Nutiu, R.; Li, Y. *Angew. Chem., Int. Ed.* **2005**, *44*, 1061. (e) Shen, Y.; Chiuman, W.; Brennan, J. D.; Li, Y. *ChemBioChem* **2006**, *7*, 1343.
- (214) (a) Hollenstein, M.; Hipolito, C.; Lam, C.; Dietrich, D.; Perrin, D. *Angew. Chem., Int. Ed.* **2008**, *47*, 4346–4350. (b) Liu, J. W.; Lu, Y. *Angew. Chem., Int. Ed.* **2007**, *46*, 7587–7590. (c) Hollenstein, M.; Hipolito, C.; Lam, C.; Dietrich, D.; Perrin, D. M. *Angew. Chem., Int. Ed.* **2008**, *47*, 4346.
- (215) (a) Li, J.; Zheng, W.; Kwon, A. H.; Lu, Y. *Nucleic Acids Res.* **2000**, *28*, 481. (b) Santoro, S. W.; Joyce, G. F.; Sakthivel, K.; Gramatikova, S.; Barbas, C. F., III. *J. Am. Chem. Soc.* **2000**, *122*, 2433. (c) Kim, H.; Liu, J.; Li, J.; Nagraj, N.; Li, M.; Pavot, C. M. B.; Lu, Y. *J. Am. Chem. Soc.* **2007**, *129*, 6896.
- (216) (a) Li, J.; Lu, Y. *J. Am. Chem. Soc.* **2000**, *122*, 10466. (b) Brown, A. K.; Li, J.; Pavot, C. M. B.; Lu, Y. *Biochemistry* **2003**, *42*, 7152.
- (217) Liu, J.; Lu, Y. *J. Am. Chem. Soc.* **2003**, *125*, 6642.
- (218) Peracchi, A. *J. Biol. Chem.* **2000**, *275*, 11693.
- (219) Liu, J.; Brown, A. K.; Meng, X.; Cropek, D. M.; Istok, J. D.; Watson, D. B.; Lu, Y. *Proc. Natl. Acad. Sci. U.S.A.* **2007**, *104*, 2056.
- (220) Roth, A.; Breaker, R. R. *Proc. Natl. Acad. Sci. U.S.A.* **1998**, *95*, 6027.
- (221) (a) Li, Y.; Geyer, C. R.; Sen, D. *Biochemistry* **1996**, *35*, 6911. (b) Travascio, P.; Li, Y.; Sen, D. *Chem. Biol.* **1998**, *5*, 505. (c) Willner, I.; Willner, B.; Katz, E. *Bioelectrochemistry* **2007**, *70*, 2. (d) Li, T.; Dong, S.; Wang, E. *Chem. Commun.* **2007**, 4209.
- (222) (a) Golub, E.; Freeman, R.; Willner, I. *Angew. Chem., Int. Ed.* **2011**, *50*, 11710. (b) Xiao, Y.; Pavlov, V.; Gill, R.; Bourenko, T.; Willner, I. *ChemBioChem* **2004**, *5*, 374. (c) Willner, I.; Baron, R.; Willner, B. *Biosens. Bioelectron.* **2007**, *22*, 1841. (d) Deng, M.; Zhang, D.; Zhou, Y.; Zhou, X. *J. Am. Chem. Soc.* **2008**, *130*, 13095.
- (223) (a) Travascio, P.; Bennet, A. J.; Wang, D. Y.; Sen, D. *Chem. Biol.* **1999**, *6*, 779. (b) Travascio, P.; Witting, P. K.; Mauk, A. G.; Sen, D. *J. Am. Chem. Soc.* **2001**, *123*, 1337. (c) Nakayama, S.; Sintim, H. O. *J. Am. Chem. Soc.* **2009**, *131*, 10320.
- (224) (a) Pan, T.; Uhlenbeck, O. C. *Biochemistry* **1992**, *31*, 3887. (b) Pan, T.; Uhlenbeck, O. C. *Nature* **1992**, *358*, 560.
- (225) (a) Cuenoud, B.; Szostak, J. W. *Nature* **1995**, *375*, 611. (b) Bartel, D. P.; Szostak, J. W. *Science* **1993**, *261*, 1411. (c) Ekland, E. H.; Szostak, J. W.; Bartel, D. P. *Science* **1995**, *269*, 364. (d) Chapman, K. B.; Szostak, J. W. *Chem. Biol.* **1995**, *2*, 325.
- (226) Curtis, E. A.; Bartel, D. P. *Nat. Struct. Mol. Biol.* **2005**, *12*, 994.
- (227) Ekland, E. H.; Bartel, D. P. *Nature* **1996**, *382*, 373.
- (228) (a) Sun, L. L.; Cui, Z. Y.; Gottlieb, R. L.; Zhang, B. L. *Chem. Biol.* **2002**, *9*, 619. (b) Zhang, B.; Cech, T. R. *Nature* **1997**, *390*, 96.
- (229) Tsukiji, S.; Pattnaik, S. B.; Suga, H. *J. Am. Chem. Soc.* **2004**, *126*, 5044.
- (230) Tsukiji, S.; Pattnaik, S. B.; Suga, H. *Nat. Struct. Biol.* **2003**, *10*, 713.
- (231) Fusz, S.; Eisenfuehr, A.; Srivatsan, S. G.; Heckel, A.; Famulok, M. *Chem. Biol.* **2005**, *12*, 941.
- (232) Sengle, G.; Eisenfuehr, A.; Arora, P. S.; Nowick, J. S.; Famulok, M. *Chem. Biol.* **2001**, *8*, 459.
- (233) Conn, M. M.; Prudent, J. R.; Schultz, P. G. *J. Am. Chem. Soc.* **1996**, *118*, 7012.
- (234) (a) Lohse, P. A.; Szostak, J. W. *Nature* **1996**, *381*, 442. (b) Jenne, A.; Famulok, M. *Chem. Biol.* **1998**, *5*, 23. (c) Suga, H.; Cowan, J. A.; Szostak, J. W. *Biochemistry* **1998**, *37*, 10118. (d) Suga, H.; Lohse, P. A.; Szostak, J. W. *J. Am. Chem. Soc.* **1998**, *120*, 1151.
- (235) (a) Illangasekare, M.; Sanchez, G.; Nickles, T.; Yarus, M. *Science* **1995**, *267*, 643. (b) Illangasekare, M.; Yarus, M. *Proc. Natl. Acad. Sci. U.S.A.* **1999**, *96*, 5470.
- (236) (a) Tarasow, T. M.; Tarasow, S. L.; Eaton, B. E. *Nature* **1997**, *389*, 54. (b) Seelig, B.; Jaschke, A. *Chem. Biol.* **1999**, *6*, 167. (c) Agresti, J. J.; Kelly, B. T.; Jaschke, A.; Griffiths, A. D. *Proc. Natl. Acad. Sci. U.S.A.* **2005**, *102*, 16170.
- (237) (a) Elbaz, J.; Shlyahovsky, B.; Willner, I. *Chem. Commun.* **2008**, 1569. (b) Teller, C.; Shimron, S.; Willner, I. *Anal. Chem.* **2009**, *81*, 9114. (c) Li, T.; Li, B.; Wang, E.; Dong, S. *Chem. Commun.* **2009**, 3551. (d) Dong, J.; Cui, X.; Deng, Y.; Tang, Z. *Biosens. Bioelectron.* **2012**, *38*, 258.
- (238) (a) Zhu, X.; Gao, X.; Liu, Q.; Lin, Z.; Qiu, B.; Chen, G. *Chem. Commun.* **2011**, *47*, 7437. (b) Elbaz, J.; Shimron, S.; Willner, I. *Chem. Commun.* **2010**, *46*, 1209. (c) Li, B.; Dong, S.; Wang, E. *Chem. Asian J.* **2010**, *5*, 1262. (d) Soukup, G. A.; Breaker, R. R. *Trends Biotechnol.* **1999**, *17*, 469.
- (239) (a) Yin, B. C.; Ye, B. C.; Tan, W.; Wang, H.; Xie, C. C. *J. Am. Chem. Soc.* **2009**, *131*, 14624. (b) Li, D.; Shlyahovsky, B.; Elbaz, J.; Willner, I. *J. Am. Chem. Soc.* **2007**, *129*, 5804. (c) Liu, J.; Lu, Y. *Angew. Chem., Int. Ed.* **2007**, *46*, 7587. (d) Zhou, W. H.; Zhu, C. L.; Lu, C. H.; Guo, X.; Chen, F.; Yang, H. H.; Wang, X. *Chem. Commun.* **2009**, 6845.
- (240) Wang, F.; Orbach, R.; Willner, I. *Chem.—Eur. J.* **2012**, *18*, 16030.
- (241) Lu, C. H.; Wang, F.; Willner, I. *J. Am. Chem. Soc.* **2012**, *134*, 10651.
- (242) Wang, F.; Elbaz, J.; Willner, I. *J. Am. Chem. Soc.* **2012**, *134*, 5504.
- (243) (a) Xiao, Y.; Rowe, A. A.; Plaxco, K. W. *J. Am. Chem. Soc.* **2007**, *129*, 262. (b) Yuan, Y.; Gou, X.; Yuan, R.; Chai, Y.; Zhuo, Y.; Mao, L.; Gan, X. *Biosens. Bioelectron.* **2011**, *26*, 4236. (c) Hu, R.; Fu, T.; Zhang, X. B.; Kong, R. M.; Qiu, L. P.; Liu, Y. R.; Liang, X. T.; Tan, W.; Shen, G. L.; Yu, R. Q. *Chem. Commun.* **2012**, *48*, 9507.
- (244) (a) Zhu, X.; Lin, Z.; Chen, L.; Qiu, B.; Chen, G. *Chem. Commun.* **2009**, 6050. (b) Sun, C.; Zhang, L.; Jiang, J.; Shen, G.; Yu, R. *Biosens. Bioelectron.* **2010**, *25*, 2483. (c) Yang, X.; Xu, J.; Tang, X.; Liu, H.; Tian, D. *Chem. Commun.* **2010**, *46*, 3107.
- (245) (a) Pelosof, G.; Tel-Vered, R.; Elbaz, J.; Willner, I. *Anal. Chem.* **2010**, *82*, 4396. (b) Chen, J.; Zhang, J.; Guo, Y.; Li, J.; Fu, F.; Yang, H. H.; Chen, G. *Chem. Commun.* **2011**, *47*, 8004. (c) Yuan, Y.; Yuan, R.; Chai, Y.; Zhuo, Y.; Ye, X.; Gan, X.; Bai, L. *Chem. Commun.* **2012**, *48*, 4621.
- (246) (a) Chen, Y.; Mao, C. *J. Am. Chem. Soc.* **2004**, *126*, 8626. (b) Chen, Y.; Wang, M.; Mao, C. *Angew. Chem., Int. Ed.* **2004**, *43*, 3554. (c) Mokany, E.; Bone, S. M.; Young, P. E.; Doan, T. B.; Todd, A. V. *J. Am. Chem. Soc.* **2010**, *132*, 1051.
- (247) (a) Lu, Y.; Liu, J. *Curr. Opin. Biotechnol.* **2006**, *17*, 580. (b) Reif, J. H.; Sahu, S. *Theor. Comput. Sci.* **2009**, *410*, 1428.

- (c) Shimron, S.; Magen, N.; Elbaz, J.; Willner, I. *Chem. Commun.* **2011**, 47, 8787.
 (248) (a) He, Y.; Liu, D. R. *Nat. Nanotechnol.* **2010**, 5, 778.
 (b) Rotaru, A.; Gothelf, K. V. *Nat. Nanotechnol.* **2010**, 5, 760.
 (c) Ayukawa, S.; Sakai, Y.; Kiga, D. *Chem. Commun.* **2012**, 48, 7556.
 (d) Beissenhirtz, M. K.; Willner, I. *Org. Biomol. Chem.* **2006**, 4, 3392.
 (249) (a) Stojanovic, M. N. *Isr. J. Chem.* **2011**, 51, 99. (d) Zhu, J.; Li, T.; Zhang, L.; Dong, S.; Wang, E. *Biomaterials* **2011**, 32, 7318. (c) Pei, R.; Macdonald, J.; Stojanovic, M. N. *Methods Mol. Biol.* **2012**, 848, 419.
 (250) (a) Liu, X.; Tang, Y.; Wang, L.; Zhang, J.; Song, S.; Fan, C.; Wang, S. *Adv. Mater.* **2007**, 19, 1471. (c) Wang, Z.; Lee, J. H.; Lu, Y. *Adv. Mater.* **2008**, 20, 3263. (b) Wei, H.; Li, B.; Li, J.; Dong, S.; Wang, E. *Nanotechnology* **2008**, 19, 095501.
 (251) (a) Liu, J.; Lu, Y. *J. Am. Chem. Soc.* **2004**, 126, 12298. (b) Liu, Q.; Jing, C.; Zheng, X.; Gu, Z.; Li, D.; Li, D. W.; Huang, Q.; Long, Y. T.; Fan, C. *Chem. Commun.* **2012**, 48, 9574.
 (252) (a) Liu, J.; Lu, Y. *J. Am. Chem. Soc.* **2005**, 127, 12677. (b) Liu, J.; Lu, Y. *Chem. Commun.* **2007**, 4872. (c) Lee, J. H.; Wang, Z.; Liu, J.; Lu, Y. *J. Am. Chem. Soc.* **2008**, 130, 14217. (d) Zheng, X.; Liu, Q.; Jing, C.; Li, Y.; Li, D.; Luo, W.; Wen, Y.; He, Y.; Huang, Q.; Long, Y. T.; Fan, C. *Angew. Chem., Int. Ed.* **2011**, 50, 11994.
 (253) (a) Schöneborn, H.; Bülle, J.; von Kiedrowski, G. *ChemBioChem* **2001**, 2, 922. (b) von Kiedrowski, G.; Eckardt, L.; Naumann, K.; Pankau, W. M.; Reimold, M.; Rein, M. *Pure Appl. Chem.* **2003**, 75, 609. (c) Achilles, K.; Kiedrowski, G. V. *Bioorg. Med. Chem. Lett.* **2005**, 15, 1229.
 (254) (a) Kindermann, M.; Stahl, I.; Reimold, M.; Pankau, W. M.; von Kiedrowski, G. *Angew. Chem., Int. Ed.* **2005**, 44, 6750. (b) Fernando, C.; Kiedrowski, G.; Szathmary, E. *J. Mol. Evol.* **2007**, 64, 572. (c) Otto, S. *Acc. Chem. Res.* **2012**, 45, 2200.
 (255) (a) Li, X. Q.; Chmielewski, J. *J. Am. Chem. Soc.* **2003**, 125, 11820. (b) Brøns, M. *J. Chem. Phys.* **2011**, 134, 144105. (c) Lou, S. J.; Peacock-López, E. *J. Biol. Phys.* **2012**, 38, 349.
 (256) (a) Sievers, D.; von Kiedrowski, G. *Chem.—Eur. J.* **1998**, 4, 629. (b) Luther, A.; Brandsch, R.; von Kiedrowski, G. *Nature* **1998**, 396, 245. (c) Eckardt, L. H.; Naumann, K.; Pankau, W. M.; Rein, M.; Schweitzer, M.; Windhab, N.; von Kiedrowski, G. *Nature* **2002**, 420, 286. (d) Islas, J. R.; Pimienta, V.; Micheau, J. C.; Buhse, T. *Biophys. Chem.* **2003**, 103, 201.
 (257) (a) Islas, J. R.; Pimienta, V.; Micheau, J. C.; Buhse, T. *Biophys. Chem.* **2003**, 103, 191. (b) Meyer, A. J.; Ellefson, J. W.; Ellington, A. D. *Acc. Chem. Res.* **2012**, 45, 2097. (c) Rubinov, B.; Wagner, N.; Matmor, M.; Regev, O.; Ashkenasy, N.; Ashkenasy, G. *ACS Nano* **2012**, 6, 7893. (d) Schulman, R.; Yurke, B.; Winfree, E. *Proc. Natl. Acad. Sci. U.S.A.* **2012**, 109, 6405.
 (258) (a) Severin, K.; Lee, D. H.; Martinez, J. A.; Ghadiri, M. R. *Chem.—Eur. J.* **1997**, 3, 1017. (b) Wang, B.; Sutherland, I. O. *Chem. Commun.* **1997**, 1495. (c) Shibata, T.; Takahashi, T.; Konishi, T.; Soai, K. *Angew. Chem., Int. Ed.* **1997**, 36, 2458. (d) Ohmori, R.; Saito, H.; Ikawa, Y.; Fujita, Y.; Inoue, T. *J. Mol. Evol.* **2011**, 73, 221.
 (259) (a) Paul, N.; Joyce, G. F. *Proc. Natl. Acad. Sci. U.S.A.* **2002**, 99, 12733. (b) Paul, N.; Joyce, G. F. *Curr. Opin. Chem. Biol.* **2004**, 8, 634.
 (260) Levy, M.; Ellington, A. D. *Proc. Natl. Acad. Sci. U.S.A.* **2003**, 100, 6416.
 (261) Lincoln, T. A.; Joyce, G. F. *Science* **2009**, 323, 1229.
 (262) Lam, B. J.; Joyce, G. F. *Nat. Biotechnol.* **2009**, 27, 288.
 (263) Pei, R.; Taylor, S. K.; Stojanovic, D.; Rudchenko, S.; Mitchell, T. E.; Stojanovic, M. N. *J. Am. Chem. Soc.* **2006**, 128, 12693.
 (264) (a) Shi, M. M. *Clin. Chem.* **2001**, 47, 164. (b) Zhao, W.; Ali, M. M.; Brook, M. A.; Li, Y. *Angew. Chem., Int. Ed.* **2008**, 47, 6330. (c) Fischer, N. O.; Tarasow, T. M.; Tok, J. B. H. *Anal. Biochem.* **2008**, 373, 121.
 (265) (a) Schweitzer, B.; Kingsmore, S. *Curr. Opin. Biotechnol.* **2001**, 12, 21. (b) Nilsson, M.; Dahl, F.; Larsson, C.; Gullberg, M.; Stenberg, J. *Trends Biotechnol.* **2006**, 24, 83. (c) Nilsson, M. *Histochem. Cell Biol.* **2006**, 126, 159. (d) Stougaard, M.; Juul, S.; Andersen, F. F.; Knudsen, B. R. *Integr. Biol.* **2011**, 3, 982.
 (266) (a) Andras, S. C.; Power, J. B.; Cocking, E. C.; Davey, M. R. *Mol. Biotechnol.* **2001**, 19, 29. (b) Demidov, V. V. *Expert Rev. Mol. Diagn.* **2002**, 2, 89. (c) Qian, X.; Lloyd, R. V. *Diagn. Mol. Pathol.* **2003**, 12, 1. (d) Zhang, D.; Wu, J.; Ye, F.; Feng, T.; Lee, I.; Yin, B. *Clin. Chim. Acta* **2006**, 363, 61.
 (267) (a) Nilsson, M.; Gullberg, M.; Dahl, F.; Szuhan, K.; Raap, A. K. *Nucleic Acids Res.* **2002**, 30, e66. (b) Smolina, I. V.; Demidov, V. V.; Cantor, C. R.; Broude, N. E. *Anal. Biochem.* **2004**, 335, 326.
 (268) (a) Pickering, J.; Bamford, A.; Godbole, V.; Briggs, J.; Scorzafava, G.; Roe, P.; Wheeler, C.; Ghouze, F.; Cuss, S. *Nucleic Acids Res.* **2002**, 30, e60. (b) Wu, Z. S.; Zhang, S.; Zhou, H.; Shen, G. L.; Yu, R. *Anal. Chem.* **2010**, 82, 2221.
 (269) (a) Lizardi, P. M.; Huang, X.; Zhu, Z.; Bray-Ward, P.; Thomas, D. C.; Ward, D. C. *Nat. Genet.* **1998**, 19, 225. (b) Hsu, H. Y.; Huang, Y. Y. *Biosens. Bioelectron.* **2004**, 20, 123. (c) Ali, M. M.; Su, S.; Filipe, C. D. M.; Pelton, R.; Li, Y. *Chem. Commun.* **2007**, 4459.
 (270) (a) Di Giusto, D. A.; Wlassoff, W. A.; Gooding, J. J.; Messerle, B. A.; King, G. C. *Nucleic Acids Res.* **2005**, 33, e64. (b) Cheng, Y.; Li, Z.; Zhang, X.; Du, B.; Fan, Y. *Anal. Biochem.* **2008**, 378, 123.
 (271) Yi, J.; Zhang, W.; Zhang, D. Y. *Nucleic Acids Res.* **2006**, 34, e81.
 (272) (a) Schweitzer, B.; Roberts, S.; Grimwade, B.; Shao, W.; Wang, M.; Fu, Q.; Shu, Q.; Laroche, I.; Zhou, Z.; Tchernev, V. T.; Christiansen, J.; Velleca, M.; Kingsmore, S. F. *Nat. Biotechnol.* **2002**, 20, 359. (b) Shao, W.; Zhou, Z.; Laroche, I.; Lu, H.; Zong, Q.; Patel, D. D.; Kingsmore, S.; Piccoli, S. P. J. *Biomed. Biotechnol.* **2003**, 5, 299. (c) Kingsmore, S. F.; Patel, D. D. *Curr. Opin. Biotechnol.* **2003**, 14, 74.
 (273) (a) Schweitzer, B.; Wiltshire, S.; Lambert, J.; O'Malley, S.; Kukanskis, K.; Zhu, Z.; Kingsmore, S. F.; Lizardi, P. M.; Ward, D. C. *Proc. Natl. Acad. Sci. U.S.A.* **2000**, 97, 10113. (b) Zhou, H.; Bouwman, K.; Schotanus, M.; Verweij, C.; JMarrero, A.; Dillon, D.; Costa, J.; Lizardi, P.; Haab, B. B. *Genome Biol.* **2004**, 5, R28. (c) Huang, Y. Y.; Hsu, H. Y.; Huang, C. J. *Biosens. Bioelectron.* **2007**, 22, 980.
 (274) Cho, E. J.; Yang, L.; Levy, M.; Ellington, A. D. *J. Am. Chem. Soc.* **2005**, 127, 2022.
 (275) (a) McManus, S. A.; Li, Y. *J. Am. Chem. Soc.* **2013**, 135, 7181. (b) Ali, M. M.; Li, Y. *Angew. Chem., Int. Ed.* **2009**, 48, 3512.
 (276) (a) Tang, L.; Liu, Y.; Ali, M. M.; Kang, D. K.; Zhao, W.; Li, J. *Anal. Chem.* **2012**, 84, 4711. (b) Wen, Y.; Xu, Y.; Mao, X.; Wei, Y.; Song, H.; Chen, N.; Huang, Q.; Fan, C.; Li, D. *Anal. Chem.* **2012**, 84, 7664.
 (277) (a) Navani, N. K.; Li, Y. *Curr. Opin. Chem. Biol.* **2006**, 10, 272. (b) Yang, L.; Fung, C. W.; Cho, E. J.; Ellington, A. D. *Anal. Chem.* **2007**, 79, 3320.
 (278) (a) Jayasena, S. D. *Clin. Chem.* **1999**, 45, 1628. (b) Gooding, J. J.; King, G. C. *J. Mater. Chem.* **2005**, 15, 4876. (c) Zhou, L.; Ou, L. J.; Chu, X.; Shen, G. L.; Yu, R. Q. *Anal. Chem.* **2007**, 79, 7492.
 (279) (a) Deng, Z.; Tian, Y.; Lee, S. H.; Ribbe, A. E.; Mao, C. *Angew. Chem., Int. Ed.* **2005**, 44, 3582. (b) Beyer, S.; Nickels, P.; Simmel, F. C. *Nano Lett.* **2005**, 5, 719. (c) Zhao, W.; Gao, Y.; Kandadai, S. A.; Brook, M. A.; Li, Y. *Angew. Chem., Int. Ed.* **2006**, 45, 2409.
 (280) (a) He, Y.; Tian, Y.; Ribbe, A. E.; Mao, C. D. *J. Am. Chem. Soc.* **2006**, 128, 15978. (b) Cheglakov, Z.; Weizmann, Y.; Braunschweig, A. B.; Wilner, O. I.; Willner, I. *Angew. Chem., Int. Ed.* **2007**, 47, 126.
 (281) (a) Tian, Y.; He, Y.; Mao, C. *ChemBioChem* **2006**, 7, 1862. (b) Cheglakov, Z.; Weizmann, Y.; Basnar, B.; Willner, I. *Org. Biomol. Chem.* **2007**, 5, 223. (c) Wang, F.; Lu, C. H.; Liu, X.; Freage, L.; Willner, I. *Anal. Chem.* **2014**, 86, 1614.
 (282) Köster, D. M.; Haselbach, D.; Lehrach, H.; Seitz, H. *Mol. Biosyst.* **2011**, 7, 2882.
 (283) (a) Green, L. S.; Jellinek, D.; Jenison, R.; Östman, A.; Heldin, C. H.; Green, N. J. *Biochemistry* **1996**, 35, 14413. (b) Fredriksson, S.; Gullberg, M.; Jarvius, J.; Olsson, C.; Pietras, K.; Gustafsdottir, S. M.; Östman, A.; Landegren, U. *Nat. Biotechnol.* **2002**, 20, 473.
 (284) (a) Lin, Z.; Yang, W.; Zhang, G.; Liu, Q.; Qiu, B.; Cai, Z.; Chen, G. *Chem. Commun.* **2011**, 47, 9069. (b) Tian, T.; Xiao, H.; Zhang, Z.; Long, Y.; Peng, S.; Wang, S.; Zhou, X.; Liu, S.; Zhou, X. *Chem.—Eur. J.* **2013**, 19, 92.
 (285) (a) Bi, S.; Zhang, J.; Zhang, S. *Chem. Commun.* **2010**, 46, 5509. (b) Huang, Y.; Chen, J.; Zhao, S.; Shi, M.; Chen, Z.; Liang, H. *Anal. Chem.* **2013**, 85, 4423.

- (286) Weizmann, Y.; Cheglakov, Z.; Willner, I. *J. Am. Chem. Soc.* **2008**, *130*, 17224.
- (287) Zhang, M.; Huang, J.; Deng, M.; Weng, X.; Ma, H.; Zhou, X. *Chem. Asian J.* **2009**, *4*, 1420.
- (288) (a) Zhou, Z.; Du, Y.; Zhang, L.; Dong, S. *Biosens. Bioelectron.* **2012**, *34*, 100. (b) Xu, H.; Xu, P.; Gao, S.; Zhang, S.; Zhao, X.; Fan, C.; Zuo, X. *Biosens. Bioelectron.* **2013**, *47*, 520.
- (289) Kong, R. M.; Zhang, X. B.; Chen, Z.; Meng, H. M.; Song, Z. L.; Tan, W.; Shen, G. L.; Yu, R. Q. *Anal. Chem.* **2011**, *83*, 7603.
- (290) Weizmann, Y.; Beissenhirtz, M. K.; Cheglakov, Z.; Nowarski, R.; Kotler, M.; Willner, I. *Angew. Chem., Int. Ed.* **2006**, *45*, 7384.
- (291) Wang, F.; Freage, L.; Orbach, R.; Willner, I. *Anal. Chem.* **2013**, *85*, 8196.
- (292) (a) Zhu, C.; Wen, Y.; Li, D.; Wang, L.; Song, S.; Fan, C.; Willner, I. *Chem.—Eur. J.* **2009**, *15*, 11898. (b) Shlyahovsky, B.; Li, D.; Weizmann, Y.; Nowarski, R.; Kotler, M.; Willner, I. *J. Am. Chem. Soc.* **2007**, *129*, 3814.
- (293) Li, D.; Wieckowska, A.; Willner, I. *Angew. Chem., Int. Ed.* **2008**, *47*, 3927.
- (294) (a) Li, W.; Liu, Z.; Lin, H.; Nie, Z.; Chen, J.; Xu, X.; Yao, S. *Anal. Chem.* **2010**, *82*, 1935. (b) Zeng, Y. P.; Hu, J.; Long, Y.; Zhang, C. Y. *Anal. Chem.* **2013**, *85*, 6143.
- (295) (a) Heithoff, D. M.; Sinsheimer, R. L.; Low, D. A.; Mahan, M. J. *Science* **1999**, *284*, 967. (b) Cheng, X.; Roberts, R. J. *Nucleic Acids Res.* **2001**, *29*, 3784. (c) Jeltsch, A. *ChemBioChem* **2002**, *3*, 274. (d) Shames, D. S.; Minna, J. D.; Gazdar, A. F. *Curr. Mol. Med.* **2007**, *7*, 85. (e) Song, G.; Chen, C.; Ren, J.; Qu, X. *ACS Nano* **2009**, *3*, 1183.
- (296) (a) Boening, D. W. *Chemosphere* **2000**, *40*, 1335. (b) Bolger, P. M.; Schwetz, B. A. N. *Engl. J. Med.* **2002**, *347*, 1735. (c) Clarkson, T. W.; Magos, L.; Myers, G. J. N. *Engl. J. Med.* **2003**, *349*, 1731. (d) Harris, H. H.; Pickering, I. J.; George, G. N. *Science* **2003**, *301*, 1203. (e) Nolan, E. M.; Lippard, S. J. *Chem. Rev.* **2008**, *108*, 3443.
- (297) Lu, L. M.; Zhang, X. B.; Kong, R. M.; Yang, B.; Tan, W. *J. Am. Chem. Soc.* **2011**, *133*, 11686.
- (298) He, K.; Li, W.; Nie, Z.; Huang, Y.; Liu, Z.; Nie, L.; Yao, S. *Chem.—Eur. J.* **2012**, *18*, 3992.
- (299) McClintock, B. *Proc. Natl. Acad. Sci. U.S.A.* **1942**, *28*, 458.
- (300) Moyzis, R. K.; Buckingham, J. M.; Cram, L. S.; Dani, M.; Deaven, L. L.; Jones, M. D.; Meyne, J.; Ratcliff, R. L.; Wu, J. R. *Proc. Natl. Acad. Sci. U.S.A.* **1988**, *85*, 6622.
- (301) (a) Wright, W. E.; Piatszek, M. A.; Rainey, W. E.; Shay, J. W. *Dev. Genet.* **1996**, *18*, 173. (b) Shay, J. W. *J. Cell. Physiol.* **1997**, *173*, 266.
- (302) (a) Makarov, V. L.; Hirose, Y.; Langmore, J. P. *Cell* **1997**, *88*, 657. (b) Hahn, W. C.; Stewart, S. A.; Brooks, M. W.; York, S. G.; Eaton, E.; Kurachi, A.; Beijersbergen, R. L.; Knoll, J. H.; Meyerson, M.; Weinberg, R. A. *Nat. Med.* **1999**, *5*, 1164.
- (303) (a) Shay, J. W.; Bacchetti, S. *Eur. J. Cancer* **1997**, *33*, 787. (b) Bryan, T. M.; Cech, T. R. *Curr. Opin. Cell Biol.* **1999**, *11*, 318.
- (304) (a) Morin, G. B. *Cell* **1989**, *59*, 521. (b) Rhyu, M. S. *Natl. J. Cancer Int.* **1995**, *87*, 884. (c) Kim, N. W. *Eur. J. Cancer* **1997**, *33*, 781.
- (305) Niazov, T.; Pavlov, V.; Xiao, Y.; Gill, R.; Willner, I. *Nano Lett.* **2004**, *4*, 1683.
- (306) (a) Izbicka, E.; Wheelhouse, R. T.; Raymond, E.; Davidson, K. K.; Lawrence, R. A.; Sun, D.; Windle, B. E.; Hurley, L. H.; Von Hoff, D. D. *Cancer Res.* **1999**, *59*, 639. (b) Neidle, S.; Read, M. A. *Biopolymers* **2001**, *56*, 195.
- (307) (a) Parkinson, G. N.; Lee, M. P. H.; Neidle, S. *Nature* **2002**, *417*, 876. (b) Cuesta, J.; Read, M. A.; Neidle, S. *Mini-Rev. Med. Chem.* **2003**, *3*, 11.
- (308) (a) Freeman, R.; Sharon, E.; Teller, C.; Henning, A.; Tzfati, Y.; Willner, I. *ChemBioChem* **2010**, *11*, 2362. (b) Tian, T.; Peng, S.; Xiao, H.; Zhang, X.; Guo, S.; Wang, S.; Zhou, X.; Liu, S.; Zhou, X. *Chem. Commun.* **2013**, *49*, 2652.
- (309) (a) Burack, W. R.; Shaw, A. S. *Curr. Opin. Cell Biol.* **2000**, *12*, 211. (b) Savage, D. F.; Afonso, B.; Chen, A. H.; Silver, P. A. *Science* **2010**, *327*, 1258.
- (310) (a) Park, S. H.; Zarrinpar, A.; Lim, W. A. *Science* **2003**, *299*, 1061. (b) Dueber, J. E.; Wu, G. C.; Malmirchegini, G. R.; Moon, T. S.; Petzold, C. J.; Ullal, A. V.; Prather, K. L.; Keasling, J. D. *Nat. Biotechnol.* **2009**, *27*, 753.
- (311) (a) Liu, X.; Freeman, R.; Golub, E.; Willner, I. *ACS Nano* **2011**, *5*, 7648. (b) Freeman, R.; Liu, X.; Willner, I. *J. Am. Chem. Soc.* **2011**, *133*, 11597.
- (312) Niazov, A.; Freeman, R.; Girsh, J.; Willner, I. *Sensors* **2011**, *11*, 10388.
- (313) Golub, E.; Niazov, A.; Freeman, R.; Zatsepina, M.; Willner, I. *J. Phys. Chem. C* **2012**, *116*, 13827.
- (314) Tacal, O.; Ozer, I. *J. Enzyme Inhib. Med. Chem.* **2006**, *21*, 783.
- (315) (a) Delebecque, C. J.; Lindner, A. B.; Silver, P. A.; Aldaye, F. A. *Science* **2011**, *333*, 470. (b) You, M.; Wang, R. W.; Zhang, X.; Chen, Y.; Wang, K.; Peng, L.; Tan, W. *ACS Nano* **2011**, *5*, 10090. (c) Piperberg, G.; Wilner, O. I.; Yehezkel, O.; Tel-Vered, R.; Willner, I. *J. Am. Chem. Soc.* **2009**, *131*, 8724. (d) Xin, L.; Zhou, C.; Yang, Z.; Liu, D. *Small* **2013**, *9*, 3088. (e) Liu, M.; Fu, J.; Hejesen, C.; Yang, Y.; Woodbury, N. W.; Gothelf, K.; Liu, Y.; Yan, H. *Nat. Commun.* **2013**, *4*, 2127.
- (316) (a) Zhou, M.; Liang, X.; Mochizuki, T.; Asanuma, H. *Angew. Chem., Int. Ed.* **2010**, *49*, 2167. (b) Liang, X.; Zhou, M.; Kato, K.; Asanuma, H. *ACS Synth. Biol.* **2013**, *2*, 194.
- (317) (a) Liang, X.; Nishioka, H.; Takenaka, N.; Asanuma, H. *ChemBioChem* **2008**, *9*, 702. (b) Han, D.; Huang, J.; Zhu, Z.; Yuan, Q.; You, M.; Chen, Y.; Tan, W. *Chem. Commun.* **2011**, *47*, 4670.
- (318) (a) Saha, K.; Agasti, S. S.; Kim, C.; Li, X.; Rotello, V. M. *Chem. Rev.* **2012**, *112*, 2739. (b) Daniel, M. C.; Astruc, D. *Chem. Rev.* **2004**, *104*, 293. (c) Katz, E.; Willner, I. *Angew. Chem., Int. Ed.* **2004**, *43*, 6042. (d) Rosi, N. L.; Mirkin, C. A. *Chem. Rev.* **2005**, *105*, 1547. (e) Wang, F.; Liu, X.; Lu, C. H.; Willner, I. *ACS Nano* **2013**, *7*, 7278.
- (319) (a) Petty, J. T.; Zheng, J.; Hud, N. V.; Dickson, R. M. *J. Am. Chem. Soc.* **2004**, *126*, 5207. (b) Guo, W.; Yuan, J.; Dong, Q.; Wang, E. *J. Am. Chem. Soc.* **2010**, *132*, 932. (c) Yeh, H. C.; Sharma, J.; Han, J. J.; Martinez, J. S.; Werner, J. H. *Nano Lett.* **2010**, *10*, 3106. (d) Liu, X.; Wang, F.; Niazov-Elkan, A.; Guo, W.; Willner, I. *Nano Lett.* **2013**, *13*, 309.
- (320) (a) Chan, W. C.; Maxwell, D. J.; Gao, X.; Bailey, R. E.; Han, M.; Nie, S. *Curr. Opin. Biotechnol.* **2002**, *13*, 40. (b) Green, M. *Angew. Chem., Int. Ed.* **2004**, *43*, 4129. (c) Michalet, X.; Pinaud, F. F.; Bentolila, L. A.; Tsay, J. M.; Doose, S.; Li, J. J.; Sundaresan, G.; Wu, A. M.; Gambhir, S. S.; Weiss, S. *Science* **2005**, *307*, 538. (d) Gill, R.; Zayats, M.; Willner, I. *Angew. Chem., Int. Ed.* **2008**, *47*, 7602. (e) Freeman, R.; Willner, I. *Chem. Soc. Rev.* **2012**, *41*, 4067. (f) Wang, F.; Liu, X.; Willner, I. *Adv. Mater.* **2013**, *25*, 349.
- (321) (a) Katz, E.; Willner, I. *ChemPhysChem* **2004**, *5*, 1084. (b) Kauffman, D. R.; Star, A. *Chem. Soc. Rev.* **2008**, *37*, 1197. (b) Vashist, S. K.; Zheng, D.; Al-Rubeaan, K.; Luong, J. H.; Sheu, F. S. *Biotechnol. Adv.* **2011**, *29*, 169. (c) Gao, C.; Guo, Z.; Liu, J. H.; Huang, X. *J. Nanoscale* **2012**, *4*, 1948. (d) De Volder, M. F.; Tawfick, S. H.; Baughman, R. H.; Hart, A. J. *Science* **2013**, *339*, 535.
- (322) (a) Lu, C. H.; Yang, H. H.; Zhu, C. L.; Chen, X.; Chen, G. N. *Angew. Chem., Int. Ed.* **2009**, *48*, 4785. (b) Pumera, M. *Chem. Soc. Rev.* **2010**, *39*, 4146. (c) Chen, D.; Tang, L.; Li, J. *Chem. Soc. Rev.* **2010**, *39*, 3157. (d) Guo, S.; Dong, S. *Chem. Soc. Rev.* **2011**, *40*, 2644. (e) Morales-Narváez, E.; Merkoçi, A. *Adv. Mater.* **2012**, *24*, 3298. (f) Liu, X.; Wang, F.; Aizen, R.; Yehezkel, O.; Willner, I. *J. Am. Chem. Soc.* **2013**, *135*, 11832.
- (323) (a) Rosenbaum, D. M.; Liu, D. R. *J. Am. Chem. Soc.* **2003**, *125*, 13924. (b) Alemdaroglu, F. E.; Ding, K.; Berger, R.; Herrmann, A. *Angew. Chem., Int. Ed.* **2006**, *45*, 4206. (c) McKee, M. L.; Milnes, P. J.; Bath, J.; Stulz, E.; Turberfield, A. J.; O'Reilly, R. K. *Angew. Chem., Int. Ed.* **2010**, *49*, 7948. (d) Ravnsbæk, J. B.; Jacobsen, M. F.; Rosen, C. B.; Voigt, N. V.; Gothelf, K. V. *Angew. Chem., Int. Ed.* **2011**, *50*, 10851. (e) Milnes, P. J.; McKee, M. L.; Bath, J.; Song, L.; Stulz, E.; Turberfield, A. J.; O'Reilly, R. K. *Chem. Commun.* **2012**, *48*, 5614. (f) McKee, M. L.; Milnes, P. J.; Bath, J.; Stulz, E.; O'Reilly, R. K.; Turberfield, A. J. *J. Am. Chem. Soc.* **2012**, *134*, 1446.
- (324) Bastian, A. A.; Marcozzi, A.; Herrmann, A. *Nat. Chem.* **2012**, *4*, 789.

- (325) (a) Fan, Z.; Govorov, A. O. *Nano Lett.* **2010**, *10*, 2580.
(b) Lange, H.; Juárez, B. H.; Carl, A.; Richter, M.; Bastús, N. G.; Weller, H.; Thomsen, C.; von Klitzing, R.; Knorr, A. *Langmuir* **2012**, *28*, 8862. (c) Acuna, G. P.; Möller, F. M.; Holzmeister, P.; Beater, S.; Lalkens, B.; Tinnefeld, P. *Science* **2012**, *338*, 506. (d) Li, Z.; Zhu, Z.; Liu, W.; Zhou, Y.; Han, B.; Gao, Y.; Tang, Z. *J. Am. Chem. Soc.* **2012**, *134*, 3322. (e) Shen, X.; Song, C.; Wang, J.; Shi, D.; Wang, Z.; Liu, N.; Ding, B. *J. Am. Chem. Soc.* **2012**, *134*, 146.
- (326) (a) Jaeger, L.; Chworos, A. *Curr. Opin. Struct. Biol.* **2006**, *16*, 531. (b) Cayrol, B.; Nogues, C.; Dawid, A.; Sagi, I.; Silberzan, P.; Isambert, H. *J. Am. Chem. Soc.* **2009**, *131*, 17270. (c) Jaeger, L.; Westhof, E.; Leontis, N. B. *Nucleic Acids Res.* **2001**, *29*, 455. (d) Severcan, I.; Geary, C.; Chworos, A.; Voss, N.; Jacovetty, E.; Jaeger, L. *Nat. Chem.* **2010**, *2*, 772. (e) Severcan, I.; Geary, C.; Verzemnieks, E.; Chworos, A.; Jaeger, L. *Nano Lett.* **2009**, *9*, 1270.
- (327) Orbach, R.; Guo, W.; Wang, F.; Lioubashevski, O.; Willner, I. *Langmuir* **2013**, *29*, 13066.
- (328) (a) Kuzyk, A.; Schreiber, R.; Fan, Z.; Pardatscher, G.; Roller, E. M.; Högele, A.; Simmel, F. C.; Govorov, A. O.; Liedl, T. *Nature* **2012**, *483*, 311. (b) Shen, X.; Asenjo-Garcia, A.; Liu, Q.; Jiang, Q.; García de Abajo, F. J.; Liu, N.; Ding, B. *Nano Lett.* **2013**, *13*, 2128.